Department of Chemistry

Amino Acid Functionalised Calixarenes: Crystal Growth Modifiers and Low Molecular Weight Gelators

Ching Yong Goh

This thesis is presented for the Degree of
Doctor of Philosophy
of
Curtin University

November 2012

Declaration

To the best of my knowledge and belief this thesis contains no material previously published by any other person except where due acknowledgement has been made. This thesis contains no material which has been accepted for the award of any other degree or diploma in any university.

Signature: _____

Date: _____

Abstract

A selection of amino acid functionalised calix[4]arenes was studied. Acidic amino acid functionalised calixarenes were investigated as crystal growth modifiers. The self-assembly behaviour of proline functionalised calixarenes were also examined.

Calix[4]arenes functionalised at the wide-rim with acidic amino acids were investigated as potential crystal growth modifiers on model mineral systems and were compared with previously investigated narrow-rim analogues. This study found that the wide-rim aspartic acid and glutamic acid functionalised calix[4]arenes had an impact on the morphology of calcium carbonate and barium sulfate. The iminodiacetic acid calix[4]arene was found to have minor impact on the morphology of calcium carbonate. In comparison with the narrow-rim analogues, the wide-rim and narrow-rim aspartic acid calix[4]arenes had similar potency on calcium carbonate while the wide-rim glutamic acid calix[4]arene appeared to be more potent than the narrow-rim calix[4]arene. Calcium carbonate crystallised in the presence of wide-rim aspartic acid and glutamic acid calix[4]arenes and their narrow-rim analogues had stepped edges which resembled calcium carbonate found in biomineral systems (e.g. mollusc shells). Desupersaturation experiments showed the wide-rim aspartic acid calix[4]arene to be a more potent inhibitor of barium sulfate crystallisation than the wide-rim glutamic acid calix[4]arene.

An aqueous solution of L-proline calix[4]arene exhibited surfactant-like properties. The self-assembly behaviour of L-proline calix[4]arene in solution was characterised by UV-visible and NMR spectroscopy. The critical aggregation concentration of L-proline calix[4]arene was determined to be 4–9 mM by monitoring a selection of dye compounds using UV-visible spectroscopy. The interaction of L-proline calix[4]arene with small molecules and in the presence of electrolytes was also characterised by NMR spectroscopy. The ^{1}H NMR spectra of L-proline calix[4]arene in the presence of small molecules (tetrahydrofuran, 1-methyl-2-pyrrolidinone, and *tert*-butyl alcohol) suggested that the calixarene was either acting as a host or self-assembling into larger aggregates. Variable temperature NMR experiments showed that these interactions were thermoreversible.

The formation of a hydrogel by proline calix[4]arenes in the presence of electrolytes was a serendipitous discovery. Investigations with selected electrolytes showed that the anion was the dominant factor in determining if a hydrogel formed, with lesser influence from the cation. The thermostability of the calixarene-electrolyte hydrogels tended to follow the Hofmeister series, where more stable hydrogels formed in the presence of anions towards the chaotropic end of the series. A racemic mixture of the proline calixarenes gave a less stable hydrogel compared with hydrogels of the enantiopure compounds. The calixarene-electrolyte hydrogels had a fibrous appearance, as characterised by atomic force microscopy. Some hydrogels collapsed slowly and deposited crystals of sufficient quality for single crystal x-ray crystallography. These structures gave some insights into how intermolecular forces may give rise to the fibrous gel structures; in particular hydrogen bonds between proline moieties, and the inclusion of a proline group into the cavity of a neighbouring calixarene, leading to spiral-like structures. A sarcosine functionalised calix[4]arene also formed hydrogels upon addition of some electrolytes, whereas the proline-functionalised calix[5]arene analogue did not.

Since a range of hydrogels have been used as matrices to control crystal growth, a proline calix[4]arene-lithium nitrate hydrogel was used as a potential template for barium sulfate crystallisation. The results suggested that lithium nitrate was the main factor in modification of the barium sulfate morphology. The hydrogel did have a minor impact by slowing the diffusion of sulfate anions into the barium-containing gel phase resulting in smaller particles.

The versatility of amino acid functionalised calix[4]arenes has been highlighted here. Wide-rim functionalised acidic amino acid calix[4]arenes were found to be effective crystal growth modifiers; having an impact on the morphology and growth kinetics of model crystallisation systems, calcium carbonate and barium sulfate. Interesting supramolecular chemistry was observed with proline functionalised calix[4]arenes; the proline calixarene interacts with small molecules in solution and either act as a host or self-assembles into large aggregates. The formation of proline calix[4]arene aggregates is interesting as they give rise to hydrogels in the presence of selected electrolytes.

Acknowledgements

I would like to acknowledge my supervisors, A/Prof. Mauro Mocerino, Prof. Mark I. Ogden, and Dr. Franca Jones, for their advice, guidance, and patience throughout this project.

I would also like to thank my colleagues in the laboratory (Dr David H. Brown, Dr Gareth L. Nealon, Dr Matthew J. McIldowie, and past and present members of the synthesis labs).

Furthermore, I would like to thank the staff of the Department of Chemistry, in particular Dr. Thomas Becker (atomic force microscopy experiments), Joyce Wong (glassware and reagents), and Tomoko Radomirovic (crystallisation experiments). In addition I would like to thank following people for their technical expertise: Elaine Miller, Centre for Materials Research, Curtin University (scanning electron microscopy); Dr. Matthias Floetenmeyer, Centre for Microscopy and Microanalysis, University of Queensland (cryo-transmission electron microscopy); Dr. Brian Skelton, School of Biomedical, Biomolecular and Chemical Sciences, University of Western Australia (x-ray crystallography); and Drs Nigel Kirby and Adrian Hawley, Australian Synchrotron (SAX/WAXS beamline scientists). The synthesis of amino acid functionalised calixarenes for crystal growth was assisted by helpful discussions with members of the Ungaro research group (University of Parma, Italy).

I would also like to acknowledge the following funding sources: the Australian Federal Government for an Australian Postgraduate Award (APA) scholarship; Curtin University for the Curtin Research Scholarship (CRS); the Australian Microscopy and Microanalysis Research Facility for travel and access to the cryo-transmission electron microscopy (cryo-TEM) facility at the University of Queensland; Australian Synchrotron for travel and access to the SAX/WAXS beamline at the Australian Synchrotron; and my supervisors (access to instruments, reagents, and consumables).

Finally, I would like to thank my family for their support and patience.

Table of Contents

Abbreviations

Ac	acetyl
AFM	atomic force microscopy
Ar	arene
Asp	aspartic acid
Asx	asparagine or aspartic acid
ax	axial
Bn	benzyl
Boc	*N*-*tert*-butoxycarbonyl
Bu	butyl
t-Bu	*tert*-butyl
c.a.c.	critical aggregation concentration
cat.	catalyst, catalytic
CD	circular dichroism
c.m.c.	critical micelle concentration
COSY	correlated spectroscopy
DAST	*N*,*N*-diethylaminosulfur trifluoride
DCC	*N*,*N*'-dicyclohexylcarbodiimide
DCE	1,2-dichloroethane
DCM	dichloromethane
dec	decomposed
DEPT	distortionless enhancement by polarisation transfer
DLS	dynamic light scattering
DMAP	4-(*N*,*N*-dimethylamino)pyridine
DMF	*N*,*N*-dimethylformamide
DMSO	dimethyl sulfoxide
E	electrophile
EAS	electrophilic aromatic substitution
EDC	*N*-(3-dimethylaminopropyl)-*N*'-ethylcarbodiimide
EDTA	ethylenediaminetetraacetic acid
EDTP	ethylenediaminetetraphosphonic acid
eq	equatorial
equiv.	equivalence
Et	ethyl
Fmoc	9-fluorenylmethoxycarbonyl
Glu	glutamic acid
Glx	glutamine or glutamic acid
h	hour(s)
HBTU	*O*-(benzotriazol-1-yl)-*N*,*N*,*N'*,*N'*-tetramethyluronium hexafluorophosphate
HEDP	hydroxyethylenediphosphonic acid
HMBC	heteronuclear multiple bond correlation
HOBt	1-hydroxybenzotriazole
HOSu	*N*-hydroxysuccinimide
HSQC	heteronuclear single quantum coherence
ISE	ion-selective electrode
J	coupling constant
Me	methyl
MEK	methyl ethyl ketone
Mes	mesityl
mp	melting point
N	nucleophile
NBS	*N*-bromosuccinimide
NMP	1-methyl-2-pyrrolidinone
PAA	poly(acrylic acid)
PFP	perfluorophenol
Ph	phenyl
PMMA	poly(methyl methacrylate)
ppm	parts per million
Pr	propyl
Pro	proline
PyBOP	benzotriazol-1-yloxy)-tripyrrolidinophosphonium hexafluorophosphate
rt	room temperature
SAXS	small angle x-ray scattering
SEM	scanning electron microscopy
TEM	transmission electron microscopy
TFA	trifluoroacetic acid
THF	tetrahydrofuran
TLC	thin layer chromatography
TOCSY	total correlation spectroscopy
VT	variable-temperature
WAXS	wide-angle x-ray scattering

1 Calixarenes, Crystallisation, and Low Molecular Weight Gelators—an Overview

1.1 Calixarenes

1.1.1 Background on calixarenes

Calixarenes are a class of cyclic oligomers, [1$_n$] metacyclophanes, formed by a condensation reaction between a phenol and an aldehyde (Figure 1.1).[1–3] Since the seminal works by Gutsche,[4] there have been numerous publications involving calixarenes, including several books devoted to calixarenes.[1, 2, 4–11] Furthermore, calixarenes can vary in size (by the number of arene units), adopt different conformations, and be readily functionalised. Their structure also allows for some degree of control over the spatial arrangement of functional groups or moieties of interest in solution.

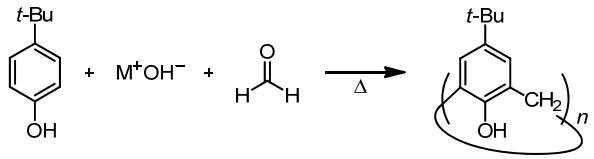

Figure 1.1 General scheme for the preparation of calix[*n*]arenes by based condensation of *tert*-butylphenol and formaldehyde. M^+ is typically an alkali metal such as Na^+ or K^+.

Much of the literature involving calixarenes typically employ the more synthetically accessible calix[*n*]arenes, where $n = 4, 6, 8$. Odd numbered calixarenes (especially calix[5]arenes[12, 13]) and higher calix[*n*]arenes (where $n \geq 7$) have also been reported. It was realised during early research into calixarenes that they could be isolated as

different conformational isomers (i.e. *conformers*).[14] Gutsche later coined the terms cone, partial cone, 1,3-alternate, and 1,2-alternate (Figure 1.2) to describe the four main conformers of calix[4]arenes.[4] Calix[4]arenes can be immobilised into these conformers by introducing sufficiently large groups to restrict exo- and endo-intraannular rotation.[15, 16] This allows further control over the spatial arrangements of functional groups.

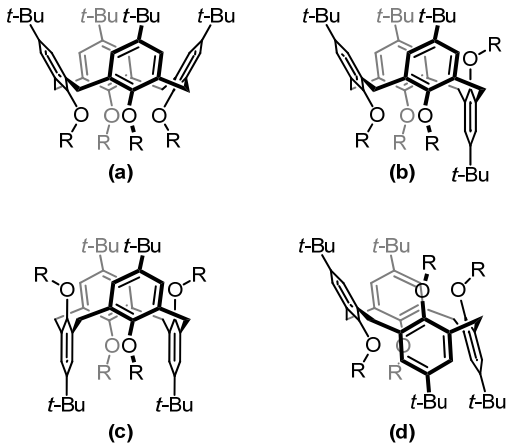

Figure 1.2 The main conformational isomers ('conformers') of calix[4]arenes: (a) cone; (b) partial cone; (c) 1,3-alternate; and (d) 1,2-alternate, where R is a sufficiently bulky group.

1.1.2 Graphical representation of calixarenes

There are many schematic representations of calixarenes in the literature. Some of the more common forms for the calix[4]arene are shown in Figure 1.3. The bracketed forms without a loop (Figure 1.3a) and with a loop (Figure 1.3b) are commonly used in the literature. However, the bracketed form without a loop can be confused for the acyclic oligomer by readers not familiar with the literature. The three-dimensional (Figure 1.3c) and 'flattened' (Figure 1.3d) structures are particularly useful for chiral, partially substituted, and intra- and intermolecular bridged calixarenes, however it becomes cumbersome to draw when the calixarenes are functionalised with large bulky substituents. This thesis will primarily use the bracketed form with a loop (Figure 1.3b), although other representations of calixarenes will be used where appropriate.

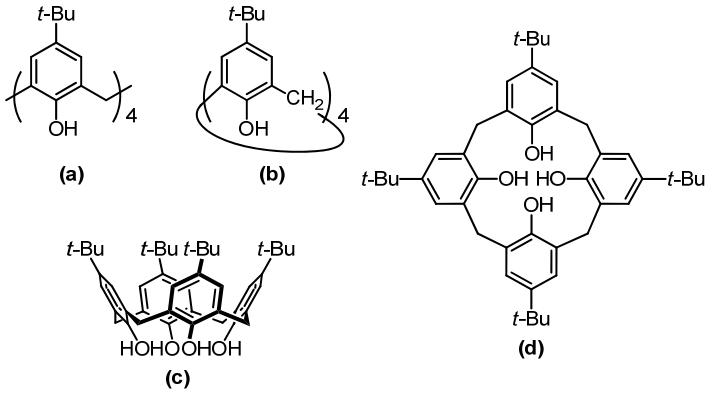

Figure 1.3 Graphical structural representation of *tert*-butylcalix[4]arene **1**: (a) bracketed form; (b) bracketed form with loop to represent cyclic structure of calixarenes; (c) three-dimensional representation; and (d) 'flattened' structure.

1.1.3 Nomenclature of calixarenes

The nomenclature of calixarenes in this thesis will follow the International Union of Pure and Applied Chemistry's (IUPAC) recommendations for the nomenclature of phanes.[17, 18] The phane parent hydride is simplified and numbered according to the following precedence rules (taken from IUPAC's *Phane Nomenclature*, *Part II*[18]) to give the lowest locant set:

1. numbering of the phane parent hydride
2. heteroatoms introduced by skeletal replacement ('a') nomenclature
3. indicated hydrogen
4. nondetachable 'hydro-'/'dehydro-' prefixes
5. principal characteristic group (named as suffix)
6. unsaturation ('-ene'/'-yne' endings and 'hydro-'/'dehydro-' prefixes)
7. substituents named as prefixes (alphabetised substituents)

The following is an example whereby the calix[4]arene **1** (Figure 1.3) is named using the phane nomenclature rules. The calix[4]arene **1** is simplified (Figure 1.4) and the resulting skeleton is named, *cyclooctaphane*, and numbered. The atoms of the *amplificants* (the result of amplification of the superatoms) are then numbered to give the lowest attachment locant set with preference for the lowest attachment locant to be adjacent to the lower amplificant locant. This gives a phane parent hydride name of 1,3,5,7(1,3)-tetrabenzenacyclooctaphane.

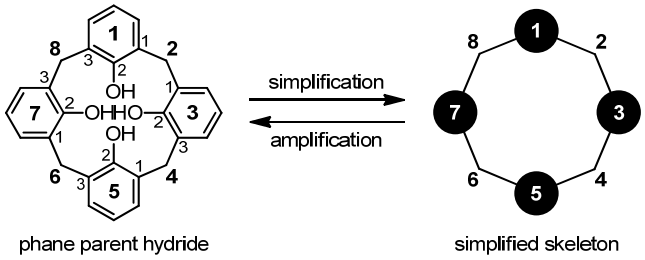

Figure 1.4 Numbering of the phane parent hydride using the recommendations from IUPAC's *Phane Nomenclature*, *Part II*.[18] Each black circle (●) represents a *superatom* (a phenarene moiety). Bold numbers are for the phane parent hydride and smaller numbers are for the amplificants.

The characteristic groups are then appended to the name by skeletal replacement nomenclature.[19] Here, the –OH, the principal characteristic group, is the suffix while the *tert*-butyl group is a prefix. The locant of the characteristic group is denoted in superscript after the amplificant locant to which it is attached (Figure 1.5). The full name of the calix[4]arene **1** (Figure 1.6) is $1^5,3^5,5^5,7^5$-tetra-*tert*-butyl-1,3,5,7(1,3)-tetrabenzenacyclooctaphane-$1^2,3^2,5^2,7^2$-tetrol. The parent hydride name, 1,3,5,7(1,3)-tetrabenzenacyclooctaphane, can be substituted with 'calix[4]arene' to give a more recognisable name, $1^5,3^5,5^5,7^5$-tetra-*tert*-butylcalix[4]arene-$1^2,3^2,5^2,7^2$-tetrol. IUPAC nomenclature can become unwieldy, especially for macrocyclic structures, so the use of the full IUPAC name will be limited in preference for the numbered structures.

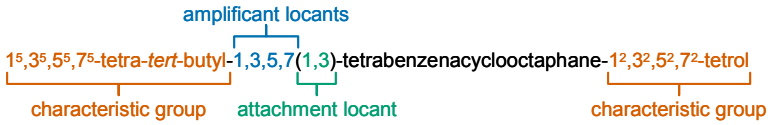

Figure 1.5 The constituents of an IUPAC name (using phane nomenclature) for calix[4]arene **1**.

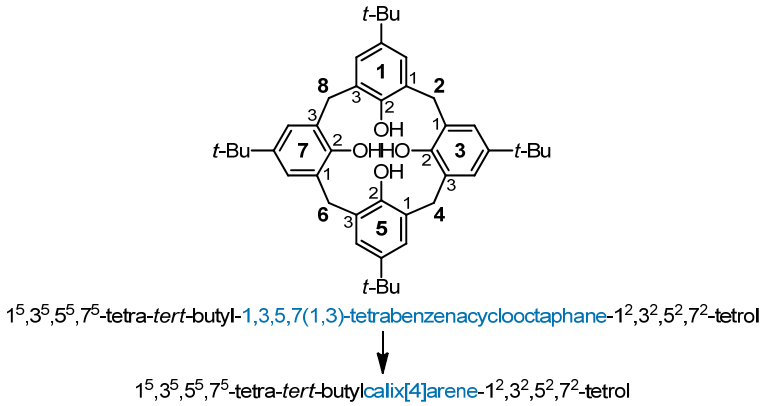

Figure 1.6 The IUPAC name for calix[4]arene **1**, based on phane nomencalture. Substitution of the phane parent name with 'calix[4]arene' gives a more familiar calixarene name.

The IUPAC nomenclature system for phanes had not been developed during the early days of calixarene research, therefore much of the literature still uses the original numbering system applied by Gutsche (Figure 1.7).[1] This numbering scheme was based on that used by the Chemical Abstracts Service (CAS). The recent systematic name assigned to calix[4]arene **1** by CAS is pentacyclo[19.3.1.13,7.19,13.115,19]-octacosa-1(25),3,5,7(28),9,11,13(27),15,17,19(26),21,23-dodecaene-25,26,27,28-tetrol, 5,11,17,23-tetrakis(1,1-dimethylethyl) (for CAS registry number 60705-62-6).

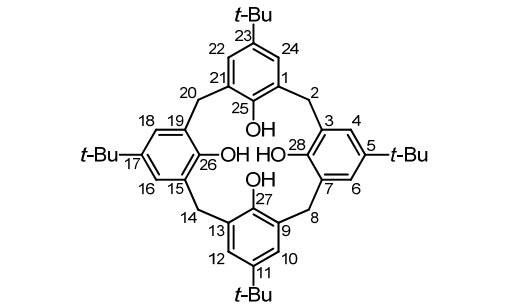

Figure 1.7 Gutsche's[1] numbering scheme for calixarene **1**.

Although a calixarene resembles a Greek *calyx krater* (a vase), it is not always practical to refer to the 'upper-rim' and 'lower-rim' of a calixarene (Figure 1.8). The upper-rim and lower-rim are also designated *exo*-rim (away from the annulus) and *endo*-rim (towards the annulus) respectively. Böhmer[20] introduced orientation-independent terms 'wide-rim' and 'narrow-rim' in place of upper-rim and lower-rim

respectively to avoid confusion. Therefore, 'wide-rim' and 'narrow-rim' are the preferred terms in this thesis.

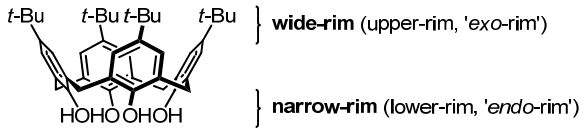

Figure 1.8 Designation of the rims of a calix[4]arene. The preferred terminology in this thesis is 'wide-rim' and 'narrow-rim'.

1.1.4 Selected methods of functionalising calixarenes

Borrowing from Gutche's idea of embroidering calixarene 'baskets',[1] some literature examples of functionalising calixarenes will be presented here. The examples will explore functionalising the calixarene at both the wide- and narrow-rims of the calix[4]arenes in the cone conformation and to a lesser extent at the methylenes.

Calixarenes are derived from phenols and they inherit many of the chemical characteristics of phenols. Therefore, calixarenes can be functionalised much like a phenol (Scheme 1.1) by electrophilic aromatic substitution (EAS) and esterification and alkylation of the phenol.[21] Because most calixarenes are prepared from *p-tert*-butylphenol, the *tert*-butyl group is removed to allow EAS to occur at the *para* position. Functional groups can also be introduced onto the methylene bridges of calixarenes. Similar to phenols, the arene groups of calixarenes can be oxidised under mild conditions.

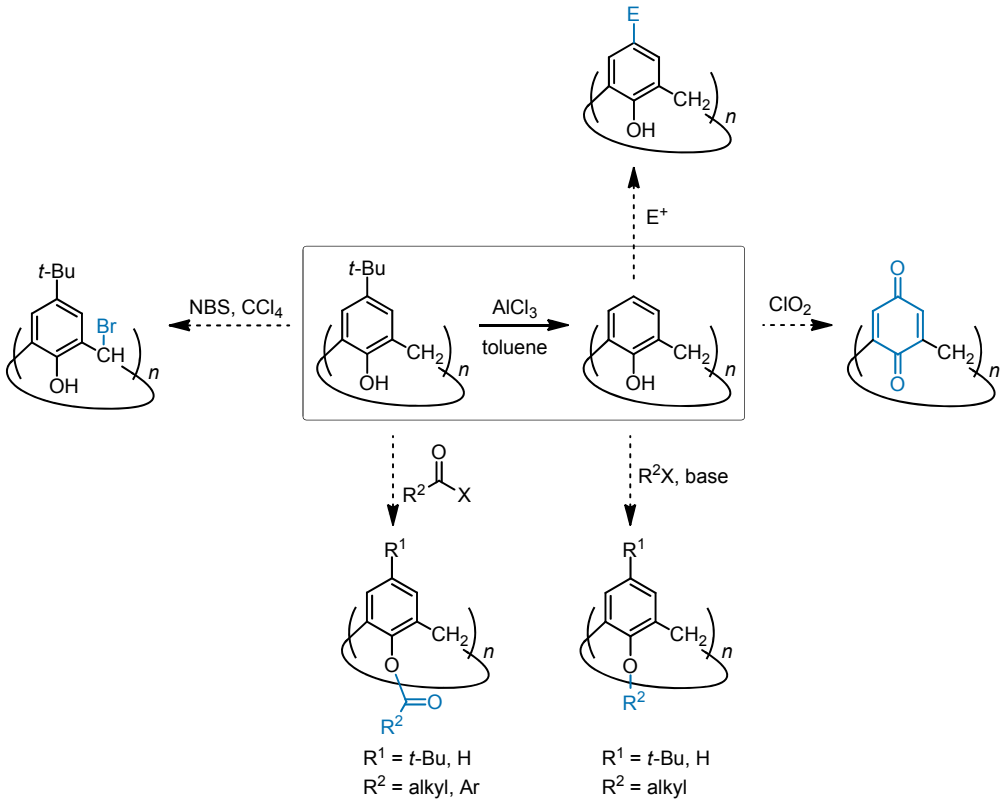

Scheme 1.1 Generic schemes for the main methods of functionalising calixarenes: electrophilic substitution at the wide-rim, nucleophilic substitution at the methylene, and esterification and etherification of the phenols.

It is not practical to review all the synthetic methodologies which have been used for the functionalisation of calixarenes. More detailed reviews of synthetic strategies can be found elsewhere.[1, 11, 21, 22] Scheme 1.2 illustrates a small selection of the large number of possible functionalities that can be introduced on to debutylated calix[4]arene **2**. The phenolic moieties can be oxidised to their para-quinones under mild oxidising conditions. Electrophilic aromatic substitutions at the position *para* to the phenol gives access to a wide range of compounds, including sulfonates, azo compounds, and amines (via reduction of a nitrated calix[4]arene) at the wide-rim. Methylation of the aminomethylene gives a good leaving group which allows for nucleophilic substitution of the ammonium group. Alkylation of the phenol with an allyl group allows access to alkene chemistry[23] at the narrow-rim. A Claisen-Cope rearrangement[24] will allow the same at the wide-rim. Alkylation of the phenol with ethyl haloacetate followed by hydrolysis of the ester introduces carboxylic acid chemistry at the narrow-rim (refer to section 1.1.4.2 for carboxylic acids at the wide-

rim). Alkylation of the phenols with a sufficiently bulky group locks the conformation of the calix[4]arene and protects the phenol at later stages of the synthesis.

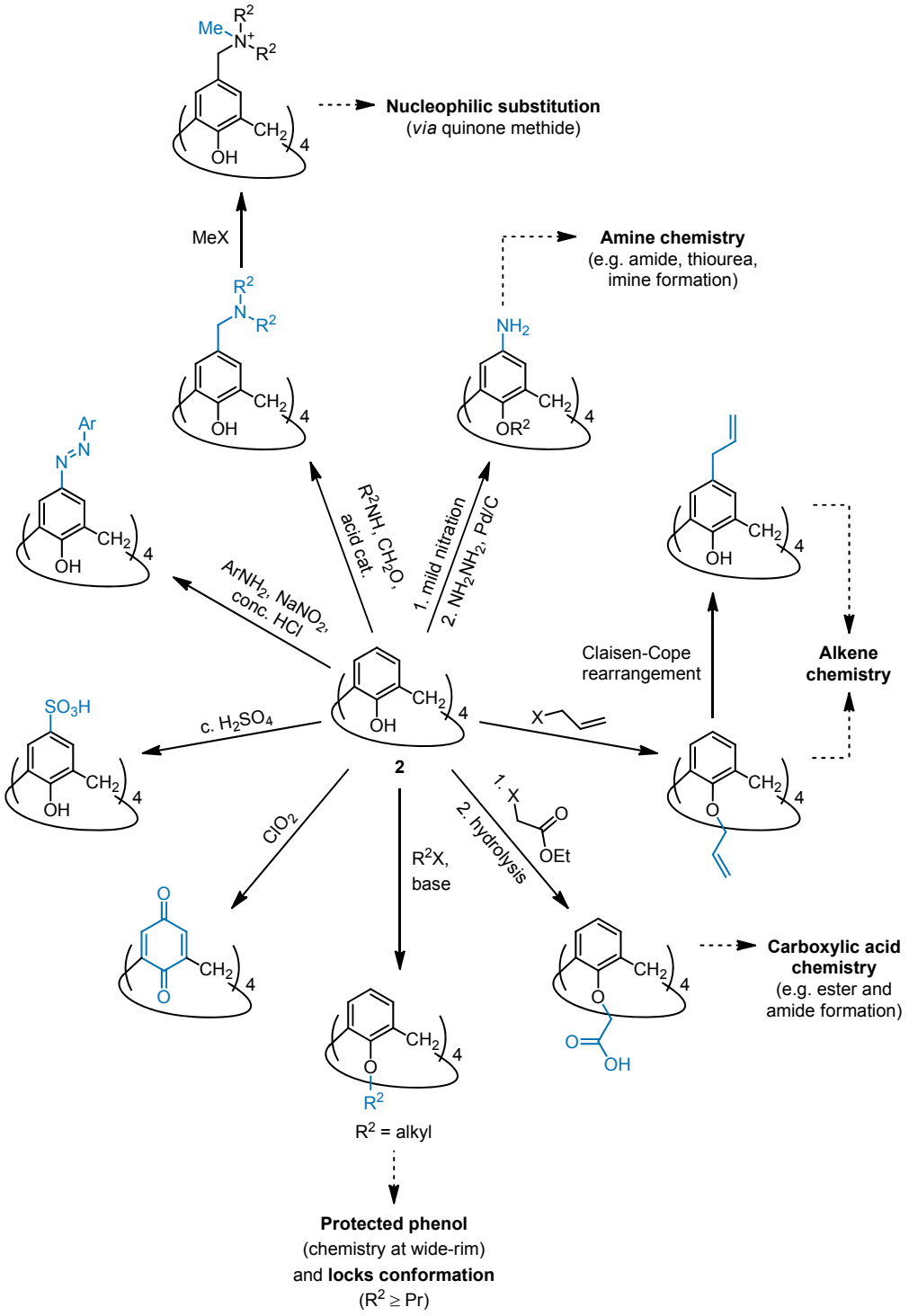

Scheme 1.2 Potential reactions of debutylated-calixarenes at the wide- and narrow-rims.

1.1.4.1 **Reactions at the phenol: narrow-rim functionalisation**

Alkylation of the phenol groups of calix[4]arenes allows the calixarene to be immobilised in a particular conformation, alters the calixarene's solubility in solvents, or direct attachment of more complex molecules to the narrow-rim. Typically, a calixarene is alkylated using an alkyl halide in the presence of a base (Scheme 1.3). The base used is dependent on the desired conformer[25] or degree of alkylation.[26] Iwamoto and Shinkai[25] also found that the proportions of the various conformers obtained (cone, partial cone, and 1,3-alternate) were dependent on the solvent, temperature of the reaction, reaction time, and the alkali cation.[27] The 1,2-alternate conformer is the least accessible[28] of the four conformers of calix[4]arenes, however Lhoták et al.[29] have described multi-gram scale preparations for the 1,2-alternate conformers of the *tert*-butylcalix[4]arene **1** (Scheme 1.4). The phenol groups can also be esterified by treatment with acid chlorides or anhydrides. Esterification is commonly used to protect the phenols (for example, Scheme 1.8).

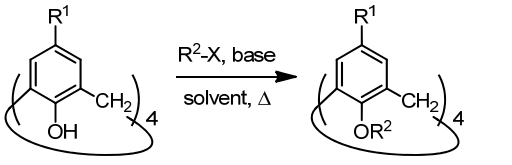

	R^1
1	*t*-Bu
2	H

	R^1	R^2
3a	*t*-Bu	Pr
3b	*t*-Bu	$CH_2(C=O)OEt$
3c	H	$CH_2(C=O)OEt$

Scheme 1.3 Direct alkylation of calix[4]arenes **1** and **2** with ethyl bromoacetate or propyl bromide. Refer to references for base, solvent, and full reaction conditions.[25, 27]

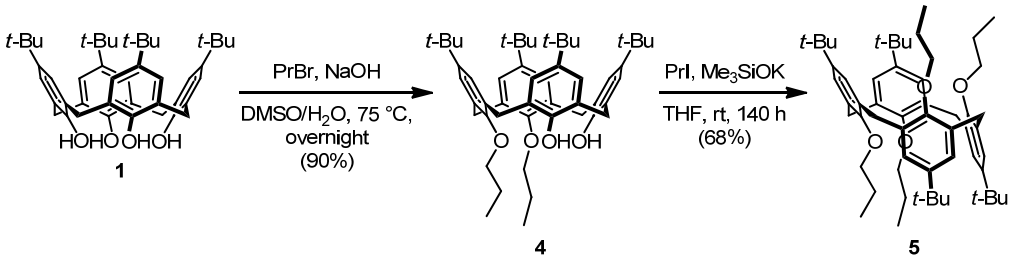

Scheme 1.4 Selected reaction condition (not the optimal condition but financially sound) investigated by Lhoták et al.[29] for the preparation of the 1,2-alternate conformation of a calix[4]arene.

Lalor et al.[30] prepared 'multi-calixarenes' **55a**,**b** and **56a** (refer to Figure 1.22, for full structures) by linking calix[4]arenes through the phenols at the narrow-rim and exploiting some of the conformers of calix[4]arenes. The selectively tris-alkylated[31] calix[4]arene **6** was alkylated with *N*-(3-bromopropyl)phthalimide in the presence of NaH to give the cone calix[4]arene **7**. Ipso-nitration of the *para*-position of the arene unit followed by reduction of *p*-nitrocalix[4]arene **8** gave the *p*-aminocalix[4]arene **9**. The wide-rim amines were protected with a Boc group or functionalised with Boc-protected glycine to give calix[4]arenes **10a** and **10b** respectively. The narrow-rim monoalkylamine was then deprotected to give calixarenes **11a**,**b**. Further functionalisation gave the desired multi-calixarenes.

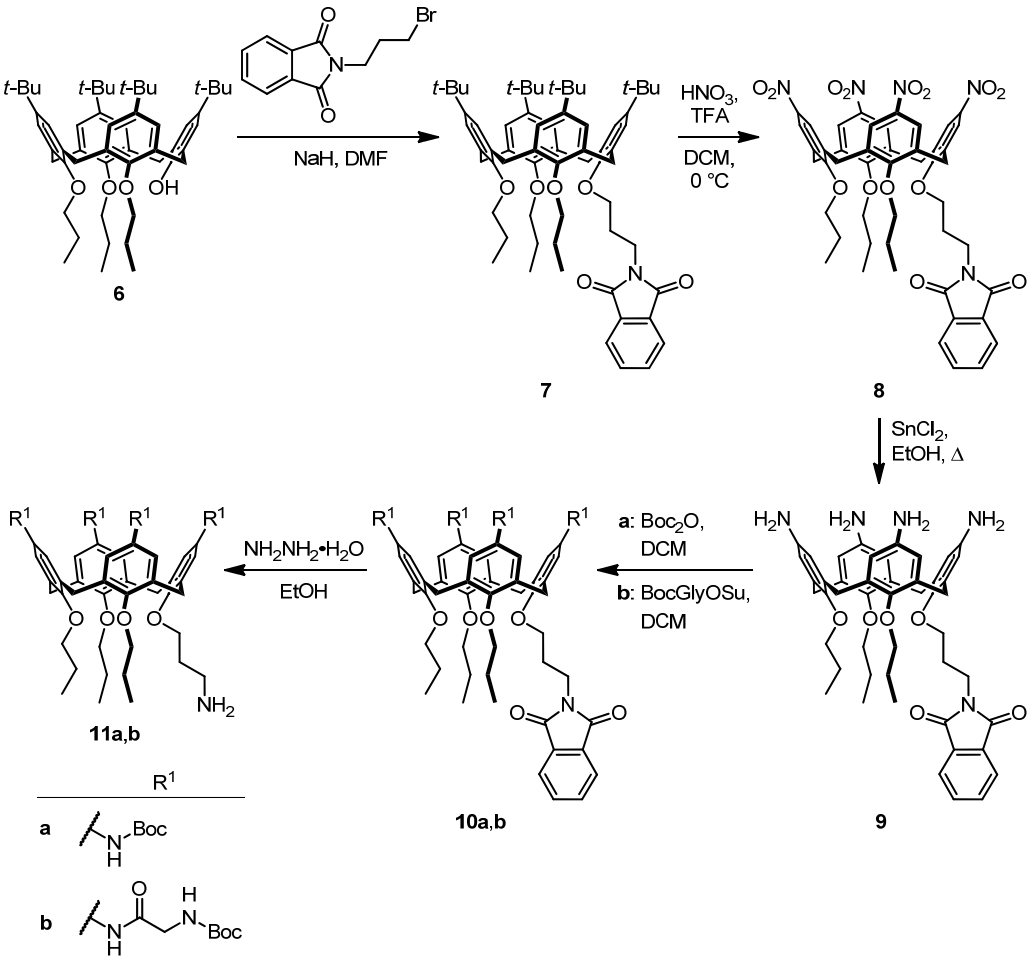

Scheme 1.5 Part of a synthetic sequence used in the preparation of dendritic 'multi-calixarenes' **55a**,**b** and **56a** by Lalor et al.[30] (refer to Figure 1.22 for the full chemical structure).

1.1.4.2 **Functionalisation of the wide-rim**

Nearly all the chemistry of the calixarenes of interest in this work occurs at the wide-rim. As such, more attention will be paid to synthesis at the wide-rim, in particular with protected phenols. From the handful of reactions shown in Scheme 1.6, it is evident that a range of synthetic chemistry can occur at the wide-rim of calixarenes giving access to a wide range of molecular functionality. The tetraalkylated calixarene can be halogenated at the *para*-position. Substitution of the *para*-halogenated calixarene with copper(I) cyanide gives a nitrile[32] which allows access to tetrazoles.[33, 34] Like other aryl halides, the halogenated calixarene can undergo cross-coupling reactions.[35] Likewise, potential boronic acid-functionalised calixarenes can also undergo cross-coupling reactions. Lithiated calixarenes can undergo nucleophilic substitution and are used to prepare boronic acids. Reaction of lithiated calixarenes with carbon dioxide give carboxylic acids.[36] Carboxylic acids can also be prepared by hydrolysis of a nitrile or oxidation[37, 38] of an aldehyde[39] (prepared by a Duff reaction[40] from the tetraalkylated calixarene). The remainder of this section explores more specific examples of chemistry at the wide-rim of calixarenes.

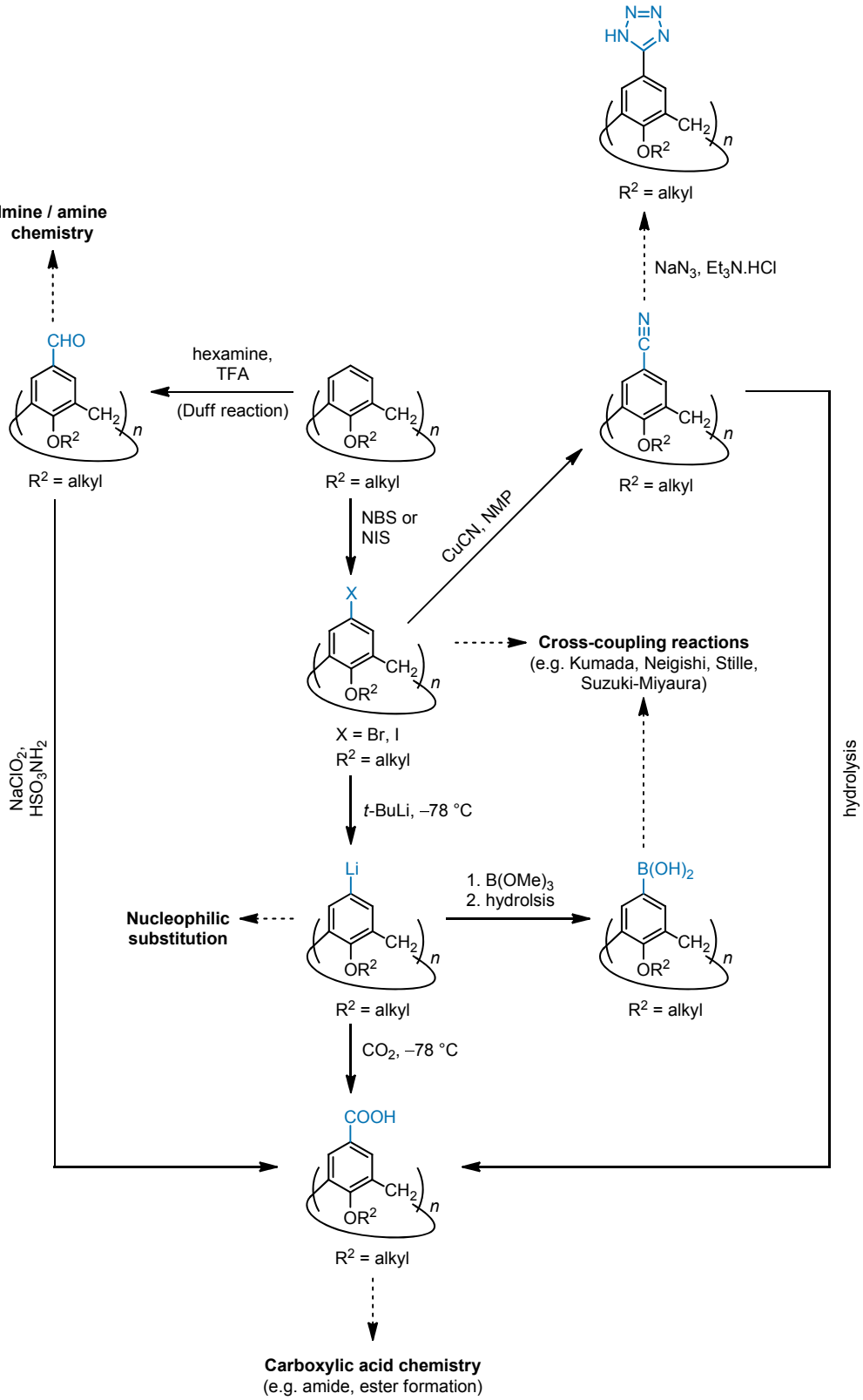

Scheme 1.6 Potential reactions at the wide-rim of phenol-protected calixarenes.

Amphiphilic calix[4]arenes **13a**,**b** and **14a**,**b** were prepared by Strobel et al.[36] using different methods at the wide-rim. Calix[4]arenes **13a**,**b** (with ammonium groups) were prepared by first generating the chloromethyl calix[4]arene and then a nucleophilic substitution with trimethylamine. This two-step method allows for aminomethylation of phenyl alkyl ethers whereas no product is obtained under Mannich conditions (refer to section 2.3 for more information). Calix[4]arenes **14a**,**b** (with carboxylic acid groups at the *para*-position) were prepared by reacting carbon dioxide with lithiated calix[4]arene.

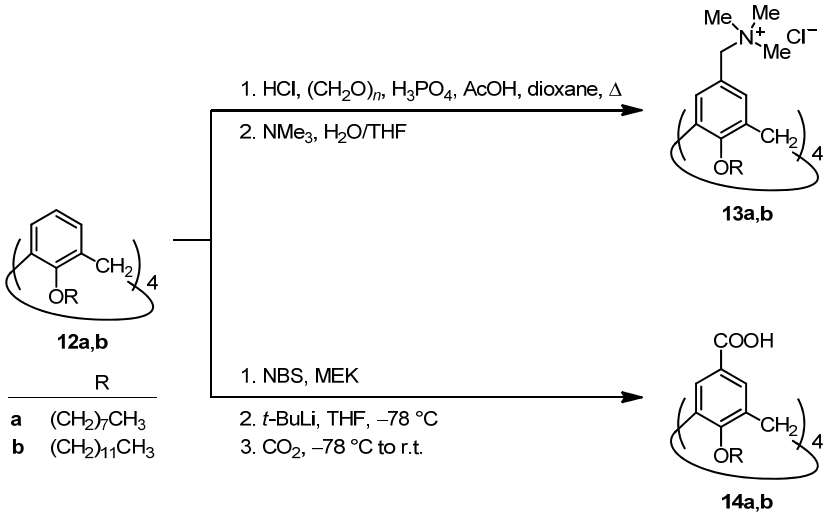

Scheme 1.7 Chloromethylation of calix[4]arene **12a**,**b** followed by an S_N2 substitution by trimethylamine to give the ammonium calix[4]arene **13a**,**b**. Bromination of calix[4]arene **12a**,**b** followed by lithiation and reaction with carbon dioxide gave the carboxylated calix[4]arene **14a**,**b**.[36]

Martin and Raston[41] prepared a series of *p*-phosphonic acid calix[*n*]arenes (where $n = 4, 5, 6, 8$). An example of the calix[4]arene is shown in Scheme 1.8 (this scheme is applicable to the other calix[*n*]arenes). Here, the authors brominated the wide-rim of calix[4]arene **2** then protected the phenols of **15** as acetates. This allowed the phosphonate to be introduced onto the aromatic ring **16** via a nickel-catalysed[42] Arbuzov reaction[43] (84% yield). The phenols of calix[4]arene **17** were then deprotected followed by removal of the esters from the phosphonate **18** to give the final product **19** (with a 98% yield after both deprotection steps). Phosphonates[44, 45] have been shown to have an impact on crystallisation of inorganic minerals such as barium sulfate (refer to section 3.1.1).

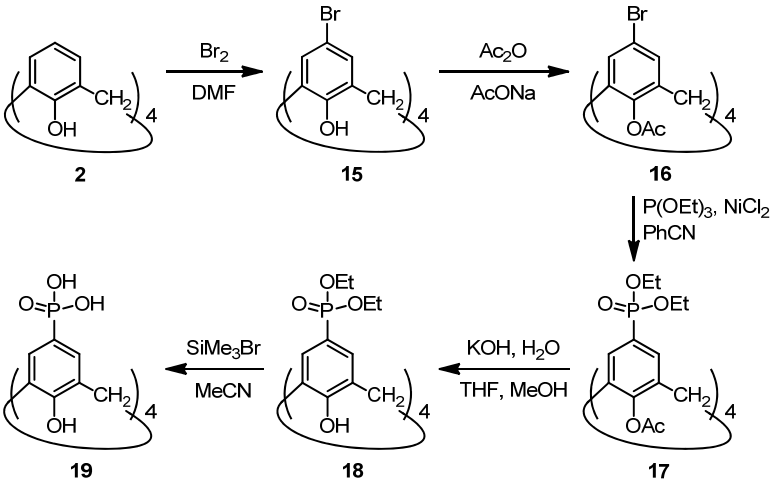

Scheme 1.8 Preparation of phosphonate calix[4]arene.[41] This scheme was also applied to other calix[*n*]arenes (where *n* = 5, 6, 8).

In contrast to phosphonates, sulfonates and nitrates can be introduced on the aromatic ring of calixarenes more directly (Scheme 1.9). Shinkai et al.[46] prepared sulfonated calix[*n*]arenes (where, *n* = 4, 6, 8; 78% yield for *n* = 4), which could then be converted to nitro calix[*n*]arenes by treating the sulfonated calixarenes with nitric acid (obtained in a low yield of 21%). It should be noted that the parent *tert*-butylcalixarene can be nitrated directly as demonstrated by Lalor et al.[30] (Scheme 1.5). Like the phosphonate calixarene **19**, sulfonated calix[4]arene **22** has also been studied[44] as a crystal growth modifier (refer to section 3.1.1).

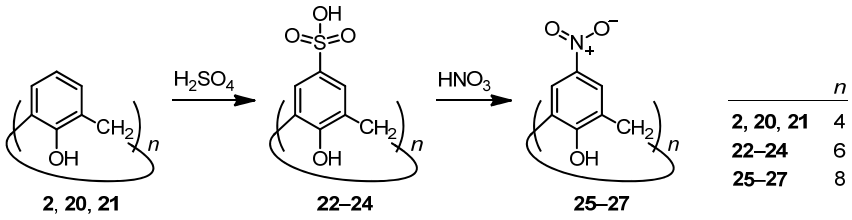

	n
2, 20, 21	4
22–24	6
25–27	8

Scheme 1.9 Direct substitution of calix[*n*]arenes (**2**, **20**, **21**) allows access to calix[*n*]arene-*p*-sulfonates (**22**–**24**) and *p*-nitrocalix[*n*]arenes (**25**–**27**).[46]

A series of amphiphilic calix[4]arenes (Scheme 1.10) were prepared by Rodik et al.[47] as gene delivery vehicles. Chloromethylation of calixarenes **28** or **12a** gave **29a**,**b** in good yields (80%). It should be noted that chloromethyl methy ether is classified as a human carcinogen[48] and is highly flammable and highly volatile.[49] Others[50] have substituted the volatile chloromethyl methyl ether for the less volatile chloromethyl

octyl ether as a safer alternative. Calix[4]arenes **30a**–**c** were then prepared by nucleophilic substitution of **29a**,**b** by tertiary amines or an imidazole with yields for **30b** and **30c** reported as 75% and 93% respectively.

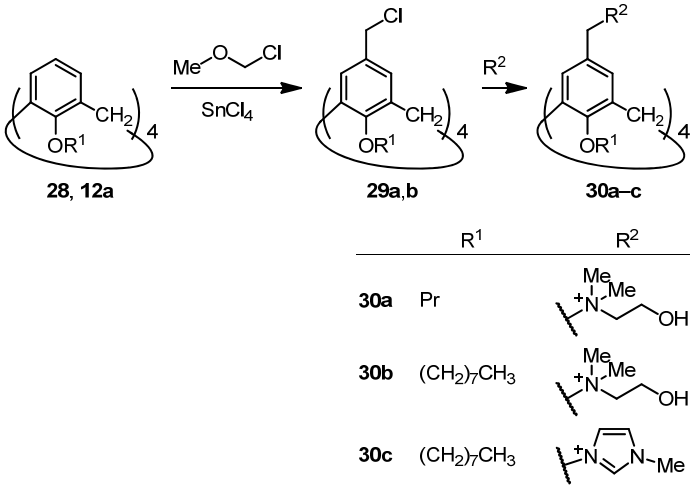

Scheme 1.10 Example of chloromethylation and controlling solubility (thus, c.m.c.) by altering chain length at narrow-rim.[47]

Using a chloromethyl calixarene as a starting point, Bew et al.[51] have successfully attached a variety of amino acids to calix[4]arenes via a 1,2,3-triazole linker (Scheme 1.11). Nucleophilic substitution of the chloromethyl calix[4]arene **29a** by a microwave-assisted reaction gave the azide calix[4]arene **31**. They then used microwave-assisted 'click' chemistry (a copper(I)-catalysed [3 + 2] dipolar cyclo-addition) to prepare the triazole link to give the amino acid substituted calix[4]arenes **32a**–**d** as a single regioisomer in good yields (40–89%). The authors further noted that heat-labile groups, trityl (triphenylmethyl) and Boc (*tert*-butoxycarbonyl) protecting groups, survived the microwave-assisted reactions.

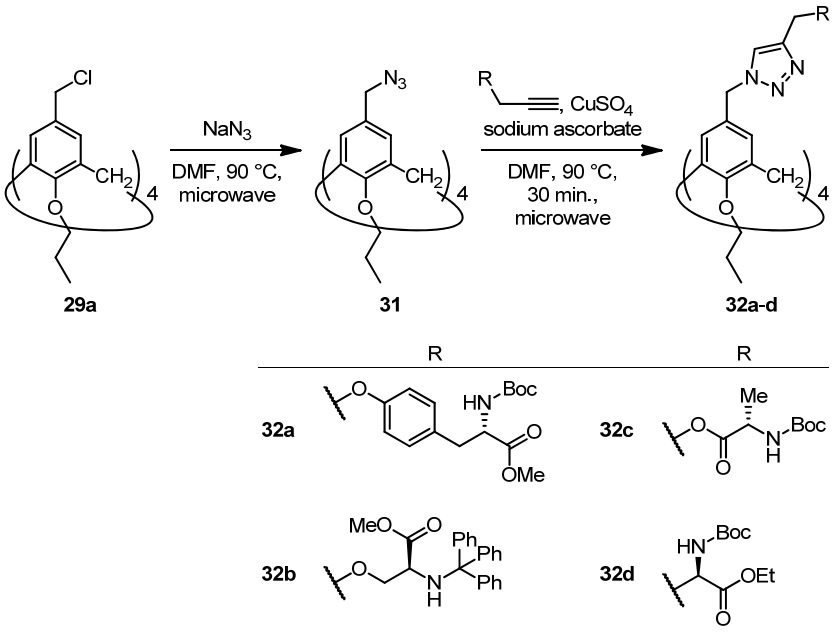

Scheme 1.11 Example of wide-rim click chemistry using microwave-assisted reactions.[51]

An alternative method for preparing *para*-functionalised carboxylic acids (refer to Scheme 1.6 for additional methods) was utilised by Conner et al.[52] The ketone **33** was prepared by Friedel-Crafts acylation of **12a**. Subsequent oxidation with sodium hypobromite gave the amphiphilic calixarene **34**.

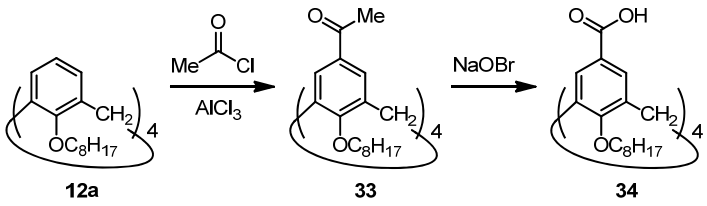

Scheme 1.12 Method of functionalisation of the wide-rim used by Conner et al.[52]

1.1.4.3 **Chemistry at the methylene bridge**

Once the methylene bridge of the calixarene has been substituted with a halide (typically radical bromination),[53, 54] it allows for the replacement of the bromide by nucleophilic substitution (Scheme 1.13). Much of the work on methylene functionalisation of calixarenes has been published by Biali, et al[55, 56] including synthesis from bisphenol[57] and partial substitution[58] at the methylenes. Tetrasubstitution at the methylenes was also investigated by Biali and Columbus.[59, 60]

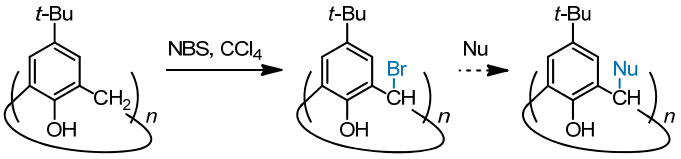

Scheme 1.13 Radical bromination followed by nucleophilic substitution at the methylene bridge.

1.1.5 Selected potential applications of calixarenes

Calixarenes have been investigated for a range of potential applications, many of which exploit their cavities for host-guest chemistry and/or their ability to act as scaffolds for various functionalities. Here, selected potential applications of calixarenes from the literature based on cation and anion receptors, recognition of small molecules and biomolecules, and catalysis will be highlighted.

1.1.5.1 Cation receptors

Many calixarene-based receptors for ions[61–64] have been investigated and have potential in applications in electrochemical sensors,[65, 66] fluorescence-based sensors,[67–70] chemical sensors,[71] and biomedicine.[72] The following section explores a small selection of chemistry based on calixarene-cation interactions, including sensors, solvent extraction, and luminescence.

Chang et al.[73] prepared calix[4]arene **35** and investigated its potential for the chromogenic sensing of cations. The design of this sensor molecule involved the use of the calixarene as a scaffold for distal 1,2,3-triazoles as binding sites at the narrow-rim for cations and distal azoanisole moieties at the wide-rim as chromophores. Calix[4]arene **35** was found to be selective towards Ca^{2+} and Pb^{2+} (from the group 1A and 2A and transition metals surveyed). Upon binding by calix[4]arene **35**, the UV-visible absorption maxima of the cations shift from 365 nm to longer wavelengths by ~175 nm.

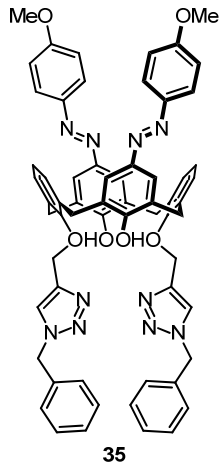

35

Figure 1.9 Chromogenic calix[4]arene **35** investigated by Chang et al.[73] for cation sensing.

Lee et al.[74] showed the potential of calix[4]arene **36** as a Hg^{2+} sensor. Calix[4]arene **36** (Figure 1.10) was appended with pyrene and rhodamine moieties and Hg^{2+}-binding azacrown moiety. Unlike previous work with a bridged calixarene system (also appended with pyrene and rhodamine),[75] the authors exploited the 1,3-alternate conformation of calix[4]arene **36** to orientate the chromophores. Fluorescence was observed for the **36•Hg^{2+}** complex in an acetonitrile solution, however, weak fluorescence was also observed in the presence of Pb^{2+}. The authors attributed this reduction of fluorescence intensity to the coordination of Pb^{2+} to the amides—not competition with the complexed Hg^{2+}.

Calixarenes have also been extensively explored as ionophores for ion-selective electrodes. Calixarene-based ISEs (ion-selective electrodes) have been aimed at the detection of cations including potassium,[76] sodium,[77] silver,[78–80] cadmium,[81, 82] mercury,[83, 84] thallium,[80, 82, 85] and lead.[86, 87] The ability to selectively functionalise and orientate cation-binding moieties (particularly carboxylates) is of importance for such applications.

Calixarenes can be functionalised such that they are good ligands for metal cations.[8] As a result of this, there is strong interest in applying calixarenes to the extraction of toxic metals[88–91] and metals associated with radioactive wastes.[92–96] Calixarene receptors **37a**,**b** were investigated by Ohto et al.[97] for the extraction of alkali metal cations. The authors found that calix[4]arene **37a** selectively extracted sodium ions at low pH (1–3) in single-ion experiments but not lithium or potassium ions. In contrast

calix[6]arene **37b** and analogous acyclic oligomers (monomer and trimer) did not show any ability to extract the ions investigated. Further experiments showed that two sodium ions were extracted simultaneously. Interestingly, competitive extraction experiments showed that potassium ions were also co-extracted with sodium ions at low pH (< 3). The authors proposed that the first sodium ion was an 'allosteric trigger' for the second ion leading to simultaneous uptake of both cations (as opposed to sequential complexation of two individual cations).

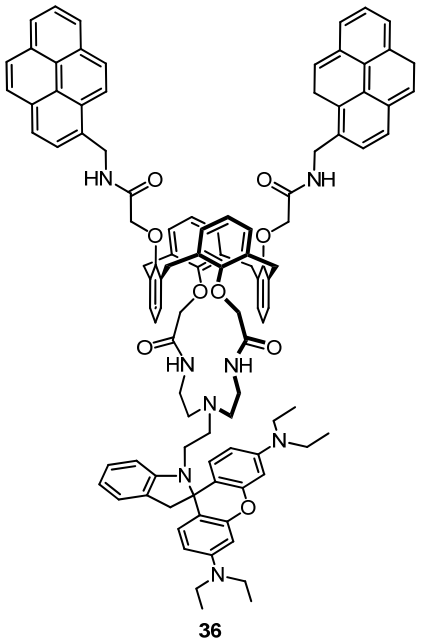

36

Figure 1.10 A 1,3-alternate calix[4]arene-based fluorescence resonance energy transfer sensor (**36**) for Hg^{2+}.[74]

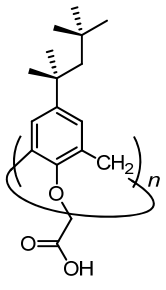

	n
37a	4
37b	6

37a,**b**

Figure 1.11 Calixarenes **37a**,**b** investigated for extraction of alkali metals.[97]

Adhikari et al.[98] prepared a series of methylene cross-linked calixarene resins bearing pyridyl groups for silver extraction from photographic wastes. The authors prepared the resins with variable loadings of calixarene **38**, cross-linked via the position *para* to the phenoxide with *s*-trioxane. The calixarene resins were able to extract Ag^+ efficiently over a pH range of 1–3. The resins were also selective for Ag^+ over Na, K, Fe, and Pb at pH < 3. In addition, >90% of the silver could be stripped from the resins with 3 M HCl, demonstrating potential for silver recovery from contaminated waters and photographic wastes.

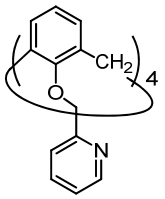

38

Figure 1.12 Calixarene **38** was cross-linked in resins as selective chelates for silver ions.[98]

The complex formed between calixarene **39** and terbium(III) was found to be luminescent.[99] The authors extended this to the preparation of transparent luminescent materials. This was achieved by cross-linking calixarene **40** with poly(methyl methacrylate) (PMMA) followed by uptake of Tb^{3+} into the polymer which was then coordinated by the calixarene ionophore. Solid state characterisation of the luminescent polymers showed similar emission profiles to that of **39**•Tb^{3+} complex in solution. This method overcomes issues with solubility of inorganic compounds during polymer preparation and the polymer itself does not appear to interfere with the luminescent properties of the calixarene-lanthanide complex.

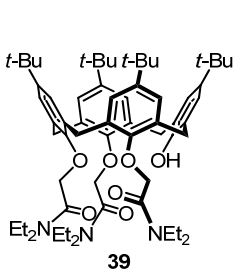

39

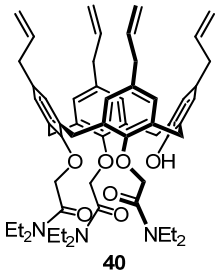

40

Figure 1.13 Tris-functionalised ethyoxyamide calix[4]arenes produces luminescent compounds when chelated with lanthanides (**39**). Cross-linking **40** with PMMA produced luminescent polymers.[99]

1.1.5.2 **Anion receptors**

The application of calixarenes as anion receptors are not as widely reported compared with cation receptors. Troisi et al.[100] investigated a series of aramido-calix[4]arenes (**41a**–**d**) as anion receptors. Results from NMR titration experiments showed that calixarenes **41b**,**c** had selectivity towards planar nitrates and benzoate anions; reduced binding by **41c** was observed due to steric hindrance from the trityl groups. Computational studies suggested favourable hydrogen bonding between the nitrate and N–H of the amides while benzoate showed additional CH–π and π–π interactions with the calixarene host.

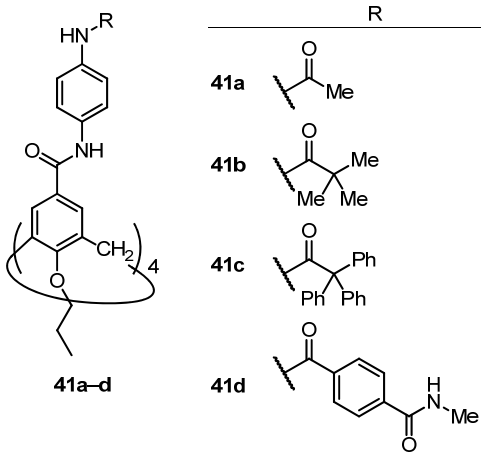

Figure 1.14 Calixarene-based anion receptors **41a**–**d** investigated by Troisi et al.[100]

Casnati et al.[101] reported wide-rim distal fluorinated calix[4]arenes **42a**,**b** and **43** as potential anion receptors. NMR titration experiments with these calixarenes against a variety of anions such as Br^-, CN^-, CH_3COO^-, $PhCOO^-$, $H_2PO_4^-$, and HSO_4^- (as Bu_4N^+ salts) showed a preference for carboxylates and dihydrogen phosphate with little binding towards Br^-, CN^-, and HSO_4^-. Their results also showed that the more mobile calixarenes **42a**,**b** were more efficient than the crown-functionalised **43**. In addition, the racemate **42a** was more efficient than *meso*-**42b**, in particular when binding carboxylates.

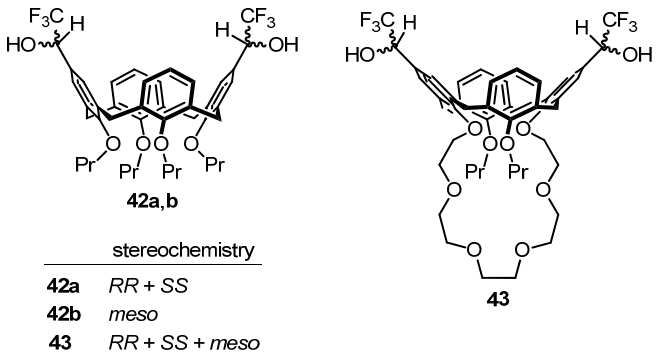

Figure 1.15 2,2,2,-Trifluoroethanol functionalised calix[4]arenes (**42a**,**b** and **43**) as potential anion receptors.[101]

A fluorescent phenylalanine-functionalised calixarene (*C*-linked) was reported by Miao et al.[102] as a selective anion sensor for the fluoride anion. The fluorescence of calixarene **44** (at 521 nm with excitation at 340 nm) was quenched by the addition of fluoride ions. Small increases in fluorescence intensity was observed with AcO^-; other anions such as NO_3^-, Cl^-, Br^-, I^- and HSO_4^- showed minimal quenching of the fluorescence intensity while $H_2PO_4^-$ showed no change in the fluorescence intensity.

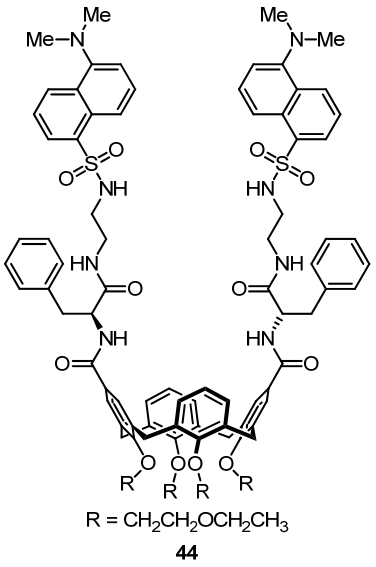

Figure 1.16 Fluorescent phenylalanine-functionalised calix[4]arene (**44**) as an anion receptor.[102]

A rather unusual application based on calixarene-anion interactions, is that of inverse phase transfer catalysis in *C*- and *O*-alkylations.[103] The authors showed that calix[*n*]-arenes **45**–**47** perform better than β-cyclodextrin, tetrabutylammonium bromide, or

hexadecyltributylphosphonium bromide in model reactions with higher yields of unsymmetrical ether products (in the case of *O*-alkylations). The authors proposed that at the interface between the organic and aqueous phases, the water-soluble calix[*n*]arenes formed host-guest complexes with either the carbanion (for *C*-alkylations) or alkoxides (for *O*-alkylations) after deprotonation by aqueous sodium hydroxide. This then allows for nucleophilic substitution of the alkyl halide at the interface. As a consequence, calixarenes with a larger cavity are more active (i.e. gives higher yield of the desired product) as they are better able to accommodate larger substrates.

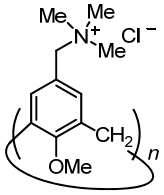

45–47

	n
45	4
46	6
47	8

Figure 1.17 Calix[*n*]arenes **45–47**, where *n* = 4, 6, 8 respectively, applied to as an inverse phase transfer catalysis for alkylation reactions.[103]

1.1.5.3 Small and neutral molecule-based applications

Early work by Bauer and Gutsche[104] showed that alkylamines could associate with calixarenes by forming an inclusion complex [assisted by protonation of the amine by the most acidic phenol of the calixarene leading to an ion pair (the phenolic protons on calixarenes have different pK_a values[105])]. McKervey et al.[106] later reported the inclusion of acetonitrile into the cavity of calixarene **3b** (functionalised with ethoxycarbonyl at the narrow-rim). Calixarene-based receptors for small molecules such as amino acids[61, 107–109] are known. Other groups have also utilised the host-guest chemistry and scaffold provided by calixarenes for other small molecules.

Work by Arena et al.[110] investigated water-soluble calix[4]arenes, **48a–d** and **22** (Figure 1.18), as hosts for small molecules such as alcohols, ketones, and nitriles. The charged wide-rim (due to the presence of sulfonate groups) and the conformation of the calixarenes (and by extension the cavity space) were found to be important to the inclusion of small molecules. Calixarene **48a** adopted a conformation with a

reduced cavity and did not allow inclusion of any small molecules, consistent with the authors' previous work.[109] Similarly, calixarene **48b**, in a 'pinched cone' conformation, had reduced access for small guests to the cavity (although host-guest activity was observed). Calixarene **48c** only included acetonitrile in water (without the assistance of the charged sulfonate groups). Calixarenes **48d** and **22** were capable of binding all the guests studied. The authors proposed that the guests were oriented such that its non-polar hydrocarbon portion was situated within the calixarene cavity while its polar portion was aligned towards the charged sulfonate groups.

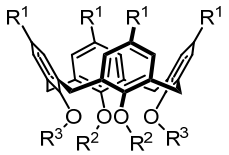

48a–d, 22

	R^1	R^2	R^3
48a	SO_3H	CH_2CH_2OEt	CH_2CH_2OEt
48b	SO_3H	H	CH_2CH_2OEt
48c	H	CH_2COOH	CH_2COOH
48d	SO_3H	CH_2COOH	CH_2COOH
22	SO_3H	H	H

Figure 1.18 Water-soluble calix[4]arenes as hosts for small neutral organic molecules.[110]

Baldini et al.[111] investigated a series of calixarenes, **49**–**51** (Figure 1.19), for the capture of carbon dioxide. The principle idea here is the reaction between carbon dioxide and alkylamines to form alkylammonium and alkylcarbamate groups. As such, the narrow-rim tetrasubstituted calixarenes (**49a**–**c**) were found to accommodate two molecules of carbon dioxide while disubstituted calixarene **50** could bind a single carbon dioxide molecule. Calix[4]arene **51** was proposed to form adducts with CO_2, however this adduct was labile. Further work showed calix[4]arene **50** could have potential as a sensor for quartz crystal microbalance devices due primarily to its fast response to the presence of CO_2.

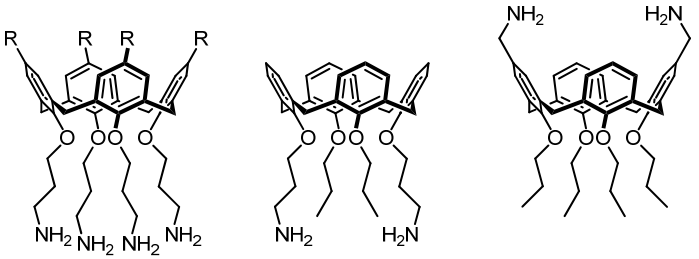

49a–c **50** **51**

	R
49a	H
49b	*t*-Bu
49c	$(CH_2)_5CH_3$

Figure 1.19 Calixarenes **49**–**51** were investigated as potential CO_2 traps.[111]

Bandela et al.[112] prepared a lower-rim dinaphthalimide calix[4]arene, **52**, for recognition of polycyclic aromatic hydrocarbons. The authors proposed that recognition occurs by π···π interactions between the naphthalimide groups from two different calixarene units and aromatic molecules which results in quenching of the fluorescence from the calixarene at 378 nm. Strong quenching was observed for polycyclic aromatic compounds (such as naphthalene- and anthracene-based compounds) while compounds with a single aromatic ring (i.e. phenyl-based compounds) showed minimal quenching. Quenching was further enhanced by electron-withdrawing or polar functional groups (such as hydroxyl groups).

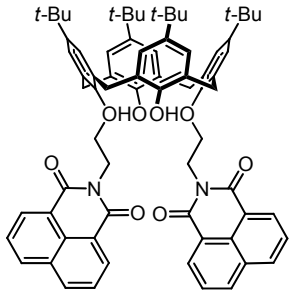

52

Figure 1.20 Distal, lower-rim–functionalised dinaphthalimide calix[4]arene for the recognition of polycyclic hydrocarbons.[112]

1.1.5.4 'Larger' molecule-based (biochemical) applications

Many calixarene-based compounds have been designed with biomedical applications in mind.[113–116] One of the main features of calixarenes is the ability to spatially direct functional groups or other small molecules such that desired interactions with

biological materials of interest (e.g. proteins, cell surfaces) are achieved. Some examples include polyanionic calix[4]arenes[117] for anti-HIV activity; guanidinium-functionalised calixarenes[118, 119] for antibacterial activity; and calixarene-based glycoclusters for trypanocidal activity.[120] Selected examples of calixarenes for biomedical applications are examined in the following section.

Sansone et al. have investigated guanidinium-functionalised calixarenes as potential cell transfection agents.[121–124] Initial work[121] with wide-rim guanine-functionalised and narrow-rim alkylated calixarenes showed that they could interact with DNA. A follow-up[122] study with a wider array of wide-rim guaninine-functionalised calix-arenes, including **53a**–**c**, revealed that three factors impacted on the type of interactions with DNA: calix[4]arenes in the cone conformer interacted by electro-static interactions; conformationally mobile calix[6]arene and calix[8]arene formed aggregates with DNA filaments; and calixarenes in the 1,3-alternate conformation condensed DNA by charge-charge interactions. Bagnacani[123] later prepared narrow-rim substituted guanidinium calixarenes. They showed that calixarenes **54a**–**c** could be efficient cell transfection agents with reduced cytotoxicity compared to the wide-rim derivatives.[122]

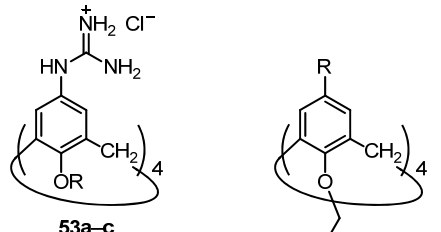

Figure 1.21 Guanidinium-functionalised calix[4]arenes investigated by Ungaro et al.[122, 123] Here, **53a** is conformationally mobile, **53b** is in the 1,3-alternate conformation, and **53c** and **54a-c** are in the cone conformation.

Along similar lines, Lalor et al.[30] investigated ammonium-functionalised dendritic calixarenes (Figure 1.22) as potential gene transfection agents. The authors found that all the 'multicalixarenes' (**55a**,**b** and **56a**) bound to DNA (by neutralising the negative charges on the DNA) and were not cytotoxic to the human cells studied. Interestingly, the control calixarene (**57a**) was found to be cytotoxic to the human cells. The glycine moiety improved DNA binding of both **55b** and **57b**. However, effective gene transfection was only observed with calix[4]arene **55b** and not the other multicalixarenes.

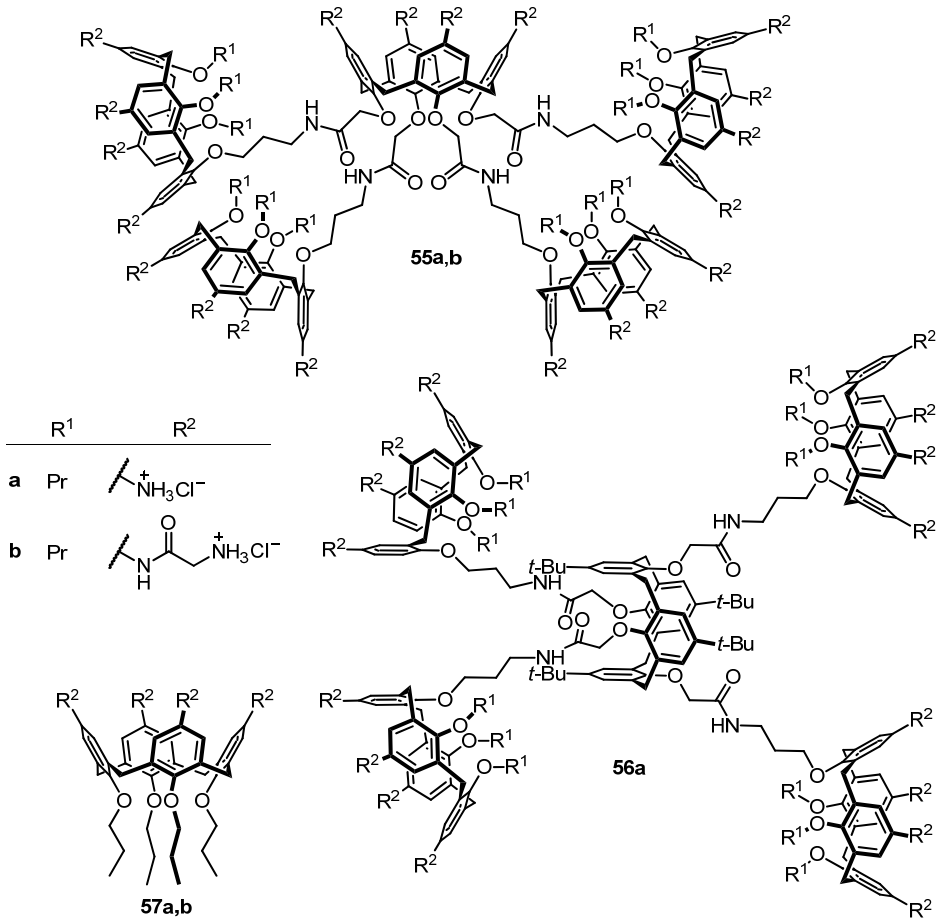

Figure 1.22 'Multicalixarenes' investigated by Lalor et al.[30] for cell transfection.

Tsuo et al.[125] functionalised calixarenes **58a**–**g** (Figure 1.23) with amino acids and tested them against HIV and the hepatitis C virus. They determined the impact of the shape and functionality on HIV, hepatitis C virus and cytotoxicity.

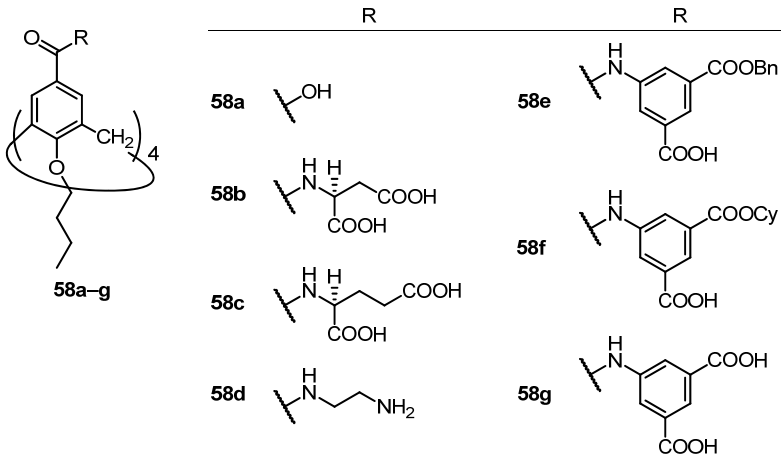

Figure 1.23 Amino acid functionalised calix[4]arenes investigated by Tsuo et al.[125] for activity against HIV and hepatitis C virus.

Carbohydrate-functionalised calix[4]arenes have been applied by Křenek et al.[126] as stimulants of natural killer cells to illicit response to tumour cells. The calixarenes **59a**,**b** (Figure 1.24) performed better than the monomeric sugar and were comparable to the dendritic octaglycan studied previously by the authors.[127] The tetrasubstituted calix[4]arene **59a** performed better than the 1,3-alternate conformer **59b** and the bis-substituted **59c**. Thus, the multivalency of carbohydrates is important for binding to the natural killer cells (as demonstrated by **59a** in the cone conformer).

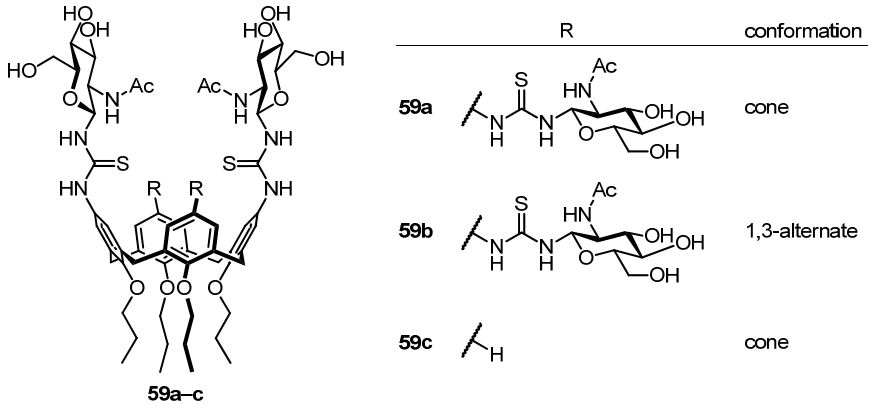

Figure 1.24 Glucopyranose-functionalised calix[4]arenes as stimulators for anti-tumour response.[126]

Lalor et al.[128] appended a fluorescent probe to a calixarene (Figure 1.25) with the aim of applying it in cell imaging. Calix[4]arene **60** was made water-soluble with ammonium groups and the fluorescent probe, 4-chloro-7-nitrobenzofurazan, attached at the narrow-rim. The authors found that calix[4]arene **60** was taken up into the

cytoplasm in Chinese Hamster Ovary cells and **60** exhibited low levels of cytotoxicity.

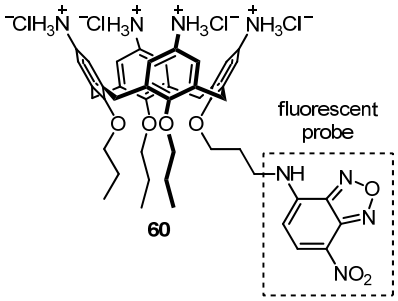

Figure 1.25 Application of calix[4]arene, functionalised with a fluorescent probe, to cell imaging.[128]

Guo et al.[129] investigated a series of sulfonate-functionalised calixarenes (**61**–**63**, Figure 1.26) as potential biosensors. Taking into account the commercialisation potential of their sensors, the authors chose to utilise commercially available **61** and fluorescent dye lucigenin for further biosensing studies. The authors employed a tandem assay (Figure 1.27) using a neurotransmitter, acetylcholine. If a strong competitor such as acetylcholine is introduced, the dye will be displaced from the **61** leading to a fluorescent response. However, a fluorescent response was not exhibited until choline is converted to the weaker binding betaine. The authors proposed that such a molecule could be applied to monitoring acetylcholinesterase (an enzyme involved in Alzheimer's dementia) during treatment for Alzheimer's dementia.

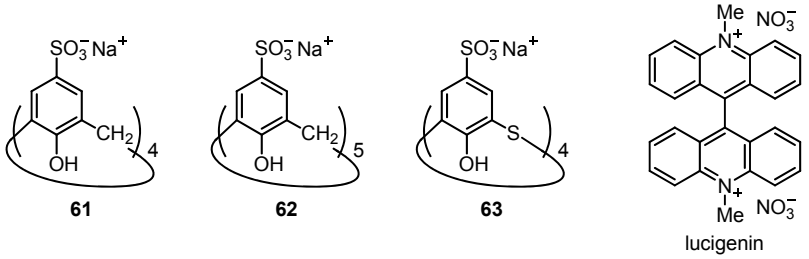

Figure 1.26 A series of calixarenes investigated by Guo et al.[129] as potential sensors with fluorescence probe, lucigenin.

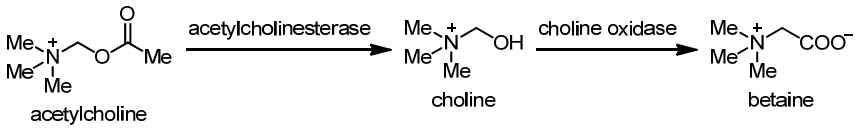

Figure 1.27 A series of enzyme-mediated reactions; the acetylcholine hydrolysis of acetylcholine to choline followed by oxidation to betaine.[129]

Much of the work on cation and amino acid sensing using calixarenes has been by Rao, et al.[130, 131] In one of their works,[131] the authors reported amino acid recognition events by a highly fluorescent calixarene complex (**64•Zn^{2+}**, Figure 1.28). The complex **64•Zn^{2+}** was found to respond to natural amino acids (e.g. aspartic acid), amino acids of peptides (e.g. glutathione), and proteins rich in α-helices or β-sheet. The authors proposed that on recognition by the complex **64•Zn^{2+}**, Zn^{2+} is released and chelated by the recognised amino acid, therefore quenching the fluorescence. The calixarene **64** itself was reported earlier[132] and found to be selective for Zn^{2+}.

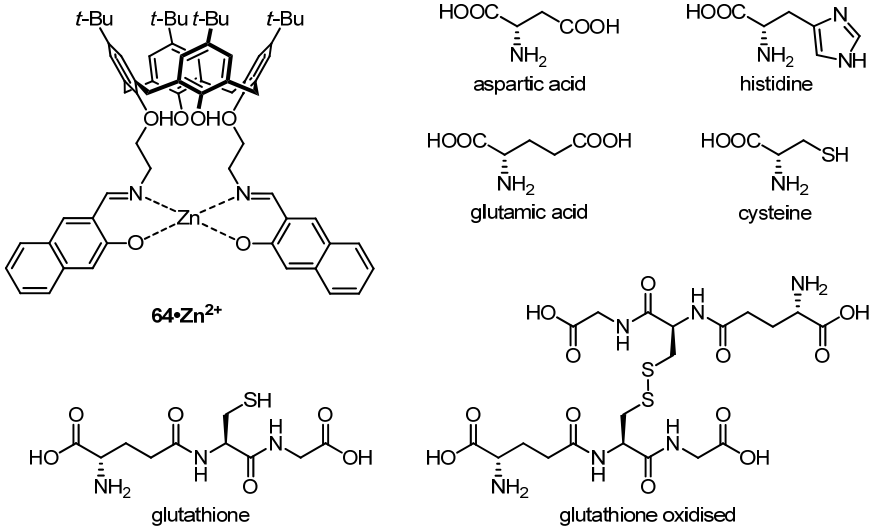

Figure 1.28 A calix[4]arene•Zn^{2+} complex investigated as an amino acid sensor by Chinta et al.[131]

1.1.5.5 **Calixarenes and catalysis**

Calixarenes have been investigated as catalysts for synthesis (in particular metal-based catalysis[133]). The appeal of calixarenes in catalysis is largely due to the scaffold it provides for the pre-organisation of molecular fragments central to catalysis. Furthermore, the cavities of the calixarenes can also assist in catalysis reactions. The following section examines some calixarene-based catalysts from the literature.

Proline is a well-known organocatalyst, particularly for aldol and Mannich reactions.[134–137] Li et al.[138] investigated prolinamide calix[4]arenes **65a**–**e** and **66a**–**e** (Figure 1.29) as potential organocatalysts for direct asymmetric aldol reactions. Tests on a model aldol reaction between an aromatic aldehyde and ketone (Scheme 1.14) under solventless conditions gave a range of results. The authors determined that calix[4]arene **65b** gave the best results and the additional hydroxy group on calix[4]-arenes **66a**–**e** did not appear to improve catalytic activity. The calixarene scaffold was demonstrated to be important as the monomeric analogue of calix[4]arene **65b** gave reduced diastereoselectivity and enantioselectivity in the model aldol reaction.

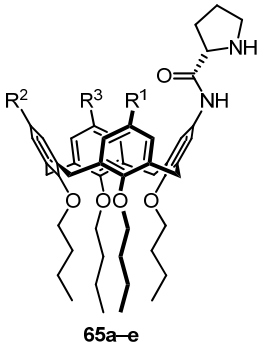

65a–e

	R^1	R^2	R^3
65a	H	H	H
65b	Pro-NHR	H	H
65c	H	Pro-NHR	H
65d	Pro-NHR	Pro-NHR	H
65e	Pro-NHR	Pro-NHR	Pro-NHR

Pro-NHR =

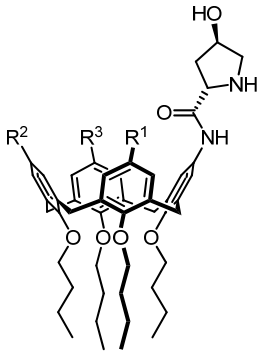

66a–e

	R^1	R^2	R^3
66a	H	H	H
66b	4-OH-Pro-NHR	H	H
66c	H	4-OH-Pro-NHR	H
66d	4-OH-Pro-NHR	4-OH-Pro-NHR	H
66e	4-OH-Pro-NHR	4-OH-Pro-NHR	4-OH-Pro-NHR

4-OH-Pro-NHR =

Figure 1.29 Prolinamide calix[4]arenes **65** and **66** investigated by Li et al.[138] for aldol catalysis.

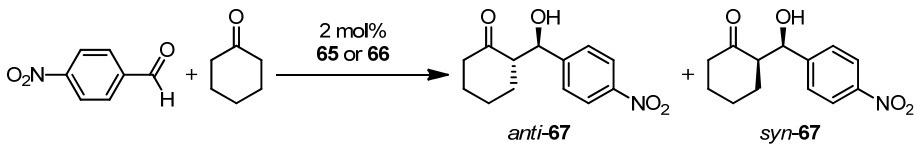

anti-**67** *syn*-**67**

Scheme 1.14 Model aldol reaction for screen prolinamide calixarene catalysts **65** and **66**.[138]

Carbon-carbon bond forming reactions are important in organic synthesis, thus calixarene-based *N*-heterocyclic carbenes palladium complexes (Figure 1.30) have been investigated as catalysts for Suzuki-Miyaura cross coupling reactions.[139–141] For example, Fahlbusch et al.[141] prepared distal-functionalised imidazolium calixarenes (**71**) as palladium complexes [amongst other complexes with silver(I), mercury(II), platinum(II), iridium(I), ruthenium(II)]. The authors found that both *cis*-**71** and *trans*-**71** gave similar yields on a model Suzuki-Miyaura reaction, suggesting that one of the imidazole units dissociated from the palladium during the catalytic cycle. Further experiments showed that there was no *cis*-to-*trans* isomerisation.

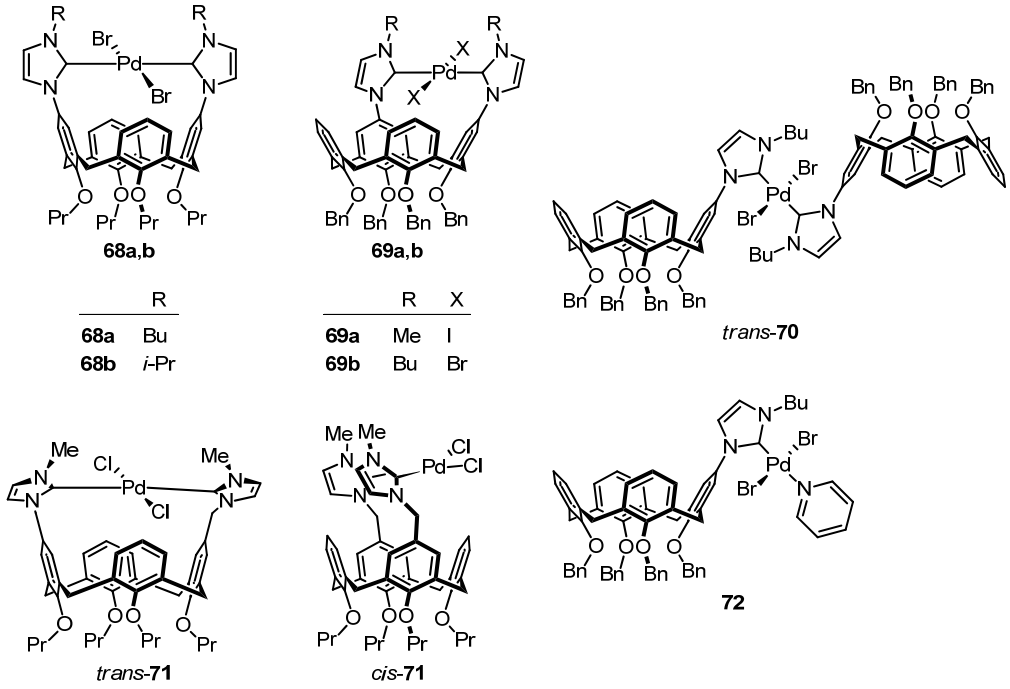

Figure 1.30 Examples of calixarene-based *N*-heterocyclic carbene palladium catalysts (**68**–**72**) for Suzuki-Miyaura cross-coupling.[139–141]

Monnereau et al.[142, 143] looked at the Suzuki-Miyaura reaction from another perspective and investigated phosphorane-functionalised calixarenes (Figure 1.31). In recent work, Monnereau et al.[142] utilised bis(iminophosphorane)-functionalised calixarenes (**74a**–**e**) in Suzuki-Miyaura cross-coupling of aryl bromides and chlorides with phenylboronic acid. The authors found that calixarenes **74a**–**e** generally performed well, with catalytic activity detected as low as 0.001 mol% Pd loading.

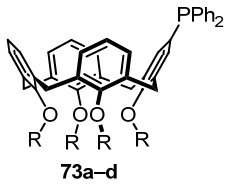

73a–d

	R
73a	$CH_2(CH_2)_4CH_3$
73b	Bn
73c	$CH_2(4\text{-}MeOC_6H_4)$
73d	$CH_2(3\text{-}MeOC_6H_4)$

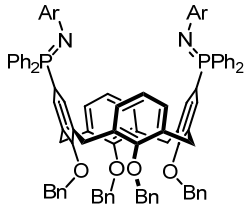

74a–e

	Ar
74a	Mes
74b	$2,4\text{-}i\text{-}Pr_2C_6H_3$
74c	$4\text{-}BuC_6H_4$
74d	$2\text{-}MeOC_6H_4$
74e	$4\text{-}MeOC_6H_4$

Figure 1.31 Examples of calixarene-based monophosphoranes[143] (**73a**–**d**) and bis(iminophosphoranes)[142] (**74a**–**e**) palladium catalysts (generated in situ) for Suzuki Miyaura cross-coupling.

1.2 Crystallisation

Crystallisation is a fascinating phenomenon in Nature and is of great importance to many industrial processes. It is of no surprise that crystallisation is a highly active area of research for both natural and artificial systems. Additives are one of the many methods used by industry to control crystallisation of desired inorganic products[144, 145] and inhibit unwanted scale formation.[146] However, Nature has had a much longer time to adapt biomineralisation processes to changing functions of various biominerals and can control biomineral formation with much greater finesse.[147, 148] Studying how Nature produces such intricate biominerals may provide strategies in preparing new and improved materials.[149–152]

1.2.1 Concise overview of biomineralisation

Biomineralization covers a wide range of topics of which a small selection will be discussed here. Other topics such as the mineral form, formation mechanism, etc are discussed elsewhere.[150, 153–158] Biominerals can be formed by 'biologically induced mineralisation' or 'biologically controlled mineralisation'.[159, 160] Biologically induced mineralisation is where the organism interacts with the environment within which the crystal is forming but has little control over crystallisation of the mineral. Biologically controlled mineralisation[148] (the idea most commonly associated with

biomineralisation) involves direct control of crystallisation by the organism. Here, the organism controls the location of nucleation, size and shape, orientation, morphology, and composition of the crystal.

There is a vast amount of literature describing a variety of biomineral systems, however a complete biomineralisation mechanism is elusive. Many biomineral systems have been studied, including: avian egg shells,[161–163] mollusc shells,[164–170] coccoliths,[171, 172] crustaceans,[173, 174] shells of cephalopods,[175] skeletal tissues in sponges,[176] shells of gastropods,[177] fish otoliths,[178, 179] bone,[180] and lenses of brittlestars (echinoderms).[181] It is remarkable that a small amount of organic material (comprising proteins and polysaccharides) can have such a large influence over the mineral formation and properties. For example, mollusc shells have ~5% organic content[182, 183] which exerts control over the crystallisation of calcium carbonate[182, 184] and gives nacre its unusual mechanical properties[185]. It has also been noted that crystallisation can be influenced by both inorganic ions and organic molecules.[145, 186] One of the emerging themes in biomineralisation is that the proteins and organic matrices involved in the formation of biominerals, particularly those associated with calcium carbonate minerals, are above of average acidity.

A study by Marin et al.[187] of mollusc shells led to the distinction of acidic proteins between 'moderately acidic' (pI 4.5–7) and 'extremely acidic' (pI <4.5). The acidity of proteins primarily arises from the larger proportion of acidic amino acids (mainly aspartic acid and glutamic acid) and to a lesser extent phosphorylated (serine, threonine, tyrosine) or sulfated (tyrosine) amino acid residues.[188] Marin and Luquet[188] further noted that even proteins with pI ~7 may have acidic domains which are offset by basic domains. Acidic proteins (and other macromolecules) have been reported to control nucleation and crystal growth;[189, 190] select polymorphs[191] (such as aragonite in the nacre layer and calcite in the prismatic layer of mollusc shells)[167, 192–194] shape crystals;[175, 195] and reinforce crystals (i.e. occluded within the crystal).[177]

Many of the acidic proteins associated with calcium carbonate biominerals have enriched aspartic acid and glutamic acid residues. Interestingly, some biomineral systems appeared to have a preference for aspartic acid over other acidic amino acids.[168, 196, 197] Much of the work with mollusc shells have identified proteins (or

peptide fragments) associated with the prismatic (calcite) layer[198, 199] or the nacre (aragonite) layer.[189, 191, 200-202] A group of aspartic acid-rich proteins, 'Asprich', in the prismatic layer of the shell of the mollusc *Atrina rigida* were studied by Gotliv et al.[168] They noted that proteins in the prismatic layer consisted of 53 mol% aspartic acid and 11 mol% glutamic acid. In contrast, earlier studies by Gotliv et al.[169] showed that proteins in the nacre layer contained 45 mol% acidic residues (as Asx and Glx). Gotliv et al.[168] proposed that the Asprich proteins, containing amino acid sequences bearing similarities to calcium-binding proteins,[203] may take part in Ca^{2+} transportation and creating localised supersaturation of calcium carbonate. Therefore, much of the crystallisation literature concerns the impact of acidic amino acids (or analogous compounds) on the crystallisation of inorganic minerals.

1.2.2 Model mineral systems of interest

1.2.2.1 Calcium carbonate

Calcium carbonate is a well studied mineral.[204] It has six known mineral phases: amorphous calcium carbonate (ACC), calcium carbonate hexahydrate (ikaite), calcium carbonate monohydrate (monohydrocalcite), calcite, vaterite, and aragonite.[205, 206] Calcite is the thermodynamically stable polymorph (at room temperature and atmospheric pressure). In the absence of additives, rhombohedral calcite forms from amorphous calcium carbonate via vaterite.[207]

Calcium carbonate is the most commonly encountered of the biominerals[208] and it is notable as a common component of industrial scale.[146] It can be found in biominerals as calcite (e.g. molluscs,[164–170] coccolithophores,[171, 172, 209, 210] foraminifera,[211] avian egg shells,[161–163] fish[212]), magnesian calcite (e.g. echinoderms[213]), aragonite (e.g. molluscs,[164–170] cephalopods[175]), vaterite (e.g. ascidians[214]), and amorphous calcium carbonate (e.g. coccoliths[213]). It is not surprising then that calcium carbonate biominerals (particularly aragonite and calcite) are also associated with much of the marine fossil record.[215] Calcium carbonate also presents a notable problem as industrial scale[146] in areas such as industrial water treatment,[216] oil fields,[217] and heat exchangers.[218] The majority of calcium carbonate-based scale is calcite, the thermodynamically stable polymorph.[219] Calcium carbonate is thus an important

mineral in Nature and industry, and hence it is a widely studied mineral both experimentally and by computational modelling.

1.2.2.2 **Barium sulfate**

Barium sulfate is another well studied mineral. Unlike calcium carbonate, it has a single known phase. It occurs as a biomineral and is found in some algae and Xenophyophore (as a gravity sensor).[220, 221] Barium sulfate also occurs as scale[222] and has spurred interest into potential crystallisation inhibitors.[223–226]

1.2.3 Additives to control crystallisation

The crystallisation of minerals can be influenced by various additives (or impurities), both inorganic and organic in nature. Inorganic ions are known to impact the crystallisation of minerals, such as calcium carbonate[227–230] and barium sulfate,[145, 231–234] however, they will not be considered further in this thesis. There is no shortage of literature on the impact of organic additives on the crystallisation of inorganic minerals.[144, 145, 159] Many types of additives have been investigated including synthetic peptides,[235, 236] peptide fragments from proteins,[191] and block copolymers.[237–240] Smaller molecules, such as amino acids,[241, 242] benzoic acids,[243] tetrazoles[244] (often used as carboxylic acid analogues in medicinal chemistry[245]), and alcohols,[246] are often used as models for larger complex macromolecules, but are also of interest as readily accessible scale inhibitors. Macrocyclic-based additives, such as calixarenes, are discussed in section 3.1.

The impact of acidic residues, such as aspartic and glutamic acids, and other organic acids have been studied. Dalas et al. found that aspartic acid[247] and glutamic acid[248] could initiate the formation of critical nuclei of Ca^{2+} and CO_3^{2-} and stabilise vaterite. Later work by Wu et al.[249] with a selection of amino acids (e.g. aspartic acid, glutamic acid) and organic acids (e.g. succinic acid, acetic acid, glutaric acid) showed the impact of these additives on etch pit morphology (during the dissolution of calcite). Their results suggested that the geometry of the additives was important, in particular the distance between calcite surface binding groups (ammonium and carboxylic acid). Some researchers have also considered the impact of inorganic additives in addition to organic additives in the same system. Meldrum and Hyde[250]

investigated Mg^{2+} incorporation into calcium carbonate in the presence of organic additives (Figure 1.32), D/L-malic acid (**75**) and sodium citrate (**76**). At high Mg^{2+} concentrations (Ca/Mg ratio ≤ 0.26 in solution), aragonite was observed along with calcite (in the presence and absence of the organic additives). The presence of both Mg and organic additives gave calcite with a variety of shapes including dumbbells, spherical particles and polycrystalline aggregates. Interestingly, the authors found that the organic additives alone were able to retard nucleation and growth, however malic acid appeared to elongate the calcite rhomb while citric acid at high concentrations gave triangular prism clusters of calcite rhombs.

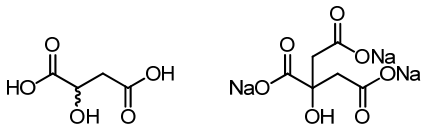

Figure 1.32 Organic additives, D/L-malic acid (**75**) and sodium citrate (**76**), investigated by Meldrum and Hyde.[250]

Many researchers have used artificial polymers to mimic natural biomacromolecules. Chen et al.[251] investigated the impact of a double-hydrophilic block copolymer on the crystallisation of calcium carbonate. They observed stacked pancake-like calcite structures which resembled the layered structure of aragonite tablets in nacre of red abalone. In another study, Song et al.[252] found that a commercial co-polyelectrolyte gave platonic calcite mesocrystals. Based on the unusual acidity exhibited by many proteins in biomineralisation systems, Sonnenberg et al.[238] utilised a diblock copolymer comprising poly(ethylene oxide) and poly(L-glutamic acid) to study the interaction between polymers and calcite by AFM. The authors found that the interaction forces varied with changes in pH and concentration of Ca^{2+}. Furthermore, the authors proposed that polypeptide-mineral interactions involved adsorption of the polypeptide on the mineral surface, transient desorption of the polypeptide, and rearrangement of the polymer.

Polymeric molecules have been used to investigate the impact of molecular weight of the additive on crystallisation. The higher molecular weight of a polymeric additive will have a lower diffusion coefficient compare to smaller molecules. However, macromolecular additives will generally have more functional groups which can

interact with the growing crystal surface. Aschauer et al.[253] found that poly(aspartic acid), poly-Asp, had a great impact on calcite crystal growth (particle size and morphology) than poly(acrylic acid), PAA, and both polymers had a much greater effect than succinic and glutaric acids. This was complemented with molecular dynamic simulations of PAA and poly-Asp on the surface of calcite.[254] The simulations suggested that the rigid backbone of PAA and the formation of stable complexes with Ca^{2+} reduced its availability for adsorption to the crystal surface. In contrast, poly-Asp was found to approach the surface in an upright manner, creating steric hindrance, and the nitrogen of the amide increased the strength of the attraction to the crystal surface.

Biomolecules, like proteins and macromolecules from biomineralization systems, can have an impact on the nucleation and growth, size and shape, orientation, morphology, and composition of inorganic crystals. These biomolecules typically affect several of these parameters during crystallisation and these parameters are often difficult to investigate independent of one another. Despite this, small molecule additives are often used as models for proteins and macromolecules[255] and typically to study an aspect of interest (for example, the impact of acidic amino acids on mineral morphology).

1.2.4 Templated crystallisation

Biominerals, composites of inorganic minerals and biological macromolecules, have a variety of forms, functions, and properties. Despite some of the elaborate structures (e.g. coccoliths[256]) and enhanced properties (e.g. nacre[183, 185]) engineered by organisms, biominerals are largely produced at room temperature.[206] Therefore, it is desirable to be able to prepare materials with similar properties using similar strategies. One such strategy is using organic molecules to 'template' crystallisation of minerals.[149, 206, 257, 258] By drawing inspiration from Nature, inorganic materials can be synthesised reproducibly with the desired orientation, size, shape, and polymorph.[259] Furthermore, by studying the interactions between the template, the inorganic mineral, and their environment, insight may be gained into the processes which occur in biomineralisation (especially 'organism-mediated' processes).

Templated crystallisation involves heterogeneous nucleation,[260] typically by organic molecules or an organic framework. The incorporation of macromolecules into the crystal may give a composite material with new properties superior to those of the mineral alone. Various 'templates' have been investigated, some of which are derived from biomineralization systems while others are non-natural and attempt to mimic the chemistry in biomineralisation systems (i.e. 'designer' molecules[206]). Examples of templates from the literature will be examined here.

Organic templates can be sourced from biomineralisation systems. Meldrum et al.[261] used apoferritin (ferritin with the ferric hydroxide core removed) to crystallise nanoparticulate iron sulfide, manganese oxide, and uranyl oxyhydroxides. In this case, the apoferritin protein shell was used as a confined space to direct the growth of the crystal and limit particle size. On a slightly larger scale, many researchers have demineralised the biomineral and remineralised the residual organic scaffold in an artificial system. Watabe et al.[262] removed calcium carbonate mineral from spicules of gorgorian *Leptogorgia virgulata* using ethylenediaminetetraacetic acid (EDTA) then remineralised the organic matrix in artificial sea water. The remineralised organic frameworks showed hollow tubular structures comprised of calcite. The authors suggested that either the aspartic acid residues or glycoproteins in the organic framework provided nucleation sites for calcium carbonate to form. This does not agree with observations by Keene et al.[202] where the absence of 'soluble' proteins from a mollusc gave rhombohedral calcite on a chitin framework. Heinemann, et al.[184] demineralised abalone nacre with EDTA to leave organic matrix comprising β-chitin, silk-fibroin-like protein, and aspartic acid-rich proteins. Crystallisation of calcium carbonate using the EDTA-insoluble material gave aragonite plates along the surface of the EDTA-insoluble matrix, as in natural nacre.[191] In contrast, crystallisation using cellulose and chitosan gave calcite and vaterite. In some cases, the authors were also able to obtain a composite material comprising the EDTA-insoluble matrix with layers of aragonite plates, similar to natural nacre.[191]

Non-natural templates generally consist of self-assembled monolayers[258, 263, 264] or gel materials.[149, 206, 259] Popescu et al.[265] have used self-organising surfactants (Figure 1.33) to investigate 'structural adaptation' of templates. Spacing between molecules in the self-assembled monolayer was controlled by surface pressure and

limited by the head group size (i.e. glycine, alanine, valine, and leucine). The glycine (**77a**) and alanine (**77b**) derived surfactants formed relatively rigid monolayers and gave mainly calcite rhombs. The valine (**77c**) and leucine (**77d**) derived surfactants formed more flexible monolayers and appear to adapt to the presence of Ca^{2+} ions. Both surfactants resulted in calcite crystals with modified habits. Furthermore, surfactant **77d** also gave a significant amount of aragonite and the authors observed that smaller calcite crystals, attributed to the nucleation of calcite at a later stage, compared with the aragonite. However, unlike calix[4]arene-based monolayers,[266] the charge densities of the surfactant monolayers do not appear to direct the orientation of the calcium carbonate crystals. Alternatively, gels have also been used as templates for crystallisation (refer to section 5.1 for more information).

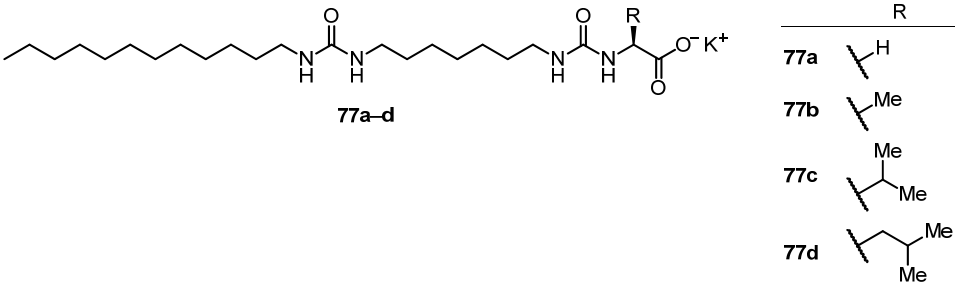

Figure 1.33 A series of bis-urea amino acid functionalised surfactants investigated by Popescu et al.[265] as self-assembled monolayers for templated crystallisation of calcium carbonate.

1.3 Small molecule gelators

1.3.1 Introduction to molecular gels

'The colloidal condition, the 'gel', is one which it is easier to recognise than to define …'[267] Although gel materials are difficult to define, Smith[268] defines a gel as 'a colloidal form of mater in which a "solid-like" network is suspended within a "liquid-like" continuous phase.' The idea that gels comprise two components (a 'solid' and 'liquid') is a central theme among many of the different definitions of a gel.[269–272] Gels are colloids but not all colloids are gels.[273]

Gels can be classified by their 'solid-like' component or their 'liquid-like' phase (Figure 1.34).[274] In chemical gels, the solid network is bound by covalent bonds

cross-linking the network (e.g. polymers). This results in robust gels but the solid network cannot break down into its constituent monomers. Physical gels in contrast, typically comprise self-assembled small molecules (in the case of supramolecular gels) linked together by non-covalent bonds (e.g. hydrogen bonds, π-π stacking, hydrophobic effect[275]). As a result of non-covalent bonding, physical gels can transform back into a free-flowing liquid. Gels can also be classified by their continuous phase. Traditionally, the liquid continuous phases considered were water and organic solvents, which gave hydrogels and organogels respectively. Some gelators are capable of gelling both water and organic phases separately.[276–278] More recently gels comprising ionic liquids ('ionogels') have been reported.[279, 280] Gels with a continuous phase comprising a gaseous phase was also possible if the organic solvent or supercritical fluid was removed, giving xerogels and aerogels[281] respectively. Of particular interest here, are low molecular weight hydrogels.

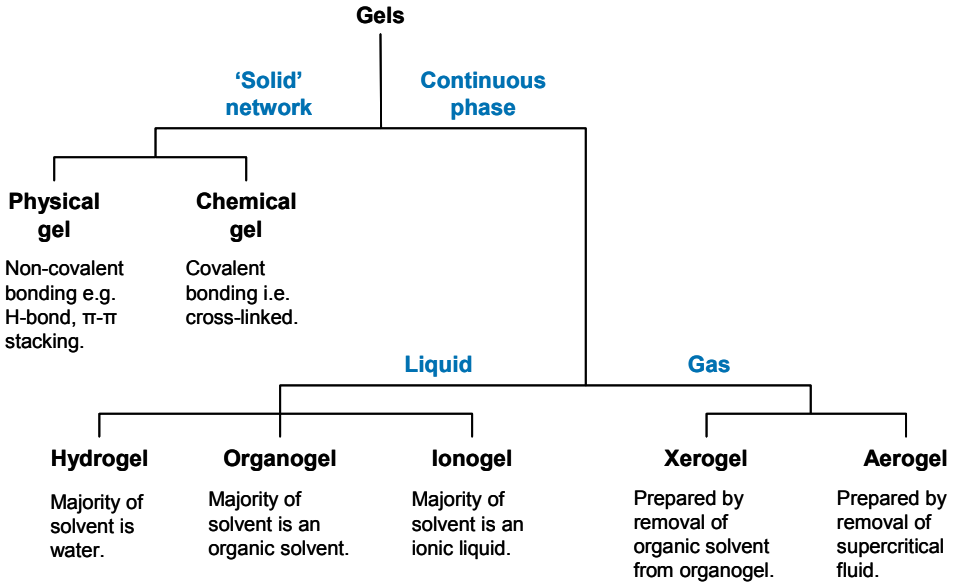

Figure 1.34 General classification scheme for gels.

Many gelators have been (and still are) discovered by serendipity[282–286]. In light of potential applications of gels,[270, 287–291] recent efforts have been directed towards the rational design of low molecular weight gelators[270, 282, 292, 293] which are primarily based on known gelator structural motifs such cholesterol[294] (Figure 1.35) and C_3-symmetric cores with hydrogen bonding motifs[295] (Figure 1.36). Physical gels or supramolecular gels[296] can be considered to be comprised of supramolecular

polymers[297, 298] thus, designing self-assembly[299, 300] would aid in the synthesis of potential gelator molecules. This section will explore examples of low molecular weight gelators from literature, selected methods of characterising gelators and gel materials, and their potential applications.

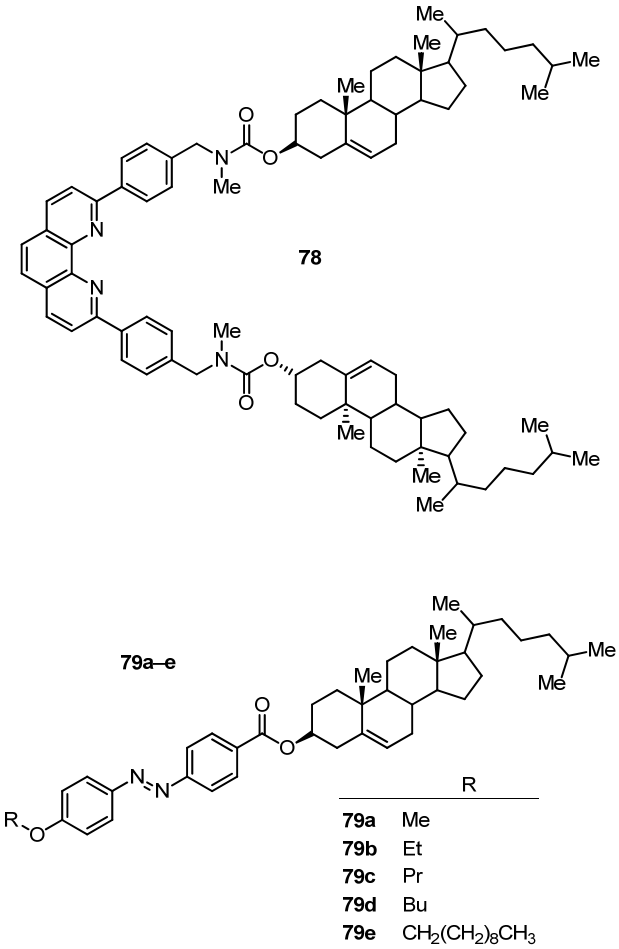

Figure 1.35 Examples of cholesterol-based organogelators.[301, 302]

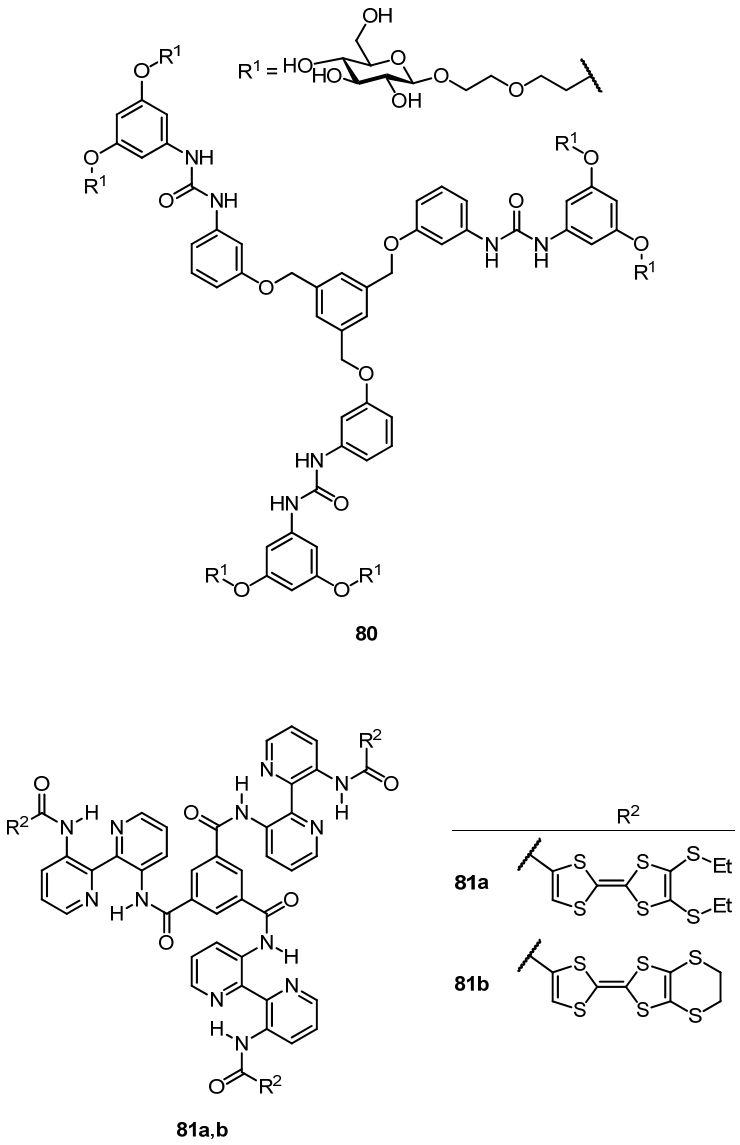

Figure 1.36 Examples C_3-symmetric gelators.[303, 304]

Gels, particularly those based on small molecule-based gelators, have generated much interest recently with a range of potential applications.[270, 274, 279, 291, 305, 306] Much of the recent literature shows that research efforts are being directed at biomedical applications[287, 288, 307, 308] (drug delivery, tissue engineering, regenerative medicine), smart materials and sensors (which are responsive to external stimuli),[303, 309, 310] and templates for crystallisation (as biomimics of organic matrices in biominerals). Other possible applications explored include using gels as reaction media,[311] for catalysis,[312–315] and water purification.[316] Some gels, albeit macromolecule-based, have also been applied to art conservation.[317, 318] The ready

accessibility and wide range of potential applications of supramolecular gels have made them a highly active research area.

1.3.2 Stimuli-responsive low molecular weight gelators

Low molecular weight gels are formed by supramolecular interactions between gelator molecules. This reduces the mechanical strength of the gels when compared with traditional high molecular weight polymer gels (although non-covalent interactions can strengthen supramolecular gels[319]). However, these supramolecular interactions allow the gels to be switched 'on' or 'off'. Many gelators are heat-responsive and are discovered by heating-and-cooling the gelator in a solvent, presumably by serendipity during recrystallisation (although Velázquez[286] has reported organogels which form on warming). Despite this, gelators have been reported to be responsive to external stimuli[320] such as pH, chemical environment,[321] cations and anions,[322–324] light (i.e. photo-responsive),[325–328] sonication,[329] redox,[330] and enzymes. The number of stimuli to which gels can respond to is primarily limited by the chemistry in which the gelator and self-assembled structures can undergo.

1.3.2.1 Anion-responsive gelators

Taking a leaf from supramolecular chemistry, researchers have investigated gelator-anion interactions in order to tune the properties of gels[331] or to develop anion-responsive gels.[332] Urea-anion binding[333, 334] is well known and thus makes it a good functional group to include in anion-responsive gelators.[332, 335] Foster et al.[336] used urea-based anion-responsive gelators (Figure 1.37) to prepare gel media for the crystallisation of pharmaceutical drug molecules. The authors prepared the organogels by heating and cooling the gelator and drug of interest in a solvent; drug crystals were then recovered by triggering a gel-sol transition using an anion (e.g. acetate) to bind to urea and disrupting gelator-gelator interactions. Similarly, Stanley et al.[337] found that a tris(urea) gelator tended to crystallise in the presence of Cl^- rather than form an organogel. Hseuh et al.[338] have reported a [2]rotaxane-urea pair that forms an organogel which is responsive to pH changes and anions. Here, the anion recognition is proposed to operate on recognition of acetate by the ammonium moiety within the urea derivative, thereby preventing the [2]rotaxane from binding

with that ammonium group; the gel can be reformed by the addition of perchlorate anion.

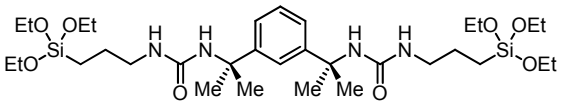

82

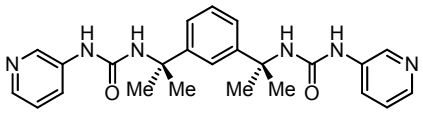

83

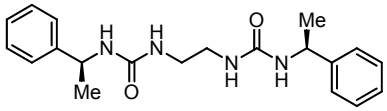

84

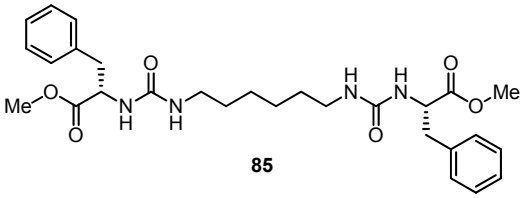

85

Figure 1.37 Gelators **82–85** (**83** forms metallogels with copper) were investigated by Foster et al.[336] for the crystallisation of pharmaceutical drugs.

1.3.2.2 **pH-Responsive gelators**

There are many examples of pH-responsive gelators.[339–342] Changes in pH interfere with supramolecular interactions between gelator molecules, for example by converting an amine to an ammonium or carboxylate to a carboxylic acid, preventing the formation of a gel. In the case of peptides, it can prevent folding into secondary structures which lead to the formation of a gel. Schneider et al.[343] reported a peptide which was in an unfolded form at low pH (<5.5) and folded into β-sheets (as observed by CD spectroscopy) under alkaline conditions (>9) forming a hydrogel. A series of compounds based on a nitrophenyl group and an aromatic dicarboxylic acid bridged by a urea (Figure 1.38) were investigated as 'pH-tuneable' hydrogelators by Wood et al.[341] The authors found that the gelators dissolved at high pH (~13) and formed a hydrogel when acidified by HCl (~pH 3) or the glucono-δ-lactone protocol

(which produces homogenous hydrogels by the controlled reduction of pH);[344] the authors did not indicate if a gel-sol transition occurred if a gel was made alkaline.

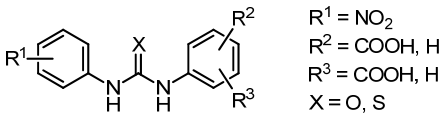

86

Figure 1.38 A series of urea-based pH-responsive hydrogelators investigated by Wood et al.[341]

1.3.2.3 **Thixotropic gels**

Some gels may also respond to external mechanical forces. Thixotropic gels become liquids when shaken (breaking non-covalent bonds between the gelator), however regain their gel state on resting (allowing supramolecular interactions to occur). Hamilton et al.[345] reported a copper metallogel (Figure 1.39), prepared in water with <5% of acetonitrile, which exhibited thixotropic behaviour; the metallogel took 3–4 hours to recover from mechanical agitation. Sobczuk et al.[346] prepared organogels from a bis-crown ether molecule hosting chiral ammonium molecules. The authors did not observe helical twists or coils by microscopic methods, however chirality of the self-assembled fibres was supported by CD spectroscopy. Remarkably, the chirality was lost through thixotropic behaviour, but recovered upon heating and cooling; the authors proposed the loss of chirality was due to mechanical disruption of anisotropic packing of the crown ether-ammonium system (although this did not prevent a gel from forming). Other organogel systems exhibiting thixotropic behaviour have been reported, such as dendritic-based[347] and anthracene-fullerene systems.[348]

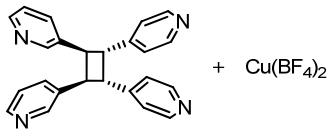

87

Figure 1.39 A metallogel investigated by Hamilton et al.[345] which exhibited thixotropic behaviour.

1.3.2.4 Enzyme-responsive gelators

A class of gelators exists which do not self-assemble until unmasked by enzymes[349] (these are also referred to as 'pre-cursors'). Hirst et al.[309] investigated a masked Fmoc-protected (9-fluorenylmethoxycarbonyl) peptide ester which transformed into the gelator upon hydrolysis by the enzyme subtilisin. Similarly, Toledano et al. examined a peptide hydrogelator formed by the action of protease on the masked gelator.[350] Yang et al.[351] reported a compound in which the gelator was masked by a phosphate group. The addition of phosphatase removed the phosphate group, altering the hydrophobicity of the molecule, leading to the formation of a hydrogel. The authors then triggered a gel-sol transition by reattaching a phosphate group using a kinase. Likewise, Yang et al.[352] reduced the solubility of their masked hydrogelator (thus, favouring hydrophobic interactions) by the addition of β-lactamase to their compound which lead to self-assembly into nanofibrils followed by formation of a hydrogel. These examples demonstrate how enzymes offer a more controlled way of accessing higher-ordered structures which can lead to gel formation.

1.3.3 Selected techniques for characterising gelators and gels

There are a number of methods for characterising gelators and gel materials. *Molecular Gels* by Weiss and Terech[271] is a good resource for methods available for characterising gel materials. Techniques employed by researchers include scattering techniques (e.g. SAXS, WAXS, small angle neutron scattering, DLS); spectroscopy (e.g. UV-visible, IR, NMR, circular dichroism); microscopy (both optical and electron microscopies); calorimetry (e.g. thermogravimetric analysis, differential scanning calorimetry, differential thermal analysis); rheometry; and scanning probe microscopy. Selected methods of interest are highlighted in this section.

1.3.3.1 Rheology

The rheological properties of soft glassy materials (such as gels, foams, and colloidal suspensions) are of interest. Gel materials possess viscoelastic properties with the storage moduli (G') and loss moduli (G'') reflecting the elastic and viscous properties respectively.[353] Smith[354] proposed a relationship which forms the basis of a quantitative definition of a gel where by '... G' should exceed G'' by about one order

of magnitude'. This definition has the advantage of avoiding confusion between gels with substances that have high viscosity or low yield-stress.[355]

Although G' and G'' are readily measured by a rheometer, 'tabletop rheology' techniques[355] are more accessible. One of the most basic tests for a gel is the 'tube inversion' test. Here, a tube of the test substance is inverted, the material is considered a gel if it does not flow. Care must be taken with interpreting these results (refer to previous paragraph). Alternatively, the bulk gel phase can be characterised by the 'dropping ball' method.[356, 357] In this method, a small dense sphere (e.g. stainless steel ball) is placed above the gel in a vial. The vial is then heated and the gel-sol transition temperature ($T_{gel–sol}$), effectively a 'melting point' for the gel, is taken at the point where the dense ball reaches the bottom of the vial. The dense ball should be placed carefully on top of the gel (and not dropped onto the gel) to avoid the effects of sheer thinning.[355] In addition, potential interactions between the dense ball and the vial walls can be eliminated by using a sufficiently large vial, however the availability of the gelator must also be considered. By determining $T_{gel-sol}$ at various concentrations of gelators, a phase diagram for the gel system can be constructed.

1.3.3.2 **Circular dichroism spectroscopy**

Circular dichroism spectroscopy[358] is a technique often applied to the measurement of asymmetric structures of chiral molecules and chiral nanostructures. The basic principle of this technique centres on the difference in the absorption of left- and right-circularly polarised light by chiral species.[359, 360] CD spectroscopy is most widely known as a technique for the investigation of biomolecules[361] (in particular structures of peptides and proteins), however it has also been applied to self-assembled systems.[362] In gel systems, gelator molecules can self-assemble into chiral structures which are then detected by CD spectroscopy where the signal is typically more intense than the gelator itself.[363–365] Although most chirality detected in gel systems arises from chiral gelator molecules or substrates,[366] chiral self-assembled structures have been reported for achiral gelators[367] Chirality of self-assembled structures can also be induced by a guest, as demonstrated by work from Sobczuk et al.[346] CD spectroscopy has also been used to monitor the chirality of photoresponsive

organogel systems,[368] recognition of chiral molecules by platinum-based metallogels,[369] and even the controversial topic of chirality induced by mechanical means[370] (i.e. stirring clockwise and counterclockwise).

1.3.3.3 **Atomic force microscopy**

Atomic force microscopy[371] is a technique well suited to the characterisation of soft matter in situ. The ability of atomic force microscopes (AFM) to image samples at high resolution in the liquid state or dry state with environmental control (such as temperature and humidity), gives it a significant advantage over other imaging methods such as scanning electron microscopy (SEM). Furthermore, the little sample preparation involved for AFM does not damage or alter the sample (e.g. drying samples for SEM). AFM is primarily used to image gel nanostrucutres, both dried and wet with solvent.[372–374] Dimensions of gel fibres are often derived from AFM micrographs which can provide information regarding the likely packing mode of gelator molecules that give rise to gel fibres.[375] Furthermore, AFM can be used to image a sol-gel transition (after heating to convert the gel to a sol) as demonstrated by Wang et al.[376] In addition, there are non-imaging applications such as work by Ikeda et al.[377] who determined the mechanical strength of gel fibres by using force curves derived from tip indentation onto fibres.

1.3.3.4 **Cryo-electron microscopy**

Another imaging technique is cryo-electron microscopy (cryo-EM). Sample preparation for cryo-EM (central to this method) involves vitrification of samples (i.e. rapid freezing to prevent crystalline ice from forming). Cryo-EM is a technique most widely known for obtaining micrographs of cellular structures[378–380] and coupled with 3D reconstruction allows for tomographic images of cellular and sub-cellular structures.[381–383] This technique has also been used for imaging self-assembled structures,[384–386] sections of nacre from mollusc shells,[387] and nanoparticles in studies of pre-nucleation clusters of calcium phosphate crystallisation.[388]

1.3.4 Chirality of gelators and its nanostructures

Chiral gels are of interest as templates for helical nanostructures.[389] Chiral gelators usually behave differently depending on whether it is a pure enantiomer or a racemic

mixture.[366] Smith[354] noted that when one enantiomer of a chiral gelator was in the presence of the other enantiomer, one of the following three scenarios typically occurred:

1. one enantiomer interfered with the self-assembly of the other leading to the dissolution of the gel (and usually followed by precipitation);
2. the enantiomer in excess imposes its chirality on the other (by a 'majority rules' or 'sergeants-and-soldiers' principles);[390-396] or
3. the enantiomers 'self-sort' into homochiral self-assembled structures.[363, 397–400]

Many of the examples of chiral gelators from literature typically form self-assembled fibres comprising a single enantiomer[401] and are more stable than their racemic mixture[402] (in addition, other properties such as gel fibre morphology are also affected). With racemic mixtures of gelators, crystallisation[403] is a common occurrence and sometimes a gel phase does not form.[404] In some cases a racemic mixture of the gelator can act synergistically to give better gels than the pure enantiomers. For example, Džolić and Žinić[405] found that homochiral two-component chiral leucine-and leucinol-based dipeptides (**88** and **89** respectively, Figure 1.40) could gel more solvent than a heterochiral pair (e.g. (*S*,*S*)-**88**) with (*R*,*R*)-**89**) or with a racemate of one compound (e.g. (*S*,*S*)-**88**) with *rac*-**89**). Frkanec and Žinić[277] later found that *rac*-**89** formed stable gels with toluene but unstable gels with dichloromethane (with the tendency to crystallise). They proposed that *rac*-**89** self-sorted into separate enantiomers in toluene whereas *rac*-**89** formed a *meso*-bilayer in dichloromethane (thereby reducing the stability of the gel-phase).

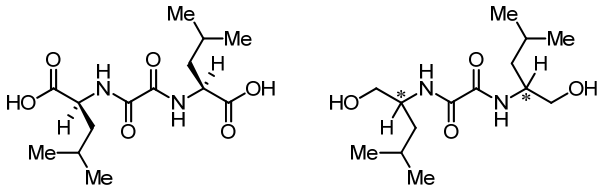

88 **89**

Figure 1.40 Synergistic chiral organogelators investigated by Džolić et al.[405]

Chiral synergistic effects were also observed by Friggeri et al.[406] who found that homochiral **90a** (either DDD or LLL), Figure 1.41, crystallised from water, however

hydrogels were obtained with the heterochiral derivatives (DDL-**90a** or LLD-**90a**). Surprisingly, a mixture of the homochiral and heterochiral derivatives (i.e. LLL-**90a** or DDD-**90a** with DDL-**90a** or LLD-**90a**) gave a higher $T_{gel\text{-}sol}$ than an equivalent concentration of the heterochiral derivative. The authors suggested that incorporation of the homochiral derivative into the fibres of the heterochiral gelator could improve the thermostability of the hydrogel. Furthermore, work with similar homochiral analogues (**90b**–**g**) with substitution at the carboxylic acids supported the idea that the effects of chirality could be 'overcome'. Watanabe et al.[407] observed improved thermostability with diastereomixtures of *myo*-inositol derivatives over comparable levels of homochiral isomers.

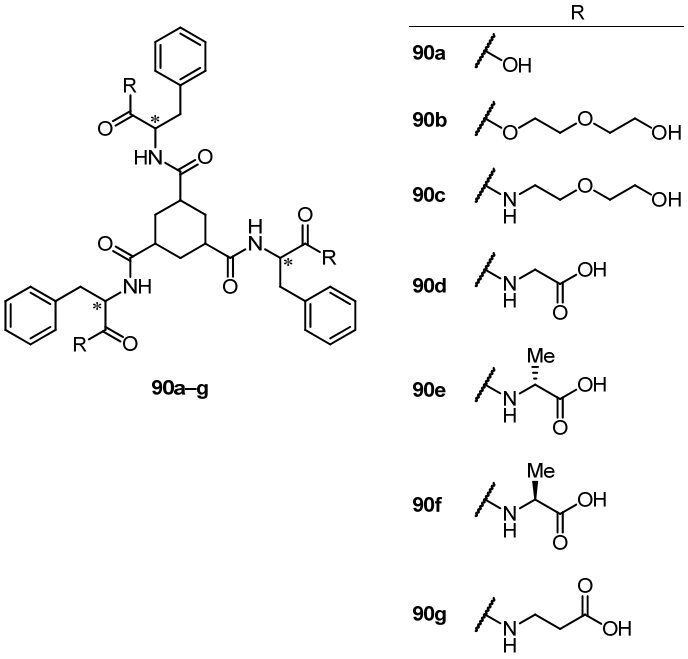

Figure 1.41 Chiral 1,3,5-substituted cyclohexane-based hydrogelators studied by Friggeri et al.[406]

Interest in the helical structures formed by gelators is driven by the ability to transcribe (or template) the helical patterns to inorganic nanostructures[408–410] (also refer to section 5.1.2). Many chiral gelators self-assemble into helical or coiled structures[411–413] In some cases helical twists in the fibres are not observable by electron microscopy,[414] while CD spectroscopy indicates the formation of chiral supramolecular structures. Smith[268] suggested that although gelators may self-assemble into chiral nanostructures, the chirality may not be reflected at larger scales

(e.g. gel fibres) or that sample preparation has altered the fine structure (e.g. removing solvent from sample in preparation for SEM). Helical or coil structures are not limited to chiral gelators, achiral gelators can also give rise to chiral nanostructures by the way they self-assemble,[415, 416] however some helices were difficult to observe by microscopy techniques.[295] Alternatively, racemic mixtures (such as **91** in the presence of a racemic mixture of tartrate, Figure 1.42) may produce gel fibres without helices or coils whereas the enantiopure gelators produced gels with helical fibres in water and chloroform.[417]

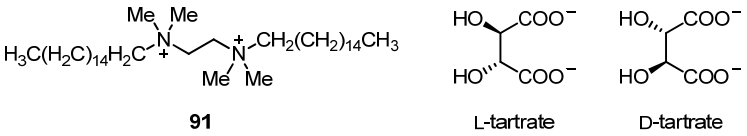

91 L-tartrate D-tartrate

Figure 1.42 Gemini surfactant **91** forms helical gel fibres in the presence of a single enantiomer of tartrate, however non-helical fibres results if a racemic mixture of tartrate is present.[417]

1.4 Objectives and outline of this research project

Amino acid functionalised calixarenes have been shown to have a wide range of interactions and properties. This thesis aims to investigate some of these properties. Of particular interest is the gelation ability of proline functionalised calixarenes and crystal growth modification by L-aspartic acid, L-glutamic acid, and iminiodiacetic acid functionalised calix[4]arene on model systems such as calcium carbonate and barium sulfate.

1.5 References

1 Gutsche, C. D. *Calixarenes: An Introduction*. 2nd ed.; RSC Publishing: Cambridge, 2008.

2 Mandolini, L.; Ungaro, R., Eds. *Calixarenes in Action*. Imperial College Press: London, 2000.

3 Böhmer, V. *Angew. Chem. Int. Ed.* **1995**, *34* (7), 713–745.

4 Gutsche, C. D. *Calixarenes*. Royal Society of Chemistry: Cambridge, 1989.

5 Gutsche, C. D. *Calixarenes Revisited*. Royal Society of Chemistry: Cambridge, 1998; p 117.

6 Vicens, J.; Böhmer, V., Eds. *Calixarenes: A Versatile Class of Macrocyclic Compounds*. Kluwer Academic Publishers: Dordrecht ; Boston, 1991.

7 Vicens, J.; Asfari, Z.; Harrowfield, J. M., Eds. *Calixarenes 50th Anniversary: Commemorative Issue*. Kluwer Academic: Dordrecht ; Boston, 1994.

8 Lumetta, G. J.; Rogers, R. D.; Gopalan, A. S., Eds. *Calixarenes for Separations*. American Chemical Society: Washington, DC, 2000; Vol. 757.

9 Asfari, Z., Ed. *Calixarenes 2001*. Kluwer Academic Publishers: Dordrecht, 2001.

10 Vicens, J.; Harrowfield, J. M.; Baklouti, L., Eds. *Calixarenes in the Nanoworld*. Springer: Dordrecht, 2007.

11 Sliwa, W.; Kozlowski, C. *Calixarenes and Resorcinarenes: Synthesis, Properties and Applications*. Wiley-VCH Verlag GmbH and Co. KGaA: Weinheim, 2009.

12 Gargiulli, C.; Gattuso, G.; Liotta, C.; Notti, A.; Parisi, M. F.; Pisagatti, I.; Pappalardo, S. *J. Org. Chem.* **2009**, *74* (11), 4350–4353.

13 Pappalardo, S.; Villari, V.; Slovak, S.; Cohen, Y.; Gattuso, G.; Notti, A.; Pappalardo, A.; Pisagatti, I.; Parisi, M. F. *Chem. Eur. J.* **2007**, *13* (29), 8164–8173.

14 Cornforth, J. W.; Hart, P. D.; Nicholls, G. A.; Rees, R. J. W.; Stock, J. A. *Br. J. Pharmacol. Chemother.* **1955**, *10* (1), 73–86.

15 Iwamoto, K.; Araki, K.; Shinkai, S. *J. Org. Chem.* **1991**, *56* (16), 4955–4962.

16 Gutsche, C. D.; Dhawan, B.; Levine, J. A.; Hyun No, K.; Bauer, L. J. *Tetrahedron* **1983**, *39* (3), 409–426.

17 Powell, W. H. *Pure Appl. Chem.* **1998**, *70* (8), 1513–1545.

18 Favre, H. A.; Hellwinkel, D.; Powell, W. H.; Smith, H. A.; Tsay, S. S.-C. *Pure Appl. Chem.* **2002**, *74* (5), 809–834.

19 Panico, R.; Powell, W. H.; Richer, J.-C., Eds. *A Guide to IUPAC Nomenclature of Organic Compounds Recommendations 1993*. Blackwell Scientific Publications: Melbourne, 1993.

20 Mogck, O.; Pons, M.; Böhmer, V.; Vogt, W. *J. Am. Chem. Soc.* **1997**, *119* (24), 5706–5712.

21 Arduini, A.; Casnati, A. Calixarenes. In *Macrocycle Synthesis: A Practical Approach*, Parker, D., Ed. Oxford University Press: Oxford, 1996; pp 145–173.

22 Diederich, F.; Stang, P. J.; Tykwinski, R. R., Eds. *Modern Supramolecular Chemistry: Strategies for Macrocycle Synthesis*. Wiley-VCH Verlag GmbH and Co. KGaA: Weinheim, 2008.

23 Chen, C.-F.; Lu, L.-G.; Hu, Z.-Q.; Peng, X.-X.; Huang, Z.-T. *Tetrahedron* **2005**, *61* (15), 3853–3858.

24 Gutsche, C. D.; Levine, J. A.; Sujeeth, P. K. *J. Org. Chem.* **1985**, *50* (26), 5802–5806.

25 Iwamoto, K.; Shinkai, S. *J. Org. Chem.* **1992**, *57* (26), 7066–7073.

26 Ogden, M. I.; Skelton, B. W.; White, A. H. *J. Chem. Soc., Dalton Trans.* **2001**, (20), 3073–3077.

27 Iwamoto, K.; Fujimoto, K.; Matsuda, T.; Shinkai, S. *Tetrahedron Lett.* **1990**, *31* (49), 7169–7172.

28 Groenen, L. C.; Van Loon, J. D.; Verboom, W.; Harkema, S.; Casnati, A.; Ungaro, R.; Pochini, A.; Ugozzoli, F.; Reinhoudt, D. N. *J. Am. Chem. Soc.* **1991**, *113* (7), 2385–2392.

29 Lhoták, P.; Bila, A.; Budka, J.; Pojarova, M.; Stibor, I. *Chem. Commun.* **2008**, (14), 1662–1664.

30 Lalor, R.; DiGesso, J. L.; Mueller, A.; Matthews, S. E. *Chem. Commun.* **2007**, (46), 4907–4909.

31 Iwamoto, K.; Araki, K.; Shinkai, S. *Tetrahedron* **1991**, *47* (25), 4325–4342.

32 Pinkhassik, E.; Sidorov, V.; Stibor, I. *J. Org. Chem.* **1998**, *63* (26), 9644–9651.

33 Pinter, T.; Jana, S.; Courtemanche, R. J. M.; Hof, F. *J. Org. Chem.* **2011**, *76* (10), 3733–3741.

34 Boyko, V.; Rodik, R.; Danylyuk, O.; Tsymbal, L.; Lampeka, Y.; Suwinska, K.; Lipkowski, J.; Kalchenko, V. *Tetrahedron* **2005**, *61* (52), 12282–12287.

35 Man, S. W.; Nicoud, J.-F. *Tetrahedron Lett.* **1993**, *34* (51), 8237–8240.

36 Strobel, M.; Kita-Tokarczyk, K.; Taubert, A.; Vebert, C.; Heiney, P. A.; Chami, M.; Meier, W. *Adv. Funct. Mater.* **2006**, *16* (1), 252–259.

37 Sansone, F.; Barboso, S.; Casnati, A.; Fabbi, M.; Pochini, A.; Ugozzoli, F.; Ungaro, R. *Eur. J. Org. Chem.* **1998**, *1998* (5), 897–905.

38 Dalcanale, E.; Montanari, F. *J. Org. Chem.* **1986**, *51* (4), 567–569.

39 Dondoni, A.; Marra, A.; Scherrmann, M.-C.; Casnati, A.; Sansone, F.; Ungaro, R. *Chem. Eur. J.* **1997**, *3* (11), 1774–1782.

40 Smith, W. E. *J. Org. Chem.* **1972**, *37* (24), 3972–3973.

41 Martin, A. D.; Raston, C. L. *Chem. Commun.* **2011**, *47* (35), 9764–9772.

42 Balthazor, T. M.; Grabiak, R. C. *J. Org. Chem.* **1980**, *45* (26), 5425–5426.

43 Bhattacharya, A. K.; Thyagarajan, G. *Chem. Rev.* **1981**, *81* (4), 415–430.

44 Baynton, A.; Ogden, M. I.; Raston, C. L.; Jones, F. *CrystEngComm* **2012**, *14* (3), 1057–1062.

45 Baynton, A.; Chandler, B. D.; Jones, F.; Nealon, G.; Ogden, M. I.; Radomirovic, T.; Shimizu, G. K. H.; Taylor, J. M. *CrystEngComm* **2011**, *13* (4), 1090–1095.

46 Shinkai, S.; Araki, K.; Tsubaki, T.; Arimura, T.; Manabe, O. *J. Chem. Soc., Perkin Trans. 1* **1987**, 2297–2299.

47 Rodik, R. V.; Klymchenko, A. S.; Jain, N.; Miroshnichenko, S. I.; Richert, L.; Kalchenko, V. I.; Mély, Y. *Chem. Eur. J.* **2011**, *17* (20), 5526–5538.

48 International Agency for Research on Cancer, World Health Organization *IARC Monographs on the Evaluation of Carcinogenic Risks to Humans, Supplement 7*. International Agency for Research on Cancer: Lyon, 1987.

49 Pohanish, R. P. Sittig's Handbook of Toxic and Hazardous Chemicals and Carcinogens. 6th ed.; Elsevier Inc.: Oxford, 2012. http://www.knovel.com/web/portal/browse/display?_EXT_KNOVEL_DISPLAY_bookid=4477&VerticalID=0 (accessed 22/2/2012).

50 Almi, M.; Arduini, A.; Casnati, A.; Pochini, A.; Ungaro, R. *Tetrahedron* **1989**, *45* (7), 2177–2182.

51 Bew, S. P.; Brimage, R. A.; L'Hermit, N.; Sharma, S. V. *Org. Lett.* **2007**, *9* (19), 3713–3716.

52 Conner, M.; Janout, V.; Regen, S. L. *J. Org. Chem.* **1992**, *57* (13), 3744–3746.

53 Klenke, B.; Näther, C.; Friedrichsen, W. *Tetrahedron Lett.* **1998**, *39* (49), 8967–8968.

54 Kumar, S.; Chawla, H. M.; Varadarajan, R. *Tetrahedron Lett.* **2002**, *43* (39), 7073–7075.

55 Kogan, K.; Columbus, I.; Biali, S. E. *J. Org. Chem.* **2008**, *73* (18), 7327–7335.

56 Kuno, L.; Biali, S. E. *J. Org. Chem.* **2011**, *76* (10), 3664–3675.

57 Biali, S. E.; Böhmer, V.; Cohen, S.; Ferguson, G.; Grüttner, C.; Grynszpan, F.; Paulus, E. F.; Thondorf, I.; Vogt, W. *J. Am. Chem. Soc.* **1996**, *118* (51), 12938–12949.

58 Simaan, S.; Agbaria, K.; Biali, S. E. *J. Org. Chem.* **2002**, *67* (17), 6136–6142.

59 Columbus, I. *J. Org. Chem.* **2008**, *73* (7), 2598–2606.

60 Columbus, I.; Biali, S. E. *Org. Lett.* **2007**, *9* (15), 2927–2929.

61 Joseph, R.; Rao, C. P. *Chem. Rev.* **2011**, *111* (8), 4658–4702.

62 Sliwa, W.; Girek, T. *J. Inclusion Phenom. Macrocyclic Chem.* **2010**, *66* (1–2), 15–41.

63 Ikeda, A.; Shinkai, S. *Chem. Rev.* **1997**, *97* (5), 1713–1734.

64 Shokova, E.; Kovalev, V. *Russ. J. Org. Chem.* **2009**, *45* (9), 1275–1314.

65 Evtugyn, G. A.; Stoikova, E. E.; Shamagsumova, R. V. *Russ. Chem. Rev.* **2010**, *79* (12), 1071–1097.

66 Diamond, D.; McKervey, M. A. *Chem. Soc. Rev.* **1996**, *25* (1), 15–24.

67 Leray, I.; Valeur, B. *Eur. J. Inorg. Chem.* **2009**, *2009* (24), 3525–3535.

68 Valeur, B.; Leray, I. *Inorg. Chim. Acta* **2007**, *360* (3), 765–774.

69 Sharma, K.; Cragg, P. J. *Chem. Sens.* **2011**, *1*, 9.

70 Kim, J. S.; Quang, D. T. *Chem. Rev.* **2007**, *107* (9), 3780–3799.

71 Kim, H. J.; Lee, M. H.; Mutihac, L.; Vicens, J.; Kim, J. S. *Chem. Soc. Rev.* **2012**, *41* (3), 1173–1190.

72 Schühle, D. T.; Peters, J. A.; Schatz, J. *Coord. Chem. Rev.* **2011**, *255* (23–24), 2727–2745.

73 Chang, K.-C.; Su, I.-H.; Lee, G.-H.; Chung, W.-S. *Tetrahedron Lett.* **2007**, *48* (41), 7274–7278.

74 Lee, Y. H.; Lee, M. H.; Zhang, J. F.; Kim, J. S. *J. Org. Chem.* **2010**, *75* (21), 7159–7165.

75 Othman, A. B.; Lee, J. W.; Wu, J.-S.; Kim, J. S.; Abidi, R.; Thuéry, P.; Strub, J. M.; Van Dorsselaer, A.; Vicens, J. *J. Org. Chem.* **2007**, *72* (20), 7634–7640.

76 Durmaz, M.; Zor, E.; Kocabas, E.; Bingol, H.; Akgemci, E. G. *Electrochim. Acta* **2011**, *56* (15), 5316–5321.

77 Sakaki, T.; Harada, T.; Deng, G.; Kawabata, H.; Kawahara, Y.; Shinkai, S. *J. Inclusion Phenom. Macrocyclic Chem.* **1992**, *14* (3), 285–302.

78 Lu, J.-Q.; Pang, D.-W.; Zeng, X.-S.; He, X.-W. *J. Electroanal. Chem.* **2004**, *568*, 37–43.

79 O'Connor, K. M.; Henderson, W.; O'Neill, E.; Arrigan, D. W. M.; Harris, S. J.; McKervey, M. A.; Svehla, G. *Electroanalysis* **1997**, *9* (4), 311–315.

80 Yajima, S.; Yoshioka, N.; Tanaka, M.; Kimura, K. *Electroanalysis* **2003**, *15* (15–16), 1319–1326.

81 Morakchi, K.; Hamel, A.; Kherrat, R. *Desalin. Water Treat.* **2012**, *46* (1–3), 168–170.

82 Dong, H.; Zheng, H.; Lin, L.; Ye, B. *Sens. Actuators, B* **2006**, *115* (1), 303–308.

83 Mahajan, R. K.; Kaur, R.; Kaur, I.; Sharma, V.; Kumar, M. *Anal. Sci.* **2004**, *20* (5), 811–814.

84 Dong, H.; Lin, L.; Zheng, H.; Zhao, G.; Ye, B. *Electroanalysis* **2006**, *18* (12), 1202–1207.

85 Kimura, K.; Tatsumi, K.; Yokoyama, M.; Ouchi, M.; Mocerino, M. *Anal. Commun.* **1999**, *36* (6), 229–230.

86 He, X.; Chen, L.; Xie, X.; Su, Z.; Qin, C.; Liu, Y.; Ma, M.; Yao, S.; Deng, L.; Xie, Q.; Tian, Y.; Qin, D.; Luo, Y. *Microchim. Acta* **2012**, *176* (1), 81–89.

87 Chen, L.; Zhang, J.; Zhao, W.; He, X.; Liu, Y. *J. Electroanal. Chem.* **2006**, *589* (1), 106–111.

88 Roundhill, D. M.; Solangi, I. B.; Memom, S.; Bhanger, M. I.; Yilmaz, M. *Pak. J. Anal. Environ. Chem.* **2009**, *10* (1–2), 1–13.

89 Sayin, S.; Ozcan, F.; Yilmaz, M. *J. Hazard. Mater.* **2010**, *178* (1–3), 312–319.

90 Ertul, Ş.; Bayrakcı, M.; Yilmaz, M. *J. Hazard. Mater.* **2010**, *181* (1–3), 1059–1065.

91 Stankovic, V.; Outarra, L.; Zonnevijlle, F.; Comninellis, C. *Sep. Purif. Technol.* **2008**, *61* (3), 366–374.

92 Ramírez, F. d. M.; Varbanov, S.; Padilla, J.; Bünzli, J.-C. G. *J. Phys. Chem. B* **2008**, *112* (35), 10976–10988.

93 Walker, D. D.; Norato, M. A.; Campbell, S. G.; Crowder, M. L.; Fink, S. D.; Fondeur, F. F.; Geeting, M. W.; Kessinger, G. F.; Pierce, R. A. *Sep. Sci. Technol.* **2005**, *40* (1–3), 297–309.

94 Antipin, I. S.; Solovieva, S. E.; Stoikov, I. I.; Vershinina, I. S.; Pribylova, G. A.; Tananaev, I. G.; Myasoedov, B. F. *Russ. Chem. Bull.* **2004**, *53* (1), 127–132.

95 Mariani, M.; Macerata, E.; Galletta, M.; Buttafava, A.; Casnati, A.; Ungaro, R.; Faucitano, A.; Giola, M. *Radiat. Phys. Chem.* **2007**, *76* (8–9), 1285–1289.

96 Sansone, F.; Fontanella, M.; Casnati, A.; Ungaro, R.; Böhmer, V.; Saadioui, M.; Liger, K.; Dozol, J.-F. *Tetrahedron* **2006**, *62* (29), 6749–6753.

97 Ohto, K.; Ishibashi, H.; Kawakita, H.; Inoue, K.; Oshima, T. *J. Inclusion Phenom. Macrocyclic Chem.* **2009**, *65* (1–2), 111–120.

98 Adhikari, B.; Hashiguchi, N.; Ohto, K.; Kawakita, H.; Inoue, K. *J. Inclusion Phenom. Macrocyclic Chem.* **2009**, *65* (1–2), 121–128.

99 Driscoll, C. R.; Reid, B. L.; McIldowie, M. J.; Muzzioli, S.; Nealon, G. L.; Skelton, B. W.; Stagni, S.; Brown, D. H.; Massi, M.; Ogden, M. I. *Chem. Commun.* **2011**, *47* (13), 3876–3878.

100 Troisi, F.; Russo, A.; Gaeta, C.; Bifulco, G.; Neri, P. *Tetrahedron Lett.* **2007**, *48* (45), 7986–7989.

101 Casnati, A.; Sartori, A.; Pirondini, L.; Bonetti, F.; Pelizzi, N.; Sansone, F.; Ugozzoli, F.; Ungaro, R. *Supramol. Chem.* **2006**, *18* (3), 199–218.

102 Miao, R.; Zheng, Q.-Y.; Chen, C.-F.; Huang, Z.-T. *Supramol. Chem.* **2007**, *19* (7), 531–535.

103 Shimizu, S.; Suzuki, T.; Shirakawa, S.; Sasaki, Y.; Hirai, C. *Adv. Synth. Catal.* **2002**, *344* (3–4), 370–378.

104 Bauer, L. J.; Gutsche, C. D. *J. Am. Chem. Soc.* **1985**, *107* (21), 6063–6069.

105 Backes, M.; Bohmer, V.; Ferguson, G.; Gruttner, C.; Schmidt, C.; Vogt, W.; Ziat, K. *J. Chem. Soc., Perkin Trans. 2* **1997**, (6), 1193–1200.

106 McKervey, M. A.; Seward, E. M.; Ferguson, G.; Ruhl, B. L. *J. Org. Chem.* **1986**, *51* (19), 3581–3584.

107 Mutihac, L.; Lee, J. H.; Kim, J. S.; Vicens, J. *Chem. Soc. Rev.* **2011**, *40* (5), 2777–2796.

108 Ludwig, R. *Microchim. Acta* **2005**, *152* (1–2), 1–19.

109 Arena, G.; Contino, A.; Giuseppe Gulino, F.; Magrì, A.; Sansone, F.; Sciotto, D.; Ungaro, R. *Tetrahedron Lett.* **1999**, *40* (8), 1597–1600.

110 Arena, G.; Contino, A.; Gulino, F. G.; Magrì, A.; Sciotto, D.; Ungaro, R. *Tetrahedron Lett.* **2000**, *41* (48), 9327–9330.

111 Baldini, L.; Melegari, M.; Bagnacani, V.; Casnati, A.; Dalcanale, E.; Sansone, F.; Ungaro, R. *J. Org. Chem.* **2011**, *76* (10), 3720–3732.

112 Bandela, A.; Chinta, J. P.; Hinge, V. K.; Dikundwar, A. G.; Row, T. N. G.; Rao, C. P. *J. Org. Chem.* **2011**, *76* (6), 1742–1750.

113 Baldini, L.; Casnati, A.; Sansone, F.; Ungaro, R. *Chem. Soc. Rev.* **2007**, *36* (2), 254–266.

114 Dondoni, A.; Marra, A. *Chem. Rev.* **2010**, *110* (9), 4949–4977.

115 Sansone, F.; Baldini, L.; Casnati, A.; Ungaro, R. *New J. Chem.* **2010**, *34* (12), 2715–2728.

116 Perret, F.; Coleman, A. W. *Chem. Commun.* **2011**, *47* (26), 7303–7319.

117 Mourer, M.; Psychogios, N.; Laumond, G.; Aubertin, A.-M.; Regnouf-de-Vains, J.-B. *Bioorg. Med. Chem.* **2010**, *18* (1), 36–45.

118 Mourer, M.; Dibama, H. M.; Fontanay, S.; Grare, M.; Duval, R. E.; Finance, C.; Regnouf-de-Vains, J.-B. *Bioorg. Med. Chem.* **2009**, *17* (15), 5496–5509.

119 Mourer, M.; Duval, R. E.; Finance, C.; Regnouf-de-Vains, J.-B. *Bioorg. Med. Chem. Lett.* **2006**, *16* (11), 2960–2963.

120 Galante, E.; Geraci, C.; Sciuto, S.; Campo, V. L.; Carvalho, I.; Sesti-Costa, R.; Guedes, P. M. M.; Silva, J. S.; Hill, L.; Nepogodiev, S. A.; Field, R. A. *Tetrahedron* **2011**, *67* (33), 5902–5912.

121 Dudic, M.; Colombo, A.; Sansone, F.; Casnati, A.; Donofrio, G.; Ungaro, R. *Tetrahedron* **2004**, *60* (50), 11613–11618.

122 Sansone, F.; Dudič, M.; Donofrio, G.; Rivetti, C.; Baldini, L.; Casnati, A.; Cellai, S.; Ungaro, R. *J. Am. Chem. Soc.* **2006**, *128* (45), 14528–14536.

123 Bagnacani, V.; Sansone, F.; Donofrio, G.; Baldini, L.; Casnati, A.; Ungaro, R. *Org. Lett.* **2008**, *10* (18), 3953–3956.

124 Takeuchi, T.; Bagnacani, V.; Sansone, F.; Matile, S. *ChemBioChem* **2009**, *10* (17), 2793–2799.

125 Tsou, L. K.; Dutschman, G. E.; Gullen, E. A.; Telpoukhovskaia, M.; Cheng, Y.-C.; Hamilton, A. D. *Bioorg. Med. Chem. Lett.* **2010**, *20* (7), 2137–2139.

126 Křenek, K.; Kuldová, M.; Hulíková, K.; Stibor, I.; Lhoták, P.; Dudič, M.; Budka, J.; Pelantová, H.; Bezouška, K.; Fišerová, A.; Křen, V. *Carbohydr. Res.* **2007**, *342* (12–13), 1781–1792.

127 Karel, B. *Rev. Mol. Biotechnol.* **2002**, *90* (3–4), 269–290.

128 Lalor, R.; Baillie-Johnson, H.; Redshaw, C.; Matthews, S. E.; Mueller, A. *J. Am. Chem. Soc.* **2008**, *130* (10), 2892–2893.

129 Guo, D.-S.; Uzunova, V. D.; Su, X.; Liu, Y.; Nau, W. M. *Chem. Sci.* **2011**, *2* (9), 1722–1734.

130 Acharya, A.; Ramanujam, B.; Chinta, J. P.; Rao, C. P. *J. Org. Chem.* **2010**, *76* (1), 127–137.

131 Chinta, J. P.; Acharya, A.; Kumar, A.; Rao, C. P. *J. Phys. Chem. B* **2009**, *113* (35), 12075–12083.

132 Dessingou, J.; Joseph, R.; Rao, C. P. *Tetrahedron Lett.* **2005**, *46* (46), 7967–7971.

133 Homden, D. M.; Redshaw, C. *Chem. Rev.* **2008**, *108* (12), 5086–5130.

134 Kumar, P. S. *Tetrahedron: Asymmetry* **2011**, *22* (20–22), 1817–1847.

135 List, B.; Pojarliev, P.; Biller, W. T.; Martin, H. J. *J. Am. Chem. Soc.* **2002**, *124* (5), 827–833.

136 List, B.; Lerner, R. A.; Barbas, C. F. *J. Am. Chem. Soc.* **2000**, *122* (10), 2395–2396.

137 Yang, J. W.; Chandler, C.; Stadler, M.; Kampen, D.; List, B. *Nature* **2008**, *452* (7186), 453–455.

138 Li, Z.-Y.; Lu, C.-X.; Huang, G.; Ma, J.-J.; Sun, H.; Wang, L.; Pan, Y. *Lett. Org. Chem.* **2010**, *7* (6), 461–466.

139 Dinarès, I.; Garcia de Miguel, C.; Font-Bardia, M.; Solans, X.; Alcalde, E. *Organometallics* **2007**, *26* (21), 5125–5128.

140 Brenner, E.; Matt, D.; Henrion, M.; Teci, M.; Toupet, L. *Dalton Trans.* **2011**, *40* (38), 9889–9898.

141 Fahlbusch, T.; Frank, M.; Maas, G.; Schatz, J. *Organometallics* **2009**, *28* (21), 6183–6193.

142 Monnereau, L.; Sémeril, D.; Matt, D. *Eur. J. Org. Chem.* **2012**, *2012* (14), 2786–2791.

143 Monnereau, L.; Sémeril, D.; Matt, D.; Toupet, L. *Chem. Eur. J.* **2010**, *16* (30), 9237–9247.

144 Song, R.-Q.; Cölfen, H. *CrystEngComm* **2011**, *13* (5), 1249–1276.

145 Jones, F.; Ogden, M. I. *CrystEngComm* **2010**, *12* (4), 1016–1023.

146 Jones, F.; Rohl, A. L.; Ogden, M. I.; Parkinson, G. M. *Mater. Forum* **2001**, *25*, 116–135.

147 Dove, P. M. *Elements* **2010**, *6* (1), 37–42.

148 Addadi, L.; Weiner, S. *Angew. Chem. Int. Ed.* **1992**, *31* (2), 153–169.

149 Behrens, P.; Baeuerlein, E., Eds. *Handbook of Biomineralization: Biomimetic and Bioinspired Chemistry*. Wiley-VCH GmbH and Co. KGaA: Weinheim, Germany, 2007; Vol. 2.

150 Epple, M.; Baeuerlein, E., Eds. *Handbook of Biomineralization: Medical and Clinical Aspects*. Wiley-VCH GmbH and Co. KGaA: Weinheim, 2007; Vol. 3.

151 Mann, S., Ed. *Biomimetic Materials Chemistry*. VCH Publishers, Inc.: New York, 1996.

152 Xu, A.-W.; Ma, Y.; Cölfen, H. *J. Mater. Chem.* **2007**, *17* (5), 415–449.

153 Mann, S.; Webb, J.; WIlliams, R. J. P., Eds. *Biomineralization: Chemical and Biochemical Perspectives*. VCH Verlagsgesellchaft: Weinheim, 1989.

154 Bäuerlein, E., Ed. *Handbook of Biomineralization: Biological Aspects and Structure Formation*. Wiley-VCH GmbH and Co. KGaA: Weinheim, Germany, 2007; Vol. 1.

155 Dove, P. M.; Yoreo, J. J. D.; Weiner, S., Eds. *Biomineralization*. Mineralogical Society of America: Washington, D.C., 2003; Vol. 54.

156 Estroff, L. A. Ed. Biomineralization. Special Issue, *Chem. Rev.* **2008**, *108* (11).

157 Addadi, L. Ed. CrystEngComm focuses on biomineralisation. Special Issue, *CrystEngComm* **2007**, *9* (12).

158 Naka, K. Ed. Biomineralization I: Crystallisation and Self-Organization Process. Special Issue, *Top. Curr. Chem.* **2007**, *270*.

159 Meldrum, F. C.; Cölfen, H. *Chem. Rev.* **2008**, *108* (11), 4332–4432.

160 Weiner, S.; Dove, P. M. An Overview of Biomineralization Processes and the Problem of the Vital Effect. In *Biomineralization*, Dove, P. M.; De Yoreo, J. J.; Weiner, S., Eds. Mineralogical Society of America: Washington, D.C., 2003; Vol. 54, pp 1–29.

161 Lakshminarayanan, R.; Kini, R. M.; Valiyaveettil, S. *Proc. Natl. Acad. Sci. U. S. A.* **2002**, *99* (8), 5155–5159.

162 Lakshminarayanan, R.; Loh, X. J.; Gayathri, S.; Sindhu, S.; Banerjee, Y.; Kini, R. M.; Valiyaveettil, S. *Biomacromolecules* **2006**, *7* (11), 3202–3209.

163 Hernández-Hernández, A.; Gómez-Morales, J.; Rodríguez-Navarro, A. B.; Gautron, J.; Nys, Y.; García-Ruiz, J. M. *Cryst. Growth Des.* **2008**, *8* (12), 4330–4339.

164 Addadi, L.; Joester, D.; Nudelman, F.; Weiner, S. *Chem. Eur. J.* **2006**, *12* (4), 980–987.

165 Weiner, S. *Biochemistry* **1983**, *22* (17), 4139–4145.

166 Khalifa, G. M.; Weiner, S.; Addadi, L. *Cryst. Growth Des.* **2011**, *11* (11), 5122–5130.

167 Nudelman, F.; Chen, H. H.; Goldberg, H. A.; Weiner, S.; Addadi, L. *Faraday Discuss.* **2007**, *136*, 9–25.

168 Gotliv, B. A.; Kessler, N.; Sumerel, J. L.; Morse, D. E.; Tuross, N.; Addadi, L.; Weiner, S. *ChemBioChem* **2005**, *6* (2), 304–314.

169 Gotliv, B.-A.; Addadi, L.; Weiner, S. *ChemBioChem* **2003**, *4* (6), 522–529.

170 Checa, A. G.; Cartwright, J. H. E.; Willinger, M.-G. *Proc. Natl. Acad. Sci. USA* **2009**, *106* (1), 38–43.

171 Henriksen, K.; Stipp, S. L. S. *Cryst. Growth Des.* **2009**, *9* (5), 2088–2097.

172 Henriksen, K.; Young, J. R.; Bown, P. R.; Stipp, S. L. S. *Palaeontology* **2004**, *47* (3), 725–743.

173 Raz, S.; Testeniere, O.; Hecker, A.; Weiner, S.; Luquet, G. *Biol. Bull.* **2002**, *203* (3), 269–274.

174 Tao, J.; Zhou, D.; Zhang, Z.; Xu, X.; Tang, R. *Proc. Natl. Acad. Sci. USA* **2009**, *106* (52), 22096–22101.

175 Marie, B.; Marin, F.; Marie, A.; Bédouet, L.; Dubost, L.; Alcaraz, G.; Milet, C.; Luquet, G. *ChemBioChem* **2009**, *10* (9), 1495–1506.

176 Aizenberg, J.; Weiner, S.; Addadi, L. *Connect. Tissue Res.* **2003**, *44* (1 supp 1), 20–25.

177 Zhang, T.; Ma, Y.; Chen, K.; Kunz, M.; Tamura, N.; Qiang, M.; Xu, J.; Qi, L. *Angew. Chem. Int. Ed.* **2011**, *50* (44), 10361–10365.

178 Söllner, C.; Burghammer, M.; Busch-Nentwich, E.; Berger, J.; Schwarz, H.; Riekel, C.; Nicolson, T. *Science* **2003**, *302* (5643), 282–286.

179 Tohse, H.; Saruwatari, K.; Kogure, T.; Nagasawa, H.; Takagi, Y. *Cryst. Growth Des.* **2009**, *9* (11), 4897–4901.

180 He, G.; Gajjeraman, S.; Schultz, D.; Cookson, D.; Qin, C.; Butler, W. T.; Hao, J.; George, A. *Biochemistry* **2005**, *44* (49), 16140–16148.

181 Aizenberg, J.; Tkachenko, A.; Weiner, S.; Addadi, L.; Hendler, G. *Nature* **2001**, *412* (6849), 819–822.

182 Gries, K.; Heinemann, F.; Gummich, M.; Ziegler, A.; Rosenauer, A.; Fritz, M. *Cryst. Growth Des.* **2011**, *11* (3), 729–734.

183 Barthelat, F. *Bioinspir. Biomim.* **2010**, *5* (3), 035001.

184 Heinemann, F.; Treccani, L.; Fritz, M. *Biochem. Biophys. Res. Commun.* **2006**, *344* (1), 45–49.

185 Meyers, M. A.; Lin, A. Y.-M.; Chen, P.-Y.; Muyco, J. *J. Mech. Behav. Biomed. Mater.* **2008**, *1* (1), 76–85.

186 Cusack, M.; Freer, A. *Chem. Rev.* **2008**, *108* (11), 4433–4454.

187 Marin, F.; Luquet, G.; Marie, B.; Medakovic, D. *Curr. Top. Dev. Biol.* **2007**, *80*, 209–276.

188 Marin, F.; Luquet, G. Unusually Acidic Proteins in Biomineralization. In *Handbook of Biomineralization: Biological Aspects and Structure Formation*, Bäeurlein, E., Ed. Wiley-VCH Verlag GmbH: Weinheim, 2008; Vol. 1, pp 273–290.

189 Fu, G.; Qiu, S.; Orme, C.; Morse, D.; De Yoreo, J. J. *Adv. Mater.* **2005**, *17* (22), 2678–2683.

190 Gotliv, B.-A.; Kessler, N.; Sumerel, J. L.; Morse, D. E.; Tuross, N.; Addadi, L.; Weiner, S. *ChemBioChem* **2005**, *6* (2), 304–314.

191 Metzler, R. A.; Evans, J. S.; Killian, C. E.; Zhou, D.; Churchill, T. H.; Appathurai, N. P.; Coppersmith, S. N.; Gilbert, P. U. P. A. *J. Am. Chem. Soc.* **2010**, *132* (18), 6329–6334.

192 Evans, J. S. *Chem. Rev.* **2008**, *108* (11), 4455–4462.

193 Politi, Y.; Mahamid, J.; Goldberg, H.; Weiner, S.; Addadi, L. *CrystEngComm* **2007**, *9* (12), 1171–1177.

194 Nudelman, F.; Gotliv, B. A.; Addadi, L.; Weiner, S. *J. Struct. Biol.* **2006**, *153* (2), 176–187.

195 De Yoreo, J. J.; Dove, P. M. *Science* **2004**, *306* (5700), 1301–1302.

196 Weiner, S. *Calcif. Tissue Int.* **1979**, *29* (1), 163–167.

197 Suzuki, M.; Saruwatari, K.; Kogure, T.; Yamamoto, Y.; Nishimura, T.; Kato, T.; Nagasawa, H. *Science* **2009**, *325* (5946), 1388–1390.

198 Metzler, R. A.; Tribello, G. A.; Parrinello, M.; Gilbert, P. U. P. A. *J. Am. Chem. Soc.* **2010**, *132* (33), 11585–11591.

199 Sarashina, I.; Endo, K. *Am. Mineral.* **1998**, *83* (11–12 Part 2), 1510–1515.

200 Kim, I. W.; Darragh, M. R.; Orme, C.; Evans, J. S. *Cryst. Growth Des.* **2005**, *6* (1), 5–10.

201 Collino, S.; Kim, I. W.; Evans, J. S. *Cryst. Growth Des.* **2006**, *6* (4), 839–842.

202 Keene, E. C.; Evans, J. S.; Estroff, L. A. *Cryst. Growth Des.* **2010**, *10* (3), 1383–1389.

203 Permyakov, E. A.; Kretsinger, R. H. *Calcium Binding Proteins*. John Wiley and Sons, Inc.: Hoboken, New Jersey, 2011.

204 Morse, J. W.; Arvidson, R. S.; Luttge, A. *Chem. Rev.* **2007**, *107* (2), 342–381.

205 Levi-Kalisman, Y.; Raz, S.; Weiner, S.; Addadi, L.; Sagi, I. *Adv. Funct. Mater.* **2002**, *12* (1), 43–48.

206 Sommerdijk, N. A. J. M.; de With, G. *Chem. Rev.* **2008**, *108* (11), 4499–4550.

207 Radha, A. V.; Forbes, T. Z.; Killian, C. E.; Gilbert, P. U. P. A.; Navrotsky, A. *Proc. Natl. Acad. Sci. U. S. A.* **2010**, *107* (38), 16438–16443.

208 Han, T. Y.-J.; Aizenberg, J. *Chem. Mater.* **2007**, *20* (3), 1064–1068.

209 Marsh, M. E. Regulation of Coccolith Calcification in *Pleurochrysis carterae*. In *Handbook of Biomineralization: Biological Aspects and Structure Formation*, Baeuerlein, E., Ed. Wiley-VCH Verlag GmbH: Weinheim, 2008; Vol. 1, pp 211–226.

210 Young, J. R.; Henriksen, K. Biomineralization Within Vesicles: The Calcite of Coccoliths. In *Biomineralization*, Dove, P. M.; De Yoreo, J. J.; Weiner, S., Eds. Mineralogical Society of America: Washington, D.C., 2003; Vol. 54, pp 189–215.

211 Erez, J. The Source of Ions for Biomineralization in Foraminifera and Their Implicationa for Paleoceanographic Proxies. In *Biomineralization*, Dove, P. M.; De Yoreo, J. J.; Weiner, S., Eds. Mineralogical Society of America: Washington, D.C., 2003; Vol. 54, pp 115–149.

212 Allemand, D.; Mayer-Gostan, N.; De Pontual, H.; Boeuf, G.; Payan, P. Fish Otolith Calcification in Relation to Endolymph Chemistry. In *Handbook of Biomineralization: Biological Aspects and Structure Formation*, Baeuerlein, E., Ed. Wiley-VCH Verlag GmbH: Weinheim, 2008; Vol. 1, pp 291–308.

213 Killian, C. E.; Wilt, F. H. *Chem. Rev.* **2008**, *108* (11), 4463–4474.

214 Lowenstam, H. A.; Abbott, D. P. *Science* **1975**, *188* (4186), 363–365.

215 Stanley, S. M. *Chem. Rev.* **2008**, *108* (11), 4483–4498.

216 Peter, K. Calcium carbonate scale control in industrial water systems. In *The Science and Technology of Industrial Water Treatment*, Amjad, Z., Ed. CRC Press: Boca Raton, 2010; pp 39–60.

217 Vetter, O. J.; Farone, W. A.; Veith, E.; Lankford, S. In *Calcium carbonate scale considerations: a practical approach*, SPE Production Technology Symposium, Lubbock, Texas, 16–17 November, 1987; Society of Petroleum Engineers: Lubbock, Texas, 1987; 17009-MS, pp 1–11.

218 MacAdam, J.; Parsons, S. A. *Rev. Environ. Sci. Biotechnol.* **2004**, *3* (2), 159–169.

219 Nancollas, G. H.; Gerard, D.; Zachowicz, W. In *Calcium carbonate scaling. A kinetics and surface energy approach*, CORROSION 2004, New Orleans, LA, March 28 - April 1, 2004; NACE International: New Orleans, LA, 2004; 04072, pp 1–8.

220 Bosselmann, F.; Epple, M. Sulfate-Containing Biominerals. In *Biomineralization: From Nature to Applications*, Sigel, A.; Sigel, H.; Sigel, R. K. O., Eds. John Wiley and Sons, Ltd: Chichester, 2010; Vol. 4, pp 207–217.

221 Krejci, M. R.; Wasserman, B.; Finney, L.; McNulty, I.; Legnini, D.; Vogt, S.; Joester, D. *J. Struct. Biol.* **2011**, *176* (2), 192–202.

222 Benton, W. J.; Collins, I. R.; Grimsey, I. M.; Parkinson, G. M.; Rodger, S. A. *Faraday Discuss.* **1993**, *95*, 281–297.

223 Jones, F.; Jones, P.; Ogden, M. I.; Richmond, W. R.; Rohl, A. L.; Saunders, M. *J. Colloid Interface Sci.* **2007**, *316* (2), 553–561.

224 Jones, F.; Stanley, A.; Oliveira, A.; Rohl, A. L.; Reyhani, M. M.; Parkinson, G. M.; Ogden, M. I. *J. Cryst. Growth* **2003**, *249* (3–4), 584–593.

225 Coveney, P. V.; Davey, R.; Griffin, J. L. W.; He, Y.; Hamlin, J. D.; Stackhouse, S.; Whiting, A. *J. Am. Chem. Soc.* **2000**, *122* (46), 11557–11558.

226 Mavredaki, E.; Neville, A.; Sorbie, K. S. *Cryst. Growth Des.* **2011**, *11* (11), 4751–4758.

227 Fernández-Díaz, L.; Putnis, A.; Prieto, M.; Putnis, C. V. *J. Sediment. Res.* **1996**, *66* (3), 482–491.

228 Falini, G.; Fermani, S.; Tosi, G.; Dinelli, E. *Cryst. Growth Des.* **2009**, *9* (5), 2065–2072.

229 Sánchez-Pastor, N.; Gigler, A. M.; Cruz, J. A.; Park, S.-H.; Jordan, G.; Fernández-Díaz, L. *Cryst. Growth Des.* **2011**, *11* (7), 3081–3089.

230 Söhnel, O.; Mullin, J. W. *J. Cryst. Growth* **1982**, *60* (2), 239–250.

231 Kowacz, M.; Prieto, M.; Putnis, A. *Geochim. Cosmochim. Acta* **2010**, *74* (2), 469–481.

232 Kowacz, M.; Putnis, A. *Geochim. Cosmochim. Acta* **2008**, *72* (18), 4476–4487.

233 Piana, S.; Jones, F.; Taylor, Z.; Raiteri, P.; Gale, J. D. *Mineral. Mag.* **2008**, *72* (1), 273–276.

234 Naka, K.; Chujo, Y. *Chem. Mater.* **2001**, *13* (10), 3245–3259.

235 Gebauer, D.; Verch, A.; Börner, H. G.; Cölfen, H. *Cryst. Growth Des.* **2009**, *9* (5), 2398–2403.

236 Volkmer, D.; Fricke, M.; Huber, T.; Sewald, N. *Chem. Commun.* **2004**, (16), 1872–1873.

237 Kulak, A. N.; Iddon, P.; Li, Y.; Armes, S. P.; Cölfen, H.; Paris, O.; Wilson, R. M.; Meldrum, F. C. *J. Am. Chem. Soc.* **2007**, *129* (12), 3729–3736.

238 Sonnenberg, L.; Luo, Y.; Schlaad, H.; Seitz, M.; Cölfen, H.; Gaub, H. E. *J. Am. Chem. Soc.* **2007**, *129* (49), 15364–15371.

239 Rudloff, J.; Antonietti, M.; Cölfen, H.; Pretula, J.; Kaluzynski, K.; Penczek, S. *Macromol. Chem. Phys.* **2002**, *203* (4), 627–635.

240 Yu, S.-H.; Antonietti, M.; Cölfen, H.; Hartmann, J. *Nano Lett.* **2002**, *3* (3), 379–382.

241 Piana, S.; Jones, F.; Gale, J. D. *CrystEngComm* **2007**, *9* (12), 1187–1191.

242 Xie, A.-J.; Shen, Y.-H.; Zhang, C.-Y.; Yuan, Z.-W.; Zhu, X.-M.; Yang, Y.-M. *J. Cryst. Growth* **2005**, *285* (3), 436–443.

243 Freeman, S. R.; Jones, F.; Ogden, M. I.; Oliviera, A.; Richmond, W. R. *Cryst. Growth Des.* **2006**, *6* (11), 2579–2587.

244 Massi, M.; Ogden, M. I.; Radomirovic, T.; Jones, F. *CrystEngComm* **2010**, *12* (12), 4205–4207.

245 Biot, C.; Bauer, H.; Schirmer, R. H.; Davioud-Charvet, E. *J. Med. Chem.* **2004**, *47* (24), 5972–5983.

246 Sand, K. K.; Rodriguez-Blanco, J. D.; Makovicky, E.; Benning, L. G.; Stipp, S. L. S. *Cryst. Growth Des.* **2012**, *12* (2), 842–853.

247 Malkaj, P.; Dalas, E. *Cryst. Growth Des.* **2004**, *4* (4), 721–723.

248 Manoli, F.; Dalas, E. *J. Cryst. Growth* **2001**, *222* (1–2), 293–297.

249 Wu, C.; Wang, X.; Zhao, K.; Cao, M.; Xu, H.; Xia, D.; Lu, J. R. *Cryst. Growth Des.* **2011**, *11* (7), 3153–3162.

250 Meldrum, F. C.; Hyde, S. T. *J. Cryst. Growth* **2001**, *231* (4), 544–558.

251 Chen, S.-F.; Yu, S.-H.; Wang, T.-X.; Jiang, J.; Cölfen, H.; Hu, B.; Yu, B. *Adv. Mater.* **2005**, *17* (12), 1461–1465.

252 Song, R.-Q.; Xu, A.-W.; Antonietti, M.; Cölfen, H. *Angew. Chem. Int. Ed.* **2009**, *48* (2), 395–399.

253 Aschauer, U.; Ebert, J.; Aimable, A.; Bowen, P. *Cryst. Growth Des.* **2010**, *10* (9), 3956–3963.

254 Aschauer, U.; Spagnoli, D.; Bowen, P.; Parker, S. C. *J. Colloid Interface Sci.* **2010**, *346* (1), 226–231.

255 Naka, K. *Top. Curr. Chem.* **2007**, *271*, 119–154.

256 Young, J. R.; Davis, S. A.; Bown, P. R.; Mann, S. *J. Struct. Biol.* **1999**, *126* (3), 195–215.

257 Naka, K. Ed. Biomineralization II: Mineralization Using Synthetic Polymers and Templates. Special Issue, *Top. Curr. Chem.* **2007**, *271*.

258 Heywood, B. R.; Mann, S. *Adv. Mater.* **1994**, *6* (1), 9–20.

259 van Bommel, K. J. C.; Friggeri, A.; Shinkai, S. *Angew. Chem. Int. Ed.* **2003**, *42* (9), 980–999.

260 Mullin, J. W. *Crystallization*. 4th ed.; Elsevier: London, 2004.

261 Meldrum, F. C.; Wade, V. J.; Nimmo, D. L.; Heywood, B. R.; Mann, S. *Nature* **1991**, *349* (6311), 684–687.

262 Watabe, N.; Bernhardt, A. M.; Kingsley, R. J.; Wilbur, K. M. *Trans. Am. Microsc. Soc.* **1986**, *105* (4), 311–318.

263 Fricke, M.; Volkmer, D. *Top. Curr. Chem.* **2007**, *270*, 1–41.

264 Tremel, W.; Küther, J.; Balz, M.; Loges, N.; Wolf, S. E. Template Surfaces for the Formation of Calcium Carbonate. In *Handbook of Biomineralization*, Behrens, P.; Baeuerlein, E., Eds. Wiley-VCH Verlag GmbH: Weinheim, 2008; Vol. 2, pp 209–232.

265 Popescu, D. C.; Smulders, M. M. J.; Pichon, B. P.; Chebotareva, N.; Kwak, S.-Y.; van Asselen, O. L. J.; Sijbesma, R. P.; DiMasi, E.; Sommerdijk, N. A. J. M. *J. Am. Chem. Soc.* **2007**, *129* (45), 14058–14067.

266 Fricke, M.; Volkmer, D.; Krill, C. E.; Kellermann, M.; Hirsch, A. *Cryst. Growth Des.* **2006**, *6* (5), 1120–1123.

267 Lloyd, D. J. The Problem of Gel Structure. In *Colloid Chemistry*, Alexander, J., Ed. Chemical Catalogue Company: New York, 1926; Vol. 1, pp 767–782.

268 Smith, D. K. *Chem. Soc. Rev.* **2009**, *38* (3), 684–694.

269 Estroff, L. A.; Hamilton, A. D. *Chem. Rev.* **2004**, *104* (3), 1201–1218.

270 de Loos, M.; Feringa, B. L.; van Esch, J. H. *Eur. J. Org. Chem.* **2005**, (17), 3615–3631.

271 Weiss, R. G.; Terech, P., Eds. *Molecular Gels: Materials with Self-Assembled Fibrillar Networks*. Springer: Dordrecht, The Netherlands, 2006.

272 Flory, P. J. *Faraday Discuss. Chem. Soc.* **1974**, *57*, 7–18.

273 Graham, T. *Philos. Trans. R. Soc. London* **1861**, *151*, 183–224.

274 Sangeetha, N. M.; Maitra, U. *Chem. Soc. Rev.* **2005**, *34* (10), 821–836.

275 Blokzijl, W.; Engberts, J. B. F. N. *Angew. Chem. Int. Ed.* **1993**, *32* (11), 1545–1579.

276 Duan, P.; Liu, M. *Langmuir* **2009**, *25* (15), 8706–8713.

277 Frkanec, L.; Žinić, M. *Chem. Commun.* **2010**, *46* (4), 522–537.

278 Yan, N.; He, G.; Zhang, H.; Ding, L.; Fang, Y. *Langmuir* **2009**, *26* (8), 5909–5917.

279 Vioux, A.; Viau, L.; Volland, S.; Le Bideau, J. *C. R. Chim.* **2010**, *13* (1–2), 242–255.

280 Taguchi, S.; Matsumoto, T.; Ichikawa, T.; Kato, T.; Ohno, H. *Chem. Commun.* **2011**, *47* (40), 11342–11344.

281 Reichenauer, G. Aerogels. In *Kirk-Othmer Encyclopedia of Chemical Technology* [Online] John Wiley & Sons, Inc.: Hoboken, N.J., 2000. http://dx.doi.org/10.1002/0471238961.010518151115.a01.pub2.

282 van Esch, J. H.; Feringa, B. L. *Angew. Chem. Int. Ed.* **2000**, *39* (13), 2263–2266.

283 Milanesi, L.; Hunter, C. A.; Tzokova, N.; Waltho, J. P.; Tomas, S. *Chem. Eur. J.* **2011**, *17* (35), 9753–9761.

284 Lin, Y. C.; Weiss, R. G. *Macromolecules* **1987**, *20* (2), 414–417.

285 Babu, P.; Sangeetha, N. M.; Maitra, U. *Macromol. Symp.* **2006**, *241* (1), 60–67.

286 Velázquez, D. G.; Díaz, D. D.; Ravelo, Á. G.; Tellado, J. J. M. *J. Am. Chem. Soc.* **2008**, *130* (25), 7967–7973.

287 Truong, W. T.; Su, Y.; Meijer, J. T.; Thordarson, P.; Braet, F. *Chem. Asian J.* **2011**, *6* (1), 30–42.

288 Zhao, F.; Ma, M. L.; Xu, B. *Chem. Soc. Rev.* **2009**, *38* (4), 883–891.

289 Xu, B. *Langmuir* **2009**, *25* (15), 8375–8377.

290 Lutolf, M. P. *Nat. Mater.* **2009**, *8* (6), 451–453.

291 Hirst, A. R.; Escuder, B.; Miravet, J. F.; Smith, D. K. *Angew. Chem. Int. Ed.* **2008**, *47* (42), 8002–8018.

292 van Esch, J. H. *Langmuir* **2009**, *25* (15), 8392–8394.

293 Dastidar, P. *Chem. Soc. Rev.* **2008**, *37* (12), 2699–2715.

294 Žinić, M.; Vögtle, F.; Fages, F. *Top. Curr. Chem.* **2005**, *256*, 39–76.

295 de Loos, M.; van Esch, J. H.; Kellogg, R. M.; Feringa, B. L. *Tetrahedron* **2007**, *63* (31), 7285–7301.

296 Buerkle, L. E.; Rowan, S. J. *Chem. Soc. Rev.* **2012**, *41* (18), 6089–6102.

297 Ciferri, A., Ed. *Supramolecular Polymers*. 2nd ed.; CRC Press: Boca Raton, Florida, 2005.

298 Brunsveld, L.; Folmer, B. J. B.; Meijer, E. W.; Sijbesma, R. P. *Chem. Rev.* **2001**, *101* (12), 4071–4098.

299 Palma, C.-A.; Cecchini, M.; Samori, P. *Chem. Soc. Rev.* **2012**, *41* (10), 3713–3730.

300 Rehm, T.; Schmuck, C. *Chem. Commun.* **2008**, (7), 801–813.

301 Jung, J. H.; Nakashima, K.; Shinkai, S. *Nano Lett.* **2001**, *1* (3), 145–148.

302 Murata, K.; Aoki, M.; Suzuki, T.; Harada, T.; Kawabata, H.; Komori, T.; Ohseto, F.; Ueda, K.; Shinkai, S. *J. Am. Chem. Soc.* **1994**, *116* (15), 6664–6676.

303 Yamanaka, M.; Haraya, N.; Yamamichi, S. *Chem. Asian J.* **2011**, *6* (4), 1022–1025.

304 Danila, I.; Riobe, F.; Puigmarti-Luis, J.; Perez del Pino, A.; Wallis, J. D.; Amabilino, D. B.; Avarvari, N. *J. Mater. Chem.* **2009**, *19* (26), 4495–4504.

305 Banerjee, S.; Das, R. K.; Maitra, U. *J. Mater. Chem.* **2009**, *19* (37), 6649–6687.

306 Dawn, A.; Shiraki, T.; Haraguchi, S.; Tamaru, S.-i.; Shinkai, S. *Chem. Asian J.* **2011**, *6* (2), 266–282.

307 Lee, K. Y.; Mooney, D. J. *Chem. Rev.* **2001**, *101* (7), 1869–1880.

308 Murdan, S. *Expert Opin. Drug Deliv.* **2005**, *2* (3), 489–505.

309 Hirst, A. R.; Roy, S.; Arora, M.; Das, A. K.; Hodson, N.; Murray, P.; Marshall, S.; Javid, N.; Sefcik, J.; Boekhoven, J.; van Esch, J. H.; Santabarbara, S.; Hunt, N. T.; Ulijn, R. V. *Nature Chem.* **2010**, *2* (12), 1089–1094.

310 Stuart, M. A. C.; Huck, W. T. S.; Genzer, J.; Muller, M.; Ober, C.; Stamm, M.; Sukhorukov, G. B.; Szleifer, I.; Tsukruk, V. V.; Urban, M.; Winnik, F.; Zauscher, S.; Luzinov, I.; Minko, S. *Nat. Mater.* **2010**, *9* (2), 101–113.

311 Díaz Díaz, D.; Kühbeck, D.; Koopmans, R. J. *Chem. Soc. Rev.* **2011**, *40* (1), 427–448.

312 Rodríguez-Llansola, F.; Miravet, J. F.; Escuder, B. *Chem. Eur. J.* **2010**, *16* (28), 8480–8486.

313 Rodríguez-Llansola, F.; Escuder, B.; Miravet, J. F. *J. Am. Chem. Soc.* **2009**, *131* (32), 11478–11484.

314 Liu, W.; Herrmann, A.-K.; Geiger, D.; Borchardt, L.; Simon, F.; Kaskel, S.; Gaponik, N.; Eychmüller, A. *Angew. Chem. Int. Ed.* **2012**, *51* (23), 5743–5747.

315 Moffat, J. R.; Coates, I. A.; Leng, F. J.; Smith, D. K. *Langmuir* **2009**, *25* (15), 8786–8793.

316 Debnath, S.; Shome, A.; Dutta, S.; Das, P. K. *Chem. Eur. J.* **2008**, *14* (23), 6870–6881.

317 Carretti, E.; Bonini, M.; Dei, L.; Berrie, B. H.; Angelova, L. V.; Baglioni, P.; Weiss, R. G. *Acc. Chem. Res.* **2010**, *43* (6), 751–760.

318 Carretti, E.; Dei, L.; Weiss, R. G. *Soft Matter* **2005**, *1* (1), 17–22.

319 Smith, D. K. *Nature Chem.* **2010**, *2* (3), 162–163.

320 de Jong, J.; Feringa, B. L.; van Esch, J. Responsive Molecular Gels. In *Molecular Switches*, 2nd edition ed.; Feringa, B. L.; Browne, W. R., Eds. Wiley-VCH Verlag GmbH & Co. KGaA: Weinheim, Germany, 2011; pp 517–561.

321 Deng, W.; Yamaguchi, H.; Takashima, Y.; Harada, A. *Angew. Chem. Int. Ed.* **2007**, *46* (27), 5144–5147.

322 Piepenbrock, M.-O. M.; Clarke, N.; Foster, J. A.; Steed, J. W. *Chem. Commun.* **2011**, *47* (7), 2095–2097.

323 Piepenbrock, M.-O. M.; Clarke, N.; Steed, J. W. *Langmuir* **2009**, *25* (15), 8451–8456.

324 Piepenbrock, M.-O. M.; Lloyd, G. O.; Clarke, N.; Steed, J. W. *Chem. Rev.* **2009**, *110* (4), 1960–2004.

325 de Jong, J. J. D.; Tiemersma-Wegman, T. D.; van Esch, J. H.; Feringa, B. L. *J. Am. Chem. Soc.* **2005**, *127* (40), 13804–13805.

326 Collier, J. H.; Hu, B. H.; Ruberti, J. W.; Zhang, J.; Shum, P.; Thompson, D. H.; Messersmith, P. B. *J. Am. Chem. Soc.* **2001**, *123* (38), 9463–9464.

327 Matsumoto, S.; Yamaguchi, S.; Ueno, S.; Komatsu, H.; Ikeda, M.; Ishizuka, K.; Iko, Y.; Tabata, K. V.; Aoki, H.; Ito, S.; Noji, H.; Hamachi, I. *Chem. Eur. J.* **2008**, *14* (13), 3977–3986.

328 Ji, Y.; Kuang, G.-C.; Jia, X.-R.; Chen, E.-Q.; Wang, B.-B.; Li, W.-S.; Wei, Y.; Lei, J. *Chem. Commun.* **2007**, (41), 4233–4235.

329 Naota, T.; Koori, H. *J. Am. Chem. Soc.* **2005**, *127* (26), 9324–9325.

330 Kawano, S.-i.; Fujita, N.; Shinkai, S. *J. Am. Chem. Soc.* **2004**, *126* (28), 8592–8593.

331 Lloyd, G. O.; Steed, J. W. *Nature Chem.* **2009**, *1* (6), 437–442.

332 Maeda, H. *Chem. Eur. J.* **2008**, *14* (36), 11274–11282.

333 Amendola, V.; Fabbrizzi, L.; Mosca, L. *Chem. Soc. Rev.* **2010**, *39* (10), 3889–3915.

334 Hay, B. P. *Chem. Soc. Rev.* **2010**, *39* (10), 3700–3708.

335 Steed, J. W. *Chem. Soc. Rev.* **2010**, *39* (10), 3686–3699.

336 Foster, J. A.; PiepenbrockMarc-Oliver, M.; Lloyd, G. O.; Clarke, N.; HowardJudith, A. K.; Steed, J. W. *Nature Chem.* **2010**, *2* (12), 1037–1043.

337 Stanley, C. E.; Clarke, N.; Anderson, K. M.; Elder, J. A.; Lenthall, J. T.; Steed, J. W. *Chem. Commun.* **2006**, (30), 3199–3201.

338 Hsueh, S.-Y.; Kuo, C.-T.; Lu, T.-W.; Lai, C.-C.; Liu, Y.-H.; Hsu, H.-F.; Peng, S.-M.; Chen, C.-h.; Chiu, S.-H. *Angew. Chem. Int. Ed.* **2010**, *49* (48), 9170–9173.

339 Ghosh, A.; Dey, J. *Langmuir* **2009**, *25* (15), 8466–8472.

340 Hwang, I.; Jeon, Woo S.; Kim, H.-J.; Kim, D.; Kim, H.; Selvapalam, N.; Fujita, N.; Shinkai, S.; Kim, K. *Angew. Chem. Int. Ed.* **2007**, *46* (1–2), 210–213.

341 Wood, D. M.; Greenland, B. W.; Acton, A. L.; Rodríguez-Llansola, F.; Murray, C. A.; Cardin, C. J.; Miravet, J. F.; Escuder, B.; Hamley, I. W.; Hayes, W. *Chem. Eur. J.* **2012**, *18* (9), 2692–2699.

342 Zhao, Y.; Yokoi, H.; Tanaka, M.; Kinoshita, T.; Tan, T. *Biomacromolecules* **2008**, *9* (6), 1511–1518.

343 Schneider, J. P.; Pochan, D. J.; Ozbas, B.; Rajagopal, K.; Pakstis, L.; Kretsinger, J. *J. Am. Chem. Soc.* **2002**, *124* (50), 15030–15037.

344 Adams, D. J.; Butler, M. F.; Frith, W. J.; Kirkland, M.; Mullen, L.; Sanderson, P. *Soft Matter* **2009**, *5* (9), 1856–1862.

345 Hamilton, T. D.; Bučar, D.-K.; Baltrusaitis, J.; Flanagan, D. R.; Li, Y.; Ghorai, S.; Tivanski, A. V.; MacGillivray, L. R. *J. Am. Chem. Soc.* **2011**, *133* (10), 3365–3371.

346 Sobczuk, A. A.; Tsuchiya, Y.; Shiraki, T.; Tamaru, S.-i.; Shinkai, S. *Chem. Eur. J.* **2012**, *18* (10), 2832–2838.

347 Percec, V.; Peterca, M.; Yurchenko, M. E.; Rudick, J. G.; Heiney, P. A. *Chem. Eur. J.* **2008**, *14* (3), 909–918.

348 Dawn, A.; Shiraki, T.; Ichikawa, H.; Takada, A.; Takahashi, Y.; Tsuchiya, Y.; Lien, L. T. N.; Shinkai, S. *J. Am. Chem. Soc.* **2011**, *134* (4), 2161–2171.

349 Yang, Z.; Liang, G.; Xu, B. *Acc. Chem. Res.* **2008**, *41* (2), 315–326.

350 Toledano, S.; Williams, R. J.; Jayawarna, V.; Ulijn, R. V. *J. Am. Chem. Soc.* **2006**, *128* (4), 1070–1071.

351 Yang, Z.; Liang, G.; Wang, L.; Xu, B. *J. Am. Chem. Soc.* **2006**, *128* (9), 3038–3043.

352 Yang, Z.; Ho, P.-L.; Liang, G.; Chow, K. H.; Wang, Q.; Cao, Y.; Guo, Z.; Xu, B. *J. Am. Chem. Soc.* **2007**, *129* (2), 266–267.

353 Hamley, I. W. *Introduction to Soft Matter: Polymers, Colloids, Amphiphiles and Liquid Crystals*. John Wiley and Sons, Ltd: Chichester, 2000.

354 Smith, D. K. Molecular Gels – Nanostructured Soft Materials. In *Organic Nanostructures*, Atwood, J. L.; Steed, J. W., Eds. Wiley-VCH Verlag GmbH and Co. KGaA: Weinheim, 2008; pp 111–154.

355 Raghavan, S. R.; Cipriano, B. H. Gel Formation: Phase Diagrams Using Tabletop Rheology and Calorimetry. In *Molecular gels: materials with self-assembled fibrillar networks*, Weiss, R. G.; Terech, P., Eds. Springer: Dordrecht, The Netherlands, 2006; pp 241–252.

356 van Esch, J. H.; Schoonbeek, F.; de Loos, M.; Kooijman, H.; Spek, A. L.; Kellogg, R. M.; Feringa, B. L. *Chem. Eur. J.* **1999**, *5* (3), 937–950.

357 Takahashi, A.; Sakai, M.; Kato, T. *Polym. J. (Tokyo, Jpn.)* **1980**, *12* (5), 335–341.

358 Berova, N.; Nakanishi, K.; Woody, R. W., Eds. *Circular Dichroism: Principles and Applications*. 2nd ed.; John Wiley and Sons, Inc: Chichester, 2000.

359 Salvadori, P.; Di Bari, L.; Rosini, C. Electronic Circular Dichroism—Fundamentals, Methods, and Applications. In *Chirality in Natural and Applied Science*, Lough, W. J.; Wainer, I. W., Eds. Blackwell Science, Ltd: Oxford, 2002; pp 203–239.

360 Snatzke, G. Circular Dichroism: An Introduction. In *Circular Dichroism: Principles and Applications*, 2nd ed.; Berova, N.; Nakanishi, K.; Woody, R. W., Eds. John Wiley and Sons, Inc: Chichester, 2000; pp 1–35.

361 Sreerama, N.; Woody, R. W. Circular Dichroism of Peptides and Proteins. In *Circular Dichroism: Principles and Applications*, 2nd ed.; Berova, N.; Nakanishi, K.; Woody, R. W., Eds. John Wiley and Sons, Inc: Chichester, 2000; pp 601–620.

362 Gottarelli, G.; Lena, S.; Masiero, S.; Pieraccini, S.; Spada, G. P. *Chirality* **2008**, *20* (3–4), 471–485.

363 Hirst, A. R.; Miravet, J. F.; Escuder, B.; Noirez, L.; Castelletto, V.; Hamley, I. W.; Smith, D. K. *Chem. Eur. J.* **2009**, *15* (2), 372–379.

364 Pham, Q. N.; Brosse, N.; Frochot, C.; Dumas, D.; Hocquet, A.; Jamart-Gregoire, B. *New J. Chem.* **2008**, *32* (7), 1131–1139.

365 Tam, A. Y.-Y.; Wong, K. M.-C.; Yam, V. W.-W. *Chem. Eur. J.* **2009**, *15* (19), 4775–778.

366 Brizard, A.; Oda, R.; Huc, I. *Top. Curr. Chem.* **2005**, *256*, 167–218.

367 Li, Y.; Wang, T.; Liu, M. *Soft Matter* **2007**, *3* (10), 1312–1317.

368 de Jong, J. J. D.; Lucas, L. N.; Kellogg, R. M.; van Esch, J. H.; Feringa, B. L. *Science* **2004**, *304* (5668), 278–281.

369 Tu, T.; Fang, W.; Bao, X.; Li, X.; Dötz, K. H. *Angew. Chem. Int. Ed.* **2011**, *50* (29), 6601–6605.

370 Okano, K.; Arteaga, O.; Ribo, J. M.; Yamashita, T. *Chem. Eur. J.* **2011**, *17* (34), 9288–9292.

371 Eaton, P.; West, P. *Atomic Force Microscopy*. Oxford University Press: Oxford, 2010.

372 Kar, T.; Debnath, S.; Das, D.; Shome, A.; Das, P. K. *Langmuir* **2009**, *25* (15), 8639–8648.

373 Shirakawa, M.; Fujita, N.; Shinkai, S. *J. Am. Chem. Soc.* **2005**, *127* (12), 4164–4165.

374 Adhikari, B.; Palui, G.; Banerjee, A. *Soft Matter* **2009**, *5* (18), 3452–3460.

375 Kuroiwa, K.; Shibata, T.; Takada, A.; Nemoto, N.; Kimizuka, N. *J. Am. Chem. Soc.* **2004**, *126* (7), 2016–2021.

376 Wang, R.; Geiger, C.; Chen, L.; Swanson, B.; Whitten, D. G. *J. Am. Chem. Soc.* **2000**, *122* (10), 2399–2400.

377 Ikeda, M.; Ochi, R.; Wada, A.; Hamachi, I. *Chem. Sci.* **2010**, *1* (4), 491–498.

378 Grigorieff, N.; Harrison, S. C. *Curr. Opin. Struct. Biol.* **2011**, *21* (2), 265–273.

379 Hryc, C. F.; Chen, D.-H.; Chiu, W. *Curr. Opin. Virol.* **2011**, *1* (2), 110–117.

380 Sander, B.; Golas, M. M. *Microsc. Res. Tech.* **2011**, *74* (7), 642–663.

381 Höög, J. L.; Bouchet-Marquis, C.; McIntosh, J. R.; Hoenger, A.; Gull, K. *J. Struct. Biol.* **2012**, *178* (2), 189–198.

382 Lacomble, S.; Vaughan, S.; Gadelha, C.; Morphew, M. K.; Shaw, M. K.; McIntosh, J. R.; Gull, K. *J. Cell Sci.* **2009**, *122* (8), 1081–1090.

383 Downing, K. H.; Sui, H.; Auer; Manfred *Anal. Chem.* **2007**, *79* (21), 7949–7957.

384 Friedrich, H.; Frederik, P. M.; de With, G.; Sommerdijk, N. A. J. M. *Angew. Chem. Int. Ed.* **2010**, *49* (43), 7850–7858.

385 Besenius, P.; van den Hout, K. P.; Albers, H. M. H. G.; de Greef, T. F. A.; Olijve, L. L. C.; Hermans, T. M.; de Waal, B. F. M.; Bomans, P. H. H.; Sommerdijk, N. A. J. M.; Portale, G.; Palmans, A. R. A.; van Genderen, M. H. P.; Vekemans, J. A. J. M.; Meijer, E. W. *Chem. Eur. J.* **2011**, *17* (18), 5193–5203.

386 Besenius, P.; Goedegebure, Y.; Driesse, M.; Koay, M.; Bomans, P. H. H.; Palmans, A. R. A.; Dankers, P. Y. W.; Meijer, E. W. *Soft Matter* **2011**, *7* (18), 7980–7983.

387 Levi-Kalisman, Y.; Falini, G.; Addadi, L.; Weiner, S. *J. Struct. Biol.* **2001**, *135* (1), 8–17.

388 Dey, A.; Bomans, P. H. H.; Müller, F. A.; Will, J.; Frederik, P. M.; de With, G.; Sommerdijk, N. A. J. M. *Nat. Mater.* **2010**, *9* (12), 1010–1014.

389 Jung, J. H.; Shinkai, S. *Top. Curr. Chem.* **2004**, *248*, 401–411.

390 Yashima, E.; Maeda, K.; Nishimura, T. *Chem. Eur. J.* **2004**, *10* (1), 42–51.

391 van Gestel, J.; Palmans, A. R. A.; Titulaer, B.; Vekemans, J. A. J. M.; Meijer, E. W. *J. Am. Chem. Soc.* **2005**, *127* (15), 5490–5494.

392 Nam, S. R.; Lee, H. Y.; Hong, J.-I. *Chem. Eur. J.* **2008**, *14* (20), 6040–6043.

393 van Gorp, J. J.; Vekemans, J. A. J. M.; Meijer, E. W. *J. Am. Chem. Soc.* **2002**, *124* (49), 14759–14769.

394 Smulders, M. M. J.; Schenning, A. P. H. J.; Meijer, E. W. *J. Am. Chem. Soc.* **2007**, *130* (2), 606–611.

395 Smulders, M. M. J.; Stals, P. J. M.; Mes, T.; Paffen, T. F. E.; Schenning, A. P. H. J.; Palmans, A. R. A.; Meijer, E. W. *J. Am. Chem. Soc.* **2009**, *132* (2), 620–626.

396 Mateos-Timoneda, M. A.; Crego-Calama, M.; Reinhoudt, D. N. *Chem. Soc. Rev.* **2004**, *33* (6), 363–372.

397 Hirst, Andrew R.; Huang, B.; Castelletto, V.; Hamley, Ian W.; Smith, David K. *Chem. Eur. J.* **2007**, *13* (8), 2180–2188.

398 Moffat, J. R.; Smith, D. K. *Chem. Commun.* **2009**, (3), 316–318.

399 Cicchi, S.; Ghini, G.; Lascialfari, L.; Brandi, A.; Betti, F.; Berti, D.; Baglioni, P.; Di Bari, L.; Pescitelli, G.; Mannini, M.; Caneschi, A. *Soft Matter* **2010**, *6* (8), 1655–1661.

400 Zhan, C.; Wang, J.; Yuan, J.; Gong, H.; Liu, Y.; Liu, M. *Langmuir* **2003**, *19* (22), 9440–9445.

401 Maitra, U.; Kumar Potluri, V.; Sangeetha, N. M.; Babu, P.; Raju, A. R. *Tetrahedron: Asymmetry* **2001**, *12* (3), 477–480.

402 Hirst, A. R.; Smith, D. K.; Feiters, M. C.; Geurts, H. P. M. *Chem. Eur. J.* **2004**, *10* (23), 5901–5910.

403 Lin, J. B.; Dasgupta, D.; Cantekin, S.; Schenning, A. P. H. J. *Beilstein J. Org. Chem.* **2010**, *6*, 960–965.

404 Becerril, J.; Escuder, B.; Miravet, J. F.; Gavara, R.; Luis, S. V. *Eur. J. Org. Chem.* **2005**, *2005* (3), 481–485.

405 Džolić, Z.; Wolsperger, K.; Žinić, M. *New J. Chem.* **2006**, *30* (10), 1411–1419.

406 Friggeri, A.; Van der Pol, C.; Van Bommel, K. J. C.; Heeres, A.; Stuart, M. C. A.; Feringa, B. L.; Van Esch, J. *Chem. Eur. J.* **2005**, *11* (18), 5353–5361.

407 Watanabe, Y.; Miyasou, T.; Hayashi, M. *Org. Lett.* **2004**, *6* (10), 1547–1550.

408 Jung, J. H.; Park, M.; Shinkai, S. *Chem. Soc. Rev.* **2010**, *39* (11), 4286–4302.

409 Yang, M.; Kotov, N. A. *J. Mater. Chem.* **2011**, *21* (19), 6775–6792.

410 Delclos, T.; Aimé, C.; Pouget, E.; Brizard, A.; Huc, I.; Delville, M.-H.; Oda, R. *Nano Lett.* **2008**, *8* (7), 1929–1935.

411 Aggeli, A.; Nyrkova, I. A.; Bell, M.; Harding, R.; Carrick, L.; McLeish, T. C.; Semenov, A. N.; Boden, N. *Proc. Natl. Acad. Sci. U. S. A.* **2001**, *98* (21), 11857–11862.

412 Ajayaghosh, A.; Praveen, V. K. *Acc. Chem. Res.* **2007**, *40* (8), 644–656.

413 Sumiyoshi, T.; Nishimura, K.; Nakano, M.; Handa, T.; Miwa, Y.; Tomioka, K. *J. Am. Chem. Soc.* **2003**, *125* (40), 12137–12142.

414 Das, R. K.; Kandanelli, R.; Linnanto, J.; Bose, K.; Maitra, U. *Langmuir* **2010**, *26* (20), 16141–16149.

415 Bao, C.; Jin, M.; Lu, R.; Song, Z.; Yang, X.; Song, D.; Xu, T.; Liu, G.; Zhao, Y. *Tetrahedron* **2007**, *63* (31), 7443–7448.

416 Koshima, H.; Moritoki, T.; Uenaka, K.; Yanase, I. *Supramol. Chem.* **2009**, *21* (5), 367–371.

417 Oda, R.; Huc, I.; Candau, S. J. *Angew. Chem. Int. Ed.* **1998**, *37* (19), 2689–2691.

2 Synthesis and characterisation of calixarenes

2.1 Amino acid-functionalised calixarenes

There are many strategies for functionalising calixarenes.[1, 2] The vast majority of the literature involves attachment at the wide-rim (particularly at the position *para* to the phenol) or narrow-rim of calixarenes. Functionalisation of calixarenes at the methylene bridges has also been reported but to a lesser extent.[3–5] Details and specific examples are provided in section 1.1.

2.1.1 Anchoring amino acids to calix[4]arenes via an amide linkage

A reliable method of attaching amino acids and peptides to calixarenes is via an amide linkage. Amino acids and peptides can be linked through the amine (N-linked) or the carboxylic acid (C-linked) groups. The choice of whether an amino acid is N- or C-linked to the calixarene will depend on the desired chemistry. In this case the interest is in having free carboxylate groups, thus aspartic acid, glutamic acid, and iminodiacetic acid were N-linked to the calix[4]arene at the wide-rim. There are many strategies available[6] for amide bond formation and peptide coupling including more novel approaches.[7] Generally, a carboxylic acid group is introduced on to the calix[4]arene (refer to section 1.1.4.2 for methods of introducing carboxylic acid groups at the wide-rim of calixarenes) then converted to an acid chloride and coupled with the C-protected amino acid. Alternatively, the carboxylic acid can be directly coupled with C-protected amino acid using peptide coupling reagents (Scheme 2.1). Both direct and indirect routes can be applied to carboxylic acid groups at the wide- and narrow-rims.

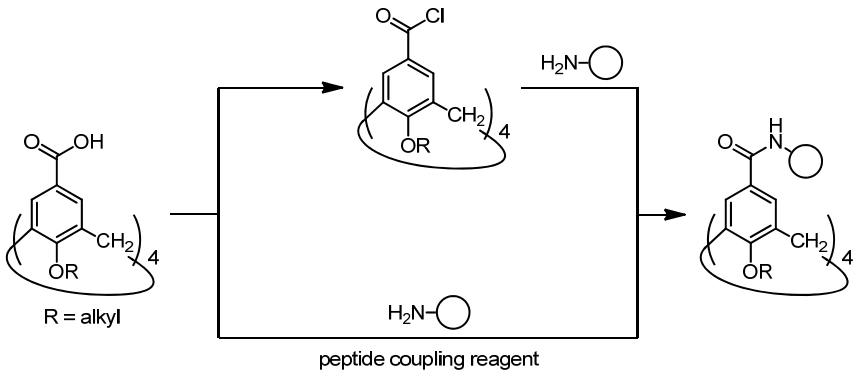

Scheme 2.1 General scheme for attaching N-linked amino acids and peptides via an amide linkage to a calix[4]arene. Here the circle represents an amino acid or peptide.

The formation of an amide via an acid chloride is accomplished in a two-step reaction. The acid halide is readily prepared by a reaction between the carboxylic acid and an acid halogenation reagent (Scheme 2.2). The most common reagents used for preparing acid chlorides at the wide-rim are thionyl chloride[8–10] and oxalyl chloride with a catalytic amount of DMF[11–13] (Figure 2.1). *N*,*N*-Diethylaminosulfur trifluoride (DAST) has also been used to prepare an acid fluoride.[14] The acid halide and the amine component are then coupled in the presence of a non-nucleophilic base to give the amide (Scheme 2.2).[8, 11–13] For example, Tsuo et al.[12] prepared a series of amino acid functionalised calix[4]arenes (Figure 1.23) to test for biological activity against HIV and hepatitis C by coupling the acid chloride calix[4]arene (prepared from oxalyl chloride/DMF) with C-protected amino acids in the presence of triethylamine. Using a similar strategy, Moridi et al.[11] prepared amphiphilic calix[4]arenes by coupling the calixarene acid chloride with the regioisomers of aminophenol in the presence of pyridine. Using a different base, Troisi et al.[15] coupled carboxylic acid calix[4]arene **92** with a 1,4-diaminobenzene fragment in the presence of 4-(*N*,*N*-dimethylamino)pyridine (DMAP), Scheme 2.3, to give the amide **93a**,**b**.

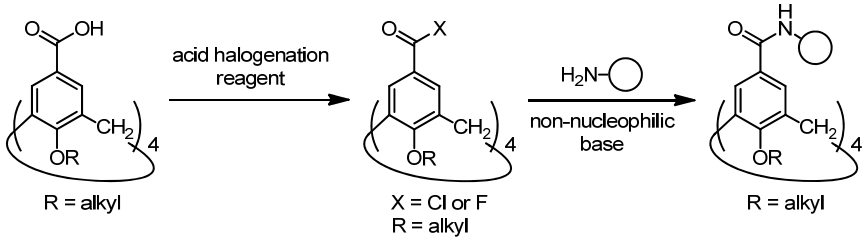

Scheme 2.2 General reaction scheme for the attachment of an amino acid or peptide to a calix[4]-arene via an acid halide.

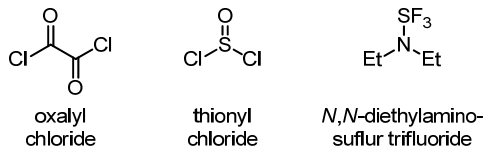

Figure 2.1 Acid halogenation reagents used to form acid halide calixarenes at the wide-rim reported in literature. Refer to main text for more details.

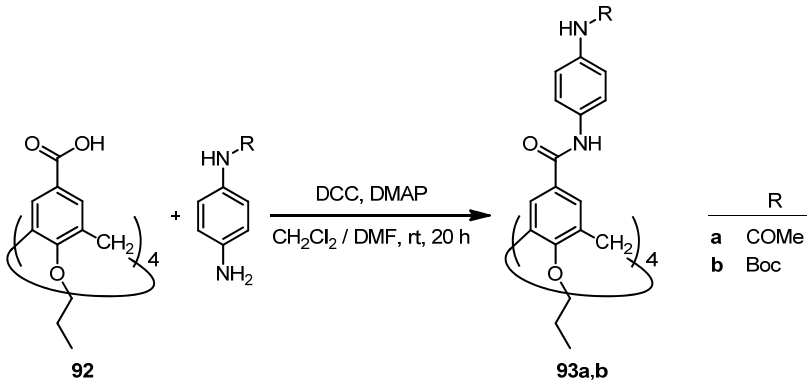

Scheme 2.3 Amide bond formed between a carboxylic acid and 1,4-diaminobenzene derivatives.[15]

A more direct method for amide formation can be found in peptide coupling chemistry. This section will focus on peptide coupling reagents (Figure 2.2) reported in the literature for preparing amide linkages at the wide-rim of calixarenes. The reader is directed to recent reviews[16–19] for general information on peptide coupling reagents. Sansone et al.[20] investigated various methods of attaching amino acids and short peptides to calix[4]arene **92** (Scheme 2.4). The coupling reagent *N*,*N*'-dicyclohexylcarbodiimide (DCC), Figure 2.1, was used to prepare activated esters with 1-hydroxybenzotriazole (HOBt) or *N*-hydroxysuccinimide (HOSu) and the carboxylic acids (Scheme 2.5). The activated esters are then reacted with the amino acids or peptides to give the amide product. Preparations using DCC/HOBt gave a 35% yield while DCC/HOSu gave 33% yield. These yields improved to 60% when *O*-(benzotriazol-1-yl)-*N*,*N*,*N*',*N*'-bis(pentamethylen)uronium tetrafluoroborate (TBPU) was used. An alternative coupling reagent, *O*-(benzotriazol-1-yl)-*N*,*N*,*N'*,*N'*-tetramethyluronium hexafluorophosphate (HTBU), was used to prepare distal N-linked and C-linked amides (Scheme 2.6) with 40–70% yields.[21] Another coupling reagent, benzotriazol-1-yloxytripyrrolidinophosphonium hexafluorophosphate (PyBOP), was found to give a good yield (~80%) when used to couple two alanine amino acids to proximal positions on a calix[4]arene.[22] In comparison, the indirect acid chloride

method investigated by Sansone et al.[20] gave overall yields of 60%. Alternatively, Phipps and Beer[23] prepared the active ester **99** from calix[4]arene **98** using DCC and perfluorophenol (PFP), Scheme 2.7, which gave a purified yield of 85%. Coupling **99** with amine **100** gave amide **101** with a purified yield of 50%. Although the direct coupling of the carboxylic acid and amine can give better yields than indirect methods, they tend to require expensive coupling reagents.

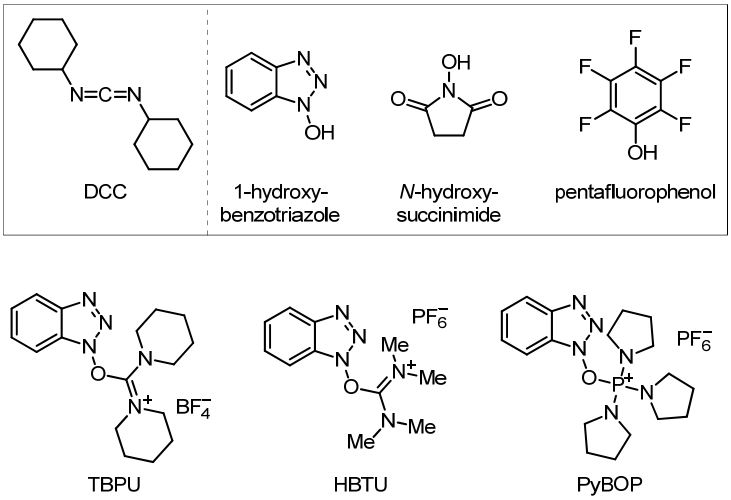

Figure 2.2 Examples of peptide coupling reagents used for preparing amides at the wide-rim.[20, 21, 23] DCC is often used with an additive to prepare an 'active ester' which is then coupled with the amine.

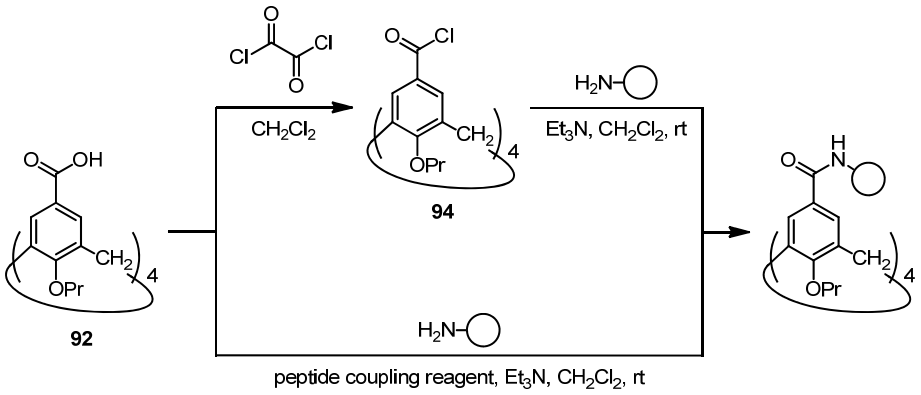

Scheme 2.4 Methods used by Sansone et al.[20] and Baldini et al.[21] for attaching C-protected amino acids and short peptides (represented by the circle) to calix[4]arene **92**.

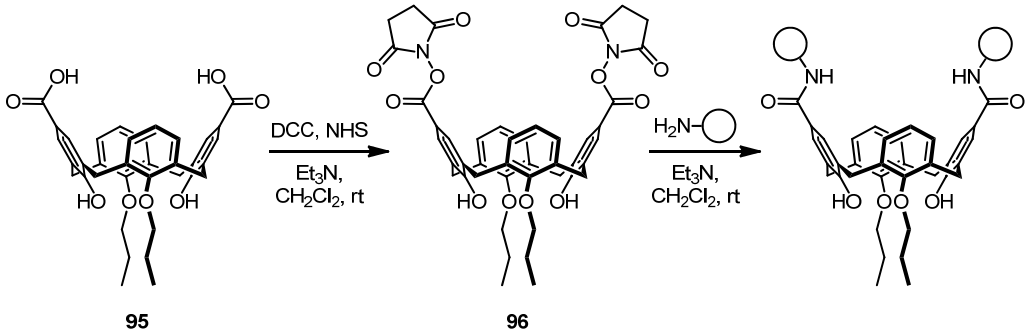

95 **96**

Scheme 2.5 Preparation of activated ester using DCC and HOSu then coupling with amino acid or peptide.[20]

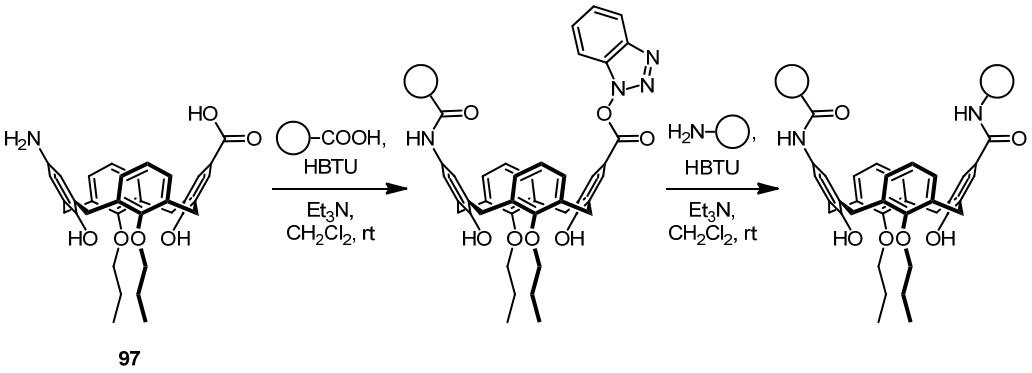

97

Scheme 2.6 Preparation of N-linked and C-linked amides by Baldini et al.[21]

Schadël et al.[24] attached aminoglucose derivatives to distal positions on calix[4]-arenes with an amide linkage. The authors found that the direct attachment of the aminoglucoside to the calix[4]arene **95** using HBTU/Et_3N did not proceed due to steric hindrance between the carboxylic acid and the aminoglucoside, thus they introduced spacer groups (Scheme 2.8). One of the spacers, L-aspartic acid, was introduced onto the calixarene using HBTU/Et_3N with subsequent coupling of the aminoglycoside to the L-aspartic acid spacer. The overall yield was 68% for **103b** when the carboxylic acid calixarene **95** was coupled to the spacer-attached glycoside. However, the authors found that the reaction between calix[4]arene **102** and the aminoglycoside gave a complex mixture and the desired calix[4]arenes **103a**,**b** could not be isolated.

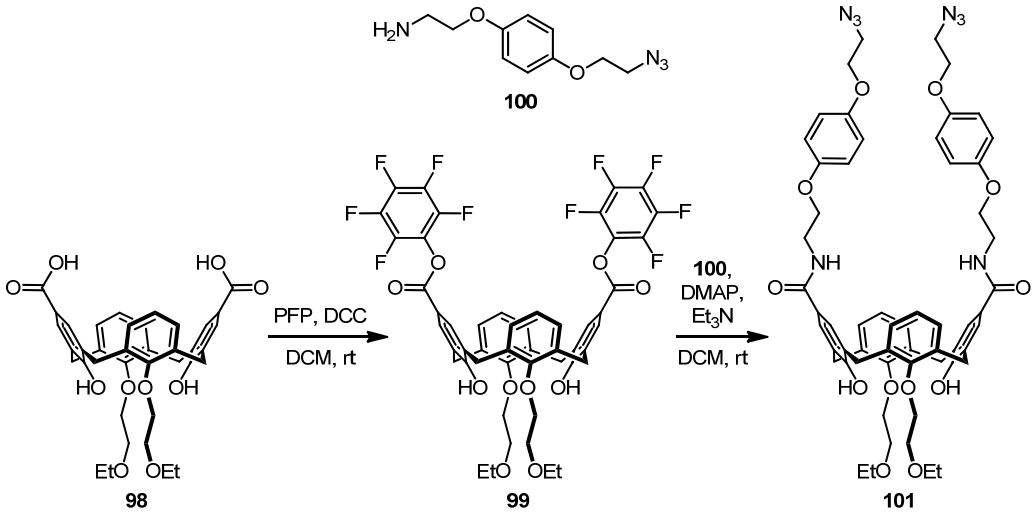

Scheme 2.7 Preparation of activated ester using DCC and PFP then coupling with amine **100**.[23]

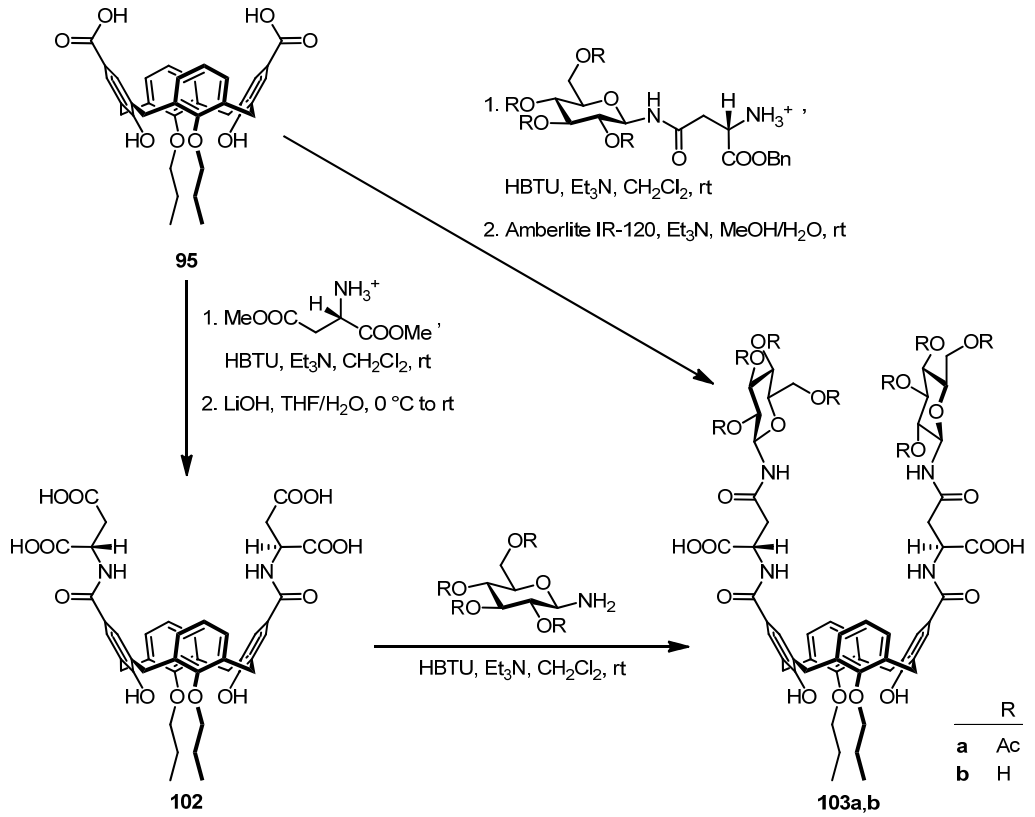

Scheme 2.8 Attachment of aminoglycoside to distal positions on calix[4]arene with an L-aspartic acid spacer.[24]

2.1.2 Attachment of amino acids to calix[4]arenes by aminomethylation

Where an amide is not desired, amines and amino acids can be attached to the wide-rim of calixarenes via a methylene. General methods to achieve this at the wide-rim of calixarenes include the Mannich reaction and halomethylation followed by a nucleophilic substitution of the halide (Scheme 2.9).

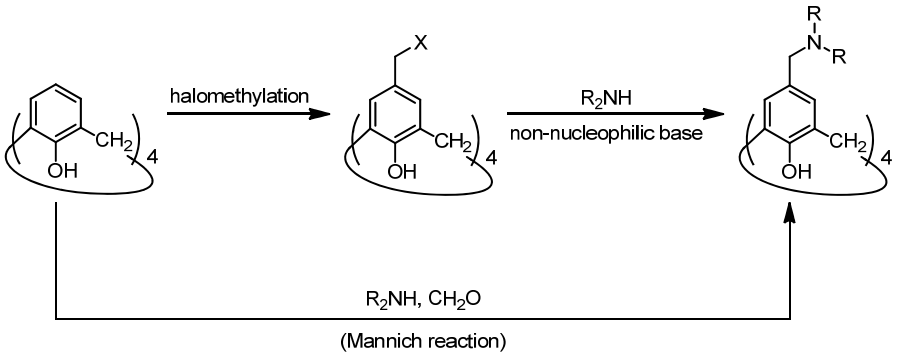

Scheme 2.9 General scheme for attaching amino acids to calixarenes via methylene linkage.

Halomethylation followed by nucleophilic substitution has been utilised for functionalisation of calixarenes at the wide-rim. Yang et al.[25] bromomethylated calix[4]arene **2** using paraformaldehyde and AcOH/HBr then investigated nucleophilic substitution of bromomethylated **104** by a variety of nucleophiles including small alcohols (e.g. MeOH), thiols (e.g. PhSH), and carboxylic acids (e.g. AcOH), Scheme 2.10. The authors achieved nucleophilic substitutions with yields of 75–85% for calixarene **106**. Cho et al.[26] prepared an amphiphilic calix[4]arene using a similar strategy (Scheme 2.11). They chloromethylated the calix[4]arene using chloromethyl octyl ether then substituted the chloride for D-alanine ethyl ester in the presence of triethylamine. The substitution step was achieved with a product yield of 48%. Further alkylation of the phenol with 1-bromododecane and deprotection gave the amphiphile **108**.

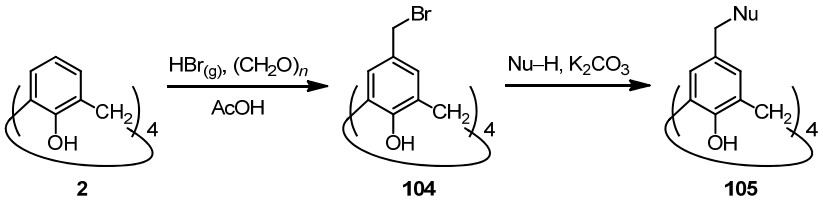

Scheme 2.10 Bromomethylation followed by nucleophilic substitution of bromomethylcalix[4]arene **104** by Yang et al.[25] The authors investigated various nucleophiles (Nu) including small alcohols, thiols, and carboxylic acids.

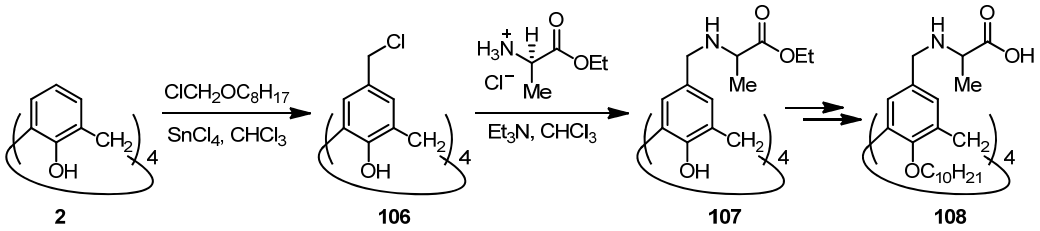

Scheme 2.11 Attachment of C-protected alanine to calix[4]arene.[26]

The Mannich reaction[27, 28] is a reaction between a C–H activated compound (such as a phenol), a primary or secondary amine, and a non-enolisable aldehyde or ketone.[29] The Mannich reaction is not limited to just amines. The review by Agababyan et al.[30] showed that amino acids could be used as the amine component in a variety of Mannich reactions. Gutsche and Nam[31] have previously prepared Mannich bases (**109a**–**e**) from calixarenes and secondary amines (Scheme 2.12). This method was extended to functionalisation of calixarenes with piperazine-based compounds.[32, 33]

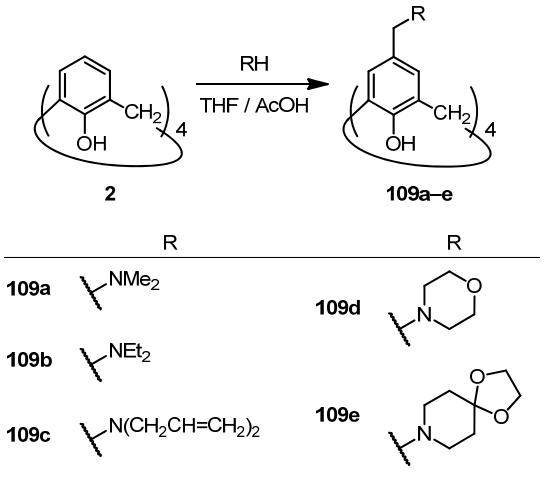

Scheme 2.12 Selected calix[4]arene Mannich prepared by Gutsche and Nam.[31]

Gutsche and Nam[31] also found that quaternising the Mannich adducts **109** with methyl iodide (without alkylation of the phenols) allowed for nucleophilic displacement of the ammonium moiety by a nucleophile (via a *p*-quinonemethide intermediate). Gutsche and Alam[34, 35] later applied this method to attach 2-ethylcarboxy moieties to the wide-rim of calix[*n*]arenes (*n* = 5–8) and these calix[*n*]arenes were investigated for complexation of aromatic hydrocarbons and catalytic studies. Interestingly, Cho et al.[26] were able to alkylate calix[4]arene **107** (Scheme 2.11) in the presence of NaH with no reported displacement of the alanine moiety from the calix[4]arene.

A similar reaction to the Mannich reaction, reductive amination, has also been applied to calixarenes. Shirakawa et al.[36] prepared inherently chiral calix[4]arenes (**112**) by reductive amination between a monoformylated calix[4]arene (**110**) and selected amines (Scheme 2.13). The chiral calixarenes (**112**) were then investigated as catalysts for Michael-type addition reactions and chiral NMR resolution of mandelic acid.

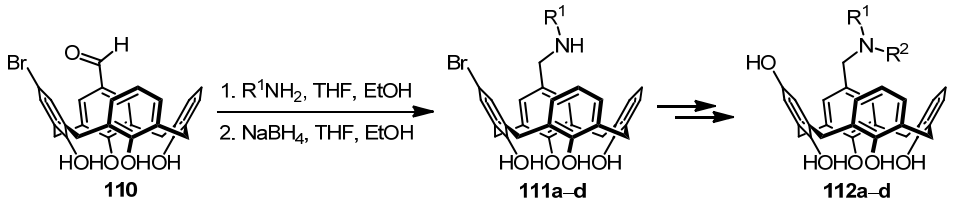

	R^1	R^2
112a	Bu	Bu
112b	Bn	Et
112c	*p*-MeO-$C_6H_4CH_2$	Et
112d	*p*-F_3C-$C_6H_4CH_2$	Et

Scheme 2.13 Reductive amination between monoformylcalix[4]arene **110** and selected amines.[36]

Resorcinarenes have also been used as the C–H active compound in Mannich reactions. Of particular interest are those which involve amino acids as the amine component. Sulfonated resorcinarene **113** was used as the scaffold for preparing a variety of water soluble aminomethylated resorcinarenes (**114a**–**i**). The reaction proceeded under Mannich conditions in the presence of resorcinarene **113**, aqueous formaldehyde, and the amine compound (Scheme 2.14) without the need for an added protic acid catalyst (unlike with calix[4]arenes, Scheme 2.12). Matsushita and

Matsui[37] reported a method for aminomethylation of resorcinarene **113** under Mannich conditions which gave good yields (64–83%); this included D-proline (not shown) and L-proline resorcinarene **114a**. Wenzel et al.[38–41] later extended this method to various proline derivatives (**114a**–**e**), pyrrolidine (**114f**) and piperidine derivatives, and other amino acids (**114g**–**i**) for the preparation of potential chiral NMR resolving agents. Wenzel et al.[38–41] reported yields of 95% for **114a**–**d,f** with the exception of **114e** (yield of 29% after a reaction time of two weeks or more under 'classical' Mannich conditions). Other proline (**116a**) and sarcosine (**116b**) functionalised resorcinarenes have been prepared in the presence of acetic acid with yields of 78% and 83% respectively (Scheme 2.15).[42]

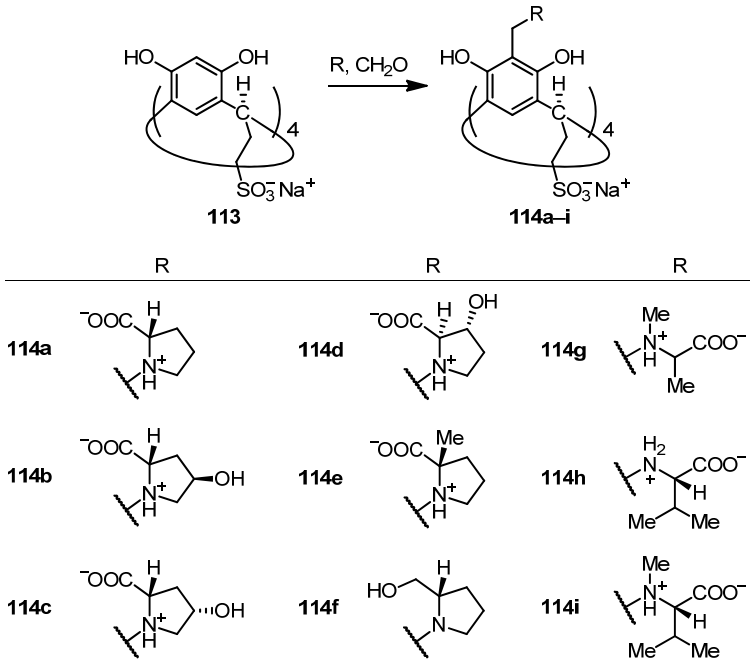

Scheme 2.14 Selected aminomethylated resorcinarenes prepared by the Mannich reaction.[38–41]

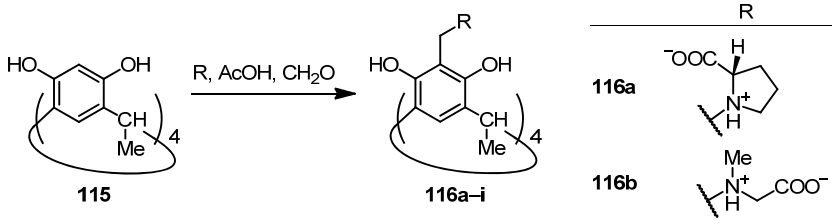

Scheme 2.15 Proline and sarcosine functionalised resorcin[4]arenes prepared by Schnieder and Schnieder.[42]

Despite the good yields reported, some amine compounds may require much longer reaction times[39] to give a Mannich base with resorcinarenes while other amines[38] do not give a Mannich base. Thus far, the examples of octahydroxyresorcinarenes are sufficiently acidic to undergo Mannich reactions in the absence of added protic acid catalysts. If the acidity of the resorcinarene is reduced (such as with **117**), the Mannich reaction will not proceed at room temperature (under the so called 'classical' condition). Despite this, Buckley et al.[43, 44] and Schmidt et al.[45] were able to prepare chiral resorcinarenes in the absence of a protic acid catalyst; of particular interest is the preparation of benzoxazines by a double Mannich reaction. The racemic benzoxazine **118** was not obtained under 'classic' Mannich conditions at room temperature, however good yields were achieved by heating the reaction at reflux in toluene (**118** obtained in 74% yield) or by pre-forming the iminium intermediate and then heating the reaction at reflux in 1,2-dichloroethane (**118** obtained in 80% yield), Scheme 2.16.[43] A similar yield was obtained by microwave-assisted reactions (**118** obtained in 82% yield), however this was achieved with a much shorter reaction time. Although the 'classic' Mannich reaction can give aminomethylated products readily under mild conditions, it may sometimes require encouragement.

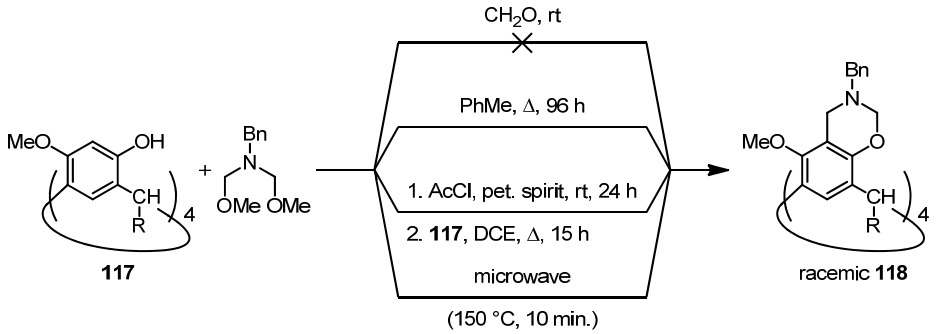

Scheme 2.16 Preparation of aminomethylated chiral resorcinarenes.[43]

2.2 Preparation of amino acid-functionalised calixarenes for crystal growth modification

2.2.1 Inspiration for amino acid-functionalised calix[4]arenes

In this work, wide-rim analogues of narrow-rim substituted calix[4]arenes **143** and **144** (refer to section 3.1.2) were prepared with the aim of investigating their impact on calcium carbonate and barium sulfate crystallisation. The wide-rim analogues are expected to have a different spatial arrangement of the attached amino acids, therefore altering their crystal growth modification behaviour relative to the narrow-rim derivatives. The acidic amino acids were attached to the calix[4]arene via an amide linkage. Another analogue of **143** was prepared by substituting L-aspartic acid for iminodiacetic acid; the L-aspartic acid derivative is linked by a secondary amide while the iminodiacetate is linked by a tertiary amide.

2.2.2 Building the calixarene scaffold

The calixarene scaffold was readily prepared by literature methods (see Scheme 2.17). The parent *p-tert*-butylcalix[4]arene (**1**) was synthesised according to the method by Gutsche;[46] the ^{1}H NMR spectrum and mp were consistent with Gutsche's data. To allow functionalisation at the wide-rim, the *tert*-butyl group was removed[47] by a Friedel-Crafts dealkylation[48] with $AlCl_3$ (Lewis acid) to give **2**. The absence of the *tert*-butyl group and appearance of doublet and triplet (integrating for two and one proton(s) respectively) in the aromatic region of the ^{1}H NMR confirmed this. The phenols of **2** were alkylated[49] with propyl bromide in the presence of a catalytic amount of imidazole and excess sodium hydride. The absence of the O–H stretch in the IR spectrum confirmed that tetraalkylation was achieved. Alkylation of the phenols served two functions: (i) protection of phenols in subsequent steps and (ii) immobilisation of the calix[4]arene **28** in a cone conformer.[50]

The calix[4]arenes were confirmed to be in the cone conformation by NMR spectroscopy. Two doublets in the ^{1}H NMR spectrum at ~4.5 ppm and 3.3 ppm (Ar–CH_2–Ar) indicates that the calix[4]arenes are in a cone conformation. The other calix[4]arene conformers have recognisable patterns for the protons on the methylene bridge.[51] This is further supported by the ^{13}C NMR spectrum of Ar–CH_2–Ar (δ approximately 31 ppm) which is consistent with a set of 'rules' proposed by de

Mendoza.[52] The conformation of the calixarene can be determined by the ^{13}C chemical shift of the Ar–CH_2–Ar carbon in the ^{13}C NMR spectrum (calixarenes in the partial cone or 1,3-alternate conformations have ^{13}C chemical shifts at ~37 ppm). This effect is independent of substituents at the *para*-position or the phenolic group and solvent.[53]

The amino acids were to be attached to the calix[4]arene via the amine group with an amide linkage, so a carboxylic acid group was introduced on the wide-rim of the calix[4]arene. The *para* position of **28** was readily formylated[49, 54] by a Duff reaction[55] to give **119** and selectively oxidised under mild conditions[49, 56] to the tetracarboxylic acid **92**. The formyl group in **119** (conjugated with an aromatic ring) was detected by IR spectroscopy (Ar–C=O stretch at 1685 cm^{-1}) and the aromatic region of the ^1H NMR spectrum showed a singlet at 7.15 ppm. Compound **92** is practically insoluble in most common laboratory solvents (with limited solubility in methanol). The carboxylic acid group was detected by IR spectroscopy (Ar–C=O stretch at 1694 cm^{-1} and broad O–H stretch, 3600–2400 cm^{-1}) and the absence of the aldehydes determined by TLC (visualised by Brady's reagent[57]—aldehydes and ketones react with 2,4-dinitrophenylhydrazine to form a yellow or orange coloured hydrazone).

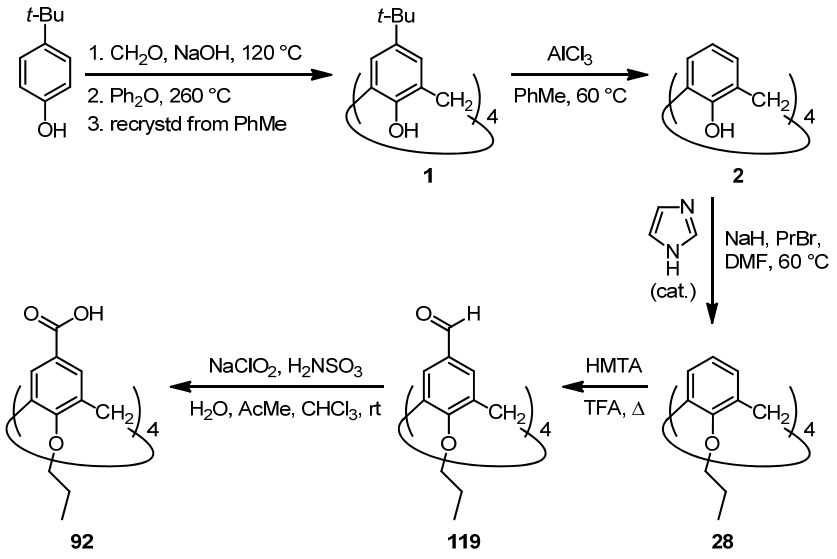

Scheme 2.17 Preparation of calix[4]arene scaffold for further functionalisation with amino acids.

2.2.3 Attaching amino acids to calixarenes via an amide linkage

L-Aspartic acid, L-glutamic acid, and iminodiacetic acid functionalised calix[4]arenes were synthesised as outlined in Scheme 2.18. Conversion of the tetracarboxylic acid **92** to the tetraacid chloride **94** (which was not isolated or characterised) allowed the amino acids of interest (**120**–**122**) to be attached to the calixarene as amides (**123a**–**c**).[49] Calix[4]arenes **123a–c** were initially obtained as a glass-like solid, which crystallised on standing at room temperature for several months.

The ^{1}H NMR spectrum of amino acid functionalised calix[4]arene **123a** showed two signals for the aromatic protons and a doublet for the amide proton (Figure 2.3). The two separate aromatic protons for the calix[4]arene is indicative of the attachment of a chiral substituent.[20] The signal at 4.6 ppm was assigned as the bridge methylene proton in the axial position while the signal at 3.3 ppm was assigned to the proton in the equatorial position. This assignment was consistent with those made by other groups for similar calixarenes.[20, 58] Signals attributed to the propoxy group were also identified at 3.9, 1.9, and 1.0 ppm. The signal at 4.9 ppm was assigned to the proton at the asymmetric carbon of the aspartic acid moiety with the vicinal diastereotopic protons[59] at 3.1–2.9 ppm (appears as two distorted doublet of doublets). The complex signal at 4.3–4.1 ppm was assigned to the diastereotopic protons on OC*H*$_2$CH$_3$ with the OCH$_2$C*H*$_3$ protons at 1.3–1.2 ppm. The ^{1}H NMR spectrum for **123b** was similar with the following main differences: the signal for the proton on the asymmetric carbon is at 4.6 ppm and for the vicinal diastereotopic protons at 2.30–2.15 ppm and 2.12–1.99 ppm; the methylene protons adjacent to the distal carboxylate appears as a complex signal at 2.5–2.3 ppm; the diastereotopic protons of OC*H*$_2$CH$_3$ appears as two nearly resolved set of complex signals at 4.3–4.0 ppm. Calix[4]arene **123c** has a tertiary amide and has no amide proton in the ^{1}H NMR spectrum. Being achiral, the Ar–*H* signal appears as a singlet. Also, the protons of NC*H*$_2$COO and OC*H*$_2$CH$_3$ appear as an overlapped signal at 4.3–4.0 ppm.

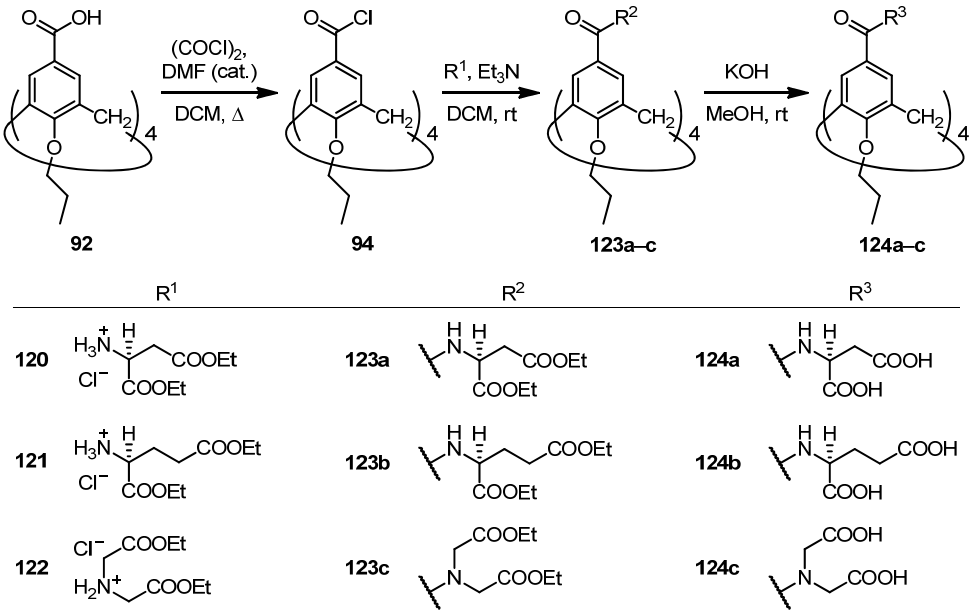

Scheme 2.18 Preparation of wide-rim, amino acid functionalized calix[4]arene as additives for crystal growth modification.

Deprotection[60] of the esters was conducted at room temperature to avoid racemisation[61] of the amino acids (and to avoid hydrolysis of the amides). ^{1}H NMR spectra (Figure 2.3) of the octacarboxylic acid calixarenes, **124a**–**c**, showed complex and slightly broadened signals suggesting that some sort of aggregation is occurring. The absence of a quartet and a triplet corresponding to the ethyl esters confirmed that selective hydrolysis was achieved. The signal in the ^{1}H NMR spectra (Figure 2.4) of calix[4]arenes **124a**–**c** sharpened slightly by changing the solvent from CD_3SOCD_3 to CD_3OD in order to reduce the formation of aggregates[22] which can broaden ^{1}H NMR signals. The IR spectrum of **124a** showed the C=O stretch for the carboxylic acid at 1720 cm^{-1} and C=O stretch for the amide at 1626 cm^{-1}. Similar C=O stretches were observed for **124b** (1731 cm^{-1} for the carboxylic acid and 1633 cm^{-1} for the amide). However, in the IR spectrum for **124c** only the C=O stretch for the carboxylic acid (1726 cm^{-1}) was visible with the C=O stretch for the amide presumably overlapped with the aromatic ring stretch signal at 1598 cm^{-1}. A signal at 169.8 ppm in the ^{13}C NMR spectrum confirmed the presence of the amide carbonyl for **124c**.

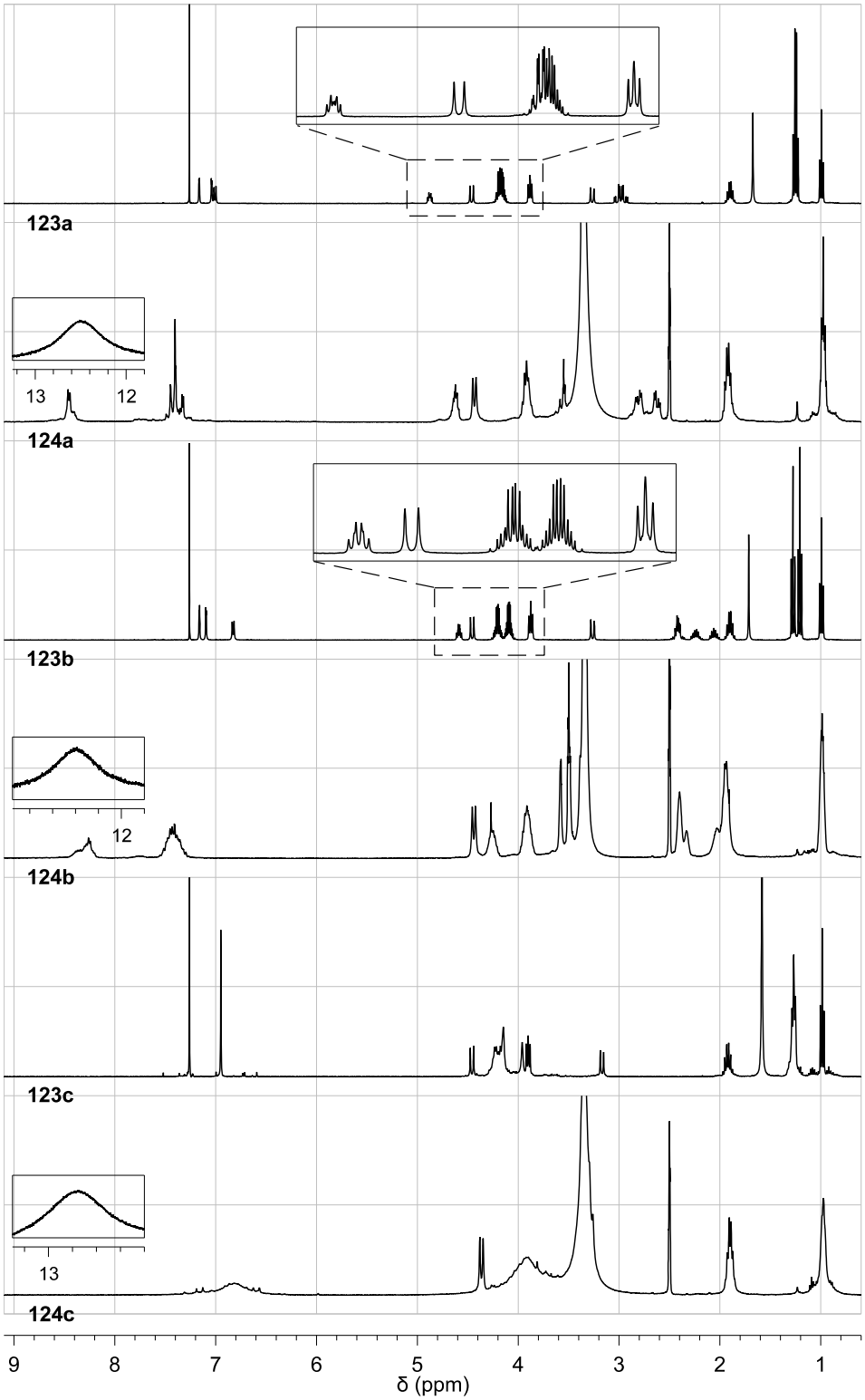

Figure 2.3 ^{1}H NMR (400 MHz) spectra of amino acid functionalised calix[4]arenes as protected esters, **123a–c** (in $CDCl_3$) and octacarboxylic acids, **124a–c** (at ~6 mg mL^{-1} in CD_3SOCD_3), with the O*H* signals shown as an inset.

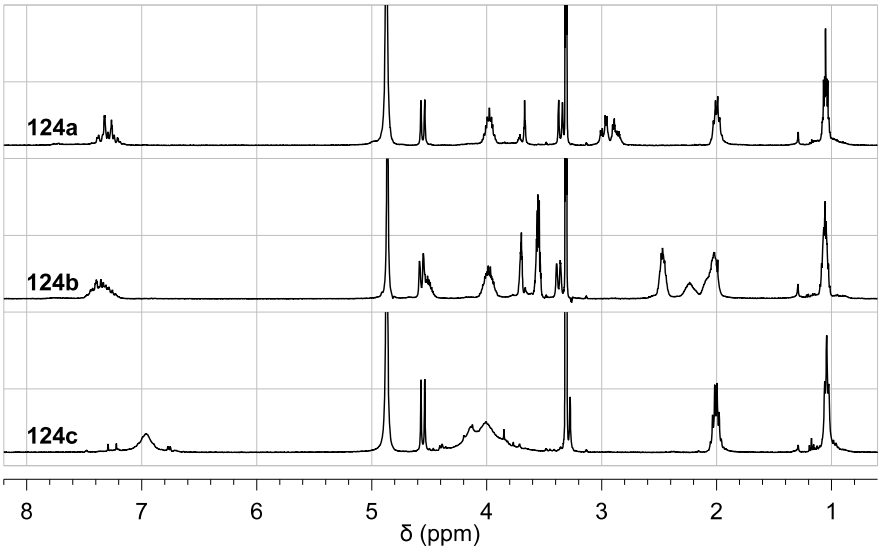

Figure 2.4 ^{1}H NMR (400 MHz) spectra of amino acid functionalised calix[4]arenes as the octa-carboxylic acids, **124a–c** (at 8–9 mg mL^{-1} in CD_3OD).

A direct method for amide bond formation using a peptide coupling reagent was also investigated. The model calixarene **123a** was prepared using the coupling method described by Sansone et al.[20] and substituting DCC for 1-ethyl-3-(3'-(dimethyl-amino)propyl)carbodiimide hydrochloride (EDC•HCl), Scheme 2.19. The reader is referred to reviews by Valeur and Bradley[18] and Montalbetti and Falque[6] for the chemistry of carbodiimide reagents and active ester formation with HOBt. A product yield of 27% was obtained after two successive purifications by column chromatography [silica gel, dichloromethane/acetone (4:1, v/v)]. An unidentified material eluted just prior to **123a** which could have contained a calix[4]arene with both the amide and HOBt active ester attached. The ^{1}H NMR spectrum of this fraction was complex and had broadened signals; these signals were tentatively assigned to the methylene of the calixarene, aromatic signals to HOBt and calixarene and alkyl signals to the ethyl esters and propoxy groups. In contrast a yield of 44% for **123a** was obtained by the acid chloride method (Scheme 2.18) and the crude compound required only a single purification step (column chromatography). Even though the coupling method was more direct and EDC was readily removed by work-up with water, the two-step acid chloride method gave a better yield and the crude material was less difficult to purify.

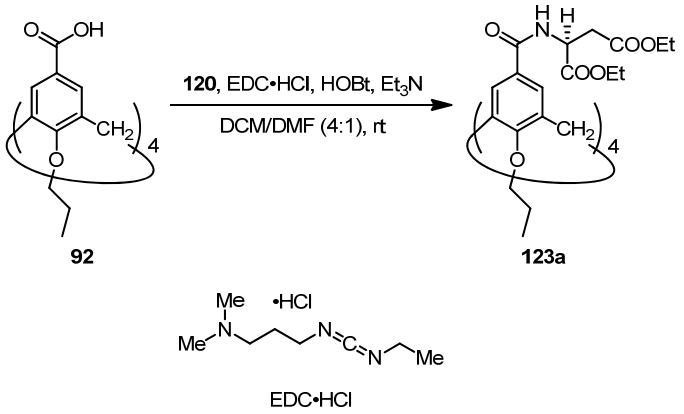

Scheme 2.19 Attaching protected aspartic acid **120** to carboxylic acid **92** using EDC•HCl.

2.3 Calixarene-based Mannich adducts

Calix[4]arenes which do not have substituents at the position *para* to the phenol can be readily functionalised at the wide-rim in a single step by a Mannich reaction. Proline was attached to the calix[4]arene **2** by the Mannich reaction in good yield. The calix[5]arene **126** was prepared as outlined in Scheme 2.20. The preparation of calix[5]arene **125** proceeded according to literature.[62] The product gave an ^{1}H NMR spectrum and mp consistent with Bew.[63] The Friedel-Crafts dealkylation was performed by a modified procedure from Bell et al.[64] and Coruzzi et al.[65] and **126** was obtained in 66% yield. As with calix[4]arene **2**, the absence of the *tert*-butyl group and the appearance of a doublet and triplet (integrating for two and one proton(s) respectively) in the aromatic region of the ^{1}H NMR spectrum confirmed the formation of **126**. The Friedel-Crafts dealkylation reaction of **125** should not be heated as this gave a brown oil upon work-up, from which only a small amount of **126** was isolated (~15% yield).

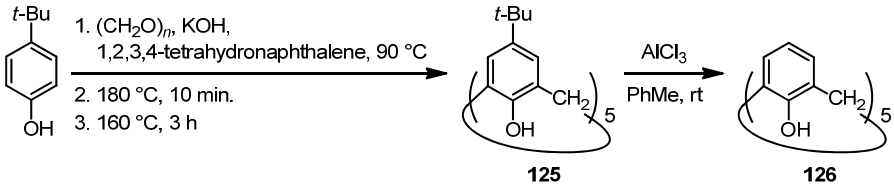

Scheme 2.20 Synthesis of penta-*tert*-butylcalix[5]arene and de-butylation to calix[5]arene.

Proline readily formed a Mannich base with calix[4]arene and calix[5]arene (Scheme 2.21). Proline calixarenes **127a**,**b** and **128** precipitated from the biphasic reaction mixture and deposited on the reaction flask wall. This allowed for a relatively simple isolation, however removing residual proline (<5 mol%, estimated from 400 MHz ^{1}H NMR spectrum; residual proline was not visible in 200 MHz NMR ^{1}H spectrum) from the proline functionalised calixarenes proved to be more difficult. Residual proline was removed by trituration of **127a**,**b** in methanol; suspension of **127a**,**b** in methanol gave a milk-like mixture which was slow to filter. The ^{1}H NMR spectrum of **127a** showed a broadened singlet in the aromatic region and significantly broadened signals in the 4.5–1.5 ppm region (refer to 2.4.2 for assignment of the ^{1}H NMR signals). The presence of a signal, in the ^{13}C NMR spectrum, at 30.4 ppm for Ar–CH_2–Ar indicates that the calix[4]arene **127a** is in a cone conformer (at room temperature).[52] Calix[4]arene **127a** also had a very high solubility in water which was estimated to be approximately 0.5 g mL^{-1}.

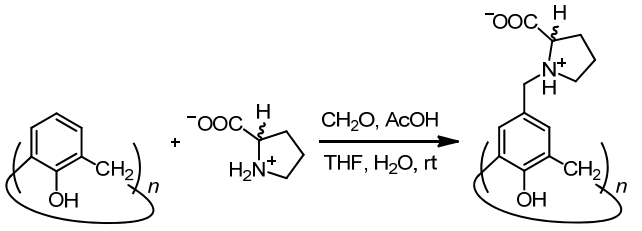

	n
2	4
126	5

	proline	*n*
127a	L-Pro	4
127b	D-Pro	4
128	L-Pro	5

Scheme 2.21 Attaching proline to the wide-rim of calix[*n*]arenes with a modified Mannich reaction.

The calix[5]arene analogue of calix[4]arene **127a** was also prepared to investigate the effect of the calixarene ring size, and as a consequence, the spatial arrangement of the proline moieties, on the self-assembly properties of such motifs. In contrast to **127a**, proline calix[5]arene **128** separated as a viscous phase on the reaction flask wall which became a white solid when treated with acetone. The purification of **128** was difficult (and only partially achieved) as **128** had appreciable solubility in methanol which prevented methanol from being used as a trituration solvent to

remove residual proline. The crude product was used for preliminary experiments (see section 4.5).

Under similar conditions, calix[6]arene **20** did not give the hexa-substituted product **129** as expected (Scheme 2.22). This was suspected to be a result of the lower solubility of the partially substituted calix[6]arene in the tetrahydrofuran-water solvent system. The calix[6]arene analogue was not pursued further as preliminary experiments with the calix[5]arene analogue **128** suggested that the increased ring size does not lead to the formation of a hydrogel under similar conditions used for compound **127**.

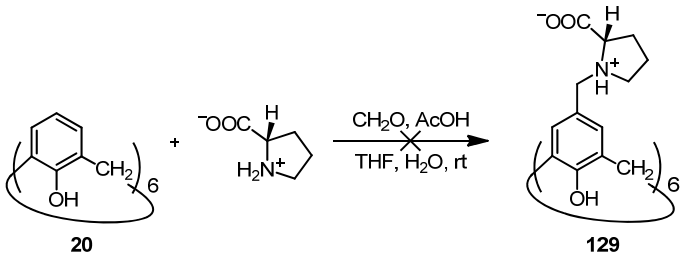

Scheme 2.22 Mannich reaction did not proceed with calix[6]arene **20** under similar conditions.

Proline (and its derivatives) has been utilised as a catalyst in many Mannich reactions.[66–68] It was hypothesised that proline may self-catalyse the Mannich reaction between it and the calixarene. In an attempt to selectively functionalise calix[4]arene with proline moieties (Scheme 2.23), the dipropoxy calix[4]arene **130**[53] was also subjected to the Mannich reaction with proline but this did not yield any product; the starting material was recovered. Van Loon et al.[69] used harsh conditions (at reflux in dioxane for 66 h) for a Mannich reaction with the dimethylated analogue of **130** and obtained a product yield of 91%. However, using similar reaction conditions, Nam and Yoon[70] did not obtain a product when the narrow-rim substituents were benzyl or allyl groups. This suggested that the hydrogen bonding between adjacent phenolic moieties was required to activate the *para* Ar-*H* for the Mannich reaction to proceed readily. This is consistent with Gutsche[71] who proposed the greater acidity of the free phenol calixarenes resulted in a greater reactivity of the *para* aromatic proton under Mannich conditions.

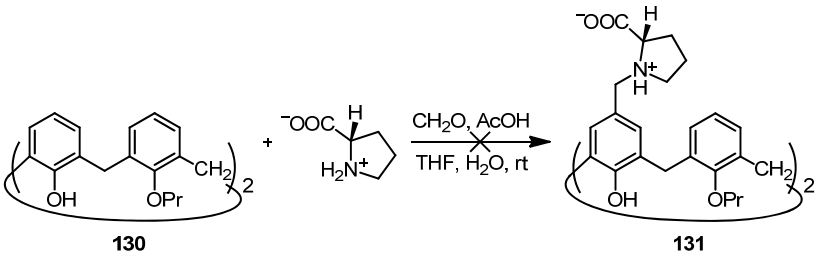

Scheme 2.23 Mannich reaction did not proceed with the dipropoxy calix[4]arene **130**.

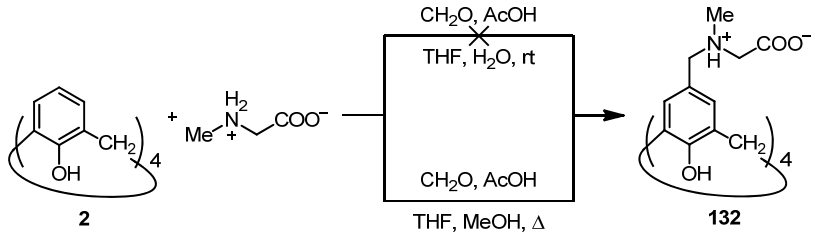

Scheme 2.24 Reaction conditions attempted for Mannich reaction between sarcosine and calix[4]arene **2**.

Since the Mannich reaction provided relatively easy access to amino acid functionalised calixarenes, other secondary amino acids were investigated. One of the targeted analogues of proline calix[4]arene **127** involved substituting proline for sarcosine. An attempt to prepare the sarcosine functionalised calix[4]arene **132** using similar reaction conditions as those used for **127** (Scheme 2.24) did not give a Mannich adduct detectable by ^{1}H NMR spectroscopy; the starting calixarene **2** was recovered. Some of the desired product **132** was obtained when the solvent system was altered to tetrahydrofuran-methanol to improve solubility of the reactants and the reaction solution heated at reflux. The reaction product precipitated from the reaction solution as a white solid. Interestingly, not all of the white powder was water soluble. The D_2O-soluble component gave a ^{1}H NMR spectrum consistent with the desired product: a singlet for the calixarene Ar–*H*; a broad methyl group for the sarcosine moiety; and two broad overlapped CH_2 groups corresponding to the methylene on the sarcosine and the newly formed methylene between the calix[4]arene and sarcosine. The crude product was used for preliminary experiments (see section 4.5).

2.4 Self-assembly behaviour of L-proline calix[4]arene

An aqueous solution of proline calix[4]arene **127** formed a foam on shaking. This behaviour is similar to detergents and suggests that **127** may be self-assembling into micelle-like structures in solution. Investigations into the self-assembly of calix[4]-arene **127** in solution were thus warranted and the results of these investigations are discussed here.

2.4.1 UV-Visible spectroscopy

Given that L-proline calix[4]arene **127a** exhibited surfactant-like properties, it was appropriate to investigate its aggregation behaviour using techniques applied to common surfactants. The 'critical aggregation concentration' (c.a.c.) can be determined by monitoring the shift of λ_{max} of a probe molecule by UV-visible spectroscopy.[72] One of the many appeals of calixarenes is the ability to include smaller molecules within their cavities or bind small molecules with appended functionality. As such, determination of the c.a.c. using a molecular 'probe' may give erroneous results if the probes preferentially included within the calixarene cavity or bind to the proline moieties. This method gave c.a.c. values ranging from 4 to 9 mM (Figure 2.5) with various dyes.

A variety of dyes were investigated (Figure 2.6); these include cationic (methylene blue and rhodamine 6G), anionic (methyl orange), and uncharged (dimethyl yellow) dyes. Methylene blue and rhodamine 6G gave c.a.c. values of 4 and 5 mM respectively while methyl orange and dimethyl yellow both gave higher c.a.c. values at 9 mM. It was not clear from this experiment alone, what role the charge on the dye played or whether the shift in λ_{max} was a result of the probe molecule interacting with the calix[4]arene itself (e.g. absorption onto the surface of aggregated structures[73]) or including within calix[4]arene aggregates. Similar experiments were also attempted with non-dye probes. 4-Nitroanisole was investigated but the λ_{max} ~300 nm for 4-nitroanisole was overlapped by the calix[4]arene absorptions at <400 nm. Dimethyl yellow, being neutral, was insoluble in water. Therefore, each of the calixarene solutions at the desired concentration were sonicated for 5 min. with ~5 mg of dimethyl yellow solid (then filtered) prior to UV-visible measurements.[74] It was noted that if the probe (in this case the methylene blue solution) was added

immediately prior to UV-visible measurement, the c.a.c. was determined to be 16 mM. Preparing the stock solutions of calix[4]arene with the probes present may allow time for the system to equilibrate. Therefore, the c.a.c. values may reflect aggregation processes under kinetic and thermodynamic control.

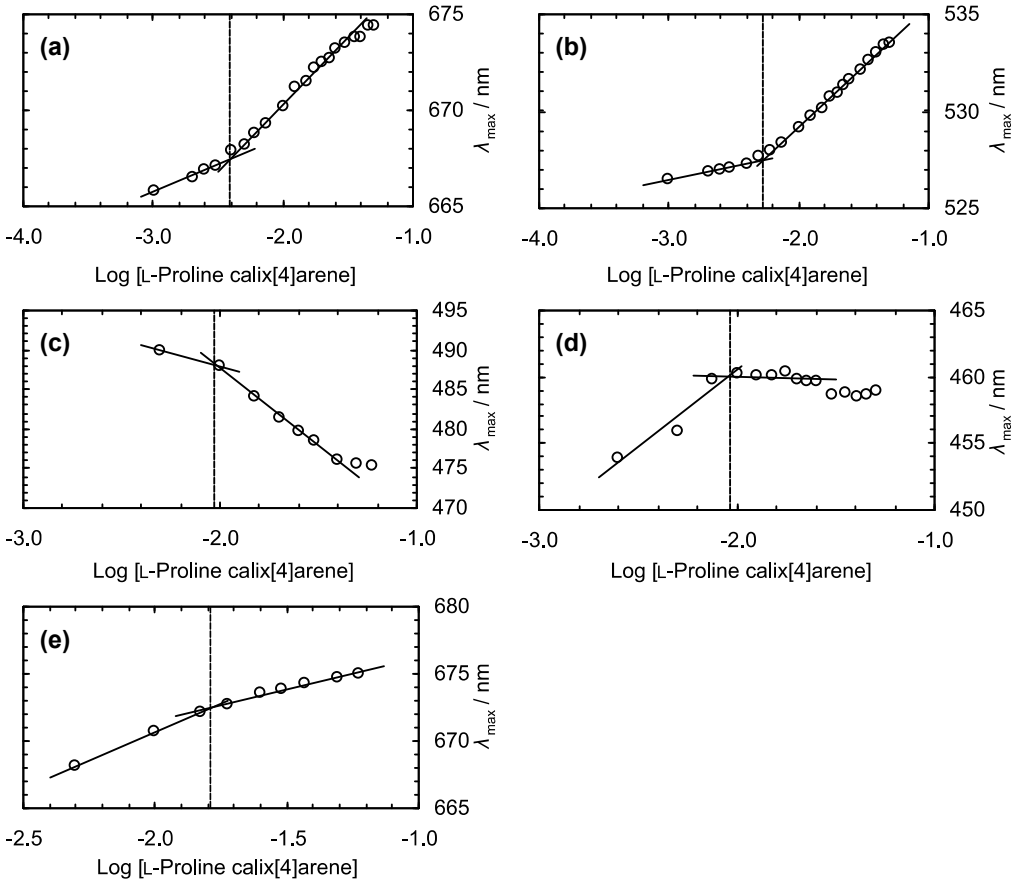

Figure 2.5 Determinations of the critical aggregation concentration by monitoring the shift of the dye's maxima at 400–700 nm in UV-visible spectroscopy. Various probes were investigated: (a) methylene blue (c.a.c. = 4 mM); (b) rhodamine 6G (c.a.c. = 5 mM); (c) methyl orange (c.a.c. = 9 mM); (d) dimethyl yellow (c.a.c. = 9 mM); and (e) methylene blue, dye added immediately prior to UV-visible measurement (c.a.c. = 16 mM).

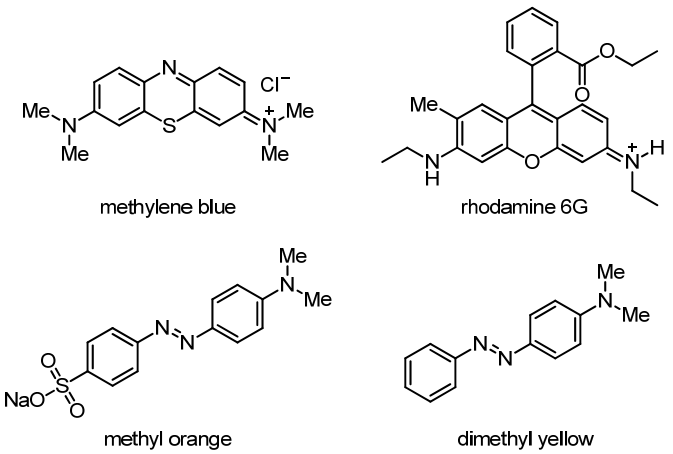

Figure 2.6 Dyes used for the determination of the c.a.c of L-proline calix[4]arene in water.

Characterisation of the size of L-proline calix[4]arene aggregates in the absence of molecular probes was performed by dynamic light scattering (DLS). The c.a.c. determined by DLS (Figure 2.7) was 11 mM. The average particle size distribution of the aggregates was approximately 1.5 nm when the solution was at a concentration below the c.a.c., but this increases to approximately 3 nm when the concentration of calixarene was greater than 20 mM and 4–5 nm when the concentration was at 40 mM. DLS instruments typically model particle size with the assumption that the particle is spherical. If the aggregates were assumed to be spherical, then this could fit six calix[4]arene units assembled into a cube-like structure (~3 nm) with a hydration shell of 1–2 nm.

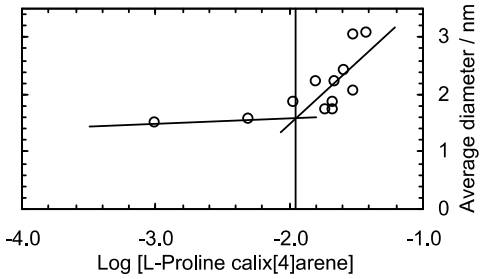

Figure 2.7 Determination of the c.a.c. by dynamic light scattering (c.a.c. = 11 mM).

Studies on the self-assembly behaviour of calixarene **127a** were based on material thought to be 'pure' based on analysis by on a 200 MHz NMR spectrometer. Analysis of the same material on a 400 MHz NMR spectrometer showed that small quantities

of residual solvent were present. Further studies by NMR spectroscopy showed that the self-assembly of calixarene **127a** could be influenced by small molecules.

2.4.2 NMR spectroscopy studies of self-aggregation

The aggregation behaviour of L-proline calixarene was further studied by nuclear magnetic resonance (NMR) spectroscopy. ^{1}H NMR spectra of L-proline calix[4]arene **127a** from 0.25 to 100 mg mL^{-1} in D_2O at 298 K (Figure 2.8) indicated that aggregation initiated at 8 mg mL^{-1} as evidenced by the formation of new peaks (3.5–2.2 ppm) and broadening of peaks in the 1.5–4.5 ppm and aromatic (7.5–7.0 ppm) regions. With the aid of ^{1}H–^{1}H COSY (correlation spectroscopy), ^{1}H–^{13}C HSQC (heteronuclear single quantum coherence), and ^{1}H–^{13}C HMBC (heteronuclear multiple bond correlation) at selected concentrations, signals at 3.3, 2.8, and 2.5 ppm were assigned to the proline moiety. At 15 mg mL^{-1}, the signals in the 4.5–1.5 ppm region broadened and the new signals increased in intensity. The Ar–*H* signal also broadened at concentrations >8 mg mL^{-1}, consistent with the signals in the 4.5–1.5 ppm region. A small peak, ~0.05 ppm upfield of the Ar–*H*, increased in intensity until 50–100 mg mL^{-1} where these signals in the aromatic region coalesced into three broad peaks (7.35–7.05 ppm).

Broadened signals indicated that the thermal motion of the aggregates were now slower on the NMR time scale. Broad signals are typical of aggregation of smaller molecular units into larger structures and larger structures typically have shorter T_2 relaxation times (leading to broad signals).[75, 76] An analysis of the normalised total integral of signals from 9–0 ppm (Figure 2.9), excluding HOD, showed the total integration increasing linearly with the concentration of **127a** up until ~10 mg mL^{-1}. Beyond this, the integration appeared to plateau and not increase linearly as expected with the increase in concentration in the solution. If the T_2 relaxation times of larger structures became too short, the signals from the larger aggregate structures would not be 'NMR-visible' (under the standard experimental parameters used), therefore decreasing the number of ^{1}H observed.

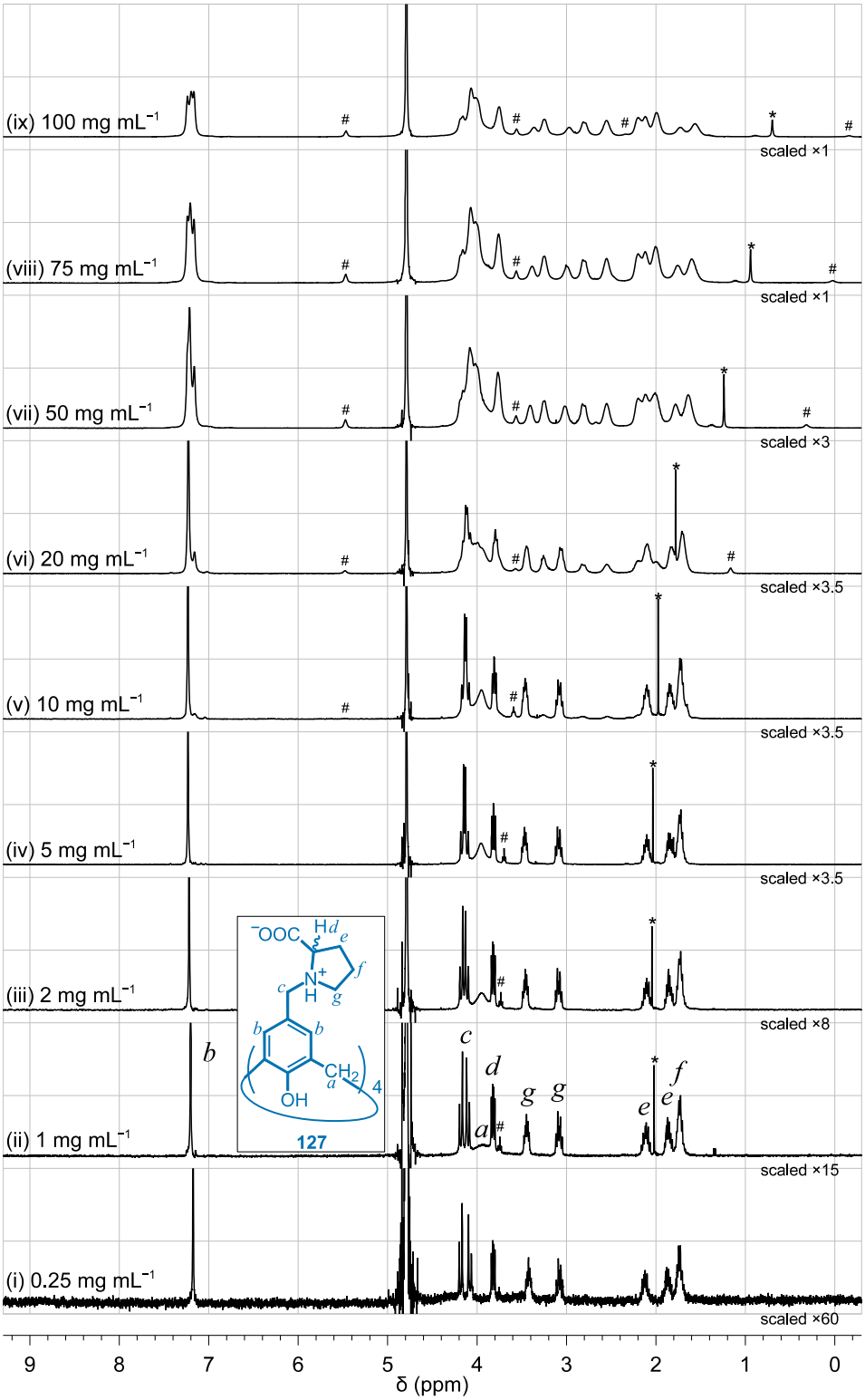

Figure 2.8 ^{1}H NMR (400 MHz) spectra of **127a** at selected concentrations from (i) 0.25 to (ix) 100 mg mL^{-1} in D_2O. The residual acetate signal (*) at ~2 ppm shifted 1.5 ppm upfield and broadened. The residual THF signals (#) shift upfield and new signals also appeared downfield at **127a** concentrations greater than 8 mg mL^{-1}. Due to changes in intensities, the spectra were scaled for clarity.

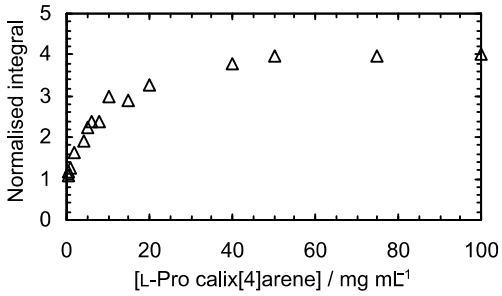

Figure 2.9 Analysis of normalised integrals from δ 9–0 ppm as the concentration of calixarene **127a** was increased.

Impurities were identified in the sample (residual L-proline, THF, and acetate). The signals from these impurities responded to changes in their environment so, they can be used to 'probe' interactions with the calix[4]arene (i.e. inclusion within the calix[4]arene cavity) or aggregated structures. The THF signals at 3.75 ppm (CH_2, C1,5) and ~1.88 ppm (overlapped, CH_2, C3,4) were consistent with THF in D_2O.[77] The signals at 3.75 and 1.88 ppm, followed with the aid of ^1H–^1H COSY experiments (Figure 2.10a), shifted upfield to 2.36 and −0.16 ppm respectively as the concentration of **127a** was increased from 0.50 to 100 mg mL^{-1}. An interesting result from the ^1H–^1H TOCSY (TOtal Correlation SpectroscoY) experiments (Figure 2.10b) for the same sample, suggested that the two signals at 5.47 and 3.56 ppm (currently unassigned) were in the same spin system as the two signals 2.36 and −0.16 ppm (assigned to THF). This was in contrast to the COSY experiments which suggested that the two pairs of signals were not coupled to each other. However, the signal at 5.47 ppm was coupled to the signal at 3.56 ppm. One possible explanation for this is that as the concentration of calix[4]arene was increased, THF included into the calix[4]arene cavity (related to the upfield shifted signals) but a portion of the THF was also aligned with the aromatic plane (the downfield shifted signals). As expected, increasing the concentration of calixarene also increased the intensity of downfield signal at 5.55 ppm (Figure 2.11).

Another impurity, acetic acid, also showed signs of inclusion in the calixarene. The acetate signal at 2.0 ppm (**127a** at 0.25 mg mL^{-1}) moved upfield to 0.7 ppm (**127a** at 100 mg mL^{-1}). Acetate is typically at 2.1 ppm in D_2O.[78] This suggested that the acetate included in the calixarene cavity as the concentration of **127a** in solution was increased.

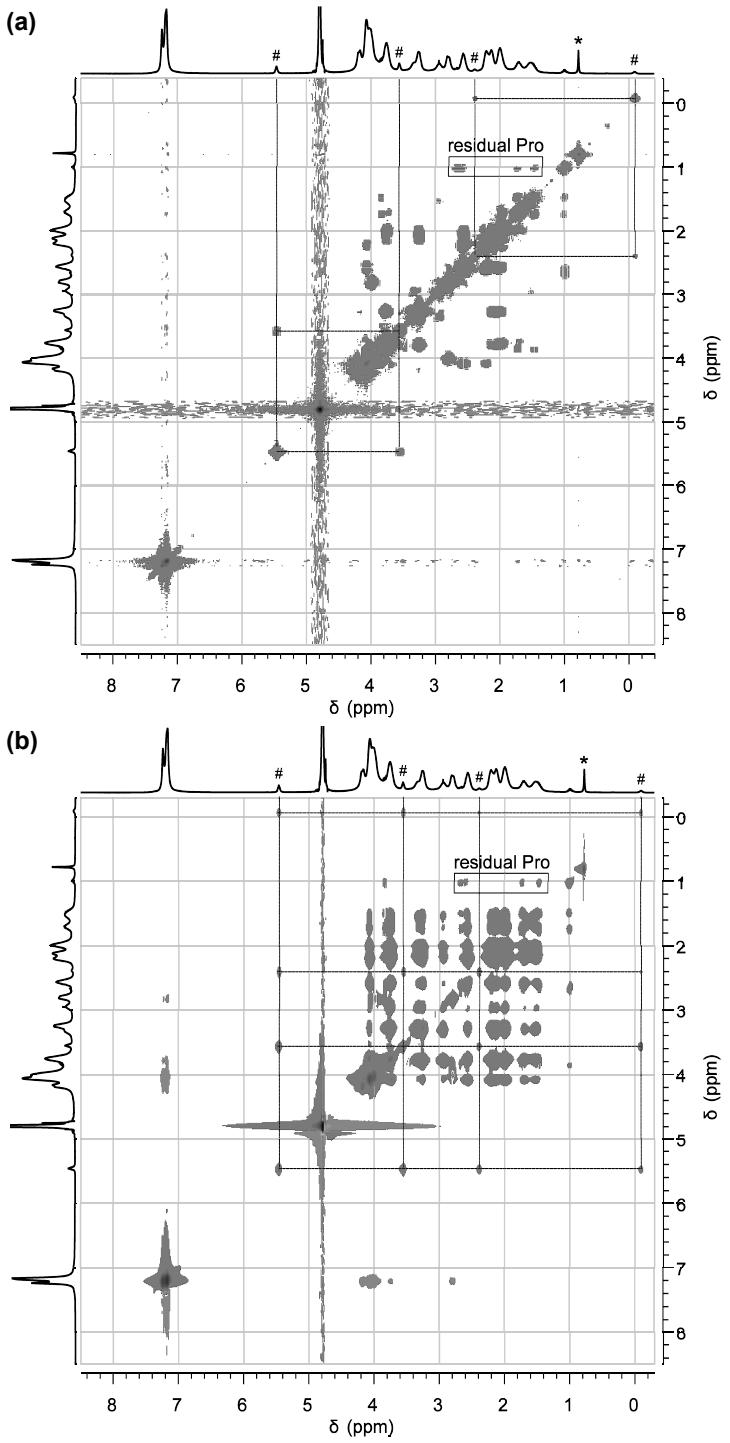

Figure 2.10 (a) ^{1}H–^{1}H COSY and (b) ^{1}H–^{1}H TOCSY NMR (400 MHz, D_2O) spectra for L-proline calix[4]arene at 100 mg mL^{-1}. Residual impurity signals: tetrahydrofuran (#) and acetate (*).

There were also indications that residual proline amino acid interacted with proline calix[4]arene as the concentration of the calixarene was increased. The proline amino

acid signal, initially at 1.80–1.65 ppm (8 mg mL^{-1}), moved upfield to 0.95–0.8 ppm (100 mg mL^{-1}) at higher concentrations of **127a**. This suggested that the proline amino acid could be included into the proline calix[4]arene cavity; an upfield shift of signals in such systems is typical of inclusion into the cavity. It is unusual for proline to include into the calixarene cavity given the high solubility of the amino acid in water (162 g/100 mL of water at 25 °C[79]). However, the high concentration of the calixarene in solution could affect the ionic characteristics of the solution therefore favouring the inclusion of proline in to the calixarene cavity. This has implications for the proposed mechanism of hydrogelation of proline calix[4]arene (refer to section 4.7).

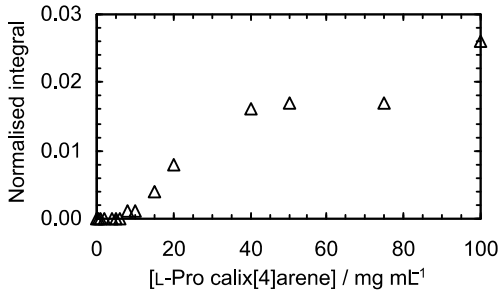

Figure 2.11 Analysis of the normalised integrals of the signal at δ 5.5 ppm.

In an attempt to elucidate the impact of small molecules in solution, a sample of calixarene **127a** was further purified. The sample was triturated with methanol then dissolved in water and concentrated *in vacuo* and the residue dried under high vacuum. The resulting ^{1}H NMR spectra (Figure 2.12) at 20 and 100 mg mL^{-1} were different compared with the previous samples. Under these conditions, the signals at 100 mg mL^{-1} were broadened but there were no additional signals at 3.3, 2.8, and 2.5 ppm from the aggregated proline calixarene **127a**. This suggests that small organic molecules could induce aggregation of proline calix[4]arene in solution.

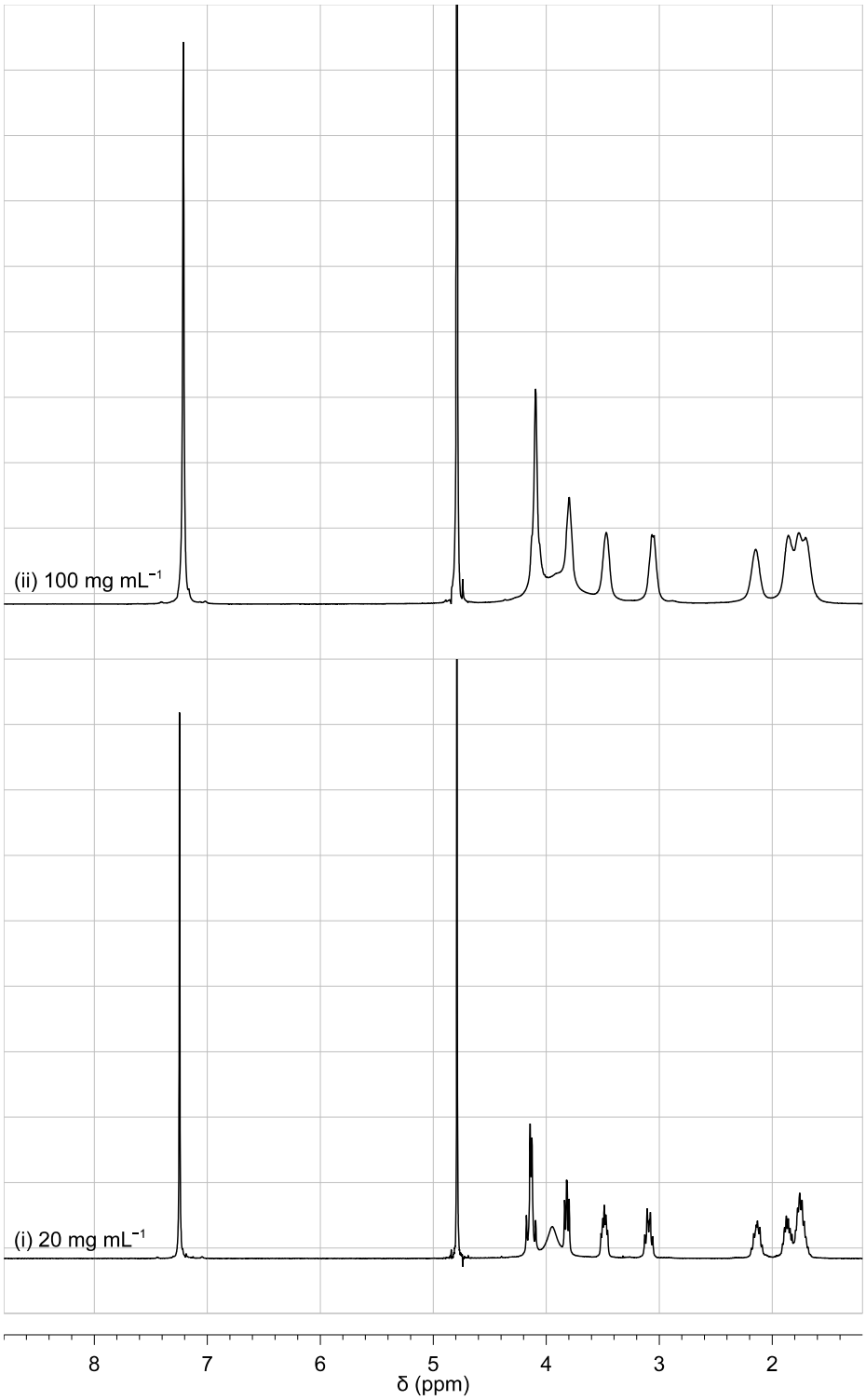

Figure 2.12 L-Proline calix[4]arene **127a** at (i) 20 mg mL^{-1} and (ii) 100 mg mL^{-1} (400 MHz, D_2O). This sample was further purified (refer to the main text above).

2.4.3 Interactions of small molecules with proline calix[4]arene

The interaction of small organic molecules with proline calix[4]arene **127a** was further investigated with tetrahydrofuran, 1-methyl-2-pyrrolidinone (NMP), and *tert*-butyl alcohol (Figure 2.13). THF was of interest as it had a dramatic impact on the aggregation of **127a** at low concentrations. NMP was selected because of its structural similarity to proline, while being more hydrophobic. *tert*-Butyl alcohol was investigated as a potential internal standard however, it too affected the ^{1}H NMR spectrum of **127a**.

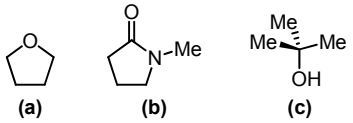

Figure 2.13 Small organic molecules of interest: (a) tetrahydrofuran, (b) 1-methyl-2-pyrrolidinone, and (c) *tert*-butyl alcohol.

NMR titration experiments (Figure 2.14) showed that THF had an impact at 0.01 equivalents. As previously observed, the signals at 3.3, 2.8, and 2.5 ppm (assigned to the proline moiety of aggregated calixarenes) increased in intensity as THF was added to a fixed concentration of calixarene **127a**. The signals due to THF moved upfield with the addition of each aliquot of THF. Furthermore, signals at 5.5 and 3.6 ppm also appeared with the addition of THF, but at a lower intensity. This result agreed with that observed previously (see section 2.4.2); the self-assembly of the calixarene was influenced by the presence of THF. Examination of the normalised integrals of these spectra (Figure 2.15a), showed a slight decrease in the aromatic region (7.5–7.0 ppm) and in the 4.5–0.5 ppm region (which included the proline moiety and THF). This indicated that there may have been (larger) structures that were not ‘NMR visible’.

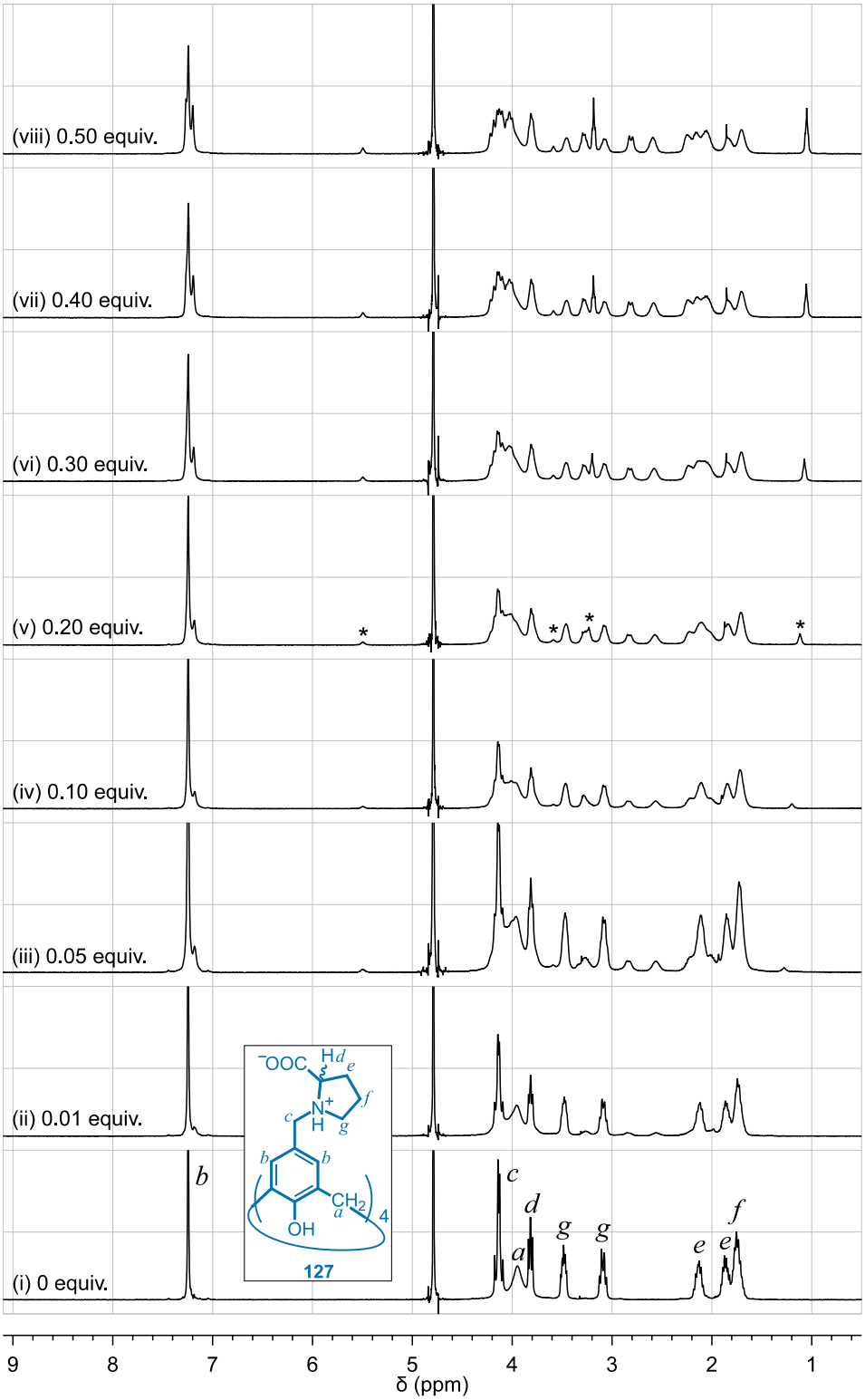

Figure 2.14 Titration of L-proline calix[4]arene **127a** (20 mg mL^{-1} in D_2O) against THF (*). An initial solution of (i) **127a** (20 mg mL^{-1}) in the presence of THF from (ii) 0.01 equiv. to (viii) 0.50 equiv. ^1H NMR spectra were acquired at 400 MHz.

Like many self-assembled systems, the calixarene **127a**-THF 'aggregate' was also reversible. Variable temperature NMR experiments (Figure 2.16) showed that the aggregated structures formed in the presence of THF were destroyed on heating to 55 °C as demonstrated by the disappearance of signals from the proline moiety (3.3, 2.8, 2.5 ppm) and 'calixarene-included' THF (5.5, 1.49 ppm). These signals have a low intensity, refer to Figure 2.17 for a scaled version of the ^{1}H NMR spectrum in Figure 2.16, (i). Supplementary analysis of the normalised integrals (Figure 2.15b) showed that the integrals increased with heating (consistent with the break-down of the calixarene aggregates); the cooling cycle did not exhibit any hysteresis.

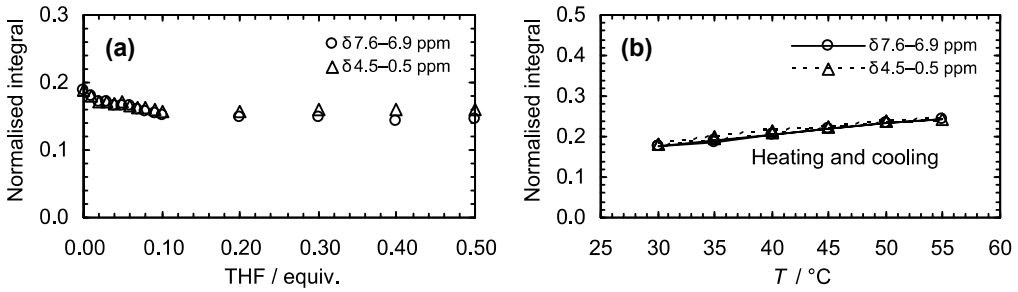

Figure 2.15 Analysis of normalised integrals from ^{1}H NMR for proline calix[4]arene **127a**-THF system. (a) **127a** (20 mg mL^{-1} in D_2O) titrated against THF; and (b) variable temperature experiments for calixarene **127a** and THF at 0.03 equiv.

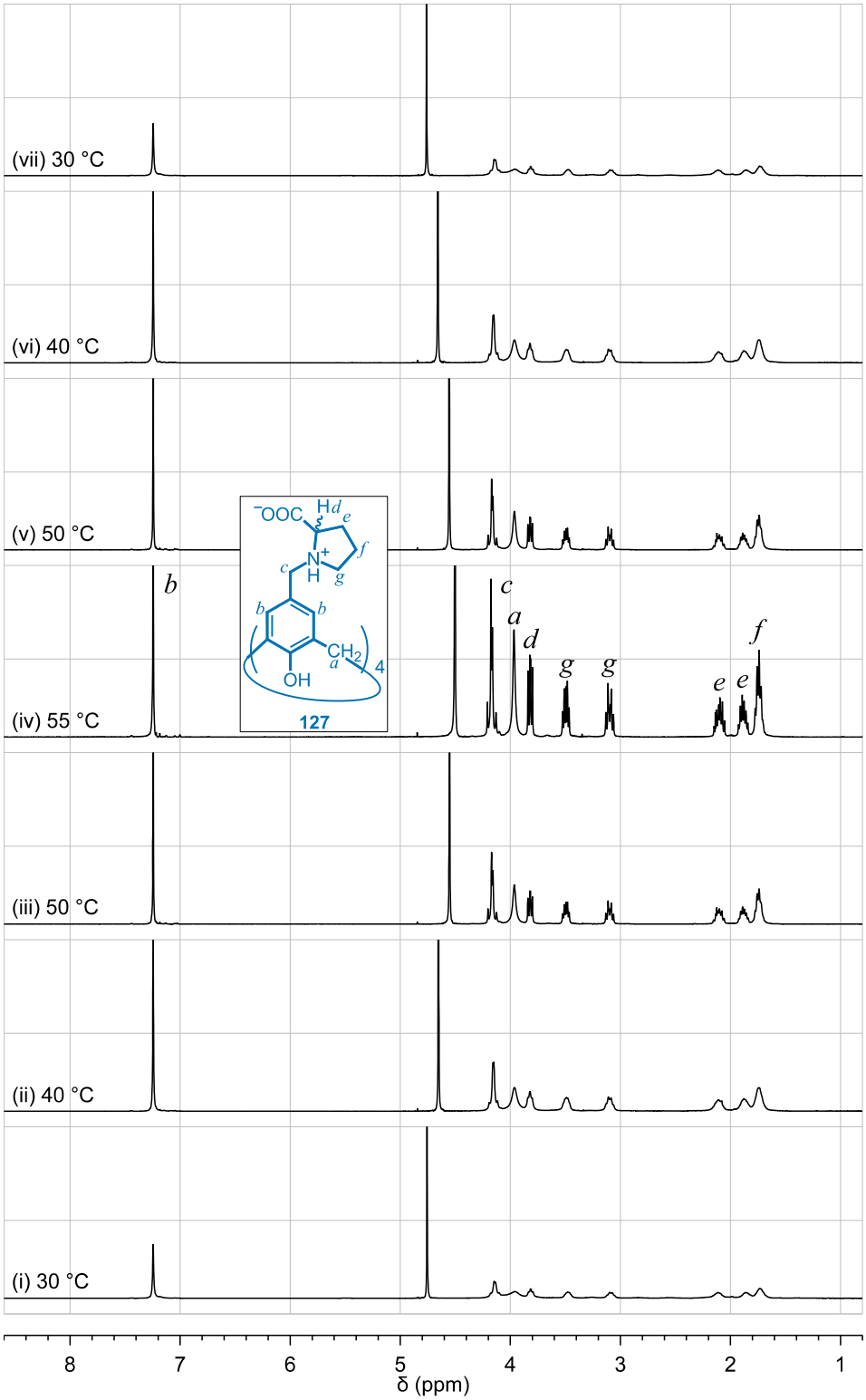

Figure 2.16 VT ^{1}H NMR (400 MHz) experiments for a L-proline calix[4]arene **127a** (20 mg mL^{-1}) and THF (0.03 equiv.) in D_2O. The solution was heated, (i) to (iv), and cooled, (v) to (vii).

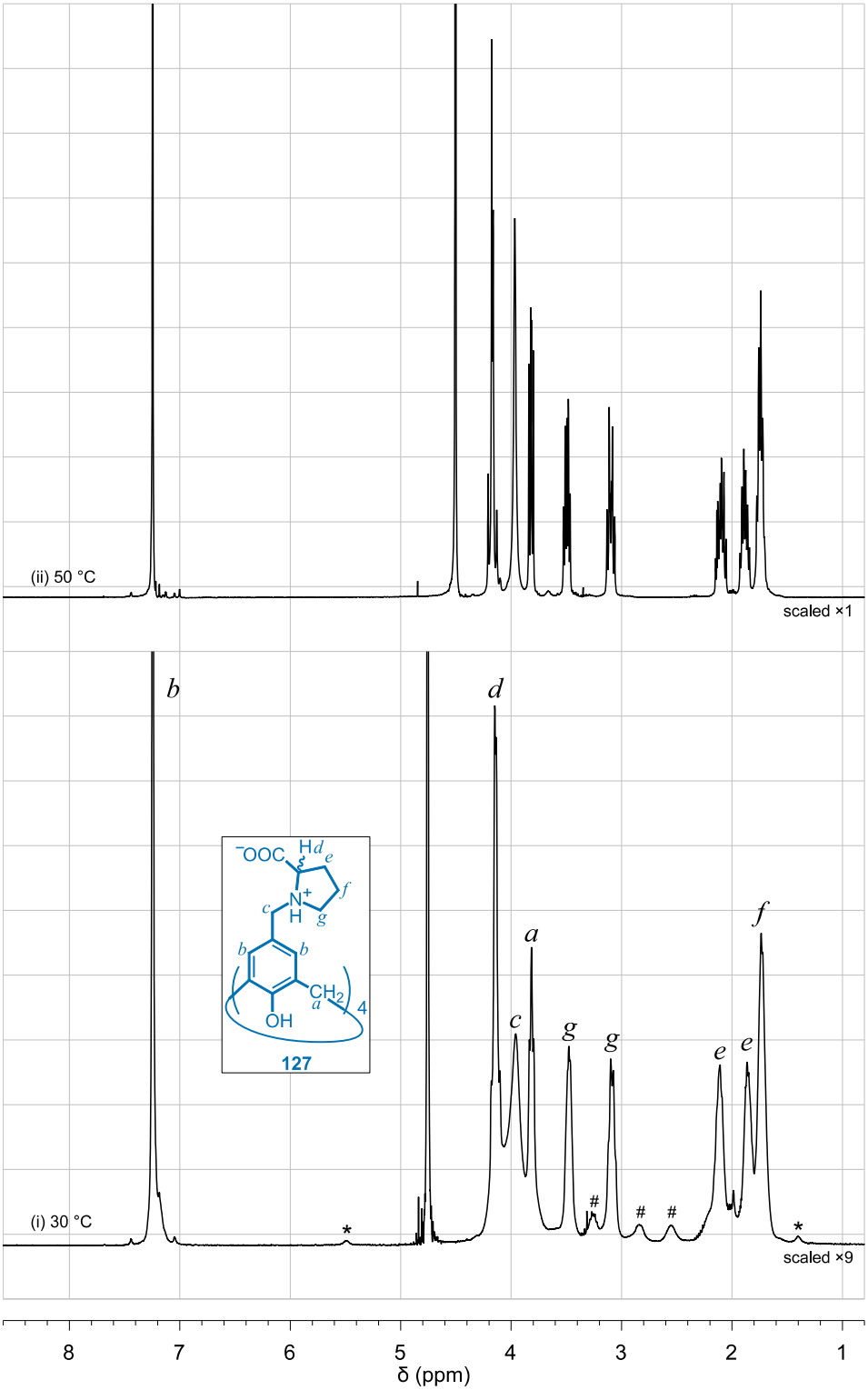

Figure 2.17 Scaled ^{1}H NMR (400 MHz) spectrum of **127a** (20 mg mL^{-1} in D_2O) and tetrahydrofuran (0.03 equiv.) in D_2O at 30 °C (Figure 2.16). The 'calixarene-included' THF signals are denoted with (*) and those belonging to the proline moiety with (#).

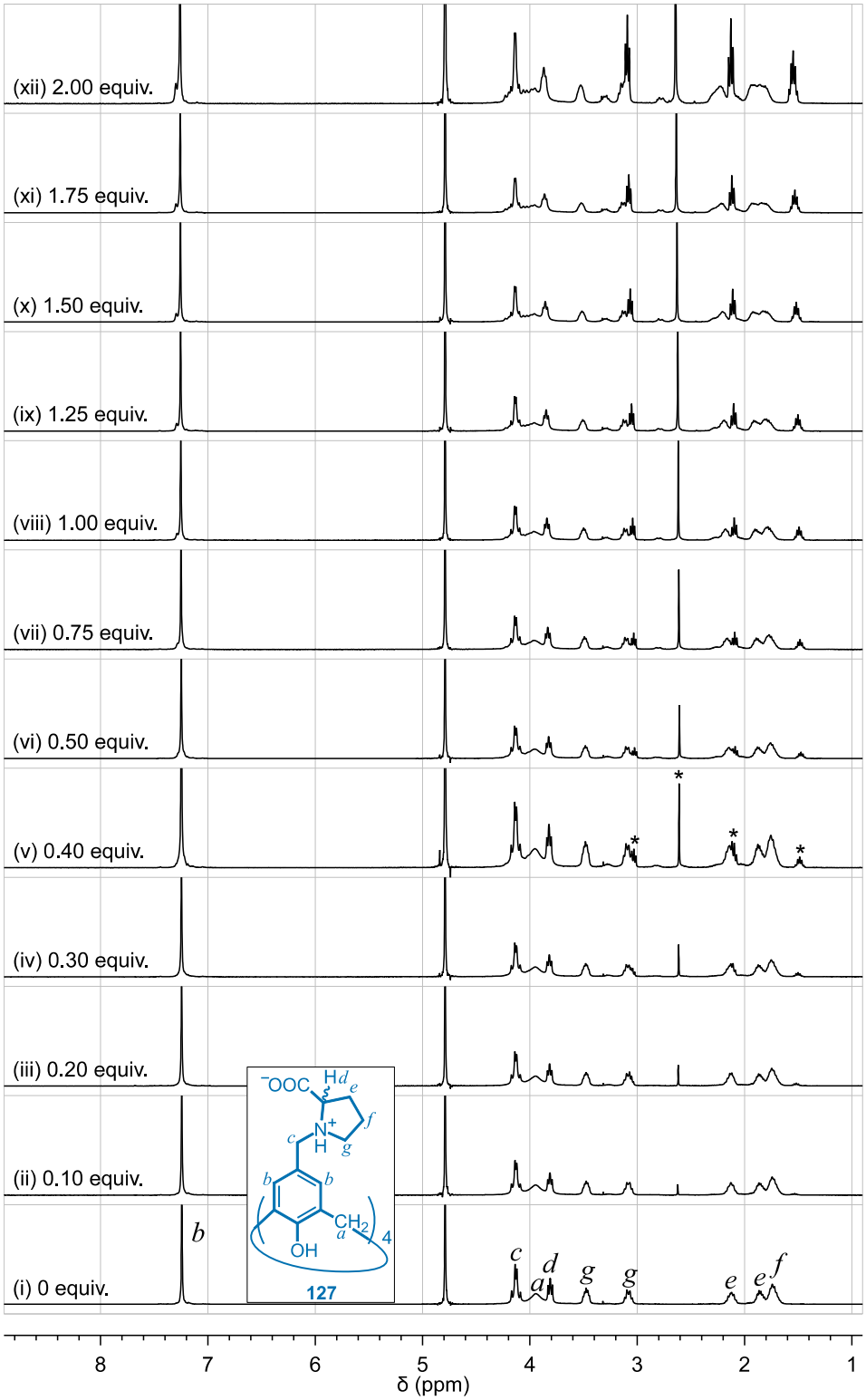

Figure 2.18 Titration of L-proline calix[4]arene **127a** against 1-methyl-2-pyrrolidinone, NMP (*) with an initial solution of (i) **127a** (20 mg mL^{-1} in D_2O) and in the presence of NMP from (ii) 0.10 equiv. to (xii) 2.00 equiv. ^1H NMR spectra were acquired at 400 MHz.

The proline analogue, 1-methyl-2-pyrrolidinone, appeared to have a lesser impact on calixarene **127a** compared with THF. NMR titration experiments of NMP into a fixed concentration of calixarene in solution (Figure 2.18) showed slight broadening of the calixarene signals and a similar set of signals (though less intense) at 3.3, 2.8, 2.6 ppm compared to the **127a**-THF system. The normalised integrals (Figure 2.19a) also showed a slight decrease with the addition of NMP. However, the integral region (3.9–3.7 ppm) is greater than the other two integral regions because of an overlap with the broadening signal of the protons of Ar–CH_2–Ar.

The **127a**-NMP system also showed reversibility. Variable temperature experiments (Figure 2.20) showed that this system was more stable with signals at 3.3, 2.8, and 2.6 ppm persisting until 50 °C and the other calixarene signals remaining broad until 70 °C. The **127a**-NMP system may be more stable as it may form stronger hydrogen bonds between the lactam carbonyl and proline moieties. The normalised integrals of these spectra (Figure 2.19b) did not reveal anything different from the **127a**-THF system.

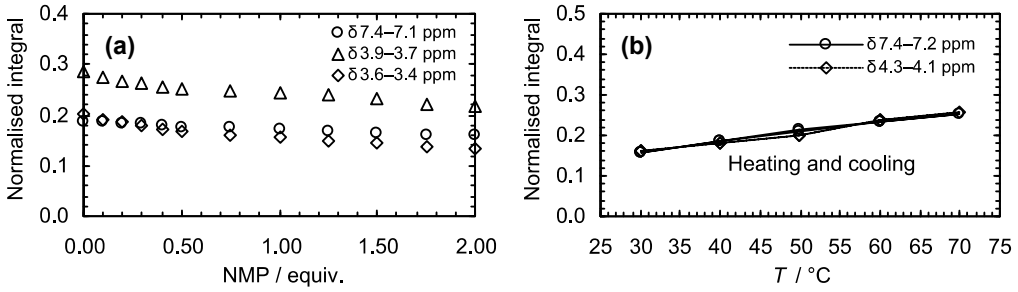

Figure 2.19 Analysis of normalised integrals from ^{1}H NMR for proline calix[4]arene **127a**–NMP system. (a) **127a** (20 mg mL^{-1} in D_2O) titrated against NMP; and (b) VT experiments for calixarene **127a** and NMP at 2.00 equiv.

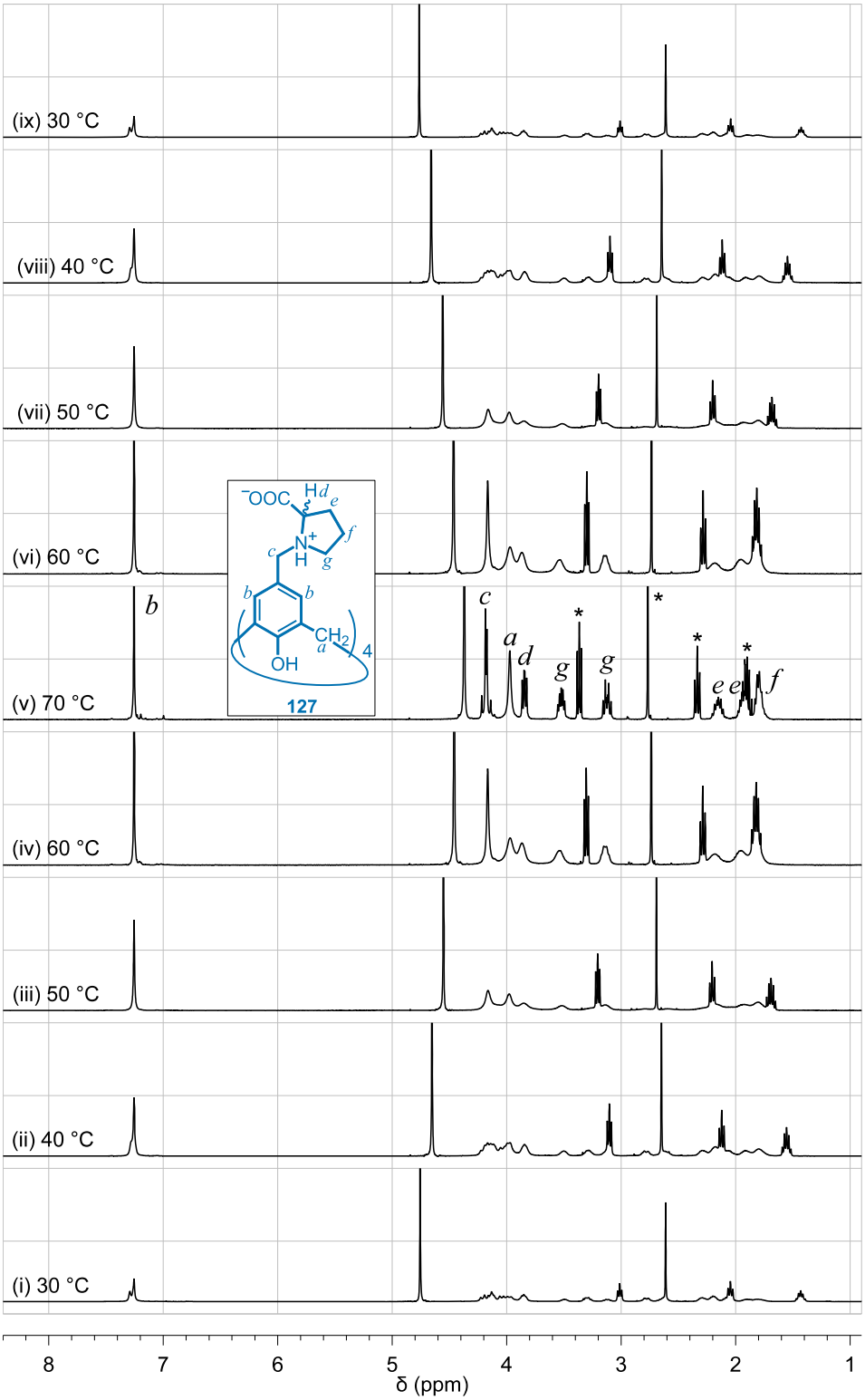

Figure 2.20 VT ^{1}H NMR (400 MHz) experiments for L-proline calix[4]arene **127a** (20 mg mL^{-1}) and NMP (*) at 2.00 equiv. in D_2O. The solution was heated, (i) to (v), and cooled, (vi) to (ix).

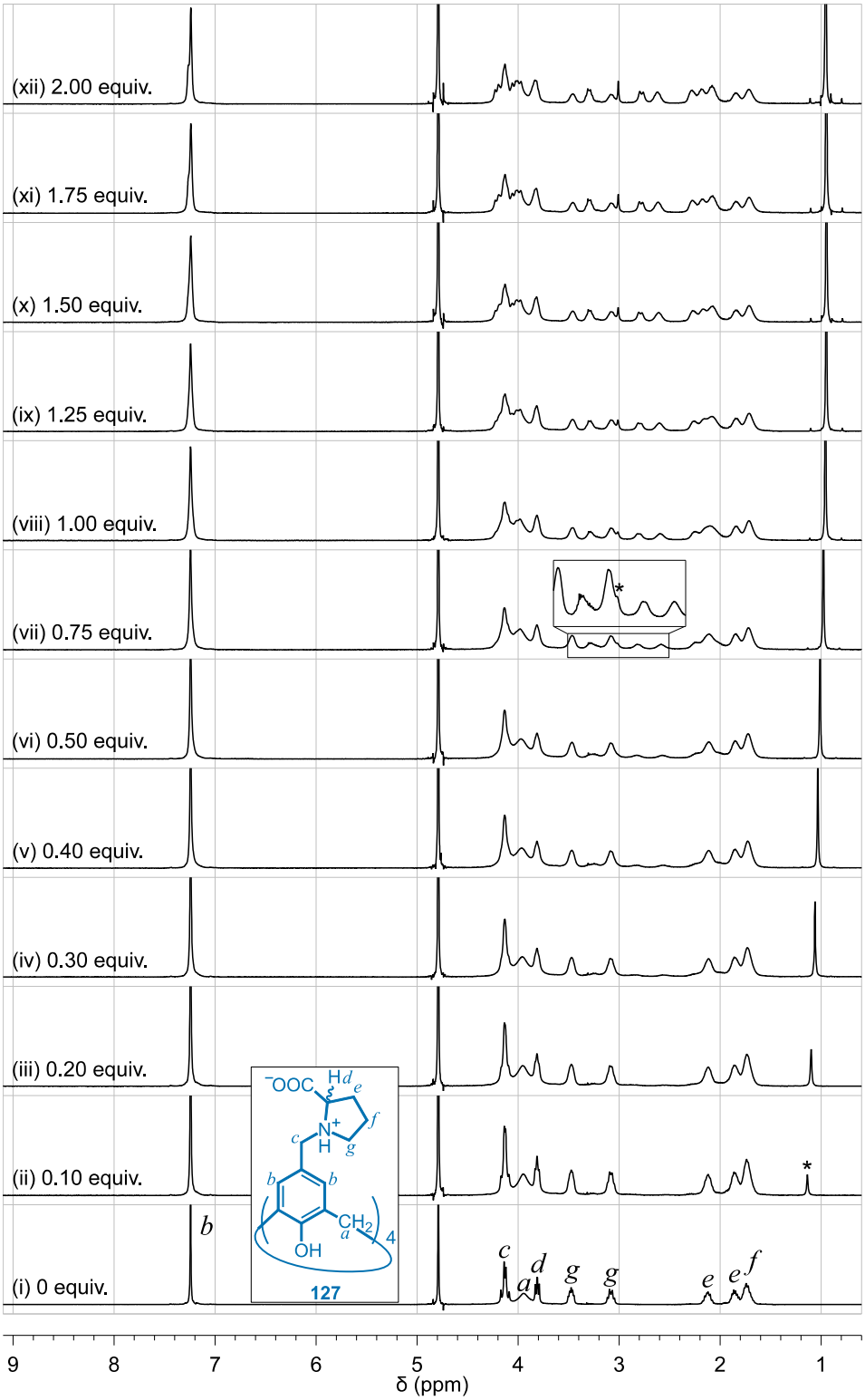

Figure 2.21 Titration of L-proline calix[4]arene **127a** against *tert*-butyl alcohol (*) with an initial solution of (i) **127a** (20 mg mL^{-1} in D_2O) and in the presence of *t*-BuOH from (ii) 0.10 equiv. to (xii) 2.00 equiv. ^1H NMR spectra were acquired at 400 MHz.

tert-Butyl alcohol initially appeared to have a similar effect as NMP and THF. NMR titrations (Figure 2.21) showed familiar signals at 3.3, 2.8, and 2.6 ppm and broadening of the calixarene signal (even at 0.1 equiv.). At 0.75 equiv. of *tert*-butyl alcohol, a small signal at ~3 ppm was visible (as a shoulder). The signal at 3 ppm was believed to be that of *tert*-butyl alcohol as it was uncharacteristically sharp compared with those of the calixarene. Typically, inclusion of guests within the calixarene cavity results in an upfield shift[80-82] in the signals of the guest as a result of shielding effects of protons positioned *over* the aromatic rings. It is hypothesised that the *tert*-butyl alcohol may be part of a larger cluster of calixarenes with its methyl groups oriented *in-plane* with the aromatic ring (explaining the downfield shift of the *tert*-butyl alcohol signal). The normalised integrals (Figure 2.22a) of these spectra were similar to those of the **127a**-THF system where there was a small decrease in the normalised integrals.

Variable temperature experiments of **127a**-*tert*-butyl alcohol system (Figure 2.23) showed that it was relatively stable. The signal at 3 ppm had disappeared at 50 °C and the calixarene signals sharpened at 65 °C. The normalised integrals (Figure 2.21b) were similar to those of the other molecules studied; it increased with heating and did not exhibit hysteresis.

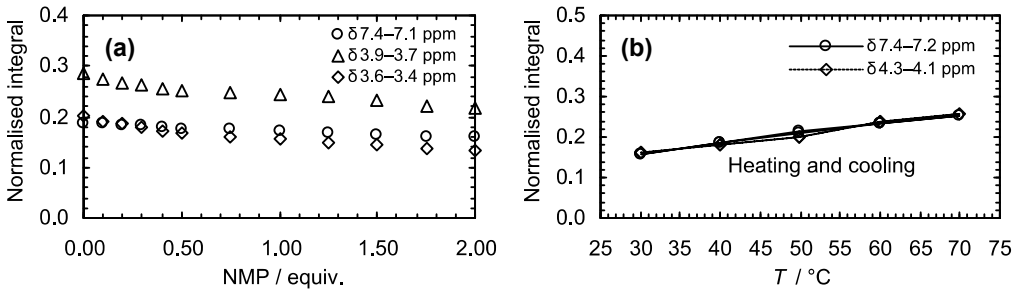

Figure 2.22 Analysis of normalised integrals from ^{1}H NMR for proline calix[4]arene **127a**–*t*-BuOH system. (a) **127a** (20 mg mL^{-1} in D_2O) titrated against *t*-BuOH; and (b) variable temperature experiments for calixarene **127a** and *t*-BuOH at 2.00 equiv.

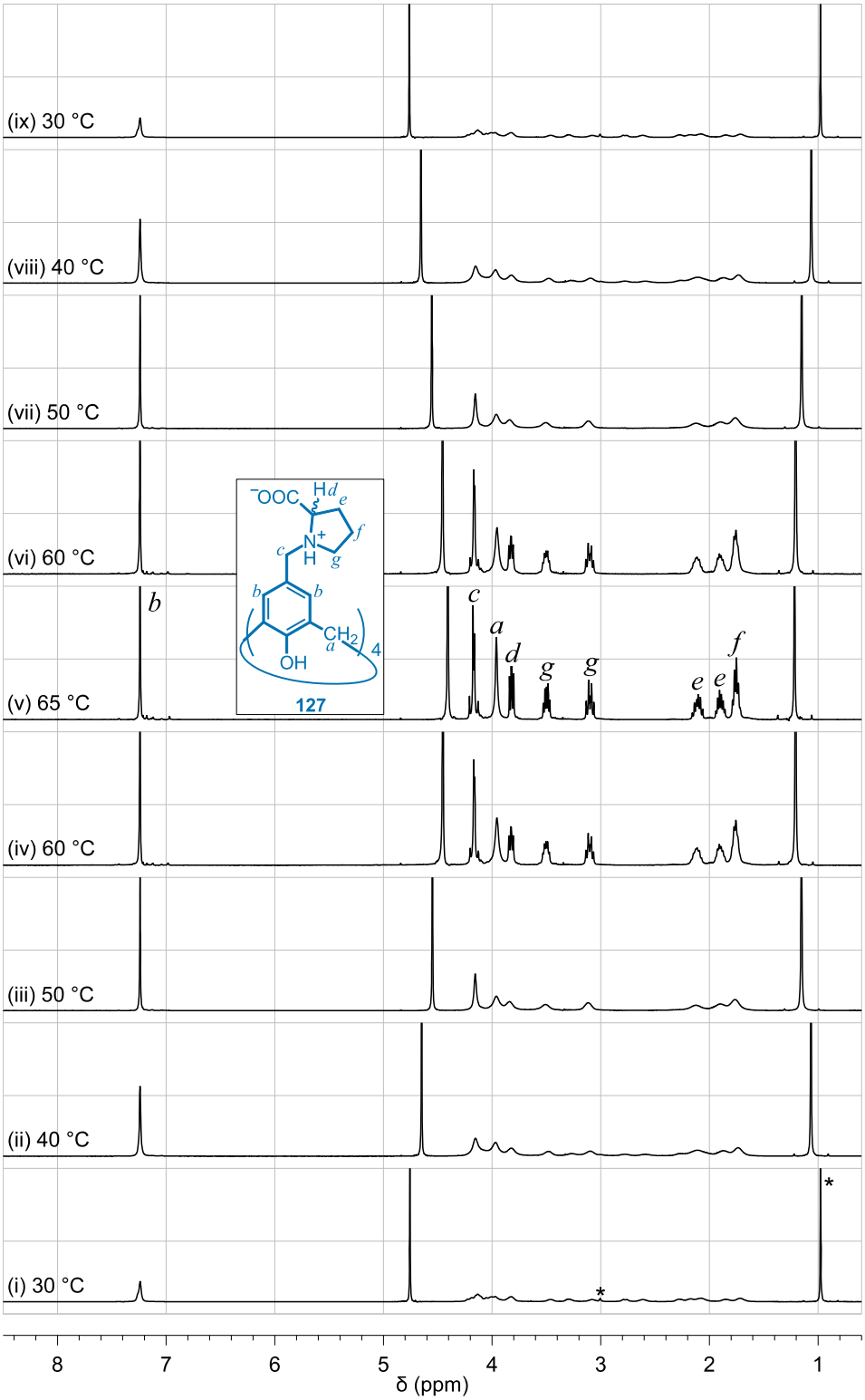

Figure 2.23 VT ^{1}H NMR (400 MHz) experiments for a L-proline calix[4]arene **127a** (20 mg mL^{-1}) and *t*-BuOH (*) at 2.00 equiv. in D_2O. The solution was heated, (i) to (v), and cooled, (vi) to (ix).

From these NMR experiments, it was shown that small organic molecules can induce the self-assembly of calixarene **127a** in solution. Variable temperature NMR experiments showed that the molecules investigated could stabilise the calixarene aggregates. The kinetics of the calixarene aggregates breaking down and reforming (on the cooling cycles) was relatively quick. This was in contrast to the calixarene in the presence of an electrolyte (see section 4.3).

2.5 Conclusions

Amino acid functionalised calix[4]arenes have been successfully synthesised. L-Aspartic acid, L-glutamic acid, and iminodiacetic acid were attached to calix[4]arenes via an amide linkage. These compounds are targeted for crystal growth modification studies (refer to Chapter 3). A proline-functionalised calix[4]-arene was also prepared. The majority of the characterisation studies discussed herein utilised the compound derived from L-proline while the D-proline analogue was used later in gelation studies (refer to Chapter 4). UV-visible spectroscopy (with a dye molecule) and ^{1}H NMR spectroscopy showed that the L-proline calix[4]arene self-assembled in water. UV-visible spectroscopy studies were performed on impure L-proline calix[4]arene and these impurities were later shown by, ^{1}H NMR experiments, to impact the self-assembly of the calixarene. Further ^{1}H NMR studies showed that it interacted with small molecules potentially acting as a host or forming larger aggregates in the presence of these smaller molecules.

2.6 Experimental

2.6.1 General remarks

Reagents were used as purchased from the manufacturer or supplier. Solvents for reactions and column chromatography were purified according to Armarego and Chai.[83]

Column chromatography was performed on Merck silica gel 60 (230–400 mesh). Reactions were monitored by TLC on aluminium backed Merck silica gel 60 F_{245} with detection by UV (for aromatic compounds), 1% $FeCl_3$ solution (for phenolic compounds), Brady's reagent[57] (for aldehydes), iodine vapour (general purpose) and/or 1% potassium permanganate solution (general purpose).

Proton and carbon NMR spectra were acquired at room temperature on a Varian Gemini™ 200 (^{1}H 200 MHz, ^{13}C 50 MHz) or a Bruker Avance™ III 400 NanoBay (^{1}H 400 MHz, ^{13}C 100 MHz) spectrometer. NMR spectra were referenced to their respective solvents:[77, 78] chloroform-*d* ($CDCl_3$, ^{1}H, δ7.26 ppm; ^{13}C, δ77.16 ppm); deuterium oxide (D_2O, ^{1}H, δ4.79 ppm); methanol-d_4 (CD_3OD, ^{1}H, δ3.31 ppm; ^{13}C, δ49.00 ppm); acetone-d_6 (CD_3COCD_3, ^{1}H, δ2.05 ppm; ^{13}C, δ29.84 or δ206.26 ppm); dimethyl sulfoxide-d_6 (CD_3SOCD_3, ^{1}H, δ2.50 ppm; ^{13}C, δ39.52 ppm). NMR signal assignments were assisted by literature data, DEPT or DEPTQ-135, and 2-dimensional NMR experiments (^{1}H–^{1}H COSY, ^{1}H–^{13}C HSQC, ^{1}H–^{13}C HMBC, ^{1}H–^{1}H TOCSY). Multiplicity is assigned as follows: s = singlet, d = doublet, t = triplet, q = quartet, sxt = sextet, br = broad.

Attenuated total reflectance Fourier Transform infrared (ATR-FT-IR) spectra were acquired on a PerkinElmer Spectrum 100 series spectrometer with a Universal ATR sampling accessory fitted with a ZnSe/diamond composite crystal. Spectra were recorded at a resolution of 4 cm^{-1} in the range of 4000–650 cm^{-1} with 16 scans accumulated. ATR correction was applied to the spectra.

Elemental analysis was performed by the Central Science Laboratory, University of Tasmania.

Melting ranges of solid samples were determined using a Barnstead/Electrothermal digital melting point apparatus (model 9100) at atmospheric pressure. Melting ranges were measured in duplicate then averaged.

2.6.2 Preparation of calixarene framework

2.6.2.1 Preparation of $1^5,3^5,5^5,7^5$-tetra-*tert*-butylcalix[4]arene-$1^2,3^2,5^2,7^2$-tetrol (1)

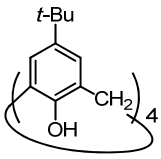

The calix[4]arene was prepared as described by Gustche.[46] Briefly, 4-*tert*-butylphenol (150.1 g, 1.00 mol), sodium hydroxide (1.80 g, 0.045 mol), and formaldehyde solution (37 wt%, 95 mL, 1.28 mol) were combined and heated at 90−100 °C for 1 hour. The resulting yellow, solid foam was cooled to room temperature, diluted with diphenyl ether (1 L), and stirred at room temperature for 1 hour. The reaction mixture was diluted with toluene (50 mL) and, under a vigorous stream of nitrogen, heated to 150−160 °C for 30 minutes then heated at reflux for 2.5 hours. The reaction mixture was allowed to cool overnight then diluted with ethyl acetate and stirred for 30 minutes. The resulting precipitate was filtered at the pump and washed with ethyl acetate (2×100 mL), acetic acid (2×100 mL), water (2×100 mL), and ethyl acetate (100 mL) to give a cream coloured solid (110.0 g). Recrystallisation of the solid from toluene gave white rhomboidal crystals (68.4 g, 0.09 mol, 37%): mp >330 °C dec (lit.[46] mp 342–344 °C); ^{1}H NMR (200 MHz, $CDCl_3$) δ 10.35 (s, 4H, Ar–O*H*), 7.36–7.13 (m, 5H, Ph–*H*, toluene), 7.05 (s, 8H, Ar–*H*), 4.26 (br d, 4H, H_{ax}, Ar–CH_2–Ar), 3.49 (br d, 4H, H_{eq}, Ar–CH_2–Ar), 2.36 (s, 3H, Ph–CH_3, toluene), 1.21 (s, 36H, C(CH_3)$_3$); IR (ATR) $\bar{\nu}_{max}$ (cm^{-1}) 3170 (O–H), 2954 (C–H).

2.6.2.2 Preparation of $1^5,3^5,5^5,7^5,9^5$-penta-*tert*-butylcalix[5]arene-$1^2,3^2,5^2,7^2,9^2$-tetrol (125)

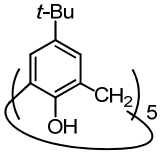

This compound was prepared according to literature.[62] A solution of potassium hydroxide (5.43 g, 0.14 mol) in water (35 mL) was added to a mixture of 4-*tert*-butylphenol (75.2 g, 0.50 mol) and para-formaldehyde (50.2 g, 1.67 mol) in 1,2,3,4-tetrahydronaphthalene (1 L). The stirring reaction mixture was heated at 80–90 °C for 1.5 hours then rapidly heated to 180 °C for 10 minutes then cooled to 160 °C for 3 hours. The reaction mixture was cooled to room temperature and the solid filtered. The solid was washed with toluene (2×50 mL). The toluene washings were combined with the reaction mixture filtrate (1,2,3,4-tetrahydronaphthalene phase) and the organic solvents removed by steam distillation. The residue was carefully acidified with hydrochloric

acid (37%, 200 mL), chloroform (500 mL) added and the biphasic solution stirred for 15 minutes. The chloroform phase was separated, filtered through diatomaceous earth, dried (Na_2SO_4), and concentrated *in vacuo*. Recrystallisation of the residue twice from acetone gave an off-white powder (7.67 g, 9.5 mmol, 7.5% yield): mp 305–311 °C (lit.[62] mp 310–312 °C); ^{1}H NMR (200 MHz, CD_3COCD_3) δ 8.59 (br s, 5H, Ar–O*H*), 7.37 (s, 10H, Ar–*H*), 3.86 (br s, 10H, Ar–C*H*$_2$–Ar), 1.23 (s, 45H, C*H*$_3$); IR (ATR) $\bar{\nu}_{max}$ (cm^{-1}) 3300 (O–H), 2956 (C–H).

2.6.2.3 Preparation of calix[4]arene-1^2,3^2,5^2,7^2-tetrol (2)

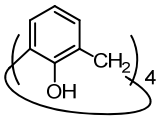

This compound was prepared as described by Strobel.[47] Briefly, **1** (18.2 g, 25 mmol) and phenol (14.0 g, 149 mmol) were suspended in toluene (250 mL) heated at 60 °C and stirred for 15 minutes. Anhydrous aluminium trichloride (26.3 g, 197 mmol) and toluene (50 mL) were carefully added to the reaction mixture and stirred for a further 4 hours at 60−70 °C. The reaction mixture was diluted with hydrochloric acid (3 M, 210 mL) and toluene (150 mL) and stirred for 1 hour at room temperature. The aqueous phase was separated and extracted with toluene (100 mL). The toluene phases were combined, dried (Na_2SO_4), and concentrated *in vacuo*. Ice-cold methanol was added to the residue and the resulting precipitate filtered at the pump. Trituration of the solid with methanol afforded a beige crystalline powder (10.3 g, 24 mmol, 98% yield): mp 301–310 °C (lit.[84] mp 315–318 °C); ^{1}H NMR (200 MHz, $CDCl_3$) δ 10.21 (s, 4H, Ar–O*H*), 7.05 (d, *J* = 7.3 Hz, 8H, Ar–*H*), 6.74 (t, *J* = 7.3 Hz, 4H, Ar–*H*), 4.24 (br s, 4H, H_{ax}, Ar–C*H*$_2$–Ar), 3.55 (br s, 4H, H_{eq}, Ar–C*H*$_2$–Ar; IR (ATR) $\bar{\nu}_{max}$ (cm^{-1}) 3140 (O–H).

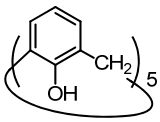

2.6.2.4 Preparation of calix[5]arene-1^2,3^2,5^2,7^2,9^2-pentol (126)

This compound was prepared from modified procedures from Bell et al.[64] and Coruzzi et al.[65] A solution of **125** (1.005 g, 1.24 mmol), and anhydrous aluminium

trichloride (1.630 g, 12.2 mmol) in dry toluene (10 mL) was stirred at room temperature for 1 hour. The reaction mixture was cooled in an ice-bath and hydrochloric acid (1 M, 20 mL) added dropwise. The reaction mixture was diluted with dichloromethane (30 mL) and the aqueous phase separated and extracted with dichloromethane (10 mL). The dichloromethane phases were combined, washed with hydrochloric acid (1 M, 10 mL), water (10 mL), saturated sodium chloride solution (10 mL), dried (Na_2SO_4), and concentrated *in vacuo*. The orange solid was dissolved in chloroform and precipitated with methanol. The solid was filtered at the pump and washed with a minimal amount of diethyl ether (note: diethyl ether removes the sticky orange residue, the product is appreciably soluble in diethyl ether). This gave an off-white powder (0.438 g, 0.83 mmol, 66% yield): mp 281 °C dec (lit.[64] mp >275 °C); ^{1}H NMR (400 MHz, $CDCl_3$) δ 8.91 (s, 5H, Ar–O*H*), 7.21 (d, *J* = 7.6 Hz, 10H, Ar–*H*), 6.84 (t, *J* = 7.6 Hz, 5H, Ar–*H*), 3.84 (br s, 10H, Ar–CH_2–Ar); IR (ATR) $\bar{\nu}_{max}$ (cm^{-1}) 3150 (O–H).

2.6.2.5 **Preparation of 1^2,3^2,5^2,7^2-tetra-*n*-propoxycalix[4]arene (28)**

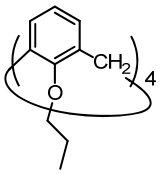

This compound was prepared from a modified procedure from Dondoni et al.[49] **2** (3.91 g, 9.22 mmol) was added to a stirring suspension of sodium hydride (4.20 g, 105 mmol, of a 60% dispersion in oil) in *N*,*N*-dimethylformamide (80 mL). A few small crystals of imidazole were added to the reaction mixture which then was stirred for 1 hour under a nitrogen atmosphere. Propyl bromide (8.6 mL, 11.6 g, 94.4 mmol) was added to the reaction mixture and was stirred at 60 °C under a nitrogen atmosphere for 18 hours. The reaction mixture was cooled to room temperature, quenched with methanol, and concentrated *in vacuo*. The residue was diluted with hydrochloric acid (3 M, 100 mL) and extracted with diethyl ether (4×50 mL). The diethyl ether extracts were combined, dried (Na_2SO_4), and concentrated *in vacuo*. Recrystallisation of the orange-brown solid from chloroform/methanol (~6:4, 10 mL) gave an off-white powder (4.10 g, 6.9 mmol, 75% yield): mp 186–194 °C (lit.[49] mp 197–199 °C); ^{1}H NMR (200 MHz, $CDCl_3$) δ 6.67–6.55 (overlapped m, Ar–*H*, 12H), 4.46 (d, *J* = 13.2 Hz, 4H, H_{ax}, Ar–CH_2–Ar), 3.85 (t, *J* = 7.5 Hz, 8H, OCH_2), 3.15 (d, *J* = 13.2 Hz,

4H, H_{eq}, Ar–C*H*$_2$–Ar), 1.93 (apparent sxt, 8H, OCH$_2$C*H*$_2$), 0.99 (t, *J* = 7.5 Hz, 12H, C*H*$_3$); IR (ATR) $\bar{\nu}_{max}$ (cm^{-1}) 2962– 2875 (C–H).

2.6.2.6 Preparation of 1^2,3^2,5^2,7^2-tetra-*n*-propoxycalix[4]arene-1^5,3^5,5^5,7^5-tetracarbaldehyde (119)

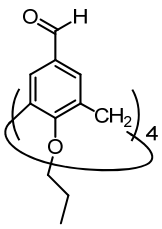

The calixarene was prepared as described by Dondoni et al.[49, 54] Briefly, a solution of **28** (1.00 g, 1.69 mmol) and hexamethylenetetramine (7.14 g, 50.9 mmol) in trifluoroacetic acid (40 mL) was heated at reflux overnight. The reaction mixture was diluted with dichloromethane (100 mL) and hydrochloric acid (1 M, 100 mL) and stirred at room temperature overnight. The aqueous phase was separated and extracted with dichloromethane (50 mL). The dichloromethane phases were combined, washed with water (2×50 mL) then saturated sodium chloride (60 mL), dried ($MgSO_4$), and concentrated *in vacuo* to give an orange solid. Trituration of the solid with methylcyclohexane afforded a beige powder (0.944 g, 1.34 mmol, 79% yield): mp >250 °C dec (lit.[49] mp 289–290 °C); ^{1}H NMR (200 MHz, $CDCl_3$) δ 9.58 (s, 4H, Ar–C*H*O), 7.15 (s, 8H, Ar–*H*), 4.15 (d, *J* = 13.9 Hz, 4H, H_{ax}, Ar–C*H*$_2$–Ar), 3.93 (t, *J* = 7.5 Hz, 8H, OC*H*$_2$), 3.35 (d, *J* = 13.9 Hz, 4H, H_{eq}, Ar–C*H*$_2$–Ar), 1.91 (apparent sxt, 8H, OCH$_2$C*H*$_2$), 1.01 (t, *J* = 7.5 Hz, 12H, C*H*$_3$); IR (ATR) $\bar{\nu}_{max}$ (cm^{-1}) 2739, 2725 (CHO), 1685 (Ar–C=O).

2.6.2.7 Preparation of 1^2,3^2,5^2,7^2-tetra-*n*-propoxycalix[4]arene-1^5,3^5,5^5,7^5-tetracarboxylic acid (92)

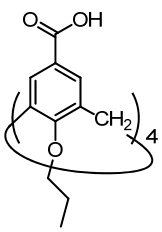

This compound was prepared according to literature.[20, 56] A freshly prepared solution of sodium chlorite (80%, 1.23 g, 10.88 mmol) and sulfamic acid (1.28 g, 13.18 mmol) in water (5 mL) was added immediately to a stirring solution of **119** (0.70 g, 0.99 mmol) dissolved in acetone (30 mL) and chloroform (30 mL) at −5 °C. The turbid reaction mixture was stirred at room temperature for two days. A second aliquot of sodium chlorite (80%, 1.245 g, 11.0 mmol) and sulfamic acid (1.24 g, 13.2 mmol) dissolve in water (5 mL) was added to the reaction mixture. After 24 hours, a third aliquot of sodium chlorite (80%, 1.24 g, 10.9 mmol) and sulfamic acid

(1.28 g, 13.2 mmol) dissolve in water (5 mL) was added to the reaction mixture along with acetone (10 mL) and chloroform (10 mL). The reaction mixture was stirred for a further five days. The reaction mixture was concentrated *in vacuo*. The residue was diluted with methanol (10 mL) and hydrochloric acid (3 M, 10 mL) and stirred at room temperature for two days. The precipitate was filtered and washed with hydrochloric acid (3 M) then cold methanol. This gave a beige solid (0.714 g, 0.93 mmol, 93% yield): mp >360 °C (lit.[20] mp >360 °C); ^{1}H NMR (200 MHz, CD_3OD) δ 7.38 (s, 8H, Ar–*H*), 4.53 (d, *J* = 13.6 Hz, 4H, H_{ax}, Ar–C*H*$_2$–Ar), 3.97 (t, *J* = 7.5 Hz, 8H, OC*H*$_2$), 3.36 (d overlapped with CD_3OD, H_{eq}, Ar–C*H*$_2$–Ar), 1.97 (m, 8H, OCH_2CH_2), 1.05 (t, J = 7.5 Hz, 12H, C*H*$_3$); IR (ATR) $\bar{\nu}_{max}$ (cm^{-1}) 3065*s* (O–H), 1694 (Ar–C=O), 1202 (C–O).

2.6.2.8 Preparation of 1^2,3^2,5^2,7^2-tetra-*n*-propoxycalix[4]arene-1^5,3^5,5^5,7^5-tetracarbonyl chloride (94)

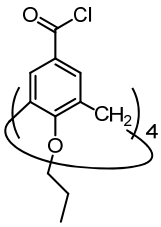

This calixarene was prepared according to literature.[20] *N,N*-Dimethylformamide (1 drop) was added to a stirring solution of oxalyl chloride (3.4 mL, 4.9 g, 38.6 mmol) and **92** (376 mg, 0.49 mmol) in dichloromethane (25 mL). The reaction solution was heated at reflux under an argon atmosphere overnight. The reaction solution was concentrated *in vacuo* and the residue used immediately without further purification or characterisation.

2.6.3 Preparation of protected amino acid fragments

2.6.3.1 Preparation of L-aspartic acid diethyl ester hydrochloride (120)

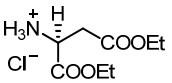

Thionyl chloride (19.3 mL, 31.6 g, 265 mmol) was added dropwise to a cold stirred suspension of L–aspartic acid (5.73 g, 43 mmol) in ethanol (150 mL) and stirred at room temperature for one week. The reaction mixture was concentrated *in vacuo* to give a pale-brown oil which solidified on cooling. Trituration of the solid with diethyl ether to gave white fine needle-like crystals (9.15 g, 40 mmol, 93% yield): mp 107–110 °C (lit.[85] mp 109–110 °C); ^{1}H NMR (400 MHz, $CDCl_3$) δ 8.79 (br s, 3H, N*H*$_3$), 4.55 (apparent t, 1H, NC*H*), 4.34–4.22 (m, 2H, OC*H*$_2$), 4.18 (q, *J* = 7.1 Hz, 2H, OC*H*$_2$), 3.30 (dd, *J* = 5.1, 17.8 Hz, 1H, H′,

NCHCH_2), 3.20 (dd, J = 5.4, 17.8 Hz, 1H, H″, NCHCH_2), 1.27 (t, J = 7.1 Hz, 3H, CH_3), 1.25 (t, J = 7.1 Hz, 3H, CH_3); ^{13}C NMR (100 MHz, $CDCl_3$) δ 170.1 (C=O), 168.1 (C=O), 63.1 (OCH$_2$), 61.9 (OCH$_2$), 49.8 (NCH), 34.2 (NCHCH$_2$), 14.2 (CH$_3$), 14.1 (CH$_3$); IR (ATR) $\bar{\nu}_{max}$ (cm^{-1}) 3129 (N–H), 1747 (C=O), 1712 (C=O), 1245, 1231, 1216 (C–O).

2.6.3.2 Preparation of L-glutamic acid diethyl ester hydrochloride (121)

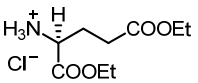

Thionyl chloride (8.3 mL, 13.60 g, 114 mmol) was added dropwise to a cold stirred suspension of L–glutamic acid (5.52 g, 38 mmol) in ethanol (70 mL). The reaction mixture was stirred at room temperature overnight then concentrated *in vacuo* to give a pale-yellow oil which crystallised on standing. Trituration of the solid with diethyl ether gave a white crystalline powder (8.99 g, 37 mmol, 97% yield): mp 112–114 °C (lit.[86] mp 113–114 °C); ^{1}H NMR (400 MHz, $CDCl_3$) δ 8.83 (br s, 3H, NH_3), 4.27 (overlapped, apparent t, 1H, NCH), 4.27 (q, J = 7.1 Hz, 2H, OCH_2), 4.12 (q, J = 7.1 Hz, 2H, OCH_2), 2.77–2.55 (m, 2H, CH_2C=O), 2.48–2.32 (m, 2H, NCHCH_2), 1.30 (t, J = 7.1 Hz, 3H, CH_3), 1.24 (t, J = 7.1 Hz, 3H, CH_3); ^{13}C NMR (100 MHz, $CDCl_3$) δ 172.4 (C=O), 169.1 (C=O), 62.9 (OCH$_2$), 61.0 (OCH$_2$), 52.7 (NCH), 30.1 (CH$_2$C=O), 25.6 (NCHCH$_2$), 14.3 (CH$_3$), 14.16 (CH$_3$); IR (ATR) $\bar{\nu}_{max}$ (cm^{-1}) 3459 (N–H), 1732 (C=O), 1224, 1198, 1185 (C–O).

2.6.3.3 Preparation of 2,2'-[(carbonyl)imino]diacetic acid diethyl ester hydrochloride (122)

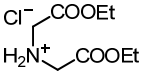

Thionyl chloride (7 mL, 11.5 g, 96 mmol) was added dropwise to a stirred suspension of iminodiacetic acid (5.23 g, 39 mmol) in ethanol (50 mL). The reaction mixture was stirred at room temperature overnight. More thionyl chloride (14 mL, 22.9 g, 193 mmol) was added to the reaction mixture and then heated at reflux. The reaction mixture was concentrated *in vacuo* to give a brown oil which crystallised on standing. Trituration of the solid with diethyl ether gave a pale-brown powder (8.91 g, 39 mmol, quantitative yield): mp 60.7–71.0 °C (lit.[87] mp 73–75); ^{1}H NMR (400 MHz, $CDCl_3$) δ 4.27 (q, J = 7.2 Hz, 4H, OCH_2), 4.01 (s, 4H, CH_2C=O), 1.29 (t, J = 7.2 Hz, 6H, CH_3); ^{13}C NMR (100 MHz, $CDCl_3$) δ

166.2 (C=O), 62.8 (O*C*H_2), 47.0 (*C*H_2C=O), 14.1 (*C*H_3); IR (ATR) $\bar{\nu}_{max}$ (cm^{-1}) 3346 (N–H), 1741 (C=O), 1220, 1202 (C–O).

2.6.4 Preparation of amino acid functionalised calixarenes for crystal growth modification studies

2.6.4.1 Preparation of 1^2,3^2,5^2,7^2-tetra-*n*-propoxycalix[4]arene-1^5,3^5,5^5,7^5-tetrakis-{(2*S*)-2-[(carbonyl)amino]}butanedioic acid diethyl ester (123a)

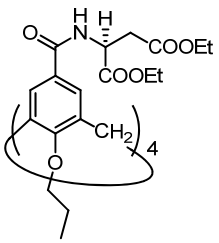

A solution of **120** (502 mg, 2.22 mmol) and triethylamine (0.61 mL, 440 mg, 4.35 mmol) dissolved in dichloromethane (15 mL) was added dropwise to a cold stirring solution of the acid chloride **94** (413 mg, 0.49 mmol) dissolved in dichloromethane (15 mL) over 15 minutes. The reaction mixture was stirred at room temperature under an argon atmosphere over the weekend. The reaction mixture was diluted with hydrochloric acid (1 M, 30 mL) and stirred for 30 minutes. The organic phase was separated and washed with hydrochloric acid (2×15 mL) then saturated sodium chloride (30 mL), dried ($MgSO_4$), and concentrated *in vacuo*. Purification of the brown residue by column chromatography [dichloromethane/acetone (9:1, v/v)] afforded a glassy yellow solid (318 mg, 0.22 mmol, 44% yield) which crystallised on standing: mp 120–130 °C (material crystallised from glassy material); ^{1}H NMR (400 MHz, $CDCl_3$) δ 7.16 (d, *J* = 2.1 Hz, 4H, Ar–*H*), 7.04 (d, *J* = 2.1 Hz, 4H, Ar–*H*), 7.01 (d, *J* = 7.9 Hz, 4H, N–*H*), 4.88 (apparent dt, 4H, NC*H*), 4.46 (d, *J* = 13.6 Hz, 4H, H_{ax}, Ar–CH_2–Ar), 4.25–4.09 (overlapped m, 16H, OC$H_2$$CH_3$), 3.88 (t, *J* = 7.5 Hz, 8H, OC$H_2$$CH_2$), 3.27 (d, *J* = 13.6 Hz, 4H, H_{eq}, Ar–CH_2–Ar), 3.02 (dd, *J* = 4.4, 16.7 Hz, 4H, H′, CH_2C=O), 2.94 (dd, *J* = 5.4, 16.7 Hz, 4H, H″, CH_2C=O), 1.90 (sxt, *J* = 7.5 Hz, 8H, OCH_2CH_2), 1.25 (overlapped, apparent q, 24H OCH_2CH_3), 0.99 (t, *J* = 7.5 Hz, 12H OCH_2CH_2CH_3); ^{13}C NMR (100 MHz, $CDCl_3$) δ 171.4 (C=O, ester), 171.2 (C=O, ester), 167.0 (C=O, amide), 159.6 (*C*–O, Ar), 135.0 (*C*–CH_2, Ar), 134.8 (*C*–CH_2, Ar), 128.3 (*C*–C=O, Ar), 128.1 (*C*–H, Ar), 127.2 (*C*–H, Ar), 77.2 (overlapped with $CDCl_3$, O*C*$H_2$$CH_2$), 61.8 (O*C*$H_2$$CH_3$), 61.1 (O*C*$H_2$$CH_3$), 49.3 (N*C*H), 36.5 (*C*H_2C=O), 31.2 (Ar–*C*H_2–Ar), 23.3 (OCH_2*C*H_2), 14.30 (OCH_2*C*H_3), 14.25 (OCH_2*C*H_3), 10.4 (OCH_2CH_2*C*H_3); IR (ATR) $\bar{\nu}_{max}$ (cm^{-1}) 3347 (N–H), 1732 (C=O, ester), 1657 (C=O, amide), 1197 (C–

O). Anal. Calcd for $C_{76}H_{100}N_4$: C, 62.80; H, 6.93; N, 3.85%). Found: C, 62.54; H, 6.75; N, 3.64%.

2.6.4.2 Preparation of $1^2,3^2,5^2,7^2$-tetra-*n*-propoxycalix[4]arene-$1^5,3^5,5^5,7^5$-tetrakis-{(2*S*)-2-[(carbonyl)amino]}pentanedioic acid diethyl ester (123b)

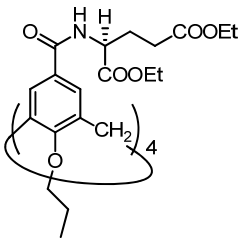

This compound was prepared according to the procedure described for **123a**. A solution of **121** (978 mg, 4.08 mmol) and triethylamine (1.40 mL, 1060 mg, 10.48 mmol) dissolved in dichloromethane (15 mL) was added dropwise to a cold stirring solution of **94** (519 mg, 0.62 mmol) dissolved in dichloromethane (20 mL) over 15 minutes. The reaction mixture was stirred a room temperature under a nitrogen atmosphere for six days. The reaction mixture was diluted with dichloromethane (25 mL) and washed with hydrochloric acid (3×25 mL) then saturated sodium chloride (25 mL), dried ($MgSO_4$), and concentrated *in vacuo*. Purification of the brown residue by column chromatography (dichloromethane/ acetone (9:1, v/v) and 0.5 v/v% triethylamine) afforded a glassy yellow solid (320 mg, 0.21 mmol, 34% yield) which crystallised on standing: mp 121–136 °C (material crystallised from glassy material); ^{1}H NMR (400 MHz, $CDCl_3$) δ 7.16 (d, *J* = 2.2 Hz, 4H, Ar–*H*), 7.10 (d, *J* = 2.2 Hz, 4H, Ar–*H*), 6.83 (d, *J* = 7.0 Hz, 4H, N–*H*), 4.59 (apparent dt, 4H, NC*H*), 4.46 (d, *J* = 13.6 Hz, 4H, H_{ax}, Ar–CH_2–Ar), 4.27–4.15 (m, 8H, OCH_2CH$_3$), 4.15–4.02 (m, 8H, OCH_2CH$_3$), 3.38 (t, *J* = 7.5 Hz, 8H, OCH_2CH$_2$), 3.26 (d, *J* = 13.6 Hz, H_{eq}, Ar–CH_2–Ar), 2.50–2.34 (m, 8H, CH_2C=O), 2.31–2.17 (m, 4H, H′, NCHCH_2), 2.12–1.99 (m, 4H, H″, NCHCH_2), 1.90 (sxt, *J* = 7.5 Hz, 8H, OCH$_2$CH_2), 1.28 (t, *J* = 7.1 Hz, 12H, OCH$_2$CH_3), 1.21 (t, *J* = 7.2 Hz, 12H, OCH$_2$CH_3), 0.99 (t, *J* = 7.5 Hz, 12H, OCH$_2$CH$_2$CH_3); ^{13}C NMR (100 MHz, $CDCl_3$) δ 173.4 (C=O, ester), 172.1 (C=O, ester), 167.3 (C=O, amide), 159.4 (*C*–O, Ar), 135.0 (*C*–CH$_2$, Ar), 134.9 (*C*–CH$_2$, Ar), 128.5 (*C*–C=O, Ar), 127.8 (*C*–H, Ar), 127.7 (*C*–H, Ar), 77.2 (overlapped with $CDCl_3$, OCH_2CH$_2$), 61.6 (OCH_2CH$_3$), 60.7 (OCH_2CH$_3$), 52.5 (NCH), 31.2 (Ar–CH_2–Ar), 30.6 (CH_2C=O), 27.4 (NCHCH_2), 23.3 (OCH$_2$CH_2), 14.30 (OCH$_2$CH_3), 10.4 (OCH$_2$CH$_2$CH_3); IR (ATR) $\bar{\nu}_{max}$ (cm^{-1}) 3382 (N–H), 1733 (C=O, ester), 1645 (C=O, amide), 1190 (C–O). Anal. Calcd for $C_{80}H_{108}N_4$: C, 63.64; H, 7.21; N, 3.71%. Found: C, 63.48; H, 7.53; N, 3.66%.

2.6.4.3 Preparation of $1^2,3^2,5^2,7^2$-tetra-*n*-propoxycalix[4]arene-$1^5,3^5,5^5,7^5$-tetrakis-2,2'-[(carbonyl)imino]diacetic acid diethyl ester (123c)

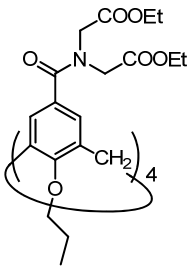

A solution of **122** (1.27 g, 5.65 mmol) and triethylamine (2.00 mL, 1.52 g, 15.0 mmol) dissolved in dichloromethane (15 mL) was added dropwise to a cold stirring solution of **94** (565 mg, 0.67 mmol) dissolved in dichloromethane (10 mL) over 15 minutes. The reaction mixture was stirred at room temperature under a nitrogen atmosphere over three days. The reaction mixture was diluted with dichloromethane (25 mL) and washed with hydrochloric acid (1 M, 3×25 mL), saturated sodium chloride (25 mL), dried (Na_2SO_4), and concentrated *in vacuo*. Purification of the brown residue by column chromatography [dichloromethane/acetone (9:1, v/v)] afforded a glassy yellow solid (296 mg, 0.20 mmol, 30% yield) which crystallised on standing: mp 110–121 °C (material crystallised from glassy material); ^{1}H NMR (400 MHz, $CDCl_3$) δ 6.95 (s, 8H, Ar–*H*), 4.46 (d, *J* = 13.3, 4H, H_{ax}, Ar–C*H*$_2$–Ar), 4.33–4.07 (overlapped m, OC*H*$_2$CH$_3$ and NC*H*$_2$), 3.90 (t, *J* = 7.7 Hz, 8H, OC*H*$_2$CH$_2$), 3.17 (d, *J* = 13.3 Hz, 8H, H_{eq}, Ar–C*H*$_2$–Ar), 1.92 (sxt, *J* = 7.7 Hz, 8H, OCH$_2$C*H*$_2$CH$_3$), 1.27 (apparent br t, 24H, OCH$_2$C*H*$_3$), 0.99 (*J* = 7.7 Hz, 12H, OCH$_2$CH$_2$C*H*$_3$); ^{13}C NMR (100 MHz, $CDCl_3$) δ 171.6 (C=O), 169.6 (C=O), 169.2 (C=O), 158.3 (*C*–O, Ar), 134.7 (*C*–CH$_2$, Ar), 128.2 (*C*–C=O, Ar), 128.3 (*C*–H, Ar), 61.7, 61.1 (O*C*H$_2$CH$_3$), 77.2 (overlapped with $CDCl_3$, O*C*H$_2$CH$_2$), 52.2, 48.1 (N*C*H$_2$C=O), 31.4 (Ar–*C*H$_2$–Ar), 23.2 (OCH$_2$*C*H$_2$CH$_3$), 14.5, 14.3 (OCH$_2$*C*H$_3$), 10.4 (OCH$_2$CH$_2$*C*H$_3$); IR (ATR) $\bar{\nu}_{max}$ (cm^{-1}) 1738 (C=O, ester), 1645 (C=O, amide), 1183 (C–O). Anal. Calcd for $C_{76}H_{100}N_4$: C, 62.80; H, 6.93; N, 3.85%. Found: C, 62.80; H, 7.00; N, 3.68%.

2.6.4.4 Preparation of $1^2,3^2,5^2,7^2$-tetrapropoxycalix[4]arene-$1^5,3^5,5^5,7^5$-tetrakis-{(2*S*)-2-[(carbonyl)amino]}butanedioic acid (124a)

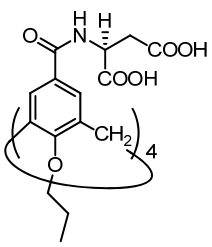

A solution of potassium carbonate (350 mg, 2.53 mmol) in water (2 mL) was added to a stirred solution of (**123a**) (286 mg, 0.20 mmol) in methanol (25 mL) at 40–50 °C. The reaction mixture was stirred for 2 hours, cooled to room temperature, and

concentrated *in vacuo*. The residue was diluted with water (30 mL), acidified with hydrochloric acid (3 M, ~2 mL) to pH ~1, and extracted with ethyl acetate (4×15 mL). The ethyl acetate extracts were combined, washed with water (30 mL) then saturated sodium chloride (30 mL), dried (Na_2SO_4), and concentrated *in vacuo*. This gave a solid (160 mg, 0.13 mmol, 66% yield): mp >240 °C dec; ^{1}H NMR (400 MHz, CD_3SOCD_3) δ 12.50 (br s, 5H, COO*H*),* 8.74–8.24 (m, 4H, N–*H*), 7.59–7.19 (m, 8H, Ar–*H*), 4.74–4.54 (m, 4H, NC*H*), 4.43, (d, *J* = 12.9, 4H, H_{ax}, Ar–CH_2–Ar), 4.02–3.92 (m, 4H, OCH_2), 3.36 (overlapped with HOD, H_{eq}, Ar–CH_2–Ar), 2.93–2.55 (m, NCHCH_2C=O), 1.92 (sxt, *J* = 7.5 Hz, 8H, $OCH_2CH_2CH_3$), 1.04–0.90 (m, 12H, CH_3); ^{13}C NMR (100 MHz, CD_3SOCD_3) δ 172.6 (C=O, carboxylic acid), 172.0 (C=O, carboxylic acid), 165.7 (C=O, amide), 158.7 (*C*–O, Ar), 134.0 (*C*–CH_2, Ar), 128.1 (overlapped, *C*–H, Ar and *C*–C=O, Ar), 76.7 (O*C*H_2), 49.3 (N*C*H), 35.9 (*C*H_2C=O), 30.7 (Ar–*C*H_2–Ar), 22.7 (OCH_2CH_2), 10.1 (*C*H_3); IR (ATR) $\bar{\nu}_{max}$ (cm^{-1}) 3340 (O–H), 1720 (C=O, carboxylic acid), 1626 (C=O, amide), 1205 (C–O).

2.6.4.5 Preparation of 1^2,3^2,5^2,7^2-tetra-*n*-propoxycalix[4]arene-1^5,3^5,5^5,7^5-tetrakis-{(2*S*)-2-[(carbonyl)amino]}pentanedioic acid (124b)

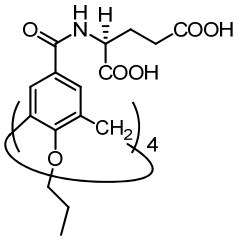

An aqueous solution of potassium hydroxide (1.92 M, 925 µL, 1.78 mmol) was added to a solution of **123b** (320 mg, 0.21 mmol) in methanol (20 mL) and stirred at room temperature for 6 hours. The reaction mixture was acidified with hydrochloric acid (3 M, ~1 mL), concentrated *in vacuo*, and the residue was diluted with water (10 mL) and ethyl acetate (10 mL). The aqueous phase was separated and extracted with ethyl acetate (3×10 mL). The ethyl acetate extracts were combined, washed with saturated sodium chloride (20 mL), dried (Na_2SO_4), and concentrated *in vacuo*. This gave a yellow solid (273 mg, 0.21 mmol, >98%): mp 121–140 °C; ^{1}H NMR (400 MHz, CD_3SOCD_3) δ 12.40 (b s, 4H, COO*H*),* 8.55–8.08 (m, 4H, N–*H*), 7.60–7.20 (m, 8H, Ar–*H*), 4.44 (d, *J* = 12.8 Hz, 4H, H_{ax}, Ar–CH_2–Ar), 4.35–4.17 (m, 4H, NC*H*), 4.02–3.81 (m, 8H, OCH_2),

* Dimethyl sulfoxide-d_6 is prepared from dimethyl sulfoxide by base-catalysed exchange of the protons with deuterium from deuterium oxide.[88] It is suspected that the under-integration of the protons of the carboxylic acid a result of residual D_2O in CD_3SOCD_3 and the small quantity of sample used.

3.37 (overlapped with HOD, H_{eq}, Ar–CH_2–Ar), 2.45–2.27 (m, 8H, CH_2C=O), 2.12–1.83 (overlapped m, 16H, NCHCH_2 and OCH$_2$CH_2), 1.06–0.90 (m, 12H, CH_3); ^{13}C NMR (100 MHz, CD_3SOCD_3) δ 173.3 (C=O, carboxylic acid), 172.9 (C=O, carboxylic acid), 166.4 (C=O, amide), 158.6 (*C*–O, Ar), 134.0 (*C*–CH$_2$, Ar), 128.3 (*C*–C=O, Ar), 128.1 (*C*–H, Ar), 76.7 (O*C*H$_2$), 52.1 (N*C*H), 30.6 (Ar–*C*H$_2$–Ar), 30.2 (*C*H$_2$C=O), 25.9 (NCH*C*H$_2$), 22.7 (OCH$_2$*C*H$_2$), 10.1 (*C*H$_3$); IR (ATR) $\bar{\nu}_{max}$ (cm^{-1}) 3352 (O–H), 1731 (C=O, carboxylic acid), 1633 (C=O, amide), 1202 (C–O).

2.6.4.6 Preparation of 1^2,3^2,5^2,7^2-tetra-*n*-propoxycalix[4]arene-1^5,3^5,5^5,7^5-tetrakis-2,2'-[(carbonyl)imino]diacetic acid (124c)

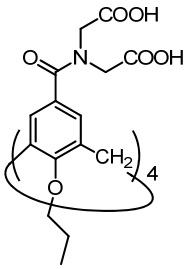

A solution of potassium carbonate (212 mg, 1.53 mmol) in water (2 mL) was added to a stirred solution of **123c** (178 mg, 0.12 mmol) in methanol (25 mL) at 40–50 °C. The reaction mixture was stirred for 2 hours, cooled to room temperature, and concentrated *in vacuo*. The residue was diluted with water (30 mL), acidified with hydrochloric acid (3 M, ~1.5 mL) to pH ~2, and extracted with ethyl acetate (4×15 mL). The ethyl acetate extracts were combined, washed with saturated sodium chloride (30 mL), dried (Na_2SO_4), and concentrated *in vacuo*. This gave a solid (140 mg, 0.11 mmol, 85% yield): mp >245 °C; ^{1}H NMR (400 MHz, CD_3SOCD_3) δ 12.76 (br s, 4H, COO*H*),* 7.48–6.30 (m, 8H, Ar–*H*), 4.36 (d, J = 13.2 Hz, 4H, H_{ax}, Ar–CH_2–Ar), 4.20–3.59 (overlapped m, 24H, NCH_2 and OCH_2), 3.28 (overlapped with HOD, H_{eq}, Ar–CH_2–Ar), 2.02–1.79 (m, 8H, OCH$_2$CH_2), 1.14–0.79 (m, 12H, CH_3); ^{13}C NMR (100 MHz, $CDCl_3$) δ 170.3 (C=O, carboxylic acid), 169.8 (C=O, amide), 157.7 (*C*–O, AR), 134.5 (*C*–CH$_2$, Ar), 128.0 (*C*–C=O, Ar), 127.2 (*C*–H, Ar), 76.7 (O*C*H$_2$), 48.3 (N*C*H$_2$), 30.4 (Ar–*C*H$_2$–Ar), 22.7 (OCH$_2$*C*H$_2$), 10.1 (*C*H$_3$); IR (ATR) $\bar{\nu}_{max}$ (cm^{-1}) 3460 (O–H), 1725 (C=O, carboxylic acid), 1196 (C–O).

---

* Dimethyl sulfoxide-d_6 is prepared from dimethyl sulfoxide by base-catalysed exchange of the protons with deuterium from deuterium oxide.[88] It is suspected that the under-integration of the protons of the carboxylic acid a result of residual D_2O in CD_3SOCD_3 and the small quantity of sample used.

2.6.5 Preparation of amino acid functionalised calixarenes for gelation studies

2.6.5.1 Preparation of $1^2,3^2,5^2,7^2$-tetrahydroxycalix[4]arene-$1^5,3^5,5^5,7^5$-tetrakis-(2*S*)-1-methylenepyrrolidine-2-carboxylic acid (127a)

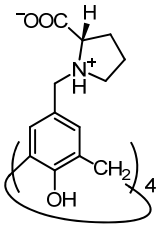

This compound was prepared according to literature.[89] A biphasic solution of L-proline (2.41 g, 20.9 mmol), **2** (2.00 g, 4.7 mmol), formalin (37 wt%, 2.15 mL, 0.86 g, 28.6 mmol), and acetic acid (5 mL) in tetrahydrofuran (45 mL) and water (5 mL) was stirred at room temperature for 2 days. The precipitated solid was filtered and triturated with acetone then methanol to give a white powder (3.47 g, 3.45 mmol, 73% yield): mp 340 °C dec (lit.[89] mp 340 °C); ^{1}H NMR (400 MHz, D_2O, 6 mg mL^{-1}) δ = 7.23 (s, 8H, Ar–*H*), 4.16 (d, *J* = 13.0 Hz, 4H, H′, Ar–C*H*$_2$–Pro), 4.11 (d, *J* = 13.0 Hz, 4H, H″, Ar–C*H*$_2$–Pro), 3.95 (br s, 8H, Ar–C*H*$_2$–Ar), 3.81 (dd, *J* = 7.0, 9.2 Hz, 4H, ProH2), 3.53–3.41 (m, 4H, H′, ProH5), 3.15–3.04 (m , 4H, H″, ProH5), 2.20–2.04 (m, 4H, H′, ProH3), 1.93–1.79 (m, 4H, H″, ProH3), 1.78–1.62 (m, 8H, ProH4); ^{13}C NMR (100 MHz, D_2O, 6 mg mL^{-1}) δ 173.4 (C=O), 151.3 (*C*–O, Ar), 131.0 (*C*–H, Ar), 129.6 (*C*–CH_2, Ar–CH_2–Ar), 122.6 (*C*–CH_2, Ar–CH_2–Pro), 67.8 (ProC2), 57.5 (Ar–*C*H_2–Pro), 53.9 (ProC5), 30.4 (Ar–*C*H_2–Ar), 28.5 (ProC3), 22.5 (ProC4); IR (ATR) $\bar{\nu}_{max}$ (cm^{-1}) 3380 (O–H), 1613 (C=O).

2.6.5.2 Preparation of $1^2,3^2,5^2,7^2$-tetrahydroxycalix[4]arene-$1^5,3^5,5^5,7^5$-tetrakis-(2*R*)-1-methylenepyrrolidine-2-carboxylic acid (127b)

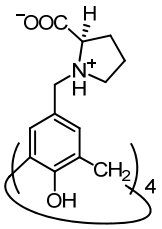

This compound was prepared according to the procedure for the L-proline isomer above. A biphasic solution of D-proline (303 mg, 2.63 mmol), **2** (249 g, 0.59 mmol), formalin (37 wt%, 265 μL, 106 mg, 3.53 mmol), and acetic acid (650 μL) in tetrahydrofuran (6 mL) and water (650 μL) was stirred at room temperature for 2 days. The solid was filtered and triturated with acetone then methanol to give a white powder (475 mg, 0.47 mmol, 80% yield): mp 330 °C dec; spectroscopic data identical to that obtained for the L-proline isomer. Anal. Calcd for $C_{52}H_{60}N_4O_{12}.6H_2O$: C, 59.99; H, 6.97; N, 5.38%. Found: C, 59.70; H, 6.93; N, 5.23%.

2.6.5.3 Preparation of $1^2,3^2,5^2,7^2,9^2$-pentahydroxycalix[5]arene-$1^5,3^5,5^5,7^5,9^5$-pentakis-(2*S*)-1-methylenepyrrolidine-2-carboxylic acid (128)

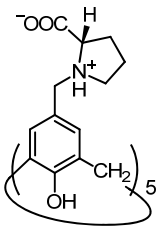

A biphasic solution of L-proline (155 mg, 1.35 mmol), **126** (121 mg, 0.23 mmol), formalin (37 wt%, 125 μL, 134 mg, 4.45 mmol), and acetic acid (0.5 mL) in tetrahydrofuran (5 mL) and water (0.5 mL) was stirred at room temperature overnight. The reaction solution was decanted and the remaining viscous phase which settled on the flask wall was treated with acetone. The resulting solid was filtered at the pump, giving a white powder (261 mg): ^{1}H NMR (400 MHz, D_2O, 7 mg mL^{-1}) δ 7.24 (s, 10 H, Ar–*H*), 4.31–4.00 (m, 10H, Ar–C*H*$_2$–Pro), 3.95–3.84 (m, 5H, ProH2), 3.84–3.70 (br s, 10H, Ar–C*H*$_2$–Ar), 3.57–3.47 (m, 5H, H′, ProH5), 3.24–3.05 (m, 5H, H″, ProH5), 2.42–2.26 (m, 5H, H′, ProH3), 2.06–1.89 (overlapped m, 10H, H″, ProH3 and H′, ProH4), 1.89–1.74 (m, 5H, H″, ProH4); ^{13}C NMR (100 MHz, 7 mg mL^{-1}) δ 173.4 (C=O), 152.8 (*C*–O, Ar), 131.1 (*C*–H, Ar), 129.3 (*C*–CH_2, Ar–CH_2–Ar), 122.2 (*C*–CH_2, Ar–CH_2–Pro), 67.9 (ProC2), 57.7 (Ar–*C*H$_2$–Pro), 54.2 (ProC5), 30.9 (Ar–*C*H$_2$–Ar), 28.7 (ProC3), 22.7 (ProC4); IR (ATR) $\bar{\nu}_{max}$ (cm^{-1}) 3370 (O–H), 1612 (C=O). Signals in the ^{1}H and ^{13}C NMR spectra have been assigned to the protons and carbons attributable to the product (estimated at not more than 85 wt% from the ^{1}H NMR spectrum) with residual L-proline as the major impurity.

2.6.5.4 Preparation of $1^2,3^2,5^2,7^2$-tetrahydroxycalix[4]arene-$1^5,3^5,5^5,7^5$-tetra-[(methylene)(methyl)amino]acetic acid (132)

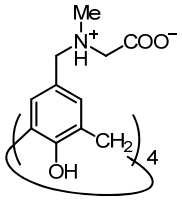

A solution of **2** (99 mg, 0.23 mmol), *N*-methylglycine (91 mg, 1.02 mmol), formalin (37 wt%, 80 μL, 32 mg, 1.07 mmol), and acetic acid (100 μL) in tetrahydrofuran (10 mL) and methanol (10 mL) was heated at reflux over the weekend. The solid was filtered at the pump and washed with a solution of methanol/acetone (1:1, v/v) to give a white solid (70 mg) which was found to be a mixture containing not more than 90 wt% of the desired product, **132** (estimated from the ^{1}H NMR spectrum): ^{1}H NMR (200 MHz, D_2O) δ = 7.20 (br s, Ar–*H*), 4.36–3.73 (m, Ar–C*H*$_2$–Ar overlapped with Ar–C*H*$_2$–N), 3.47 (br s, NC*H*$_2$COOH), 2.64 (br s, C*H*$_3$). Other major signals at 3.61 (s, C*H*$_2$) and 2.72 (s, C*H*$_3$) were attributed to the free *N*-methylglycine.

2.7 References

1 Gutsche, C. D. *Calixarenes: An Introduction*. 2nd ed.; RSC Publishing: Cambridge, 2008.

2 Sliwa, W.; Kozlowski, C. *Calixarenes and Resorcinarenes: Synthesis, Properties and Applications*. Wiley-VCH Verlag GmbH and Co. KGaA: Weinheim, 2009.

3 Columbus, I. *J. Org. Chem.* **2008**, *73* (7), 2598–2606.

4 Kogan, K.; Columbus, I.; Biali, S. E. *J. Org. Chem.* **2008**, *73* (18), 7327–7335.

5 Fischer, C.; Gruber, T.; Seichter, W.; Weber, E. *Org. Biomol. Chem.* **2011**, *9* (11), 4347–4352.

6 Montalbetti, C. A. G. N.; Falque, V. *Tetrahedron* **2005**, *61* (46), 10827–10852.

7 Pattabiraman, V. R.; Bode, J. W. *Nature* **2011**, *480* (7378), 471–479.

8 Mai, J. H.; Liu, J. M.; Li, S. Y.; Jiang, H. F. *Chin. Chem. Lett.* **2009**, *20* (10), 1191–1194.

9 Miao, R.; Zheng, Q.-Y.; Chen, C.-F.; Huang, Z.-T. *Supramol. Chem.* **2007**, *19* (7), 531–535.

10 Corbellini, F.; Knegtel, R. M. A.; Grootenhuis, P. D. J.; Crego-Calama, M.; Reinhoudt, D. N. *Chem. Eur. J.* **2005**, *11* (1), 298–307.

11 Moridi, N.; Elend, D.; Danylyuk, O.; Suwinska, K.; Shahgaldian, P. *Langmuir* **2011**, *27* (15), 9116–9121.

12 Tsou, L. K.; Dutschman, G. E.; Gullen, E. A.; Telpoukhovskaia, M.; Cheng, Y.-C.; Hamilton, A. D. *Bioorg. Med. Chem. Lett.* **2010**, *20* (7), 2137–2139.

13 Iwamoto, H.; Niimi, K.; Haino, T.; Fukazawa, Y. *Tetrahedron* **2009**, *65* (35), 7259–7267.

14 Sasine, J. S.; Brewster, R. E.; Caran, K. L.; Bentley, A. M.; Shuker, S. B. *Org. Lett.* **2006**, *8* (14), 2913–2915.

15 Troisi, F.; Russo, A.; Gaeta, C.; Bifulco, G.; Neri, P. *Tetrahedron Lett.* **2007**, *48* (45), 7986–7989.

16 Al-Warhi, T. I.; Al-Hazimi, H. M. A.; El-Faham, A. *J. Saudi Chem. Soc.* **2012**, *16* (2), 97–116.

17 El-Faham, A.; Albericio, F. *Chem. Rev.* **2011**, *111* (11), 6557–6602.

18 Valeur, E.; Bradley, M. *Chem. Soc. Rev.* **2009**, *38* (2), 606–631.

19 Han, S.-Y.; Kim, Y.-A. *Tetrahedron* **2004**, *60* (11), 2447–2467.

20 Sansone, F.; Barboso, S.; Casnati, A.; Fabbi, M.; Pochini, A.; Ugozzoli, F.; Ungaro, R. *Eur. J. Org. Chem.* **1998**, *1998* (5), 897–905.

21 Baldini, L.; Sansone, F.; Faimani, G.; Massera, C.; Casnati, A.; Ungaro, R. *Eur. J. Org. Chem.* **2008**, *2008* (5), 869–886.

22 Baldini, L.; Sansone, F.; Scaravelli, F.; Casnati, A.; Ungaro, R. *Supramol. Chem.* **2010**, *22* (11), 776–788.

23 Phipps, D. E.; Beer, P. D. *Tetrahedron Lett.* **2009**, *50* (26), 3454–3457.

24 Schädel, U.; Sansone, F.; Casnati, A.; Ungaro, R. *Tetrahedron* **2005**, *61* (5), 1149–1154.

25 Yang, L.-M.; Zheng, Y.-S.; Huang, Z.-T. *Synth. Commun.* **1999**, *29* (24), 4451–4460.

26 Cho, E. J.; Kang, J. K.; Han, W. S.; Jung, J. H. *Langmuir* **2008**, *24* (10), 5229–5232.

27 Córdova, A. *Acc. Chem. Res.* **2004**, *37* (2), 102–112.

28 Verkade, J. M. M.; Hemert, L. J. C. v.; Quaedflieg, P. J. L. M.; Rutjes, F. P. J. T. *Chem. Soc. Rev.* **2008**, *37* (1), 29–41.

29 Kürti, L.; Czakó, B. *Strategic Applications of Named Reactions in Organic Synthesis: Background and Detailed Mechanisms*. Elsevier Inc.: London, 2005; p 274–275.

30 Agababyan, A. G.; Gevorgyan, G. A.; Mndzhoyan, O. L. *Russ. Chem. Rev.* **1982**, *51* (4), 387–396.

31 Gutsche, C. D.; Nam, K. C. *J. Am. Chem. Soc.* **1988**, *110* (18), 6153–6162.

32 Atwood, J. L.; Orr, G. W.; Robinson, K. D.; Hamada, F. *Supramol. Chem.* **1993**, *2* (4), 309–317.

33 Atwood, J. L.; Orr, G. W.; Bott, S. G.; Robinson, K. D. *Angew. Chem. Int. Ed.* **1993**, *32* (7), 1093–1094.

34 Gutsche, C. D.; Alam, I. *Tetrahedron* **1988**, *44* (15), 4689–4694.

35 Alam, I.; Gutsche, C. D. *J. Org. Chem.* **1990**, *55* (14), 4487–4489.

36 Shirakawa, S.; Moriyama, A.; Shimizu, S. *Eur. J. Org. Chem.* **2008**, *2008* (35), 5957–5964.

37 Matsushita, Y.-i.; Matsui, T. *Tetrahedron Lett.* **1993**, *34* (46), 7433–7436.

38 O'Farrell, C. M.; Chudomel, J. M.; Collins, J. M.; Dignam, C. F.; Wenzel, T. J. *J. Org. Chem.* **2008**, *73* (7), 2843–2851.

39 Pham, N. H.; Wenzel, T. J. *J. Org. Chem.* **2011**, *76* (3), 986–989.

40 Dignam, C. F.; Richards, C. J.; Zopf, J. J.; Wacker, L. S.; Wenzel, T. J. *Org. Lett.* **2005**, *7* (9), 1773–1776.

41 Pham, N. H.; Wenzel, T. J. *Tetrahedron: Asymmetry* **2011**, *22* (14–15), 1574–1580.

42 Schneider, U.; Schneider, H.-J. *Chem. Ber.* **1994**, *127* (12), 2455–2469.

43 Buckley, B. R.; Boxhall, J. Y.; Page, P. C. B.; Chan, Y.; Elsegood, M. R. J.; Heaney, H.; Holmes, K. E.; McIldowie, M. J.; McKee, V.; McGrath, M. J.; Mocerino, M.; Poulton, A. M.; Sampler, E. P.; Skelton, B. W.; White, A. H. *Eur. J. Org. Chem.* **2006**, *2006* (22), 5117–5134.

44 Buckley, B. R.; Page, P. C. B.; Heaney, H.; Sampler, E. P.; Carley, S.; Brocke, C.; Brimble, M. A. *Tetrahedron* **2005**, *61* (24), 5876–5888.

45 Schmidt, C.; Straub, T.; Falàbu, D.; Paulus, Erich F.; Wegelius, E.; Kolehmainen, E.; Böhmer, V.; Rissanen, K.; Vogt, W. *Eur. J. Org. Chem.* **2000**, *2000* (23), 3937–3944.

46 Gutsche, C. D.; Iqbal, M. *Org. Synth.* **1990**, *68*, 234–237.

47 Strobel, M.; Kita-Tokarczyk, K.; Taubert, A.; Vebert, C.; Heiney, P. A.; Chami, M.; Meier, W. *Adv. Funct. Mater.* **2006**, *16* (1), 252–259.

48 Smith, M. B.; March, J. *March's Advanced Organic Chemistry: Reactions, Mechanisms, and Structure*. John Wiley and Sons, Inc.: Hoboken, New Jersey, 2007; p 742–744.

49 Dondoni, A.; Marra, A.; Scherrmann, M.-C.; Casnati, A.; Sansone, F.; Ungaro, R. *Chem. Eur. J.* **1997**, *3* (11), 1774–1782.

50 Iwamoto, K.; Araki, K.; Shinkai, S. *J. Org. Chem.* **1991**, *56* (16), 4955–4962.

51 Iwamoto, K.; Fujimoto, K.; Matsuda, T.; Shinkai, S. *Tetrahedron Lett.* **1990**, *31* (49), 7169–7172.

52 Jaime, C.; De Mendoza, J.; Prados, P.; Nieto, P. M.; Sanchez, C. *J. Org. Chem.* **1991**, *56* (10), 3372–3376.

53 Arduini, A.; Fabbi, M.; Mantovani, M.; Mirone, L.; Pochini, A.; Secchi, A.; Ungaro, R. *J. Org. Chem.* **1995**, *60* (5), 1454–1457.

54 Smith, W. E. *J. Org. Chem.* **1972**, *37* (24), 3972–3973.

55 Ogata, Y.; Kawasaki, A.; Sugiura, F. *Tetrahedron* **1968**, *24* (14), 5001–5010.

56 Dalcanale, E.; Montanari, F. *J. Org. Chem.* **1986**, *51* (4), 567–569.

57 Brady, O. L.; Elsmie, G. V. *Analyst* **1926**, *51* (599), 77–78.

58 Iki, H.; Kikuchi, T.; Shinkai, S. *J. Chem. Soc., Perkin Trans. 1* **1993**, (2), 205–210.

59 Nair, P. M.; Roberts, J. D. *J. Am. Chem. Soc.* **1957**, *79* (16), 4565–4566.

60 Jones, F.; Mocerino, M.; Ogden, M. I.; Oliveira, A.; Parkinson, G. M. *Cryst. Growth Des.* **2005**, *5* (6), 2336–2343.

61 Liardon, R.; Hurrell, R. F. *J. Agric. Food Chem.* **1983**, *31* (2), 432–437.

62 Stewart, D. R.; Gutsche, C. D. *Org. Prep. Proced. Int.* **1993**, *25* (1), 137–139.

63 Bew, S. P.; Cheesman, M. R.; Sharma, S. V. *Chem. Commun.* **2008**, (44), 5731–5733.

64 Bell, S. E. J.; Browne, J. K.; McKee, V.; McKervey, M. A.; Malone, J. F.; O'Lear, M.; Walker, A.; Arnaud-Neu, F.; Boulangeot, O.; Mauprivez, O.; Schwing-Weill, M.-J. *J. Org. Chem.* **1998**, *63* (3), 489–501.

65 Coruzzi, M.; Andreetti, G. D.; Bocchi, V.; Pochini, A.; Ungaro, R. *J. Chem. Soc., Perkin Trans. 2* **1982**, (9), 1133–1138.

66 Notz, W.; Tanaka, F.; Barbas, C. F. *Acc. Chem. Res.* **2004**, *37* (8), 580–591.

67 List, B.; Pojarliev, P.; Biller, W. T.; Martin, H. J. *J. Am. Chem. Soc.* **2002**, *124* (5), 827–833.

68 Yang, J. W.; Chandler, C.; Stadler, M.; Kampen, D.; List, B. *Nature* **2008**, *452* (7186), 453–455.

69 Van Loon, J. D.; Arduini, A.; Coppi, L.; Verboom, W.; Pochini, A.; Ungaro, R.; Harkema, S.; Reinhoudt, D. N. *J. Org. Chem.* **1990**, *55* (21), 5639–5646.

70 Nam, K. C.; Yoon, T. H. *Bull. Korean Chem. Soc.* **1993**, *14* (2), 169–171.

71 Gutsche, C. D. *Calixarenes Revisited*. Royal Society of Chemistry: Cambridge, 1998; p 117.

72 Fuguet, E.; Ràfols, C.; Rosés, M.; Bosch, E. *Anal. Chim. Acta* **2005**, *548* (1–2), 95–100.

73 Becherer, M. S. New amphiphilic dendrocalix[4]arenes as building blocks of micellar architectures. Doctoral thesis, Friedrich-Alexander-University of Erlangen-Nürnberg, Erlangen, 2009.

74 Buwalda, R. T.; Jonker, J. M.; Engberts, J. B. F. N. *Langmuir* **1999**, *15* (4), 1083–1089.

75 Barhoum, S.; Yethiraj, A. *J. Chem. Phys.* **2010**, *132*, 024909.

76 Alexandrescu, A. T.; Rathgeb-Szabo, K. *J. Mol. Biol.* **1999**, *291* (5), 1191–1206.

77 Gottlieb, H. E.; Kotlyar, V.; Nudelman, A. *J. Org. Chem.* **1997**, *62* (21), 7512–7515.

78 Fulmer, G. R.; Miller, A. J. M.; Sherden, N. H.; Gottlieb, H. E.; Nudelman, A.; Stoltz, B. M.; Bercaw, J. E.; Goldberg, K. I. *Organometallics* **2010**, *29* (9), 2176–2179.

79 O'Neil, M. J. *The Merck Index: An Encyclopedia of Chemicals, Drugs, and Biologicals*. 14th ed.; Merck: Whitehouse Station, N.J., 2006.

80 Arena, G.; Contino, A.; Gulino, F. G.; Magrì, A.; Sciotto, D.; Ungaro, R. *Tetrahedron Lett.* **2000**, *41* (48), 9327–9330.

81 Arena, G.; Contino, A.; Giuseppe Gulino, F.; Magrì, A.; Sansone, F.; Sciotto, D.; Ungaro, R. *Tetrahedron Lett.* **1999**, *40* (8), 1597–1600.

82 Kon, N.; Iki, N.; Miyano, S. *Org. Biomol. Chem.* **2003**, *1* (4), 751–755.

83 Armarego, W. L. F.; Chai, C. L. L. *Purification of Laboratory Chemicals*. 5th ed.; Elsevier: Sydney, 2003.

84 Gutsche, C. D.; Levine, J. A. *J. Am. Chem. Soc.* **1982**, *104* (9), 2652–2653.

85 Neuman, R. E.; Smith, E. L. *J. Biol. Chem.* **1951**, *193* (1), 97–111.

86 Angier, R. B.; Waller, C. W.; Hutchings, B. L.; Boothe, J. H.; Mowat, J. H.; Semb, J.; Row, Y. S. *J. Am. Chem. Soc.* **1950**, *72* (1), 74–77.

87 Keimatsu, S.; Kato, C. *Yakugaku Zasshi* **1929**, *49* (8), 731–736.

88 Fruhstorfer, W.; Hampel, B. Verfahren zur Herstellung von Hexadeuterodimethylsulfoxid. DE 1171422 (B), 4 June, 1964.

89 Becker, T.; Goh, C. Y.; Jones, F.; McIldowie, M. J.; Mocerino, M.; Ogden, M. I. *Chem. Commun.* **2008**, (33), 3900–3902.

3 Amino acid-functionalised crystal growth modifiers

3.1 Calixarene- and resorcinarene-based crystal growth modifiers

Crystallisation is an extremely large field of research. A short introduction to biomineralisation, calcium carbonate, barium sulfate, and crystal growth additives has been *briefly* discussed in section 1.2. Therefore, this section will be restricted to calixarene- and resorcinarene-based compounds that have been applied as crystal growth modifiers of inorganic minerals.

3.1.1 Additives with calixarene and resorcinarene frameworks

Calixarene and resorcinarene frameworks have previously been used as crystal growth modifiers. Volkmer et al.[1–4] crystallised calcium carbonate underneath monolayers of amphiphilic resorcinarenes and calixarenes (Figure 3.1) at the air-water interface. At high surface pressures (20 mN m^{-1}), calcium carbonate crystallised underneath monolayers of **133** with aragonite being the major phase, calcite as a minor phase and trace amounts of vaterite. An increase in the latter two phases was observed with a reduction of surface pressures, which became dominated by vaterite at 0–2 mN m^{-1}.[3] In contrast, crystallisation of calcium carbonate underneath monolayers of resorcinarene **134** and calixarenes **135** and **136** gave truncated rhombohedral shaped single calcite crystals (no other phases observed) and orientated crystals (at the monolayer) at low surface pressure (0.1 mN m^{-1}).[1–4] Further investigation by Volkmer et al.[5] showed that calcium carbonate crystallised as vaterite rosettes underneath dendron-calix[4]arene **137** monolayers (0.5 mN m^{-1}). The authors noted that the higher charge density of **137** monolayers were able to

induce and stabilise the metastable polymorphs such as vaterite—possibly by kinetic control. From these experiments Volkmer et al.[5] proposed that by varying the charge densities of the monolayers, the desired polymorph of calcium carbonate could be selectively crystallised. Crystallisation of inorganic minerals underneath monolayers is of interest as biomimetics for oriented crystallisation at the biomineral–organic matrix interface.[6–9]

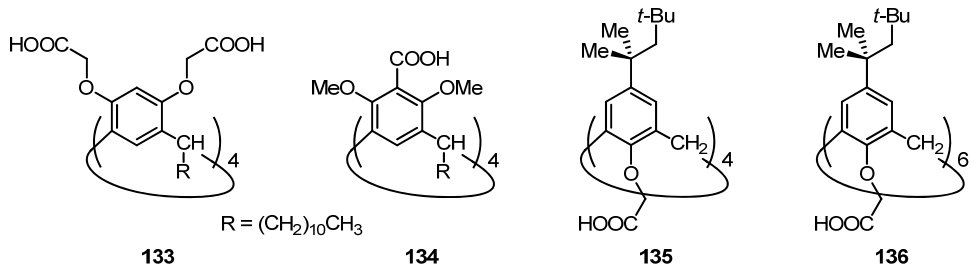

Figure 3.1 Resorcinarenes (**133** and **134**) and calixarenes (**135** and **136**) where investigated by Volkmer et al.[1–4] as potential templates (Langmuir monolayers) for calcium carbonate crystallisation.

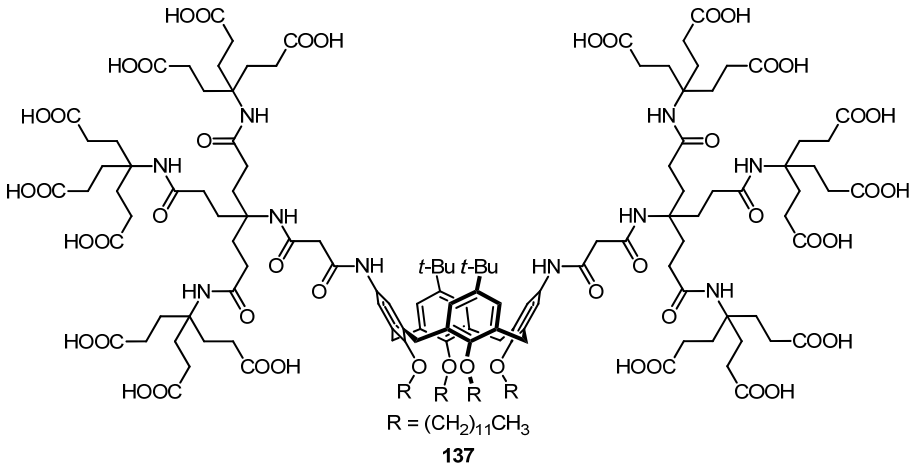

Figure 3.2 Stable monolayers formed by dendron-calix[4]arene **137** were investigated by Volkmer et al.[5] as templates for calcium carbonate crystallisation.

Calixarenes are good scaffolds for other functional groups. Baynton et al.[10] functionalised the wide-rim of calix[4]arenes with sulfonate and phosphonate groups (Figure 3.3). The phosphonate derivative **19** was found to be more potent than the sulfonate derivative **22**. This was expected since phosphonates are typically potent crystal growth modifiers for barium sulfate.[11, 12] They noted that the phosphonate **19** was able to inhibit barium sulfate crystallisation (at supersaturation $S = 25$)

completely with as little as 13–14 μM while the sulfonate **22** only achieved 34% inhibition at 200 μM. The ability of calix[4]arene **19** to direct all its phosphonate groups along a surface contributes to its potency and its efficacy is comparable to other small molecule phosphonate inhibitors (Figure 3.4); hydroxyethylenediphosphonic acid (HEDP), **138**, and ethylenediaminetetraphosphonic acid (EDTP), **139**, can achieve complete inhibition of barium sulfate at 24 μM and 1 μM respectively ($S = 25$).[12] Additionally, barium sulfate particles crystallised at higher calixarene concentrations (~10 μM) of **19** were shown to be mesocrystals rather than single crystals. Bayton et al.[13] later showed that **22** could also form barium sulfate mesocrystals (at $S = 5$), however the nanoparticles comprising the mesocrystals fused readily. They also noted that the calixarene additives **22** and **19** were incorporated within the mesocrystals. Furthermore, these additives were shown to impact on the (001) face promoting both nucleation at the surface and growth of this face leading to elongated particles.

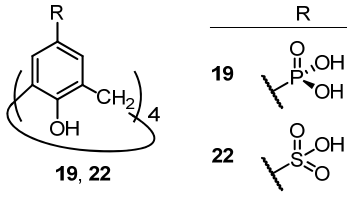

Figure 3.3 Sulfonate (**22**) and phosphonate (**19**) functionalized calix[4]arenes investigated by Massi et al.[14]

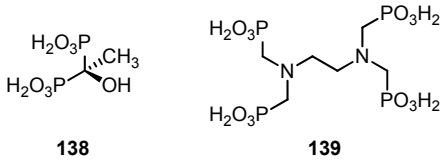

Figure 3.4 Example of organophosphonate barium sulfate inhibitors.[12]

Heywood and Ovens[15] previously studied the impact of O-alkylated derivatives (Figure 3.5) of calix[4]arene **22**, as the water soluble sodium salt, on calcium carbonate. The authors found that calix[4]arenes **140a**–**c** formed a mixture of polymorphs, calcite and vaterite, with vaterite being the dominant phase with shorter alkyl chains on the calix[4]arene **140**. As the alkyl chain length increased to butyl and octyl chains, **140d**,**e**, calcite became the dominant phase. The authors noted that

all calcite particles grown in the presence of **140a**–**e** had marked alterations of their morphology and were oriented. They suggested that the sulfonated calix[4]arenes had sufficient amphiphilic property to aggregate at the liquid/gas interface (in particular **140d**,**e**) which allowed oriented calcite to crystallise along the <10.0> or <1.2> plane as a results of matching sulfonate functional groups with these lattice planes. However, unlike work by Volkmer et al.,[1–4] Heywood and Ovens indicated[15] that there was no evidence for the formation of air/water monolayers by calix[4]arenes **140a**–**e**.

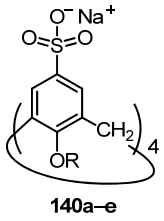

140a–e

	R
140a	Me
140b	Et
140c	Pr
140d	Bu
140e	$(CH_2)_7CH_3$

Figure 3.5 Sulfonate-functionalised calix[4]arenes investigated by Heywood[15] on calcium carbonate crystallisation.

3.1.2 Bio-inspired calixarene crystal growth modifiers

Bioinspired approaches to crystallisation are not new.[16] Continuing with the theme of using calixarenes as scaffolds, Bartlett et al.[17] showed that amino acid functionalised calix[4]arenes (**141**–**143**) were more effective crystal growth modifiers of calcium carbonate and calcium oxalate than the equivalent concentration of the amino acid monomers. Furthermore, the aspartic acid derivative (**143**) was more potent than the alanine (**141**) or the sarcosine (**142**) calix[4]arene derivatives. Following from this earlier work, Jones, et al.,[18] investigated the impact of aspartic acid (**143**) and glutamic acid (**144**) functionalised calix[4]arenes on calcium carbonate, barium sulfate, and calcium oxalate. Calix[4]arenes **143** and **144** were found to have an impact on the morphology and crystallisation kinetics of the model minerals investigated at very low concentrations (<1.5 μM); the aspartic acid derivative **143** was more potent than the glutamic acid derivative **144**.

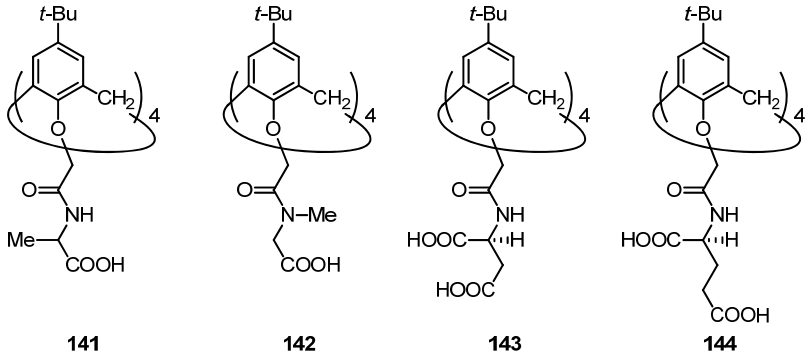

Figure 3.6 Narrow-rim functionalised calix[4]arene investigated by Bartlett, et al.[17] (**141**–**143**) and Jones, et al.[18] (**143**, **144**) for crystal growth modification properties of inorganic minerals.

3.1.3 Amino acids at the wide-rim

Calixarenes can also be functionalised at the wide-rim (in addition to the narrow-rim). Attachment of amino acids at the wide-rim of calix[4]arenes may allow for increased flexibility in the spatial arrangement of amino acids compared to attachment at the narrow-rim of calix[4]arenes. Wide-rim amino acid functionalised calix[4]arenes (Figure 3.7) were synthesised as detailed in Chapter 2. Calixarenes **124a** and **124b** are functionalised with aspartic acid and glutamic acid respectively. Calixarene **124c**, functionalised with iminodiacetic acid, is a structural isomer of **124a**, which lacks chirality and has a tertiary amide linkage. The impact of the amino acid functionalised calixarenes on model mineral systems, calcium carbonate and barium sulfate, were investigated and the results are presented here.

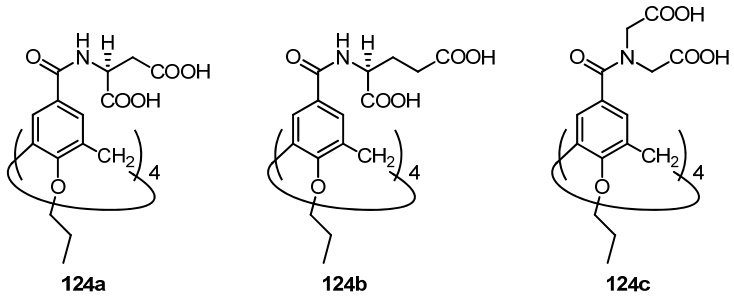

Figure 3.7 Wide-rim functionalised calix[4]arene used in this project to study the effects of acidic amino acids on the crystallisation of inorganic minerals. Here, the calixarenes were functionalised with aspartic acid (**124a**), glutamic acid (**124b**), and imino diacetic acid (**124c**) and locked in the cone conformer with propyl chains.

The crystal growth modification properties of proline calix[4]arene **127a** (and similar aminomethylated calix[4]arenes) on barium sulfate was previously investigated by Oliveira (Oliveira, A. Curtin University, Bentley, Western Australia. Unpublished work, 1997). The results suggested that calix[4]arene **127a** had a similar level of impact as a single amino acidic acid (such as aspartic acid). Therefore, the crystal growth modification properties of proline calix[4]arene **127a** and proline-derived analogues will not be pursued in this thesis.

3.2 Results from calcium carbonate crystallisation

Calcium carbonate was crystallised using the gas-diffusion method.[19] In this method, ammonium carbonate decomposes to give carbon dioxide and ammonia, which dissolve into the calcium chloride solutions; this is the source of carbonate and the ammonia increases the pH of the solution. This method of calcium carbonate crystallisation has a well known sequence progressing from the crystallisation of spherical vaterite or needle-like aragonite, which subsequently undergoes a solution-mediated transformation to rhombohedral calcite.[20] In the absence of additives, calcium carbonate precipitated predominantly as calcite (Figure 3.8a) with the typical rhombohedral shape; however, vaterite was observed in a few instances (Figure 3.8b). The spherical vaterite was likely a result of the calcium carbonate not having enough time to transform to calcite. This is consistent with literature where calcite is shown to form from amorphous calcium carbonate via less stable polymorphs such as vaterite and aragonite.[21] The calixarene additives, **124a**–**c**, altered the morphology of calcite, even at concentrations less than 1 ppm.

The L-aspartic acid additive **124a** was more potent than **124b** and **124c**. The impact of the additive was evident, even at the lowest concentration investigated (0.4 μM). The calcite particles (Figure 3.8c–e) had the general rhombohedral profile, which was lost at higher concentrations of the additive. Similarly, the edges became more rounded with increasing additive concentrations as found for Asprich-c protein.[22] The authors suggested that for ‘slow growth’ calcium carbonate in the presence of mollusc shell protein, Asprich-c, (similar to the conditions used here) the rounded

morphology was possibly caused by irreversible adsorption of the protein at step and kink sites. In contrast to calcite particles grown in the presence of the narrow-rim analogue **143** (Figure 3.6), the calcite particles here did not exhibit notches along the edges of the rhombohedron.

The L-glutamic derivative **124b** appeared to have less impact on the morphology of the calcite particles than **124a**. The calcite particles grown in the presence of **124b** showed notches along one corner (Figure 3.8f) or edge (Figure 3.8h) of the rhomb and had microsteps along the faces. At the highest concentration (1.2 μM) studied (Figure 3.8h), the calcite rhomb retained much of its edges with mild stepped faces like those grown in the presence of the narrow-rim analogue **144** at 1.4 μM. However, the wide-rim calix[4]arene **124b** appears to be more potent than the narrow-rim calix[4]arene **144** (where the lowest concentration reported for **144**, 1.4 μM, was greater than the highest concentration studied for **124b**). The stepped morphology resembles that of calcite grown in the presence of nacre proteins (isolated from the aragonitic layer of red abalone, *Haliotis rufescens*), in particular the aspartic acid/asparagine- and glycine-rich protein 'AP8'.[23, 24]

The iminodiacetic acid derivative **124c** appeared to require a greater concentration to have an impact on the calcite morphology. At concentrations of 0.8 μM of **124c**, stepped faces begin to appear on the calcite particles (Figure 3.8j); at lower concentrations, the calcite particles appeared to retain the typical rhombohedral shape (not shown here). Interestingly, spherical particles (Figure 3.8i), presumably vaterite, were also observed for calcium carbonate grown in the presence of **124c** (0.4 μM). Vaterite phases have been known to be stabilised by aspartic acid,[25] glutamic acid,[26] poly(aspartic acid)[27] and egg ovalbulmin[28] preventing it from transforming into calcite. Calixarene **124c** was not used in the original work by Jones et al.,[18] so no comparison can be made to the narrow-rim analogue.

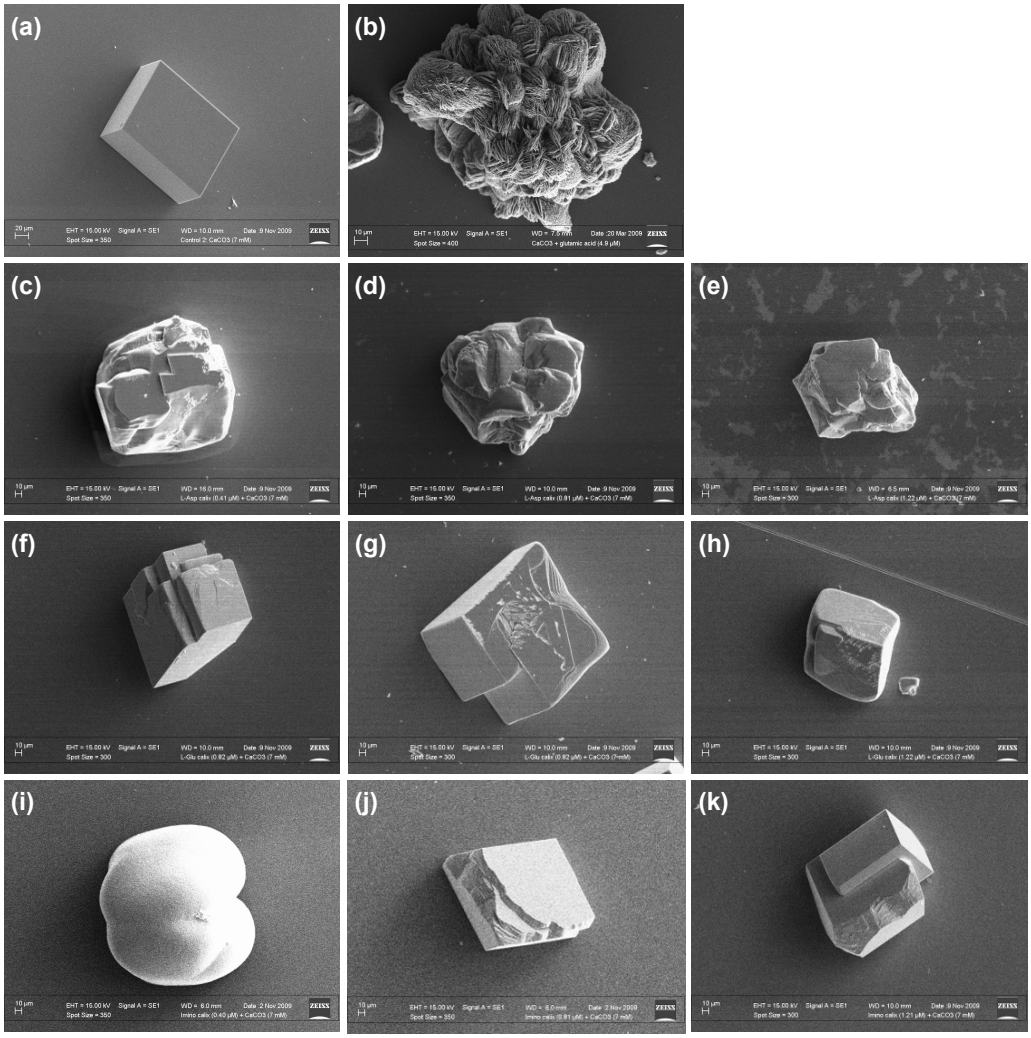

Figure 3.8 SEM micrographs of calcium carbonate in the absence of additives: (a) calcite (major polymorph) and (b) vaterite (observed occasionally). Calcite morphology in the presence of amino acid functionalised calix[4]arene: L-Asp **124a** at (c) 0.4 μM, (d) 0.8 μM, (e) 1.2 μM; L-Glu **124b** at (f) 0.4 μM, (g) 0.8 μM, (h) 1.2 μM; iminodiacetate **124c** at (i) 0.4 μM, (j) 0.8 μM, (k) 1.2 μM.

3.3 Results from barium sulfate crystallisation

3.3.1 Impact on crystallisation kinetics—crystal growth

The impact of calix[4]arene additives **124a** and **124b** on barium sulfate was determined by desupersaturation experiments.[29] In these experiments, the conductivity of the reaction solution (barium chloride, sodium sulfate, and additives) was logged over time; starting with an initial barium sulfate concentration of 0.25

mM (giving an approximate supersaturation of 25). The desupersaturation rate could then be determined from the linear region of the desupersaturation curve. From these experiments (Figure 3.9), the aspartic acid derivative **124a** was approximately ten times more potent than the glutamic acid derivative **124b** at inhibiting barium sulfate crystallisation. The calixarene **124a** was able to achieve complete inhibition (over the time scale of the experiment) at 0.3 μM whereas **124b** required 3.9 μM to do the same. The glutamic acid derivative **124b** was comparable to the narrow-rim derivative **143** (which achieved complete inhibition at 3.6 μM). The aspartic acid derivative **124a** was more potent than its narrow-rim analogue **144** (which achieved complete inhibition at 3.6 μM). Calix[4]arene **124a** was slightly more potent than the phosphonate calixarene **19** (complete inhibition at 13–14 μM) and is approaching the efficacy of some organophosphonate inhibitors (Figure 3.4); under the conditions used here, HEDP (**138**) can achieve complete inhibition at 24 μM while ethylenediaminetetraphosphonic acid (**139**) only requires levels at 1 μM.[12]

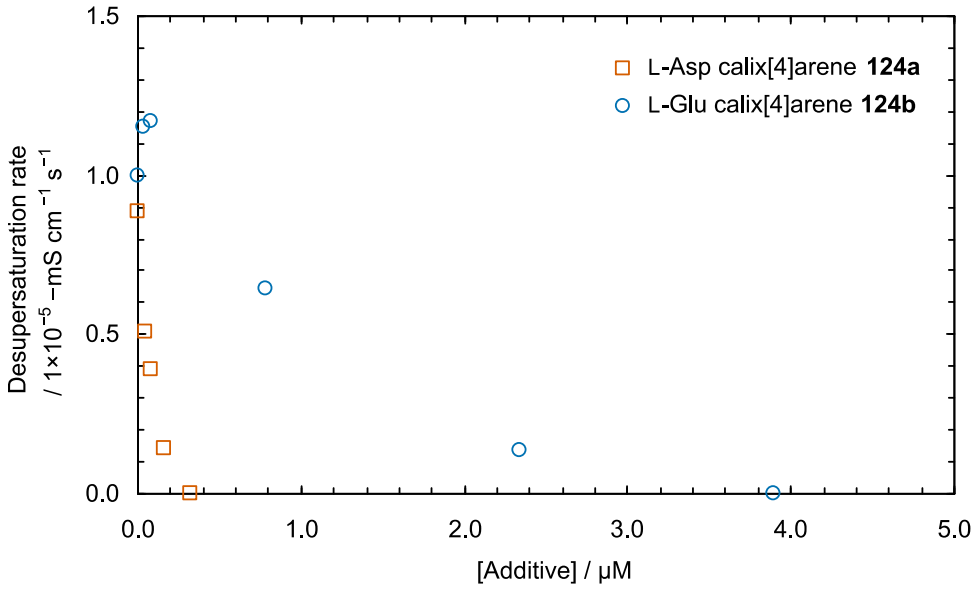

Figure 3.9 Desupersaturation experiments to assess the impact of upper-rim amino acid functionalised cailx[4]arene on the growth of barium sulfate.

While aspartic and glutamic acids are often associated as 'acidic components' in proteins associated with biominerals,[30] some authors have observed differences in the impact of the amino acids[31] and their oligomers.[32] The greater potency of aspartic acid calixarene **124a** could be attributed to the greater flexibility of the side-chain

carboxylate of the glutamic acid moieties at the wide-rim of calixarene **124b**. The slightly longer side-chain could promote intramolecular hydrogen bonding (for example with the amide linkage) thus, reducing the availability of the side-chain carboxylate for binding to the crystal surface. This would also account for the similar potency of glutamic acid calix[4]arenes **124b** and **144** (irrespective of whether the glutamate is at the wide- or narrow-rim of the calixarene).

3.3.2 Impact on barium sulfate morphology

Barium sulfate particles were obtained from desupersaturation experiments.[18] A supersaturated solution of barium sulfate was obtained by mixing barium chloride and sodium sulfate to give initial barium sulfate concentrations of 0.25 mM (giving an approximate supersaturation of 25). In low ionic strength solutions, the supersaturation, S, can be approximated as $S = c/c_0$, where c is the initial concentration of barium sulfate in solution and c_0 is the equilibrium solubility concentration at 25 °C.[33] The equilibrium solubility concentration for $BaSO_4$ at 25 °C was taken as 9.82×10^{-11} mol^2 L^{-2}.[34]

In the absence of any additives, the barium sulfate particles had the expected 'pillow-shaped' morphology with rounded (*hk*0) faces and (001) ends (Figure 3.10a). The two additives investigated here, **124a** and **124b**, showed some impact on the morphology of barium sulfate but were highly potent in the inhibition of barium sulfate crystallisation.

Barium sulfate grown in the presence of **124a** was found to form polycrystalline assemblies. These crystals (Figure 3.10) were isolated at the end of the desupersaturation experiments. At additive levels of 0.16 μM and less, some of the clusters appeared lengthened along the *c*-axis exceeding the typical 2:1 *c*/*a* aspect ratio (refer to Jones et al.[33] for micrographs of control barium sulfate particles at $S = 25$). At higher concentrations the barium sulfate particles are smaller and have distorted morphologies; this is especially true at additive levels of 0.8 μM (Figure 3.10h). This is consistent with the inhibitory effect of the additive. Where the desupersaturation experiments did not result in a precipitate at the end of the experiment (at additive levels greater then 0.8 μM), an aliquot of the solution was allowed to stand for up to 15 days over a microscope slide. Only at additive levels of

0.16 μM (Figure 3.10d,e) were polycrystalline 'ribbons' observed. The 'ribbons' appeared to be comprised of smaller orthorhombic-like particles. These polycrystalline 'ribbons' resemble results obtained by Heywood and Mann[35, 36] who crystallised barium sulfate underneath compressed *n*-eicosyl sulfate monolayers (43–47 mN m^{-1}) with the (100) face parallel to the monolayer. However, it is not clear from the micrographs (Figure 3.10d,e) if there is selectivity for a particular crystal face. The morphology of barium sulfate crystallised in the presence of **124a** retained its typical rectangular shape (at concentrations less than 0.31 μM): in contrast barium sulfate crystallised in the presence of the narrow-rim analogue **143** had elongated morphologies. Both aspartic acid-based additives resulted in polycrystalline barium sulfate particles.

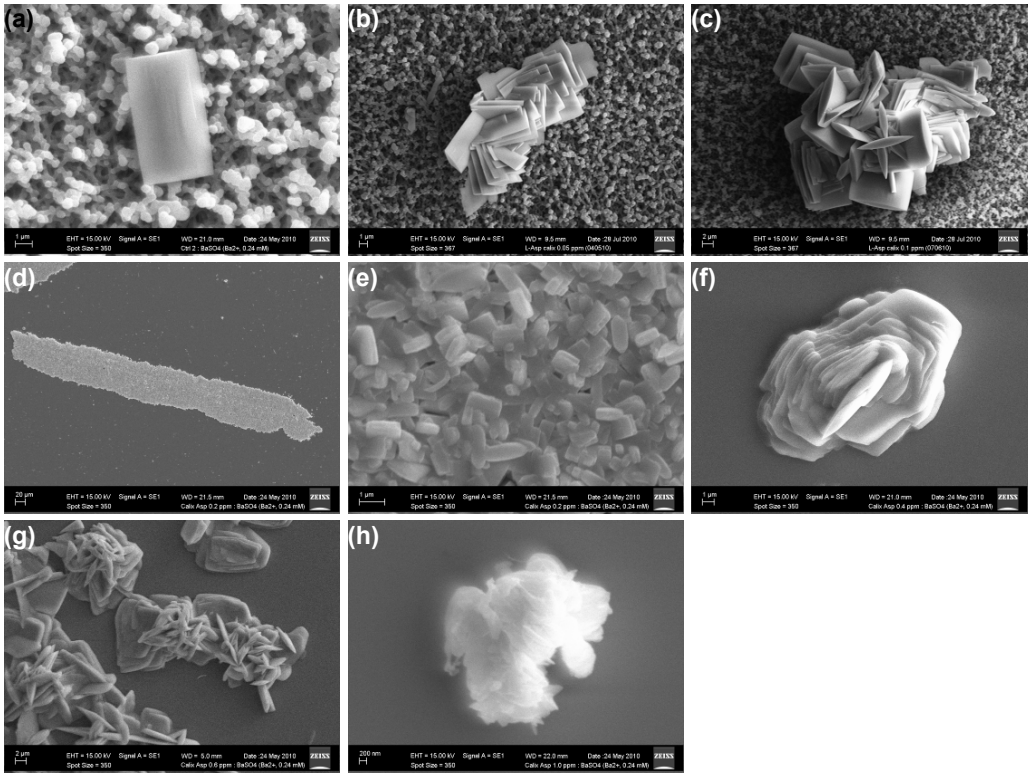

Figure 3.10 SEM micrographs showing the impact on the morphology of barium sulfate by L-Asp calix[4]arene at, (a) 0 μM (control), (b) 0.04 μM, (c) 0.08 μM, (d) 0.16 μM, (e) 0.16 μM close-up, (f) 0.31 μM, (g) 0.49 μM, and (h) 0.81 μM. At L-Asp calix[4]arene concentrations of 0.16–0.81 μM, the filtrates from the conductivity experiments were allowed to stand for 5–14 days over coverslips.

The morphology of barium sulfate grown in the presence of the glutamic acid derivative **124b** was similar to those grown in the presence of **124a**. This was true for

low concentrations of the additive (<0.39 μM) where the barium sulfate was polycrystalline and the constituents of the clusters had a lengthened *c*-axis (Figure 3.11a–c). Similar to **124a**, the barium sulfate particles grown with higher levels of additives (>0.78 μM) were rounded and did not have a rectangular shape (Figure 3.11d–e). At low concentrations (≤0.39 μM), barium sulfate crystallised in the presence of **124b** were similar to those crystallised presence of the narrow-rim analogue **144**; the barite particles had a rectangular shape (like in the control experiments) and were polycrystalline. At higher concentrations (>0.39 μM), barium sulfate crystallised in the presence of **144** were polycrystalline and had elongated morphologies (similar to the aspartic acid analogue **143**), however **124b** resulted in smaller rounded barite particles.

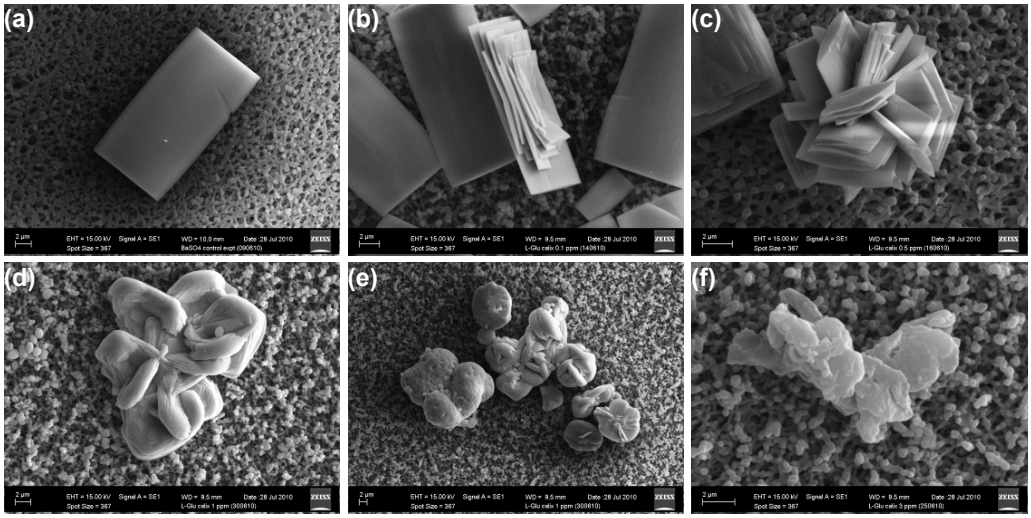

Figure 3.11 SEM micrographs showing the impact on the morphology of barium sulfate by L-Glu calix[4]arene at, (a) 0 μM (control), (b) 0.08 μM, (c) 0.39 μM, (d) 0.78 μM, (e) 0.78 μM, and (f) 2.33 μM. Where the L-Glu calix[4]arene concentration was at 2.33 μM, the filtrate from the conductivity experiments were allowed to stand over a coverslip for 14 days.

3.3.3 Impact on crystallisation kinetics—nucleation

The induction period can not be reliably determined from the desupersaturation curve as it is often shorter than the latent period (though the latent period can sometimes be indistinguishable from the induction period).[37] Therefore, the induction period for barium sulfate crystallisation was determined by a light scattering method.[38] Here, the turbidity of the solution was monitored (using a UV-visible spectrophotometer) and the induction period defined as the time where the turbidity increased above the

background turbidity.[39] This was achieved by monitoring the absorbance (i.e. scattering of light by the barium sulfate particles) of the reaction solution at 900 nm (the calixarene additives do not absorb at this wavelength). The results indicated that the presence of additives lengthened the induction period compared with control experiments. Mullin[37] defines the induction time to include the time taken to form stable nuclei and the growth of the nuclei to a measurable size. Therefore, an increase in the induction time can be an indication of an increase in time required to form stable nuclei and/or time required for the nuclei to grow to a detectable size.

The results (Table 3.1) showed that the amino acid functionalised calixarene additives lengthened the induction period of barium sulfate. The aspartic acid derivative **124a** (Figure 3.12) doubled the induction period for barium sulfate at a concentration of 0.04 μM. The gluatmic acid derivative **124b** (Figure 3.13) was less potent requiring ten times the additive level of **124b** to induce a doubling of the induction period. These additives had an impact on both the nucleation events and crystal growth phase of barium sulfate. This suggests that both the L-aspartic acid and L-glutamic calixarene additives acted as inhibitors of both bulk nucleation and crystal growth.

Table 3.1 Approximate induction times for the autonucleation of $BaSO_4$ in the presence of calixarene additives determined by UV-visible spectroscopy.

Additive	Concentration / μM	Approximate induction time / s
None (control)	—	100
L-Asp calix[4]arene **124a**	0.04	200
L-Glu calix[4]arene **124b**	0.39	250
L-Glu calix[4]arene **124b**	0.58	700
L-Glu calix[4]arene **124b**	0.78	900

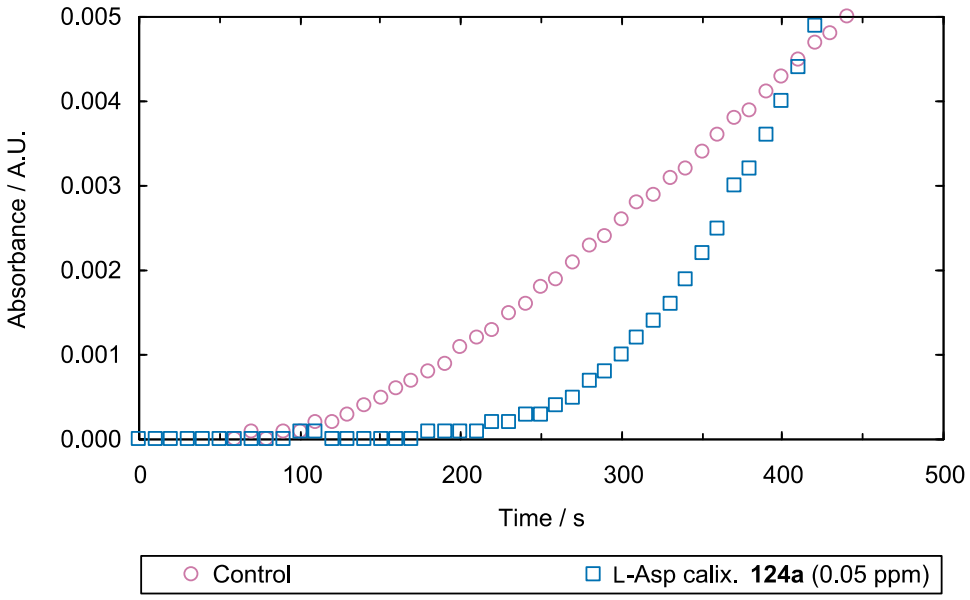

Figure 3.12 Determination of induction time for autonucleated barium sulfate in the presence of L-aspartic acid functionalised calix[4]arenes (**124a**). Absorbance of reaction solution measured overtime with additive levels at 0 μm of additive (control) and 0.04 μM (0.05 ppm).

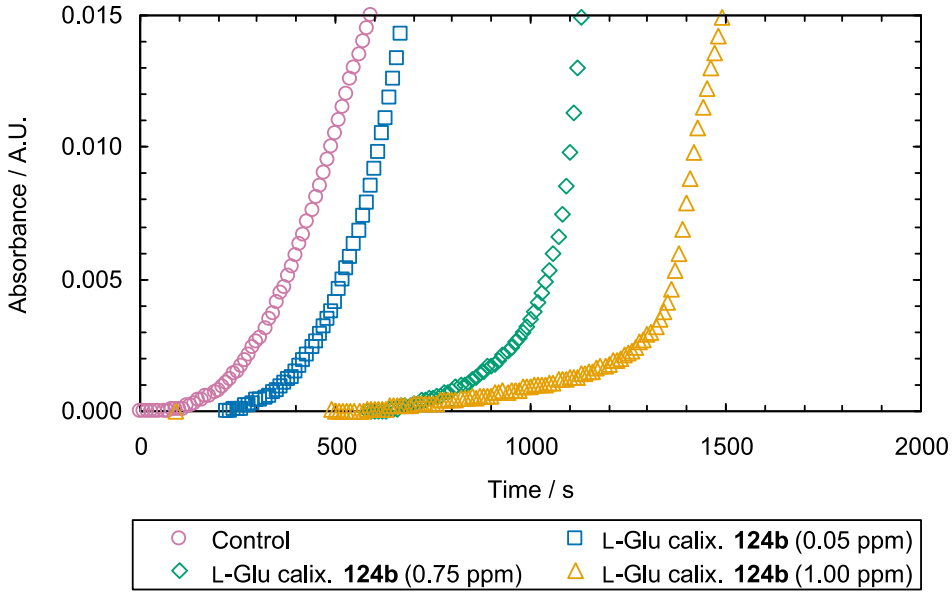

Figure 3.13 Determination of induction time for autonucleated barium sulfate in the presence of L-glutamic acid functionalised calix[4]arene (**124b**). Absorbance of reaction solution measured overtime with additive levels from 0 μM (0 ppm) of additive (control) to 0.78 μM (1 ppm).

3.4 Conclusions

The amino acid functionalised calixarenes, **124a**–**c**, had an impact on the crystallisation of model mineral systems, calcium carbonate and barium sulfate. The aspartic acid functionalised calixarene **124a** appeared to affect the morphology of calcium carbonate more than the glutamic acid derivative **124b**. Whilst **124b** appeared to behave similarly to its narrow-rim counter part in the crystallisation of calcium carbonate, **124a** resulted in a different calcite morphology compared with its narrow-rim analogue. The iminodiacetic acid derivative **124c** required a higher additive level to alter the calcite morphology. Barium sulfate grown in the presence of **124a** and **124b** gave similar morphologies. The kinetics of crystallisation, however suggested that the aspartic calixarene **124a** was a more potent crystal growth inhibitor than the glutamic calixarene **124b**. The aspartic derivative **124a** was also a more potent barium sulfate growth inhibitor than the narrow-rim analogue; **124b** showed similar potency to its narrow-rim analogue.

3.5 Experimental

3.5.1 General remarks

Reagents were used as purchased from the manufacturer or supplier. MilliQ water, having a resistance of 0.055 cm/Ω, was used throughout crystallisation experiments. The calixarene-based additives used in these experiments (**124a**, **124b**, and **124c**) were prepared by methods described in Chapter 2.

3.5.2 Calcium carbonate

The impact of the synthesised crystal growth modifiers on morphology of calcite was investigated using literature methods.[18, 19] Briefly, glass vials containing calcium chloride (7 mmol, 20 mL) with the appropriate concentration of additives and a microscope coverslip (10 mm diameter), were placed in a sealed desiccator (20 cm) along with a vial of ammonium carbonate. The vials were covered with Parafilm®, with pinholes to allow the diffusion of ammonia and carbon dioxide. After seven

days, the microscope coverslips were recovered and dried. After gold coating, the crystals were examined under a scanning electron microscope (Zeiss Evo 40XVP).

3.5.3 Barium sulfate

The impact of the synthesised additives on autonucleated desupersaturation rate and morphology of barium sulfate were investigated by literature methods.[12, 18] Briefly, barium chloride (0.100 M, 500 μL, final Ba^{2+} concentration 0.249 mM) and the additive (as a solution, neutralised with sodium hydroxide) were added to milliQ water (200 mL) and allowed to equilibrate at 25 °C while stirred. Equivalent sodium sulfate (0.100 M, 500 μL) was added to initiate autonucleation and the conductivity meter (WTW model LF 197) set to measure (the data was recorded by a computer). After 3–5 hours, the reaction mixture was filtered through a 0.2 μm filter membrane. If there was no decrease in the conductivity over the experiment period, the solution was placed in a vial with a microscope coverslip and allowed to crystallise for 5 to 14 days. Filter membranes and microscope coverslips were dried, gold coated, and the morphology examined under a scanning electron microscope (Zeiss Evo 40XVP). The desupersaturation rate was determined from the linear region of the desupersaturation curve.

Induction times were determined by a similar set-up to the desupersatuaration experiments. Barium chloride (0.100 M, 500 μL, final Ba^{2+} concentration 0.249 mM) and the additive (as a solution, neutralised with sodium hydroxide) were added to milliQ water (200 mL) and allowed to equilibrate at 25 °C while stirred. Equivalent sodium sulfate (0.100 M, 500 μL) was added to initiate crystallisation. The reaction mixture was pumped through Masterflex® Tygon® tubing (no. 14) by a Masterflex® L/S® Easy-Load® pump head (model 7518-00) at 250 rpm into a quartz flow cell. The absorbance at 900 nm was recorded by a GBC UV/VIS 916 spectrometer at 10 s intervals over 2 hours. The reaction mixture was filtered through a 0.2 μm filter membrane. Filter membranes were dried, gold coated, and the morphology examined under a scanning electron microscope (Zeiss Evo 40XVP). Induction times were determined from graphs of absorbance versus time.

3.6 References

1 Volkmer, D.; Fricke, M. *Z. Anorg. Allg. Chem.* **2003**, *629* (12–13), 2381–2390.

2 Volkmer, D.; Fricke, M.; Agena, C.; Mattay, J. *CrystEngComm* **2002**, *4* (52), 288–295.

3 Volkmer, D.; Fricke, M.; Agena, C.; Mattay, J. *J. Mater. Chem.* **2004**, *14* (14), 2249–2259.

4 Volkmer, D.; Fricke, M.; Vollhardt, D.; Siegel, S. *J. Chem. Soc., Dalton Trans.* **2002**, (24), 4547–4554.

5 Fricke, M.; Volkmer, D.; Krill, C. E.; Kellermann, M.; Hirsch, A. *Cryst. Growth Des.* **2006**, *6* (5), 1120–1123.

6 Volkmer, D. Biologically Inspired Crystallization of Calcium Carbonate Beneath Monolayers: A Critical Overview. In *Handbook of Biomineralization: Biomimetic and Bioinspired Chemistry*, Behrens, P.; Bäeuerlein, E., Eds. Wiley-VCH GmbH and Co. KGaA: Weinheim, 2008; Vol. 2, pp 65–87.

7 Fricke, M.; Volkmer, D. *Top. Curr. Chem.* **2007**, *270*, 1–41.

8 Meldrum, F. C.; Fendler, J. H. Construction of Organized Particulate Films by the Langmuir-Blodgett Technique. In *Biomimetic Materials Chemistry*, Mann, S., Ed. VCH Publishers, Inc.: New York, 1996; pp 175–219.

9 DiMasi, E.; Kwak, S.-Y.; Pichon, B. P.; Sommerdijk, N. A. J. M. *CrystEngComm* **2007**, *9* (12), 1192–1204.

10 Baynton, A.; Radomirovic, T.; Ogden, M. I.; Raston, C. L.; Richmond, W. R.; Jones, F. *CrystEngComm* **2011**, *13* (1), 109–112.

11 Jones, F.; Clegg, J.; Oliveira, A.; Rohl, A. L.; Ogden, M. I.; Parkinson, G. M.; Fogg, A. M.; Reyhani, M. M. *CrystEngComm* **2001**, *3* (40), 165–167.

12 Jones, F.; Oliveira, A.; Rohl, A. L.; Parkinson, G. M.; Ogden, M. I.; Reyhani, M. M. *J. Cryst. Growth* **2002**, *237–239* (Part 1), 424–429.

13 Baynton, A.; Ogden, M. I.; Raston, C. L.; Jones, F. *CrystEngComm* **2012**, *14* (3), 1057–1062.

14 Massi, M.; Ogden, M. I.; Radomirovic, T.; Jones, F. *CrystEngComm* **2010**, *12* (12), 4205–4207.

15 Heywood, B. R.; Ovens, A. C. D. *MRS Proceedings* **2006**, *923*, 0923-V05-09.

16 Stephen, M. *Endeavour* **1991**, *15* (3), 120–125.

17 Bartlett, M. J.; Mocerino, M.; Ogden, M. I.; Oliveira, A.; Parkinson, G. M.; Pettersen, J. K.; Reyhani, M. M. *J. Mater. Sci. Technol.* **2005**, *21* (Suppl.1), 1–5.

18 Jones, F.; Mocerino, M.; Ogden, M. I.; Oliveira, A.; Parkinson, G. M. *Cryst. Growth Des.* **2005**, *5* (6), 2336–2343.

19 Gower, L. A.; Tirrell, D. A. *J. Cryst. Growth* **1998**, *191* (1–2), 153–160.

20 Gehrke, N.; Cölfen, H.; Pinna, N.; Antonietti, M.; Nassif, N. *Cryst. Growth Des.* **2005**, *5* (4), 1317–1319.

21 Radha, A. V.; Forbes, T. Z.; Killian, C. E.; Gilbert, P. U. P. A.; Navrotsky, A. *Proc. Natl. Acad. Sci. U. S. A.* **2010**, *107* (38), 16438–16443.

22 Politi, Y.; Mahamid, J.; Goldberg, H.; Weiner, S.; Addadi, L. *CrystEngComm* **2007**, *9* (12), 1171–1177.

23 Fu, G.; Qiu, S.; Orme, C.; Morse, D.; De Yoreo, J. J. *Adv. Mater.* **2005**, *17* (22), 2678–2683.

24 Fu, G.; Valiyaveettil, S.; Wopenka, B.; Morse, D. E. *Biomacromolecules* **2005**, *6* (3), 1289–1298.

25 Malkaj, P.; Dalas, E. *Cryst. Growth Des.* **2004**, *4* (4), 721–723.

26 Manoli, F.; Dalas, E. *J. Cryst. Growth* **2001**, *222* (1–2), 293–297.

27 Zhang, Z.; Gao, D.; Zhao, H.; Xie, C.; Guan, G.; Wang, D.; Yu, S.-H. *J. Phys. Chem. B* **2006**, *110* (17), 8613–8618.

28 Wang, X.; Kong, R.; Pan, X.; Xu, H.; Xia, D.; Shan, H.; Lu, J. R. *J. Phys. Chem. B* **2009**, *113* (26), 8975–8982.

29 Klepetsanis, P. G.; Dalas, E.; Koutsoukos, P. G. *Langmuir* **1999**, *15* (4), 1534–1540.

30 Marin, F.; Luquet, G. Unusually Acidic Proteins in Biomineralization. In *Handbook of Biomineralization: Biological Aspects and Structure Formation*, Bäeurlein, E., Ed. Wiley-VCH Verlag GmbH: Weinheim, 2008; Vol. 1, pp 273–290.

31 Mann, S.; Didymus, J. M.; Sanderson, N. P.; Heywood, B. R.; Samper, E. J. A. *J. Chem. Soc., Faraday Trans.* **1990**, *86* (10), 1873–1880.

32 Addadi, L.; Weiner, S. *Proc. Natl. Acad. Sci. U. S. A.* **1985**, *82* (12), 4110–4114.

33 Jones, F.; Jones, P.; Ogden, M. I.; Richmond, W. R.; Rohl, A. L.; Saunders, M. *J. Colloid Interface Sci.* **2007**, *316* (2), 553–561.

34 Kucher, M.; Babic, D.; Kind, M. *Chem. Eng. Process.* **2006**, *45* (10), 900–907.

35 Heywood, B. R.; Mann, S. *J. Am. Chem. Soc.* **1992**, *114* (12), 4681–4686.

36 Heywood, B. R.; Mann, S. *Adv. Mater.* **1994**, *6* (1), 9–20.

37 Mullin, J. W. *Crystallization*. 4th ed.; Elsevier: London, 2004.

38 Yang, K. C.; Hogg, R. *Anal. Chem.* **1979**, *51* (6), 758–763.

39 Baynton, A.; Chandler, B. D.; Jones, F.; Nealon, G.; Ogden, M. I.; Radomirovic, T.; Shimizu, G. K. H.; Taylor, J. M. *CrystEngComm* **2011**, *13* (4), 1090–1095.

4 Proline-functionalised calixarene low molecular weight hydrogelators*

4.1 Calixarene- and resorcinarene-based gelators

A large number of gelators have been reported in the literature, however only a handful of these are macrocycles, the majority of which are calixarene- or resorcinarene-based. This section will discuss calixarene- and resorcinarene-based gelators; an introduction to small molecule gelators is provided in section 1.3. All the known calixarene-based gelators published in the literature thus far (aside from work associated with proline-functionalised calixarenes and one report of an ammonium-triazole calixarene) are organogelators. In contrast, all the known resorcinarene-based gelators reported are hydrogelators.

4.1.1 Calixarene-based gelators

Some early examples of calixarene-based gelators were reported by Aoki et al.[1, 2] Calixarenes **145**–**147** (Figure 4.1) were acylated at the wide-rim with variable length alkyl chains. The best gelators were found to be **145c** and **147b**,**c** and were capable of gelling solvents such as carbon disulfide, hexane, decane, butanol, and isopropyl alcohol (by heating and cooling the gelator in the solvent). The authors proposed that C=O···HO(calixarene) hydrogen bonds and C=O···C=O dipole-dipole interactions

* Some of this work is based on work previously published: Becker, T.; Goh, C. Y.; Jones, F.; McIldowie, M. J.; Mocerino, M.; Ogden, M. I., *Chem. Commun.* **2008,** (33), 3900–3902; Goh, C. Y.; Becker, T.; Brown, D. H.; Skelton, B. W.; Jones, F.; Mocerino, M.; Ogden, M. I., *Chem. Commun.* **2011,** *47* (21), 6057–6059.

were the key in inducing self-assembly in organic solvents; the strength of the C=O···HO(calixarene) interactions were sufficient to overcome C=O···HO(alcohol) interactions to gel alcohols.

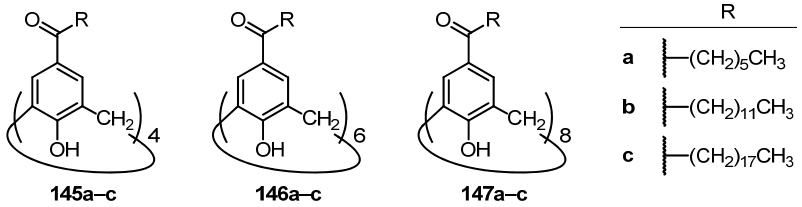

Figure 4.1 Calixarene-based organogelators investigated by Shinkai's group.[1, 2]

In some cases, the gelator formed a gel in the presence of a second component (Figure 4.2). Xing et al.[3] showed that extended polymeric networks could be formed by coordination of the 3-pyridylazo moiety of calix[4]arene **148** to $[Pd(en)(H_2O)_2]$-$(NO_3)_2$ forming a metallogel. A metallogel was observed for a range of organic solvents such as dimethylsulfoxide, tetrahydrofuran, acetic acid, chloroform, and dichloromethane. The metallogel formed in dimethylsulfoxide showed remarkable stability over a wide pH range (pH 1–13) and high temperatures (100 °C). In addition, the authors found that the metallogel could 'uptake' toluene from an aqueous solution with performance comparable to activated carbon.

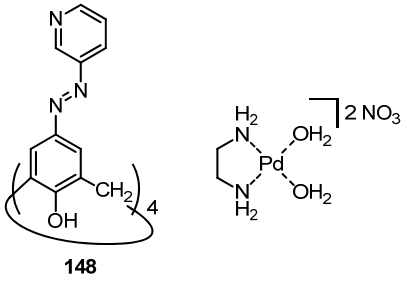

Figure 4.2 Calixarene **148**, functionalised with pyridyl-azobenezene moieties, formed metallogels with $[Pd(en)(H_2O)_2](NO_3)_2$, where en = ethylenediamine ligand.[3]

New gelators can be designed incorporating functionalities known to facilitate gel formation.[4] Cholesterol-based organogelators are well known[5] and cholesterol has been appended to the narrow-rim of calix[4]arenes by Cai et al[6] (Figure 4.3). Calix[4]arene **149** was found to form gels (>1.0 wt/vol%) in a mixed solvent system, acetonitrile/decane, however the acetonitrile content must be 10–60 vol/vol%.

Further investigation by the authors showed that the gel was like an 'oil-in-oil' emulsion where acetonitrile was trapped within the **149**-decane gel; calix[4]arene **149** is soluble in decane. In addition, the **149** organogel was found to posses thixotropic properties.

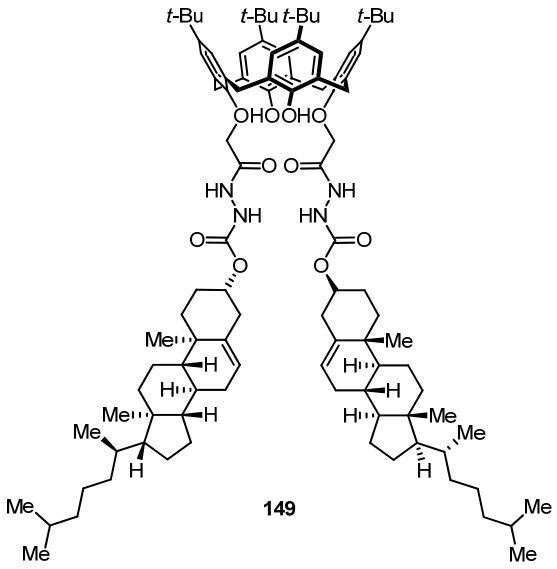

149

Figure 4.3 Cholesterol-functionalised calix[4]arene investigated by Cai et al.[6] as an organogelator.

Zheng et al.[7] investigated the formation of organogels by amine functionalised calix[4]arenes **150a**–**d** (Figure 4.4). The authors found that calix[4]arenes **150a** and **150b** could enantioselectively form a gel in the presence of 2,3-dibenzoyltartaric acid **151** (i.e. **150a**–D-**151** and **150b**–L-**151**). Gels could be formed in a variety of solvents such as dichloromethane and benzene but not in solvents that can form hydrogen bonds (e.g. diethyl ether, acetone). Characterisation of the organogels by atomic force microscopy and scanning electron microscopy (of the xerogel) showed that the gelators and tartaric acid self-assembled into fibrils. Further investigations by the group showed that achiral calix[4]arene **150c** did not form a gel whereas calix[4]arene **150d** formed a gel although it was not enantioselective.

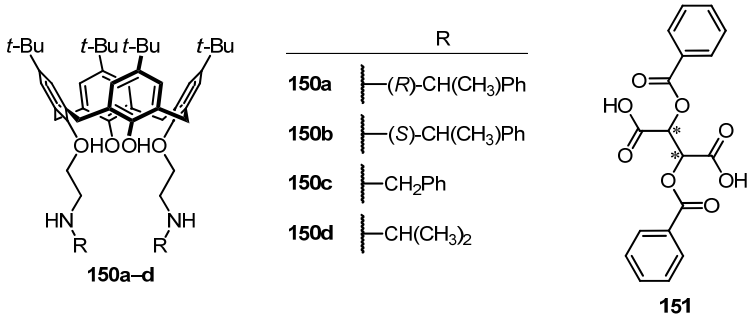

Figure 4.4 Chiral calix[4]arenes investigated by Zheng et al.[7]. **150a–b**,**d** formed organogels in the presence of **151**.

Zhou et al.[8] extended their investigation into calix[4]arenes **150a**–**d** by substituting the *tert*-butyl substituent with long alkyl chains. Calix[4]arenes **152a**–**c** (Figure 4.5) and 2,3-dibenzoyltataric acid **151** also formed organogels. The authors found that a solid mixture of **152a** and L-**151** (produced by dissolving both compounds in chloroform followed by removal of the solvent) dissolved in cyclohexane formed a gel after heating to 60 °C then cooling to 20 °C (like many gelators published in literature). However, heating a solid mixture of **152a** and D-**151** in cyclohexane formed a gel at 60 °C but the gel returned to a solution when cooled to 20 °C. Similar observations were made for **152b**,**c** with L- and D-**151**. Interestingly, **152** and L-**151** organogels formed fibres whereas **152** and D-**151** organogels formed a mixture of fibres and vesicles. The calix[4]arene **152** and D-**151** formed vesicles in cyclohexane solution (as opposed to fibrous structures). They suggested that the mixed chirality between **152** and D-**151** led to the formation of unstable fibres, therefore heat was required to destabilise the more stable vesicles.

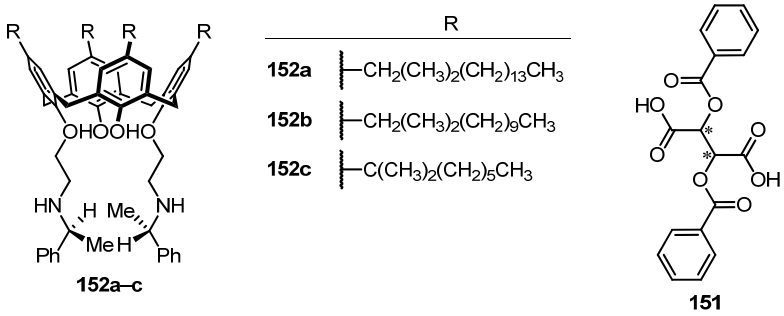

Figure 4.5 Chiral calix[4]arenes investigated by Zhou et al.[8] **152** formed organogels in cyclohexane with L-**151** after heat and cooling. **152** and D-**151** formed organogels when heated to 60 °C but formed a solution on cooling to 20 °C.

Zheng et al.[9] further examined chiral amine interactions with 2,3-dibenzoyltartaric acid by exchanging it with the narrow-rim substituted amine. The authors attached L-2,3-dibenzoyltartaric acid via a hydrazide to the narrow-rim of a calix[4]arene to give **153** (Figure 4.6). Calix[4]arene **153** formed an organogel with amine (*R*)-**154** in 1,2-dichloroethane whereas (*S*)-**154** remained a solution. The calix[4]arene **153** did not form gels or exhibit chiral recognition with amines **155**–**157** in 1,2-dichloroethane. However, altering the solvent to a mixture of 1,2-dichloroethane and cyclohexane gave an organogel with calix[4]arene **153** and amino alcohol (*S*)-**155**. Calix[4]arene **153** with amino alcohol (1*R*,2*S*)-**156**, and diamine (1*S*,2*S*)-**157** gave a suspension in mixtures of 1,2-dichloroethane and cyclohexanol. Characterisation of the gels and suspensions showed solid spherical structures unlike the fibrils observed with organogels of calix[4]arenes **150a**,**b** and **152**.

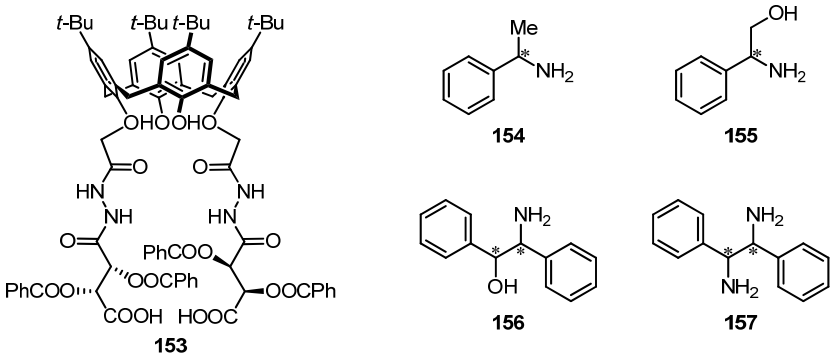

Figure 4.6 Calix[4]arene **153** investigated by Zheng et al. for gel formation with chiral amines.[9]

Another two-component organogel system was reported by Vreekamp et al.[10] Calix[4]arene **158** (Figure 4.7) substituted with 1,3,5-triazine at the wide-rim formed an organogel in the presence of an equimolar equivalent of barbituric acid **159** in chloroform. This serendipitous discovery was made during NMR experiments and the organogel was not further characterised.

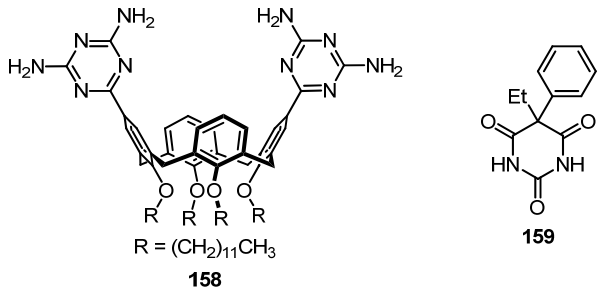

Figure 4.7 Calix[4]arene **158** forms a two-component organogel with **159**.[10]

Dudic et al.[11] may have unintentionally prepared a hydrogelator during their investigation of guanidinium-functionalised calix[4]arenes for binding to plasmid DNA. They noted that calix[4]arene **160** formed 'a gelatinous macroscopic aggregate in water' whereas the other calixarenes under investigation did not show signs of micellar aggregation by ^{1}H NMR spectroscopy.

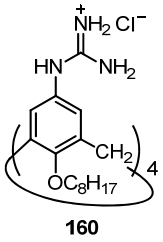

Figure 4.8 Potential hydrogelator prepared by Dudic et al.[11]

An amphiphilic calixarene-based hydrogel was briefly mentioned by Fujii et al.[12] (Figure 4.9) amongst their studies of calixarene-based micelles. The authors noted that an aqueous solution of **161** in sodium chloride formed spheres at pH <6 and cylindrical structures at pH >10 (and a mixture of structures at intermediate pH). It was not surprising that a macroscopic gel formed at pH >10. The gel phenomenon was not reported for the propyl and nonyl alkyl derivatives studied.

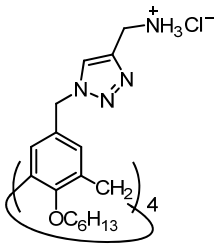

161

Figure 4.9 An amphiphilic calix[4]arene-based hydrogel investigated by Fujii et al.[12]

Zhang et al.[13] recently reported that proline calix[4]arene **127a** formed hydrogels in the presence of basic amino acids at low pH. The authors found that calix[4]arene **127a** (5 mM) formed hydrogels in the presence of arginine, histidine, or lysine (20 mM) at pH 3 (pH adjusted with hydrochloric acid). The hydrogel consisted of nanofibres, however the xerogel morphology ranged from fibres to plate-like or ribbon-like structures (dependent on the amino acid). Although the authors did not report this, it would be of interest to see if **127a** could enantioselectively form hydrogels with the basic amino acids, and also if gels would form if the pH was adjusted with phosphoric acid rather than hydrochloric acid.

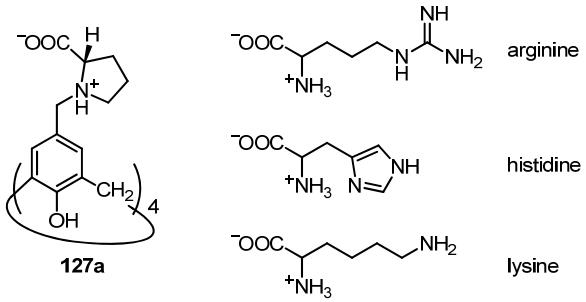

127a

Figure 4.10 Proline calix[4]arene **127a** formed hydrogels with basic amino acids at pH 3.[13]

4.1.2 Resorcinarene-based gelators

Resorcinarenes have also been shown to form gels. Haines and Harrison[14] showed that a resorcinarene functionalised with iminodiacetate **162** (Figure 4.11) formed hydrogels under acidic conditions. The gel was found to be pH-responsive and the gelation ability was diminished in the presence of Fe^{2+} and Co^{2+} and suppressed by Cu^{2+} (presumably by the preference for coordination to copper, however this was not indicated in the paper).

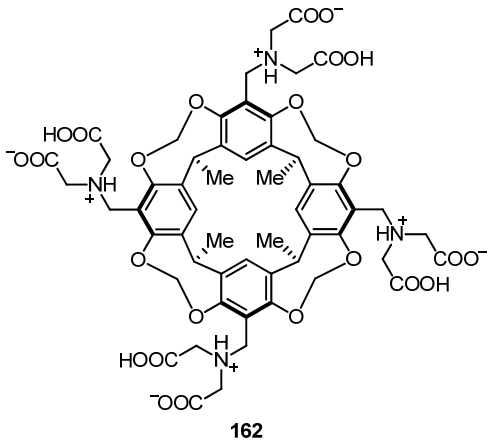

162

Figure 4.11 Resorcinarene-based hydrogelator **162**.[14]

Amino-amide functionalised resorcin[4]arene **163c** also formed hydrogels under acidic conditions.[15] The primary amines appeared to be important for gelation as **163d** did not form a gel. Similarly, the long alkyl chains appear to be involved in gelation since **163a**,**b** were not reported by the authors to form gels.

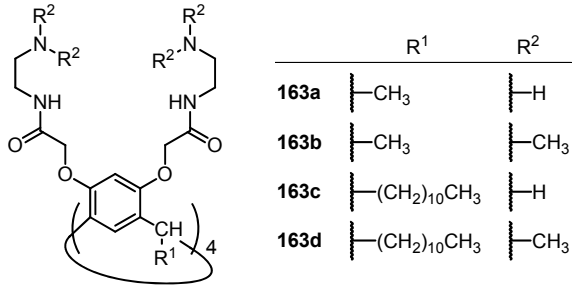

163a–d

Figure 4.12 Resorcinarene-based hydrogelator **163a–d**.[15]

4.1.3 Other macrocyclic gelators

A structural analogue of calixarenes, calix[4]pyrrole **164**, formed hydrogels in the presence of tetramethylammonium chloride and an alkali hydroxide.[16] The authors found that hydrogels formed with sodium hydroxide but not with lithium or potassium hydroxides. However, reducing the pH of the solution to neutral by exposure to CO_2 gave hydrogels with all of the alkali hydroxides (not just sodium hydroxide).

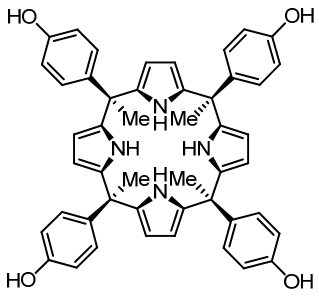

164

Figure 4.13 Calix[4]pyrrole **164** formed hydrogels in the presence of tetramethylammonium chloride and an alkali hydroxide.[16]

Cucurbit[*n*]urils[17, 18] are another class of macrocycles. Hwang et al.[19] reported a cucurbit[7]uril-based hydrogel which was not only pH- and thermo-responsive, the hydrogel underwent a gel-sol transition in the presence of Na^+ and K^+ cations (with the cucurbit[7]uril binding to the cations). Furthermore, the inclusion of *trans*-4,4′-diaminostilbene dihydrochloride guest within the cucurbit[7]uril host (**165**, Figure 4.14) allowed the authors to switch between gel and sol states by UV-irradiation; a gel was formed in the presence of *trans*-4,4′-diaminostilbene dihydrochloride while the *cis*-isomer disrupted the formation cucurbit[7]uril fibrils.

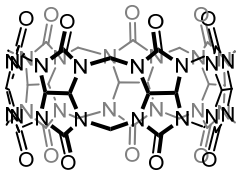

165

Figure 4.14 Cucurbit[7]uril-based hydrogelator **165** investigated by Hwang et al.[19]

4.2 Anion-triggered gelation with proline-functionalised calixarenes

Proline calix[4]arene (**127a**) (Figure 4.15) hydrogels were discovered by serendipity. The discovery was made during NMR titration experiments to study cation binding by **127a** (McIldowie, M. J. Curtin University, Perth, Australia. Personal communication, 2008). It was initially hypothesised that the cation had a dominant influence on gel formation with calixarene **127a** through cation-carboxylate interactions.

However, further investigation (Table 4.1) showed that gelation was dominated by the nature of the anion with some influence from the cation. The ability of the anion to trigger gelation was later shown to correlate with the Hofmeister series (see section 4.2.2).

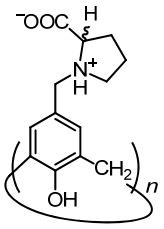

127, **128**

	proline	*n*
127a	L-Pro	4
127b	D-Pro	4
128	L-Pro	5

Figure 4.15 Proline calix[*n*]arenes investigated as potential hydrogelators.

Table 4.1 Summary of selected electrolyte effect on gel formation by L-proline calix[4]arene (20 mM, final solution), where G = stable gel; TG(*x*) transient gel (followed by crystallisation after *x* hours or 'w' for one week); I = incomplete gel (i.e. not stable to vial inversion); L = liquid; and C = crystallisation. The concentrations listed refer to the final concentration of the electrolyte (and not individual ions).

		Anion								
		SO_4^{2-}	$H_2PO_4^-$	F^-	Cl^-	Br^-	I^-	NO_3^-	ClO_4^-	SCN^-
Cation	Al^{3+}				0.05 M G			0.05 M G		
	Mg^{2+}				0.08 M G			0.05 M G		
	Ca^{2+}				0.05 M G			0.05 M TG(12)		
	H^+	0.05 M L	0.05 M L		0.05 M L	0.05 M G	0.05 M G	0.05 M G	0.05 M TG(<0.1)	
	Li^+				0.05 M L			0.12 M G		
	Na^+	0.05 M L	0.05 M L	0.05 M L	0.05 M L	0.05 M IG	0.05 M TG(1)	0.05 M TG(w)	0.05 M TG(0.1)	0.05 M TG(2)
	K^+				0.05 M L			0.05 M TG(108)		
	NH_4^+				0.05 M L			0.05 M TG(w)		
	NBu_4^+							0.05 M G		

In order to form gel fibres, gelators typically have limited solubility in a solvent and self-assemble in one direction.[20] The solubility of gelator **127a** was determined to be in excess of 0.5 g/mL. This is unusual in that there is generally a balance between the

solubility of the gelator in the solvent (the gelator will not form the solid-like structures if it is highly soluble in the solvent) and the ability to precipitate from solution (if the gelator has low solubility then it can not be dissolved). The high solubility of compound **127a** in water and its ability to form a hydrogel is a puzzle. It is possible that the electrolyte may modify the solubility of the gelator **127a** in solution. The solubility of a gelator in a solvent is known to have an impact on gel formation[21–23] and Muro-Small et al.[24] have suggested that the thermodynamic parameters for dissolution (solvent-dependent) are also related to gel formation. Salts have been reported to alter the gelation ability of some molecules, such as guanosine-based[25] and calix[4]pyrrole[16] gelators.

4.2.1 Gel-sol transition temperature

The gel-sol transition temperature ($T_{gel\text{-}sol}$) was determined for L-proline calix[4]-arene hydrogels formed with selected electrolytes. $T_{gel\text{-}sol}$ was determined by the 'dropping ball' method modified from that described by de Loos.[26] The hydrogels typically formed rapidly when the electrolyte solutions were added to solutions of **127a** (at the concentrations of interest); there were concerns that the gels may not be homogenous for the 'dropping ball' (or 'falling spheres') experiments. To overcome concerns with the homogeneity of the hydrogels, the initial hydrogels (formed by the addition of the electrolyte solution to **127a** solution) were heated briefly in an oven at 100 °C then allowed to cool to room temperature.

Preliminary dropping ball experiments with selected lanthanide nitrates (Figure 4.16) showed that this process had minimal impact on the $T_{gel\text{-}sol}$ determination. However, the heating and cooling cycle did lead to precipitation in some gel systems. A compromise between homogeneity and crystallisation was made by allowing the gel to stand at room temperature for a period of time before commencing $T_{gel\text{-}sol}$ measurements. The equilibration time period is variable (due to potential for the gel to crystallise) and depended on the electrolytes under investigation. It was also observed that the hydrogel was not necessarily a liquid, even though the ball had reached the bottom of the vial. Therefore, the dropping ball experiment was supplemented with the 'tube-inversion' method; both of these methods give a qualitative indication of the yield stress of the hydrogel.[27, 28]

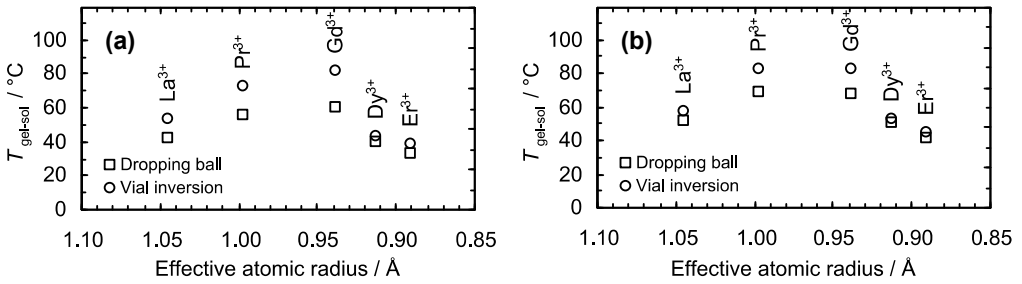

Figure 4.16 Comparison of the effect of sample preparation on $T_{gel–sol}$ determination (a) at room temperature and (b) heated in an oven at 100 °C for 5 min. with both 'dropping ball' and 'tube inversion' methods. The effective atomic radii are for lanthanides with coordination 6 in the solid state.[29]

The effect of gelator concentration on $T_{gel\text{-}sol}$ was investigated using **127a**-$La(NO_3)_3$ hydrogel system. As the concentration of gelator was increased with a fixed concentration of $La(NO_3)_3$, $T_{gel\text{-}sol}$ increased nearly linearly (Figure 4.17). The experiments were stopped at $T_{gel\text{-}sol}$ at approximately 80 °C for safety reasons. The linear increase in $T_{gel\text{-}sol}$ with increasing concentration of gelator was consistent with observations by de Loos[26] for urea-based organogels. Furthermore, Figure 4.17 shows a gel-sol phase boundary for this specific system.

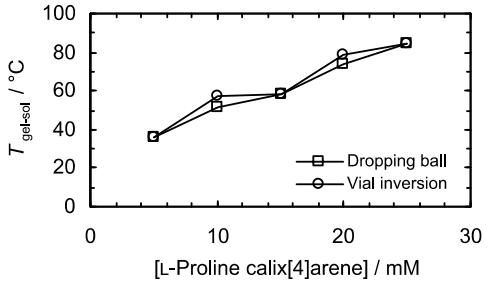

Figure 4.17 Effect of L-proline calix[4]arene concentration (**127a**) on thermostability of hydrogels, $La(NO_3)_3$ at 20 mM.

4.2.2 The Hofmeister series

The Hofmeister series (also referred to as the lyotropic series or specific ion effect) was named after Franz Hofmeister[30–36] who first studied specific ion effects. Hofmeister's original papers, written in archaic German, are not well read[37] but a translation of his second and third publications are available.[37] The Hofmeister series is better defined for anions (Figure 4.18) than cations;[38] the sequence of anions in the series is often varied slightly to suit the system under consideration. Anions to the left are known as kosmotropes while those to the right are chaotropes. Traditionally

the Hofmeister series was thought to operate on the ions' ability to influence 'bulk water' structure thus, kosmotropes are associated with 'water structure making' while chaotropes are associated with 'water structure breaking'.[38] The chloride anion is generally considered to be the pivotal point of the Hofmeister series, having little effect on the water-structure.[39] Despite the early observations by Hofmeister, research into Hofmeister effects has not reached a consensus on the underlying mechanism (although it is believed to be more than just the ion's impact on 'bulk water' structure) and it is quite possible that there may be more than one factor responsible.[38, 40-47] Furthermore, the sequence has been known to invert due to changes in concentration[48, 49] or the pH of proteins relative to the pI.[50] Regardless, the Hofmeister effect has been observed in many biological, supramolecular, and colloidal systems.[51, 52]

Figure 4.18 A typical Hofmeister series for anions.[38]

The Hofmeister effect is typically observed over moderate concentrations, 0.01–1.0 M.[53–55] Here, experiments with sodium salts of anions in the Hofmeister series showed that the $T_{gel\text{-}sol}$ generally increased (Figure 4.19) as the anion is situated towards the chaotropic end of the series. However, at the chaotropic end of the series (in particular perchlorate and thiocyanate) the hydrogels were found to have lower thermostability and a tendency to crystallise, thereby rapidly decomposing the hydrogel. The addition of sodium perchlorate to a solution of **127a** led mainly to precipitation with the formation of some clumps of gel-like material. The **127a**-NaSCN hydrogels had lower yield stress with some samples not able to hold the steel ball at the surface of the hydrogel (although they were self-supporting to tube inversion). The anions towards the middle of the Hofmeister series (nitrate, bromide, and iodide) formed relatively more thermostable hydrogels with **127a**. Both the **127a**-NaBr and **127a**-NaI samples precipitated on cooling after the gel-sol transition while the **127a**-$NaNO_3$ reformed the hydrogel then crystallised on standing overnight. The **127a**-NaCl sample formed a hydrogel (stable to vial inversion) when cooled in a fridge (~5 °C) but not at room temperature; $T_{gel\text{-}sol}$ was estimated from the

127a-NaCl solution on warming to room temperature. This lower $T_{gel\text{-}sol}$ value is consistent with chloride being the 'pivot' of the Hofmeister series. The **127a**-NaCl sample formed thin crystals after the gel-sol transition. From this experiment, it was observed that the $T_{gel\text{-}sol}$ and the tendency to crystallise generally correlated with the Hofmeister series for anions.

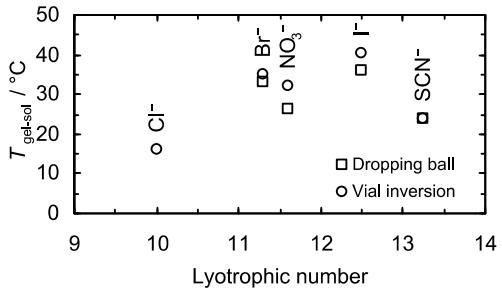

Figure 4.19 The effect of the anion on the L-proline calix[4]arene hydrogel thermal stability. Here the gels were composed of L-proline calix[4]arene at 20 mM and sodium salts at 50 mM. Lyotropic number (derived from impact of electrolytes on the cloud point of a surfactant) obtained from Schott.[56]

No attempts were made to measure the cation effect by the 'dropping ball' method. However, it has been observed that hydrogels formed from electrolytes of alkali salts are generally less stable hydrogels than di- and trivalent cation salts, and in cases where hydrogels are formed, the hydrogels had a tendency to crystallise. Trivalent lanthanides generally formed the most stable gels. Divalent cations showed mixed results with calcium salts being much less stable than magnesium salts. This difference between Ca^{2+} and Mg^{2+} electrolytes could be due to differences in their surface charge densities.[57] In addition, differences between the hydration of Ca^{2+} and Mg^{2+} have been shown to have an impact on crystallisation;[58] Ca^{2+} is easier to dehydrate (requiring less energy compared to Mg^{2+}). In this case, the interaction between Ca^{2+} and the carboxylates of **127a** may tip the delicate balance (between a gel phase and solid) towards crystallisation. Unfortunately, crystals formed from **127a**-Ca^{2+} hydrogels were very thin plate-like crystals, and diffracted weakly, or not at all, in attempts to obtain a single crystal x-ray structure determination.

Gel-sol transition temperatures determined for hydrogels formed from **127a** and lanthanide nitrates (Figure 4.20) gave an unexpected result. The $T_{gel\text{-}sol}$ was generally higher for hydrogels formed in the presence of Ce^{3+}, Pr^{3+}, Nd^{3+}, Eu^{3+}, and Gd^{3+} and a

lower in the presence of Dy^{3+} and Er^{3+}. **127a**-$Yb(NO_3)_3$ had a transient hydrogel phase which led to crystallisation within half an hour. These results could suggest that charge density reaches an optimum value for gel formation in the middle of the lanthanide series. Alternatively, there may be a structural change in the metal complexation with the heavier lanthanides, which impacts negatively on the gel stability. Certainly, structural changes across the lanthanide series have been reported for other calixarene ligands.[59]

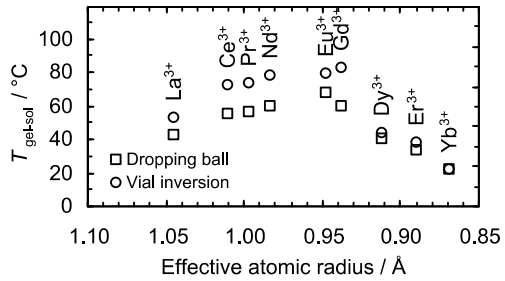

Figure 4.20 $T_{gel-sol}$ determined for lanthanide nitrates by the 'dropping ball' and 'tube inversion' methods. The effective atomic radii are for lanthanides with coordination 6 in the solid state.[29]

Bulk water structure 'breaking' and 'making' was thought to be central to the mechanism of the Hofmeister effect. Recent work has shown that this may not be the case and it has been hypothesised that the ion-specific effects are a result of ion interactions at the macromolecule/water interface.[60] Omta et al.[61] have shown that the effect of the ions does not extend beyond the first hydration shell, and thus does not affect hydrogen bonding network of water molecules in the immediate vicinity. Collins and Washabaugh[39] have shown that ion effects are at the interface and on bulk water. Recently, Parsons et al.[48] noted that the Hofmeister effect involved complex interactions between ion polarisabilities, ion size, nonelectrostatic potentials, and specific surface chemistry. Furthermore, Hofmeister described his observations for electrolytes[37] not individual ions in solution (which is not practical in any case). Recent tetrahertz and femtosecond infrared spectroscopic results by Tielrooij et al.[62] indicated that there may be a 'cooperative' effect between hydrated cations and anions in solution which are interdependent and not additive. This makes it difficult to interpret the impact of individual cations and anions on the self-assembly (and by extension, the gel formation) of proline calix[4]arene **127**.

The role of the anion in gel systems can be broadly placed into two groups: anions can behave as in the Hofmeister series or participate more directly by supramolecular anion-binding.[63, 64] Liu et al.[65] noted that kosmotropic anions reduced the heat capacity of hydroxypropylmethylcellulose (promoting gelation) and increased the storage moduli; an opposite trend was observed towards the chaotropic end of the Hofmeister series. In contrast, Steed et al.[66, 67] reported organogels which formed from supramolecular anion-binding by urea-based gelators. Similarly, supramolecular interactions between protonated melamine and selected anions were reported to form hydrogels.[68] Regardless of the precise mechanism, the impact of anions is of interest as noted by Lloyd and Steed[69] who suggested that anions may be used to chemically tune the properties of gels.

4.3 Characterisation of self-assembled structures in the presence of electrolytes

4.3.1 Physical characterisation of gel phase structures

The structures formed by proline calix[4]arene **127** in the gel phase were visualised by physical characterisation methods. Some methods gave results indicating fibrous structures in the hydrogel while other methods were limited by issues with sample preparation or interference from the sample matrix.

4.3.1.1 Scanning electron microscopy

Initial attempts to visualise hydrogel structures under scanning electron microscopy (SEM) proved unsuccessful. The sample preparation procedure for SEM (air drying then drying *in vacuo* to remove water) resulted in a structureless mass. Removal of water from hydrogels is known to cause collapse of the gel,[70, 71] primarily by surface tension acting on the gel fibres.[72] Hydrogels have been imaged by SEM, however lengthy sample preparation is required (e.g. freeze drying or chemical fixation)[13, 73] or requires variable pressure SEM instrumentation.[74] Alternatively, gel fibre morphology can be visualised *in situ* by atomic force microscopy (AFM).

4.3.1.2 **Atomic force microscopy**

A selection of hydrogels prepared from **127a** and selected electrolytes (LiCl, NaBr, $NaNO_3$, $CaCl_2$, and $La(NO_3)_3$) were imaged by AFM (Figure 4.21). The nature of the electrolyte appears to have had an impact on the morphology of the gel fibres with chloride electrolytes generally resulting in shorter and thinner fibres with **127a** than nitrate electrolytes. The diameter of the hydrogel fibres was estimated from AFM micrographs.

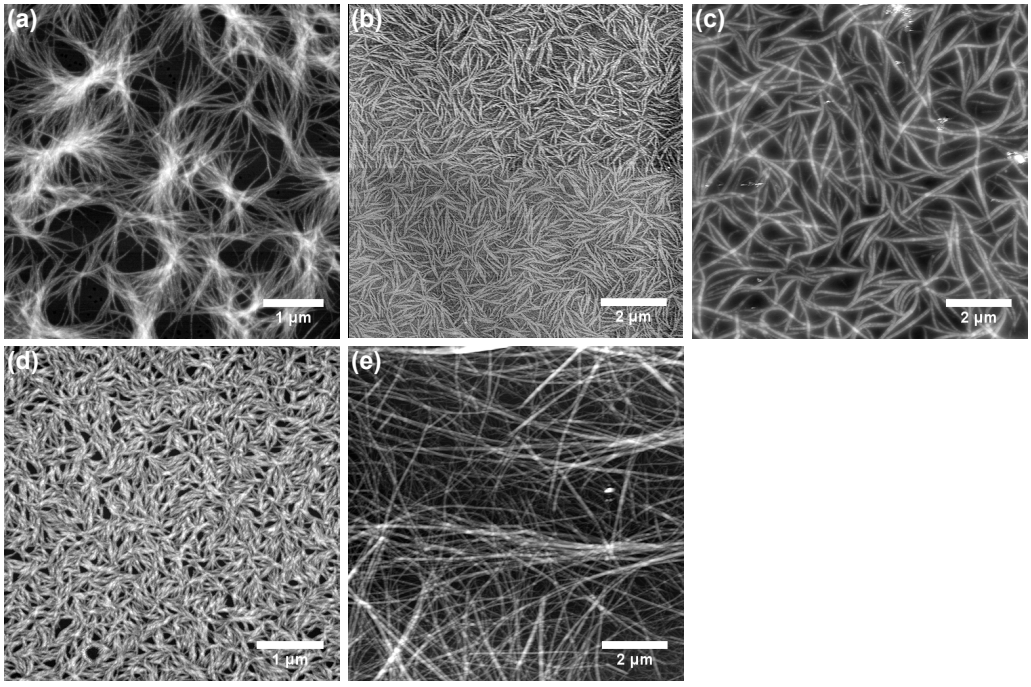

Figure 4.21 AFM micrographs of L-proline calix[4]arene **127a** (20 mM) in the presence of (a) LiCl (25 mM), (b) NaBr (25 mM), (c) $NaNO_3$ (25 mM), (d) $CaCl_2$ (25 mM), and (e) $La(NO_3)_3$ (25 mM).

Height measurements of selected (observable) gel fibres of **127a**-$La(NO_3)_3$ (Figure 4.22) revealed that the fibre bundles have diameters ranging from 5 to 40 nm (Table 4.2) and with increments of the fibre diameters of 5 ± 2 nm. In contrast, results from **127a**-LiCl hydrogel (Figure 4.23) showed that the gel fibres were generally more uniform with diameters of 2–6 nm. High resolution images to resolve the superstructures of the gel fibres were not readily achieved. Since the calix[4]arenes **127a**,**b** are chiral, the gel fibre morphology was expected to exhibit some chirality (i.e. twist in the fibres). However, this was not apparent from the AFM micrographs of the gels. In some cases the chirality of the gelator is not translated to

the supramolecular structure or altered during sample preparation (though less likely when analysed by AFM).[20] Alternatively, the pitch may be too close to be observed under the conditions used; pitch of fibres can vary over several orders of magnitude from 10 nm to 1 mm for twisted fibres or helices.[75]

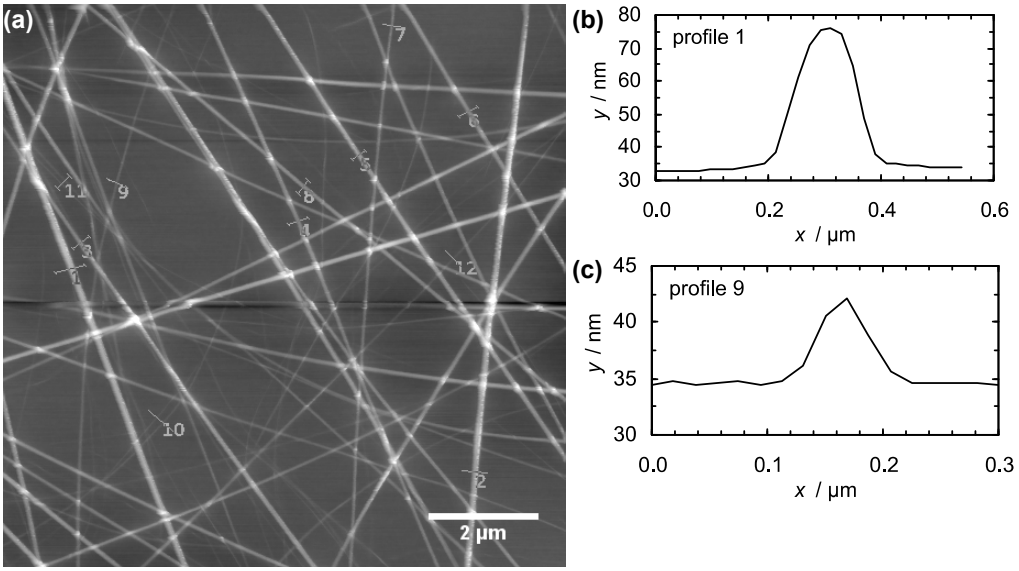

Figure 4.22 Estimation of gel fibre diameter from height profiles, L-proline calix[4]arene **127a** (20 mM) and $La(NO_3)_3$ (25 mM), from an (a) AFM micrograph and (b, c) associated line profiles.

Table 4.2 Height measurement from line profiles from selected gel fibres from an AFM micrograph in Figure 4.22. Height measurements are ±0.2 nm.

Profile	Height (nm)	Profile	Height (nm)
1	39	7	16
2	39	8	25
3	21	9	7
4	21	10	3, 5
5	31	11	3, 4
6	21	12	6

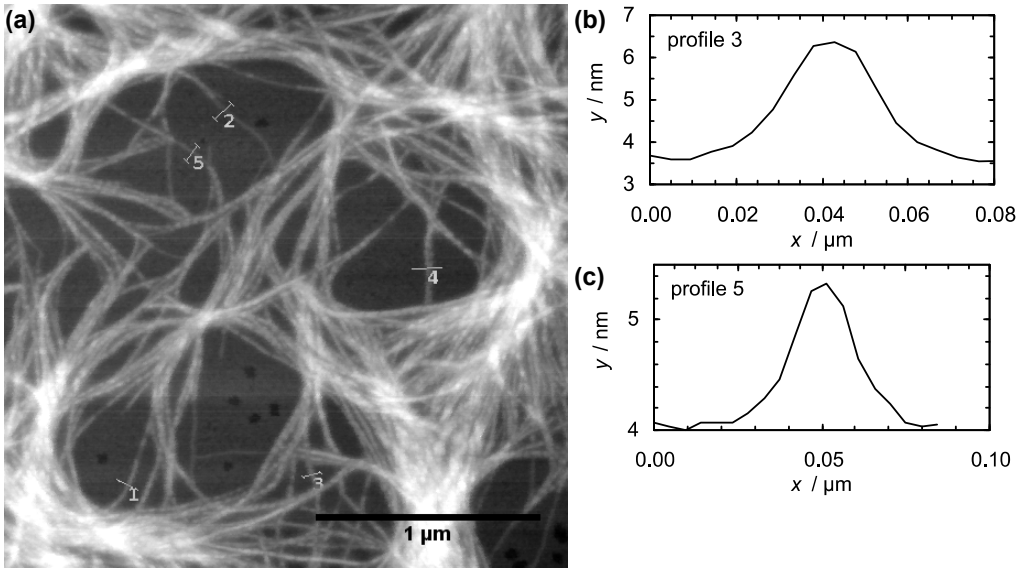

Figure 4.23 Estimation of gel fibre diameter from height profiles, L-proline calix[4]arene (20 mM) and LiCl (25 mM), from an (a) AFM micrograph and (b, c) associated line profiles.

4.3.1.3 **Cryo-transmission electron microscopy**

The absence of a hydrogel at the macroscale, does not exclude the formation of fibrous structures at the microscale by **127a** in the presence of electrolyte. Investigations using cryogenic-transmission electron microscopy (cryo-TEM) showed fibres in *solutions* of **127a**-electrolyte systems that were known to form hydrogels at room temperature (Figure 4.24). By reducing the concentration of the electrolyte, the formation of a hydrogel was avoided. Cryo-TEM micrographs of **127a** in the presence of selected electrolytes (LiCl, NaBr, $CaCl_2$, and $La(NO_3)_3$) all showed the formation of long fibrous structures despite a free flowing solution at the macroscale level. No fibrous structures were observed in the absence of an electrolyte, however Zhang et al.[13] reported the formation of nanoscale spherical micelles for **127** (at pH 3) in the presence of hydrochloric acid. These micrographs (Figure 4.24) suggest that **127a** formed fibres in the presence of electrolytes, although there may not be enough fibres present to entangle and trap the water to form a hydrogel. It should be noted that the samples were cooled to 5 °C prior to vitrification. Cooling **127a**-electrolyte solutions can lead to the formation of a gel (which forms a solution on warming to room temperature).

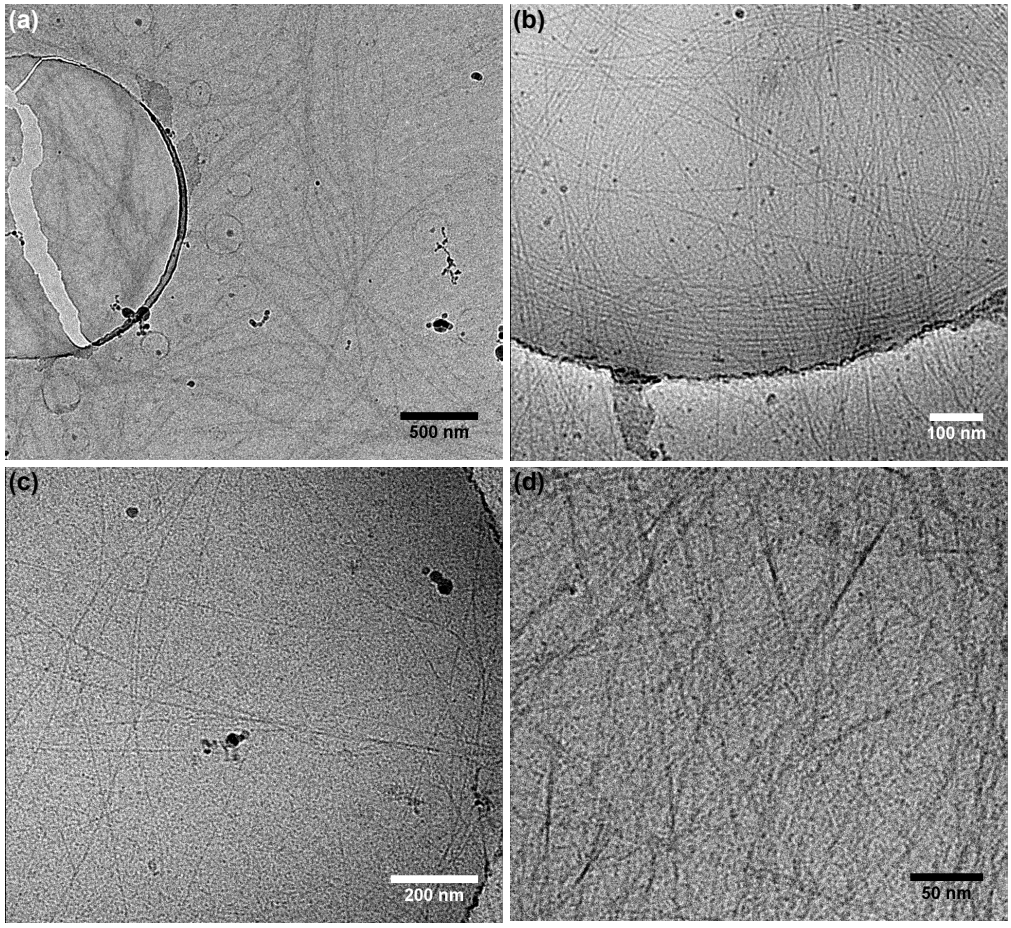

Figure 4.24 Cryo-TEM micrographs of calix[4]arene **127a** (~20 mM) in the presence of (a) LiCl (20 mM), (b) NaBr (10 mM), (c) $CaCl_2$ (21 mM), and (d) $La(NO_3)_3$ (5 mM). All samples were blotted for 5 s (except **127a**-LiCl sample, 30 s) at 5 °C. Dark round structures are crystalline ice.

4.3.1.4 **Circular dichroism spectroscopy**

Self-assembled chiral nanostructures tend to have much more intense absorptions in CD spectroscopy (refer to section 1.3.3.2 for a brief overview of CD spectroscopy) compared to that of the chiral monomer.[76] This is a good method for detecting chirality in the solid-like structures of gels, even if the gel fibres do not reveal any helices or coils by microscopy methods. Preliminary experiments with gelator **127a** in the presence of $La(NO_3)_3$ and NaBr showed that the features of interest coincided with the background UV-absorption of these anions (especially from the nitrate anion absorbing at less than 240 nm[77, 78]). Unfortunately this prevented extraction of any information regarding the chirality of the self-assembled structures. Zhang et al.[13]

showed that there was a change in the ellipticity for **127** above its c.a.c. at pH 3, suggesting that **127** could self-assemble into chiral structures.

4.3.2 Characterisation of behaviour in solution and gel phase

4.3.2.1 UV-visible spectroscopy

The self-assembly of proline calixarene **127a** was investigated by measuring the critical aggregation concentration using a probe molecule and by UV-visible spectroscopy (refer to section 2.4.1). A relatively 'weak' gel-inducing electrolyte, $MgCl_2$, was selected for further investigation with **127a** and with rhodamine 6G as the 'probe' molecule. The results (Figure 4.25) suggested a c.a.c. value close to where the solution appeared viscous on the bulk scale. The c.a.c. values obtained for **127a**-$MgCl_2$ system were greater than that for **127a** in the absence of $MgCl_2$ (c.a.c. = 5 mM). This suggests that the shift in the maxima of the wavelength of rhodamine 6G may be due to interactions with self-assembled structures formed by **127a**-$MgCl_2$. Care is required in interpreting these results since small molecules can interfere with the self-assembly of **127a** (see section 2.4.3). However, rhodamine 6G did not prevent the formation of a gel by **127a**-$MgCl_2$.

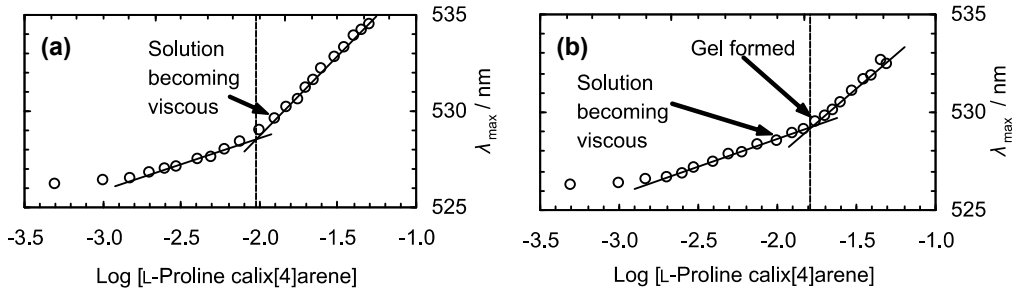

Figure 4.25 Critical aggregation concentration of L-Pro calix[4]arene determined with a rhodamine 6G probe/UV-visisble spectroscopy method. The c.a.c. values were determined in the presence of $MgCl_2$ at (a) 25 mM (c.a.c. = 9 mM) and (b) 50 mM (c.a.c. = 16 mM).

4.3.2.2 Zeta-potential by dynamic light scattering

The charge distribution on the surface of particles can be determined by measuring their zeta-potential.[79] This zeta-potential would have indicated if the electrolyte was localised along the surface of the calixarene aggregates. An attempt was made to measure the zeta-potential of **127a** alone, however the concentration range of interest was below the sensitivity of the instrument. A similar attempt was made to measure

the zeta-potential of the **127a** in the presence of LiCl, this resulted in a redox reaction at the copper contacts of the zeta-potential cell. Zeta-potential measurements for **127a** were not pursued any further.

4.3.2.3 **Nuclear magnetic resonance spectroscopy**

Nuclear magnetic resonance spectroscopy (NMR) was used to study self-assembly of proline calix[4]arene **127** in the presence of an electrolyte. The addition of small aliquots of $La(NO_3)_3$ to a solution of **127a** (20 mg mL^{-1} in D_2O) led to a broadening of signals in the ^1H NMR spectra (Figure 4.26). On the addition of 0.15 equiv. of $La(NO_3)_3$ to the solution of **127a**, the sample appeared more viscous in the NMR tube and small air bubbles trapped near the top of the sample[27]—an indication of a gel. Amanokura et al.[80] attributed broadening of ^1H NMR signals of an organogelator to changes in the molecular motion in different environments. The authors found that the relatively sharp ^1H NMR signal of a phenol broadened when the sample cooled below the $T_{gel\text{-}sol}$.

Analysis of the integrals of calix[4]arene **127a**–$La(NO_3)_3$ titration NMR spectra showed that as more $La(NO_3)_3$ was added, the intensity of the signals attributed to the calixarene were reduced compared with the HOD signal (Figure 4.29a). The signals were normalised against the HOD signal and the number of protons in the integral region. Aggregation of the calixarenes will result in a larger structure and consequently reduced spin-spin relaxation times (T_2). The reduced T_2 of the larger aggregates were presumably less than the delay time of ~10 μs (the delay time for the zg pulse sequence used). Therefore, the larger structures were not detected during the experiments (since bulk magnetisation was lost). Reduction in T_2 for some compounds leads to the broadening of signals in the NMR spectrum.[81] From the analysis, the intensities reduced rapidly after 0.13 equiv. of $La(NO_3)_3$ was added to the calixarene solution. Furthermore, the intensity of the aromatic signal at ~7.25 ppm decays at the same rate as the other signals 4.5–1.5 ppm (Ar-CH_2-Ar, Ar-CH_2-Pro, and proline moiety), suggesting that the entire calixarene molecule was effectively part of the aggregated structure.

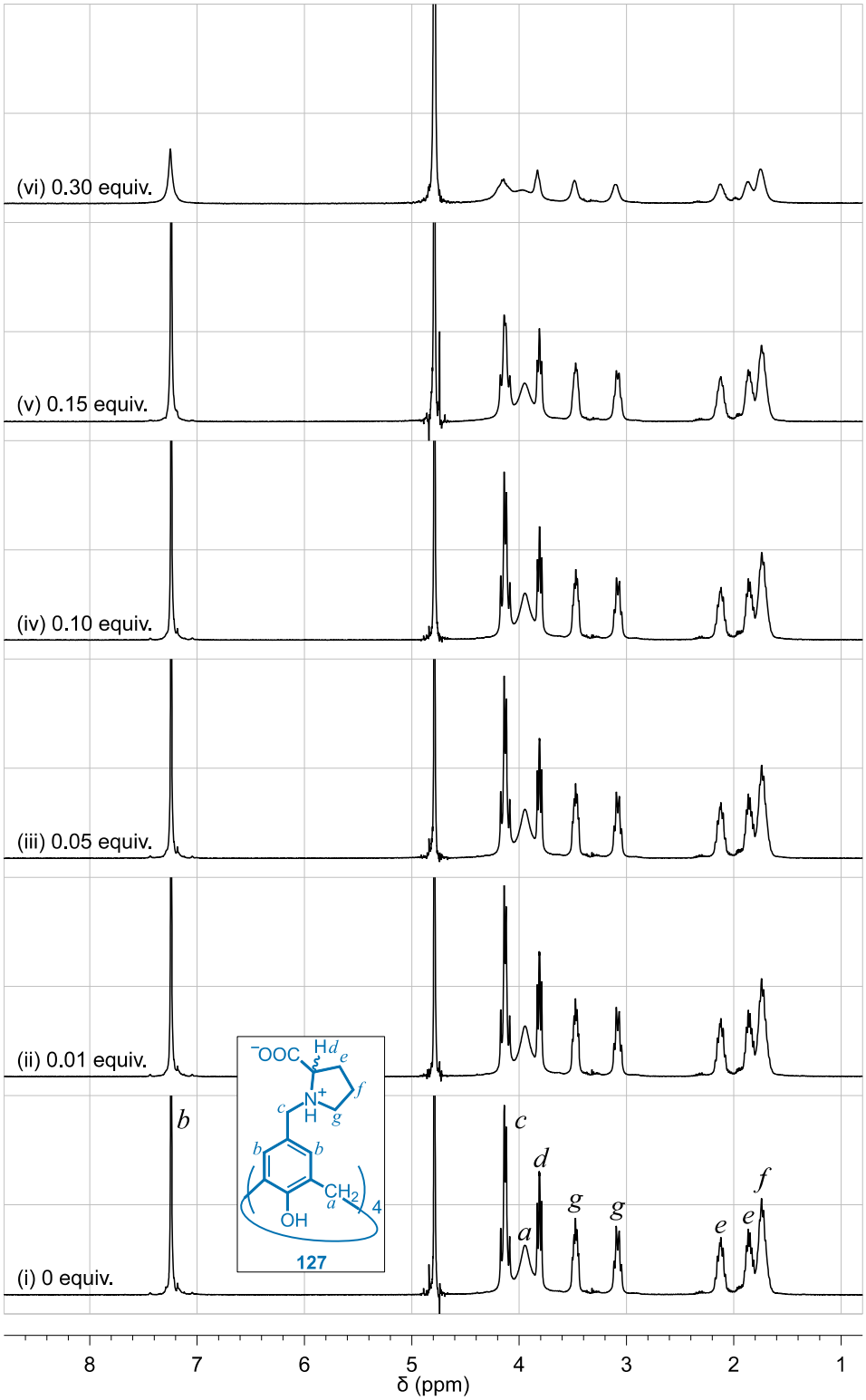

Figure 4.26 Titration of L-proline calix[4]arene (20 mg mL^{-1} in D_2O) against $La(NO_3)_3$. An initial solution of (i) **127a** (20 mg mL^{-1}) in the presence of $La(NO_3)_3$ from (ii) 0.01 equiv. to (vi) 0.30 equiv. ^1H NMR spectra were acquired at 400 MHz.

Variable temperature NMR experiments of **127a** (20 mg mL^{-1}) and $La(NO_3)_3$ at 0.15 equiv., indicated that the majority of aggregated structures had disassembled at approximately 50 °C (Figure 4.27). The signals in the ^1H NMR spectrum sharpened on heating and broadened on cooling. The integrals of these spectra (Figure 4.29b) showed hysteresis—the rate in reduction in the intensities on cooling of the sample was slower compared with the increase in intensity on the heating cycle. This 'lag' suggests that the aggregation of the calixarene molecules in solution is under kinetic control.

The variable temperature experiments were repeated after a further 0.15 equiv. of $La(NO_3)_3$ was added to the gel sample in the NMR tube (taking the total $La(NO_3)_3$ content to 0.3 equiv.). Here, the NMR sample was briefly heated to 60 °C to convert the gel to a liquid and the aliquot of $La(NO_3)_3$ added, homogenised, and allowed to stand overnight. The VT-NMR experiments (Figure 4.28) showed similar results as before. The maximum temperature for the signals to sharpen (and aggregates to disassemble) was now 70 °C. Increasing the $La(NO_3)_3$ content appears to have a stabilising effect on the aggregates. Similar to previous VT experiments at 0.15 equiv. $La(NO_3)_3$, there was a lag in the decrease in the intensity of the signals on the cooling cycle (Figure 4.29c).

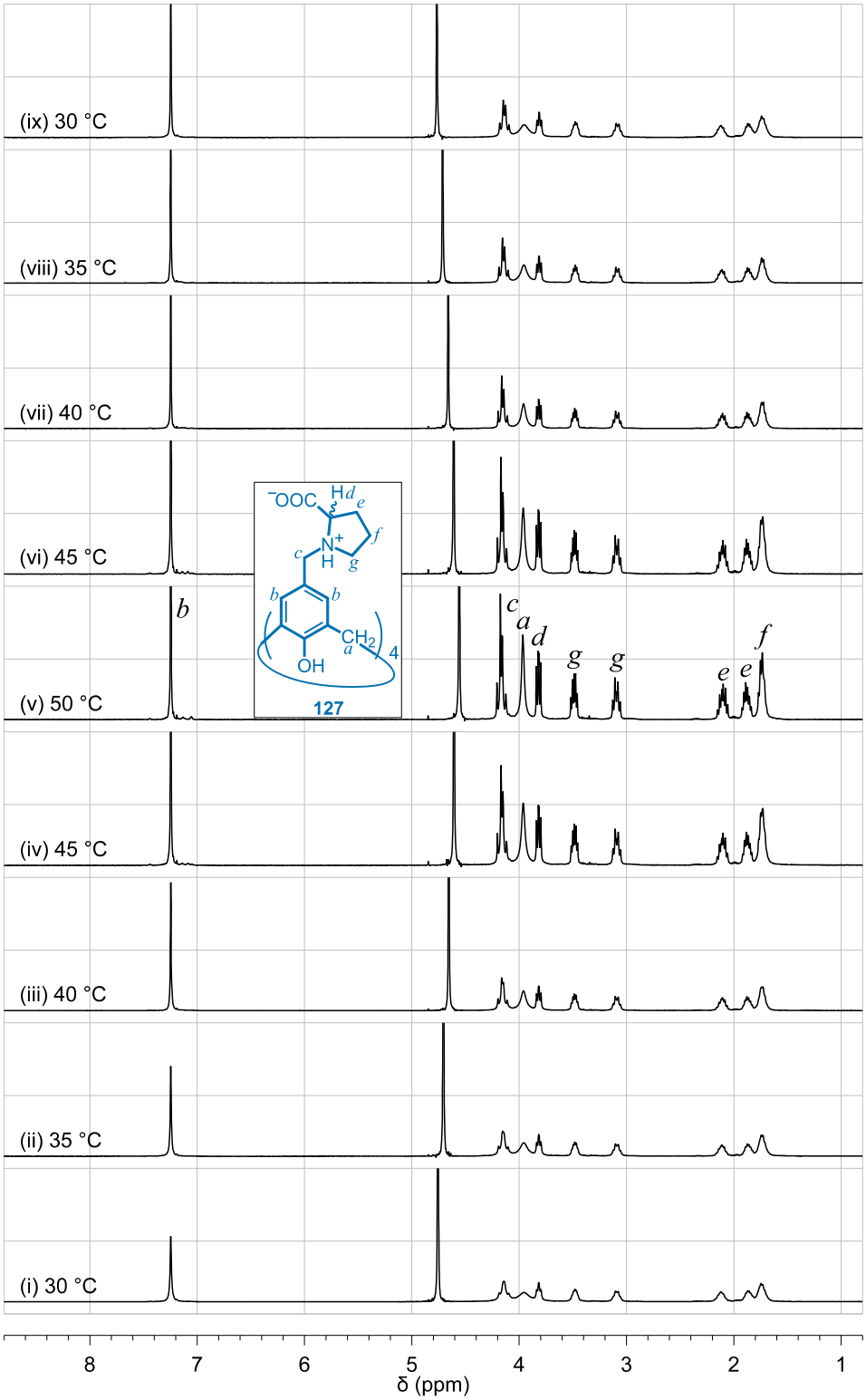

Figure 4.27 VT ^{1}H NMR (400 MHz) experiments for a gel composed of L-proline calix[4]arene (20 mg mL^{-1}) and $La(NO_3)_3$ (0.15 equiv.) in D_2O. ^{1}H NMR signals for **127a** sharpened on heating, (i) to (v), and the same features broaden on cooling, (vi) to (ix).

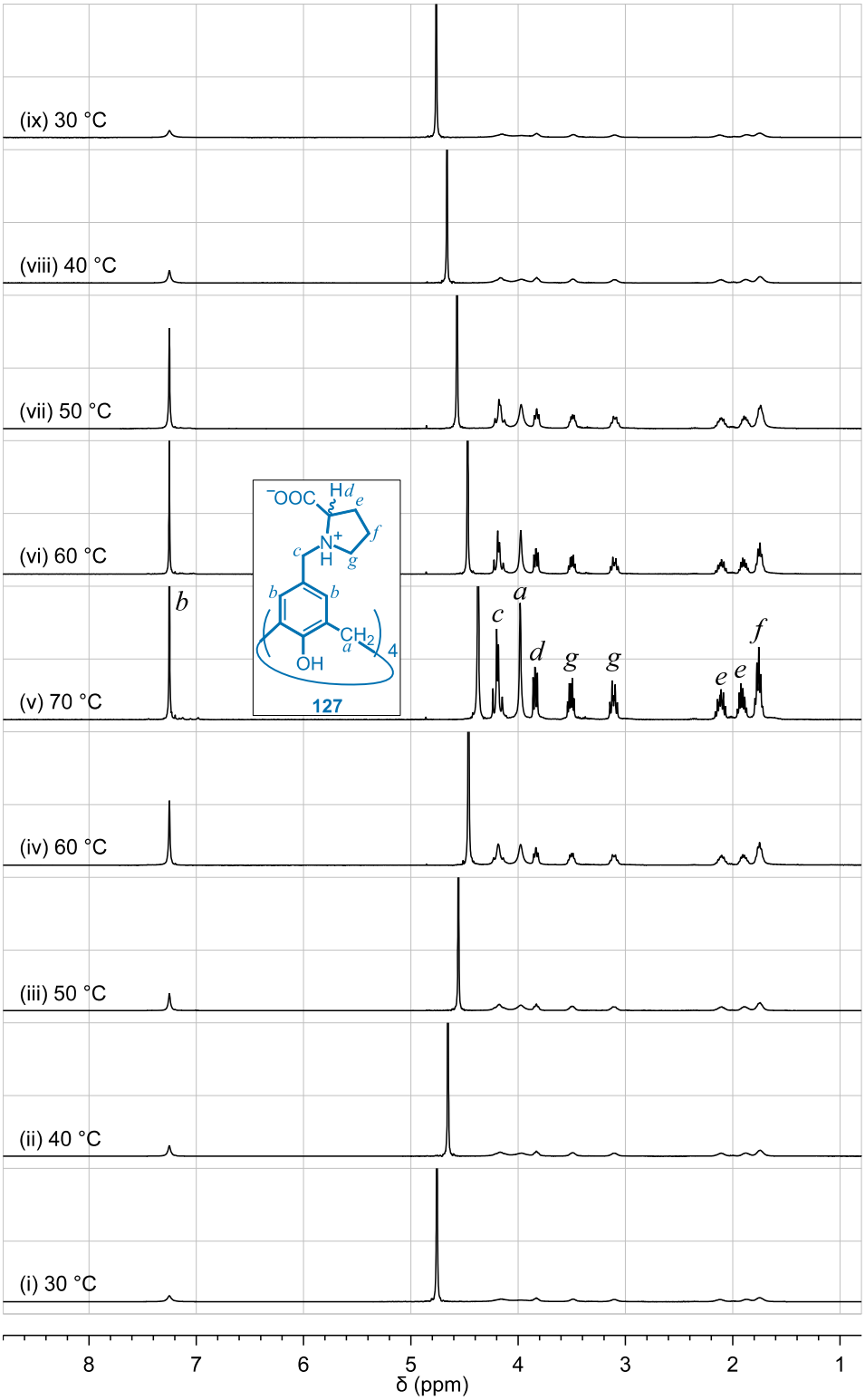

Figure 4.28 VT ^{1}H NMR (400 MHz) experiments for a gel composed of L-proline calix[4]arene (20 mg mL^{-1}) and $La(NO_3)_3$ (0.30 equiv.) in D_2O. The gel was heated, (i) to (v), and cooled, (vi) to (ix).

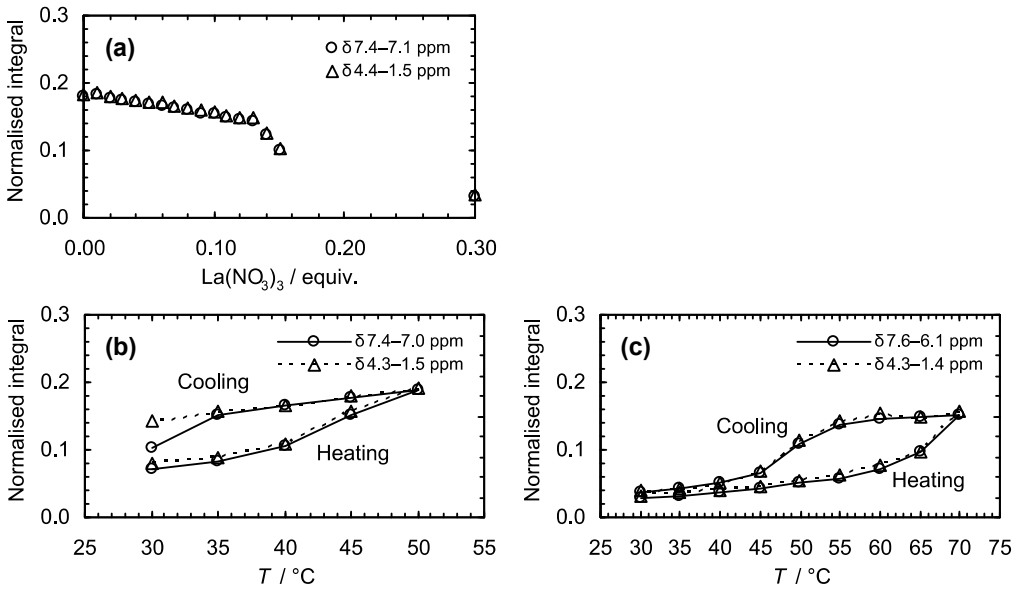

Figure 4.29 Analysis of normalised integrals from ^{1}H NMR for proline calix[4]arene **127a**–$La(NO_3)_3$ system. (a) **127a** (20 mg mL^{-1} in D_2O) titrated against $La(NO_3)_3$; (b) variable-temperature experiments for **127a** (20 mg mL^{-1} in D_2O) and $La(NO_3)_3$ at 0.15 equiv.; and (c) variable-temperature experiments for **127a** (20 mg mL^{-1} in D_2O) and $La(NO_3)_3$ at 0.30 equiv.

Previous investigations have shown that small molecules can induce the aggregation of calix[4]arene **127a** (refer to section 2.4.3). The ability of small organic molecules to interfere with the gel formation of **127a** was investigated using the same **127a**-THF sample from section 2.4.3. A 0.30 equiv. aliquot of $La(NO_3)_3$ was added to the sample of calixarene **127a** (20 mg mL^{-1}) and THF (0.50 equiv.). The sample formed a hydrogel. VT-NMR experiments of this gel (Figure 4.30) showed broad signals consistent with the **127a**-THF system (Figure 2.14) at 30 °C (the peaks were much broader as a result of the presence of $La(NO_3)_3$). The calixarene signals sharpened at 60 °C on heating compared with 70 °C in the absence of THF (Figure 4.28). Like the **127a**-$La(NO_3)_3$ system, the normalised integrals showed that the **127a**-THF-$La(NO_3)_3$ system exhibited hysteresis. This indicated that THF could compete with $La(NO_3)_3$ for calixarene **127a** and the system existed in an equilibrium of THF-induced aggregates and gel fibres.

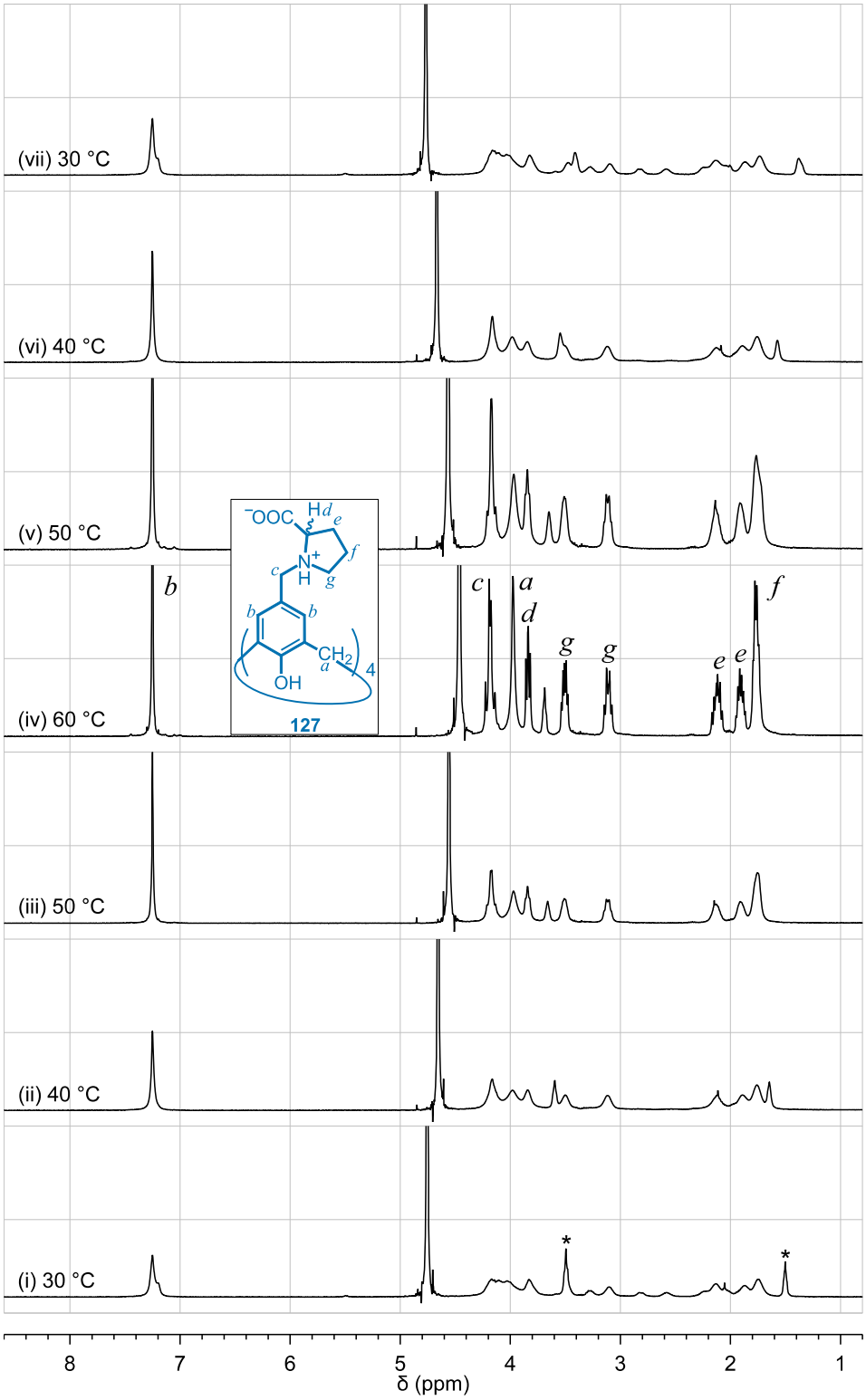

Figure 4.30 VT ^{1}H NMR (400 MHz) experiments for a gel composed of calix[4]arene **127a** (20 mg mL^{-1}), tetrahydrofuran (0.50 equiv.) (*), and $La(NO_3)_3$ (0.30 equiv.) in D_2O. The gel was heated, (i) to (iv), and cooled, (v) to (vii).

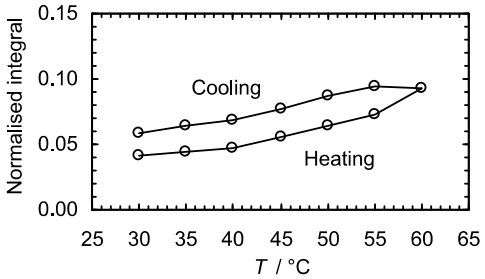

Figure 4.31 Analysis of normalised integrals from VT-NMR experiments for a gel composed of calix[4]arene **127a** (20 mg mL^{-1}), tetrahydrofuran (0.50 equiv.), and $La(NO_3)_3$ (0.30 equiv.) in D_2O.

Nitric acid was a useful electrolyte to investigate the effect of the nitrate anion. NMR titration experiments (Figure 4.32) showed little change with the addition of HNO_3 (as a solution prepared from HNO_3 70 wt/wt% in D_2O). The Ar–*H* signal exhibited little broadening unlike the Ar–CH_2–Pro (δ 4.1 ppm) and proline moieties (2.2–1.6 ppm). Analysis of the normalised integrals (Figure 4.33) showed that the intensities of the signals had decreased as HNO_3 was added. Like the bulk gel experiments, the **127a**-HNO_3 system was expected to gel *then* crystallise. However, thin plates were observed at the bottom of the NMR tube and a gel phase was not observed during the course of this experiment. Despite the sample crystallising from solution, there was sufficient sample dissolved in solution for subsequent ^{1}H NMR experiments. The addition of each aliquot of HNO_3 and agitation of the sample in the NMR tube, could have favoured crystallisation over gelation (i.e. the expected gel phase was not observed).

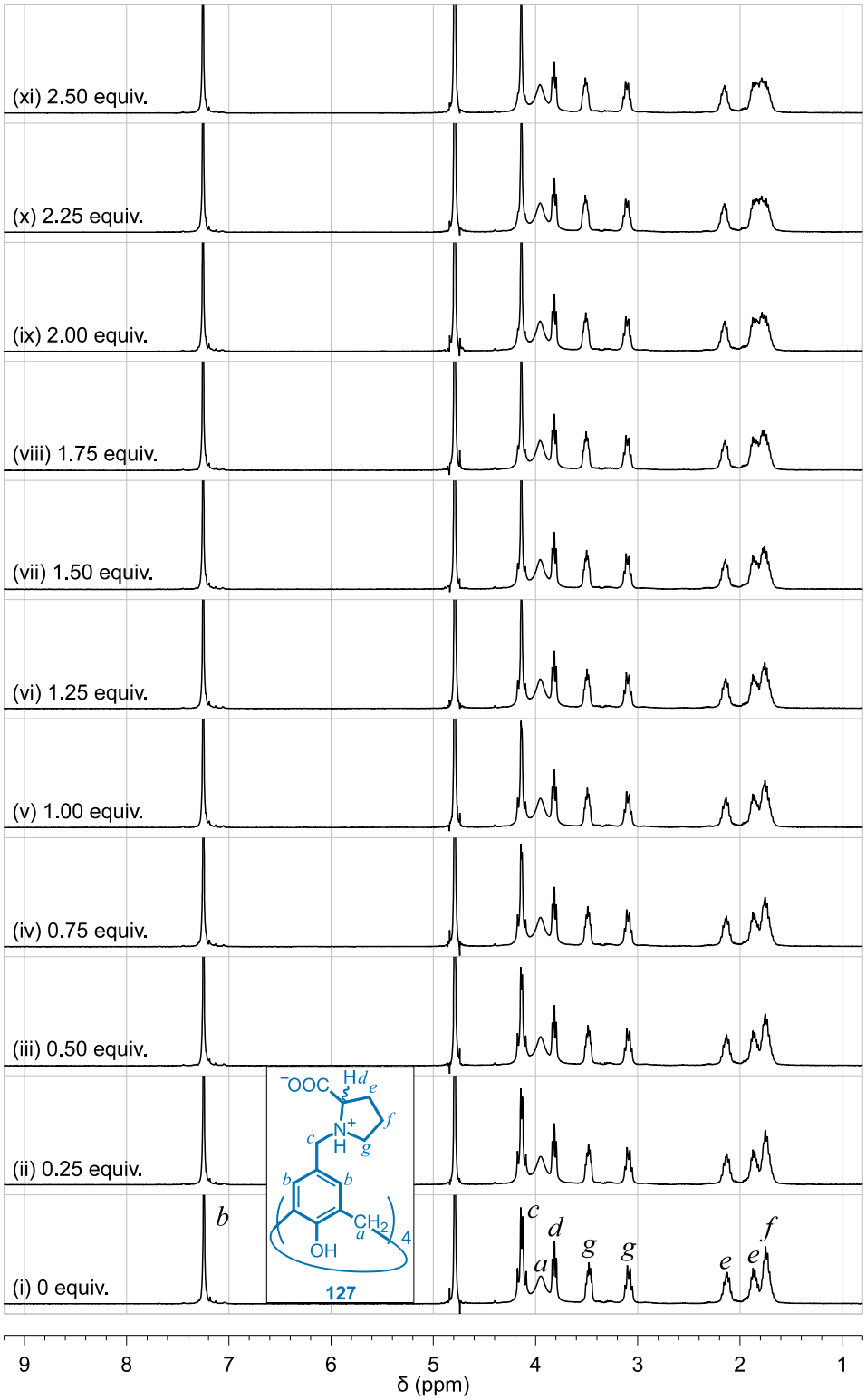

Figure 4.32 Titration of L-proline calix[4]arene (20 mg mL^{-1} in D_2O) against HNO_3. An initial solution of (i) **127a** (20 mg mL^{-1}) in the presence of HNO_3 from (ii) 0.025 equiv. to (xi) 0.250 equiv. ^1H NMR spectra were acquired at 400 MHz.

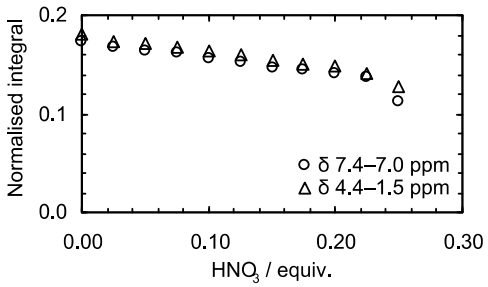

Figure 4.33 Analysis of normalised integrals from ^{1}H NMR for proline calix[4]arene **127a**-HNO_3 system. **127a** (20 mg mL^{-1} in D_2O) titrated against HNO_3.

4.4 Racemate gels

The racemate hydrogels, comprising mixtures of L-proline calix[4]arene (**127a**) and D-proline calix[4]arene (**127b**), were observed to form hydrogels, albeit less stable one than the pure enantiomers. The gel-sol transition temperature for racemate proline calix[4]arene hydrogels is reduced by up to ~10 °C for a 1:1 mixture of the each enantiomer. $T_{gel\text{-}sol}$ and general stability for the racemate gel (Figure 4.34) is dependent on the ratio of L-proline calix[4]arene to D-proline calix[4]arene. The maximum $T_{gel\text{-}sol}$ was obtained with enantiopure compounds while the minimum $T_{gel\text{-}sol}$ was obtained with the racemate.[20, 82]

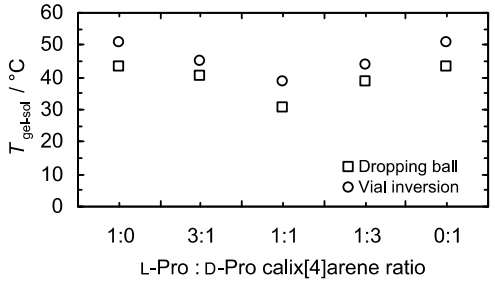

Figure 4.34 $T_{gel\text{–}sol}$ determined for racemate proline calix[4]arene hydrogels. Proline calix[4]arene (10 mM) and $La(NO_3)_3$ (20 mM).

Initially, all the proline calix[4]arene hydrogels had a transparent appearance (Figure 4.35), however they became slightly cloudy on standing. The racemate hydrogel readily collapsed and transitioned from the gel phase to the solid phase (precipitating as a white solid). Examination of the gels under AFM (Figure 4.36) revealed that the racemate hydrogels had a different fibre morphology compared with

the hydrogels of a single enantiomer. The racemate hydrogels were composed of shorter fibres. The reduced stability and changes in gel fibre morphology of racemic mixtures of gelators compared with the pure enantiomers is consistent with results reported for many racemate gels.[82–85] However, some racemic mixtures of chiral gelators are known to form stronger gels compared with their enantiomers[86] or self-sort into their enantiomers.[87, 88] In some cases, racemic mixtures did not form gels whereas the enantiopure compounds were gelators.[89] Brizard et al.[75] noted that the tendency of racemic mixtures of gelators to crystallise was likely a result of the greater number ways of packing the racemic mixture of molecules in a crystal. An x-ray single crystal structure was obtained for a viable crystal formed from a **127a**,**b**-$La(NO_3)_3$ hydrogel with equimolar portions of each enantiomer (refer to the next section for more information).

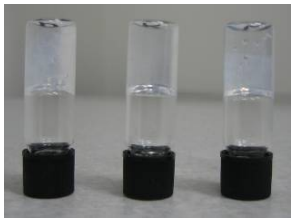

Figure 4.35 Images of hydrogels prepared from proline calixarenes **127a**,**b** (20 mM) in the presence of $La(NO_3)_3$ (20 mM). (Left) D-proline calix[4]arene, (centre) racemate, L-Pro:D-Pro calix[4]arene ratio = 1:1, (right) L-proline calix[4]arene.

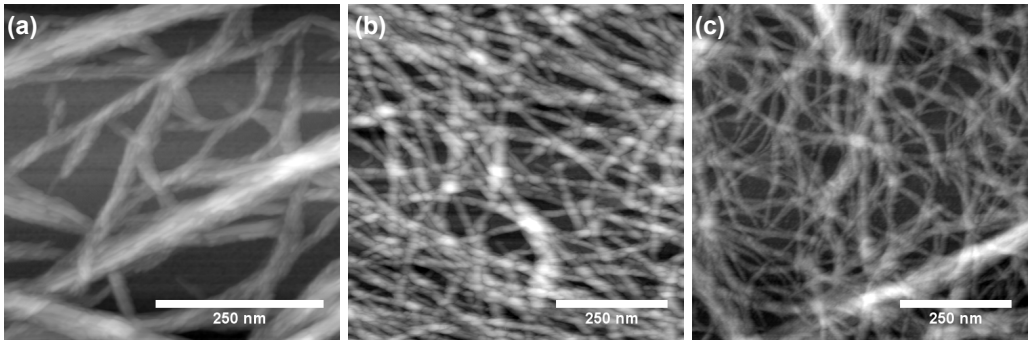

Figure 4.36 AFM micrographs of (a) L-proline calix[4]arene (20 mM), (b) 1:1 mixture of D-/L-proline calix[4]arene (20 mM), (c) D-proline calix[4]arene (20 mM) in the presence of $La(NO_3)_3$ (25 mM).

4.5 Analogous compounds

Attempts were also made to develop other anion-responsive gelators based on proline calix[4]arene gelators, **127**. The proline moiety was thought to be central to gel formation, hence the proline calix[5]arene (**128**) was prepared. Preliminary gelation studies with crude **128** did not show signs of increased viscosity of the solution or gel formation at the macroscopic scale, thus further experiments were not pursued. Another target analogue was the sarcosine-functionalised calix[4]arene **132**. Preliminary experiments with **132** showed that an aqueous solution of **132** and selected electrolytes produced viscous solutions or clumps of gel-like material. However, it did produce a reasonably stable opaque gel with $Cu(NO_3)_2$. Since calix[4]arene **132** did not appear to be a better gelator than **127** and had issues with its synthesis, compound **132** was not further pursued in this study.

4.6 From the gel phase to the solid state

It is often difficult to obtain crystals of a gelator from a gel phase that are of sufficient quality for single crystal x-ray crystallography.[90, 91] Many crystals formed within a variety of **127a**-electrolyte hydrogels were not viable for x-ray crystallography (mainly because they were poor quality crystals or were very thin plates). Despite this, two crystal structures were obtained from crystals grown from hydrogels; **127a**-$MgCl_2$ and racemate **127a**,**b**-$La(NO_3)_3$. In addition, a crystal structure of the gelator **127a** was obtained by diffusion of tetrahydrofuran into an aqueous solution of **127a**. This particular calixarene had a long history of forming crystals that did not diffract well enough to resolve the crystal structure (McIldowie, M. J. Curtin University, Perth, Australia. Personal communication, 2008).

The crystal structure of L-proline calix[4]arene•THF **127a** (Figure 4.37) shows the carboxylate groups of the proline moieties oriented away from the calixarene cavity. Here, the calix[4]arene adopted a cone conformation. In contrast, Zheng et al.[13] reported a pinched cone structure for **127a** with the carboxylates of two distal proline moieties pointed away from the cavity (at low pH and in the presence of hydrochloric acid). A disordered THF molecule is situated over the cavity, however

O···N distances between THF and proline (>4 Å) suggests that the THF is a solvent of crystallisation and is not included within the calixarene cavity. An interesting cubic structure was observed in the extended crystal structure (Figure 4.38). Here, an oxygen atom from the carboxylate could hydrogen bond to an ammonium group on a proline moiety on an adjacent calixarene molecule (N41···O42, 2.896 Å). The distances between the centroid of the aromatic rings of adjacent calixarene molecules (>4 Å) did not support the presence of π···π stacking.

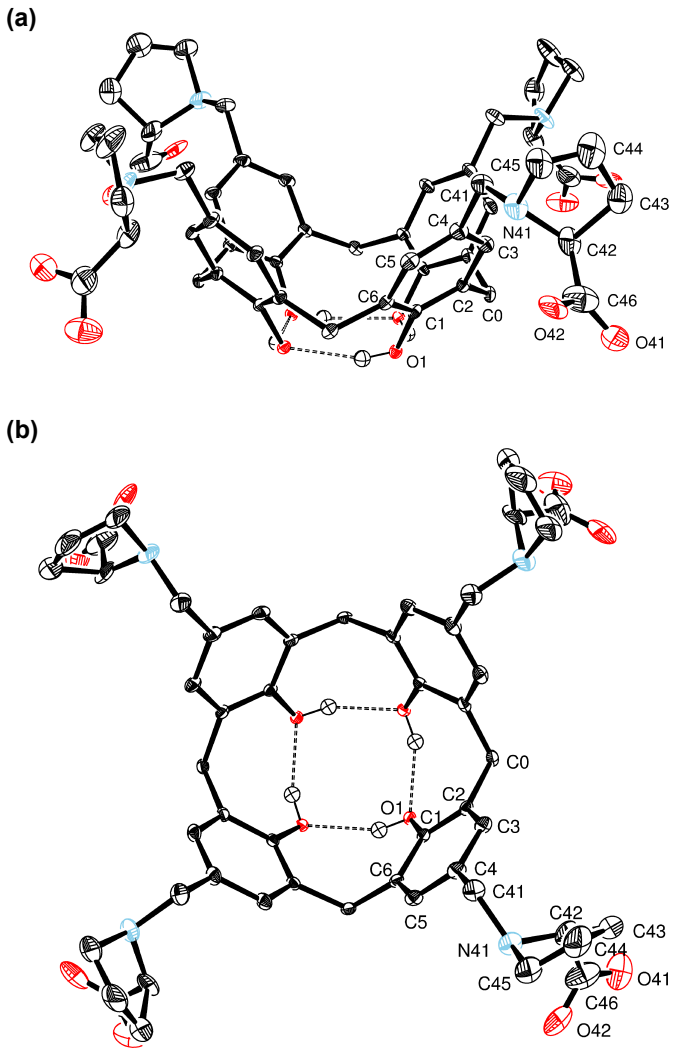

Figure 4.37 Crystal structure obtained from diffusion of tetrahydrofuran into an aqueous solution of **127**, viewed from (a) the side and (b) top of the calixarene. A tetrahydrofuran molecule sits above the cavity of the calixarene (omitted from these figures) though is not included within the cavity. Potential hydrogen bonds are depicted between the phenols. Ellipsoid probability at 25%.

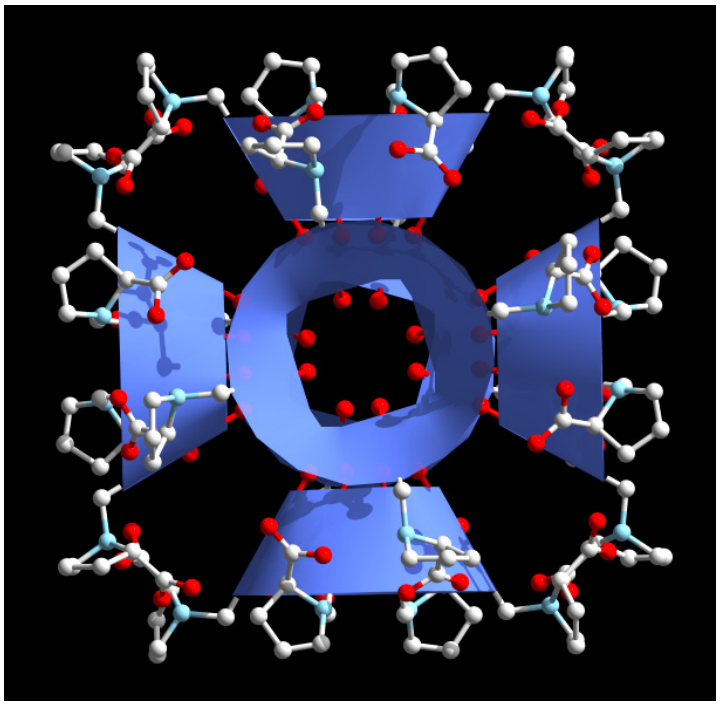

Figure 4.38 Crystal packing of **127a** shows six calixarene molecules arranged in a cube with hydrogen bonding between the carboxylate and ammonium groups of the proline moieties on adjacent calixarenes. Here the blue ribbon represents the calixarene structure and protons have been omitted for clarity.

The crystal structure of **127a**-$MgCl_2$ contrasted with the previous crystal structure of **127a**. In this case, the carboxylates of all four proline moieties were coordinated to Mg^{2+} (Figure 4.39) with four equivalent Mg1···O141 distances (2.039 Å). The radius of an Mg^{2+} cation (0.860 Å for coordination number 6)[92] is small enough for this divalent cation to fit over the cavity of the calixarene. Like the previous **127a** crystal structure, there is likely to be intramolecular hydrogen bonding between adjacent proline moieties (N241···O242, 2.764 Å). The packing structure showed that there may be π···π interactions between adjacent calixarenes (distances between the centroid of aromatic rings, C1–C6, of 3.639 Å).

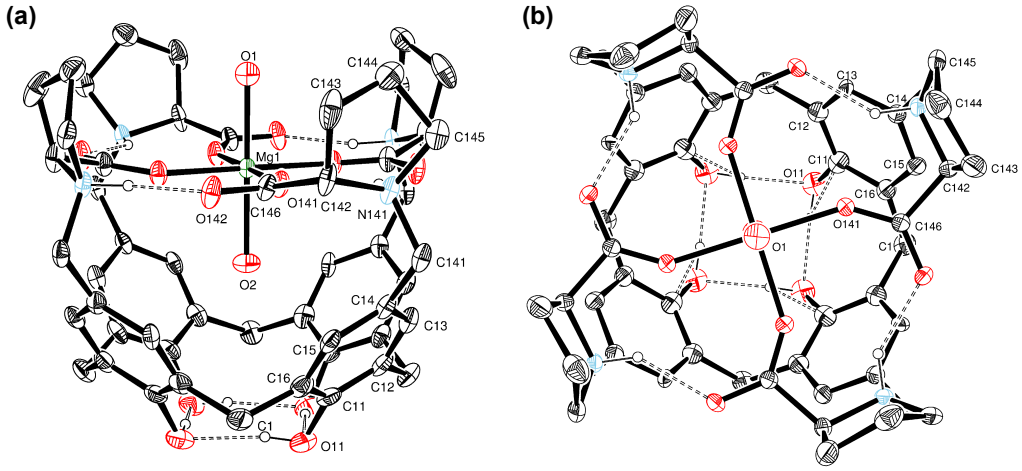

Figure 4.39 Single X-ray crystal structure obtained *from* a **127a**-$MgCl_2$ hydrogel gave a crystal, viewed from the (a) side and (b) top of the calixarene. Ellipsoid probability at 25%.

The other crystal structure was obtained from the racemate **127a**,**b**-$La(NO_3)_3$ hydrogel. Racemates tended to crystallise more readily compared with the pure enantiomer and contributes to the reduced thermostability of the hydrogels (refer to section 4.4). The two main features of this crystal structure (Figure 4.40) are that a lanthanum cation bridges two calixarene units by coordination to the proline carboxylates (Figure 4.40a) and the intermolecular inclusion of the proline into a calixarene cavity (Figure 4.40b). The size of the La^{3+} cation (with a radius of 1.045 Å for coordination number 6)[29] may prevent it from coordinating to proline moieties over the calixarene cavity like Mg^{2+} in the **127a**-$MgCl_2$ structure. The La atoms is disordered over two sites in the crystal structure and each La atom appears to be coordinated to proline moieties of two different calixarene molecules (Figure 4.40a). The remaining proline units (not coordinated to La) show inclusion into a neighbouring calixarene cavity (Figure 4.40b). The bond distances (Figure 4.40c) supported the possibility of hydrogen bonds between the carboxylate of the proline and the electron deficient methylene of Ar–CH_2–Pro and C–H···π interactions between hydrophobic ring of proline and the aromatic rings of the calixarene.

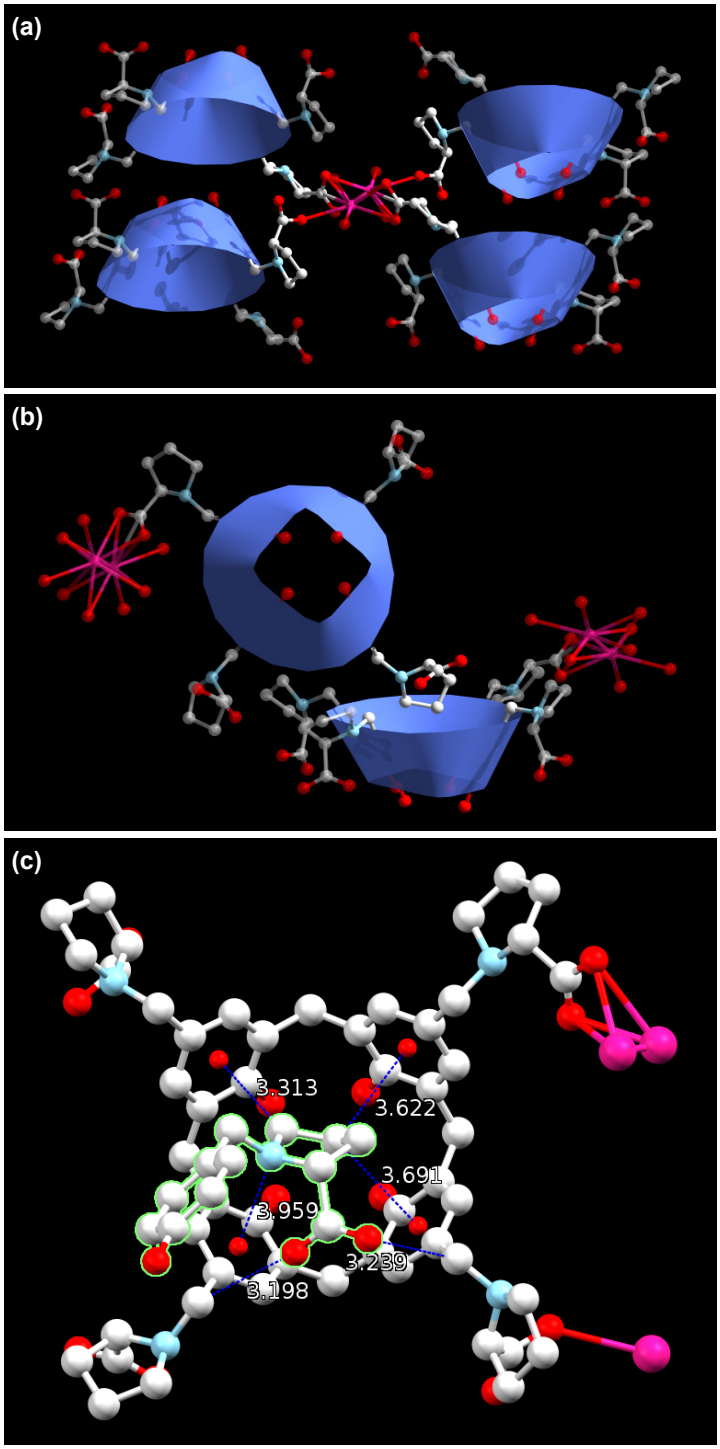

Figure 4.40 Single crystal X-ray crystal structure obtained *from* a **127a**,**b**-$La(NO_3)_3$ hydrogel. (a) Two lanthanum atoms dislocated over two sites coordinated to four calix[4]arene units, with **127a** (L-proline) on the left and **127b** (D-proline) on the right. (b) The proline moieties not coordinated to lanthanum appear to be self-included within another calixarene molecule with the same stereochemistry (c) Distances for points of interest in the crystal structure (between the centroid of the aromatic ring, smaller red sphere, and the nearest carbon of included-proline). Here the protons have been omitted for clarity.

What was remarkable about the **127a**,**b**-$La(NO_3)_3$ crystal structure was that the self-inclusion appeared to be self-sorting into the two stereoisomers. An L-proline moiety includes into another calixarene cavity where the calixarene is functionalised with L-proline and likewise with calixarenes functionalised with the D-proline moiety. The crystal packing structure (Figure 4.41) showed the two stereoisomers self-sorted into two helical strands and the two strands are bridged by two La^{3+} ions. Self-sorting of chiral supramolecular systems from racemates into aggregates of each enantiomer is known.[20, 93] This arrangement of calixarenes could provide some insight into how the calix[4]arene molecules self-assemble into fibrous structures to form a hydrogel (discussed in section 4.7).

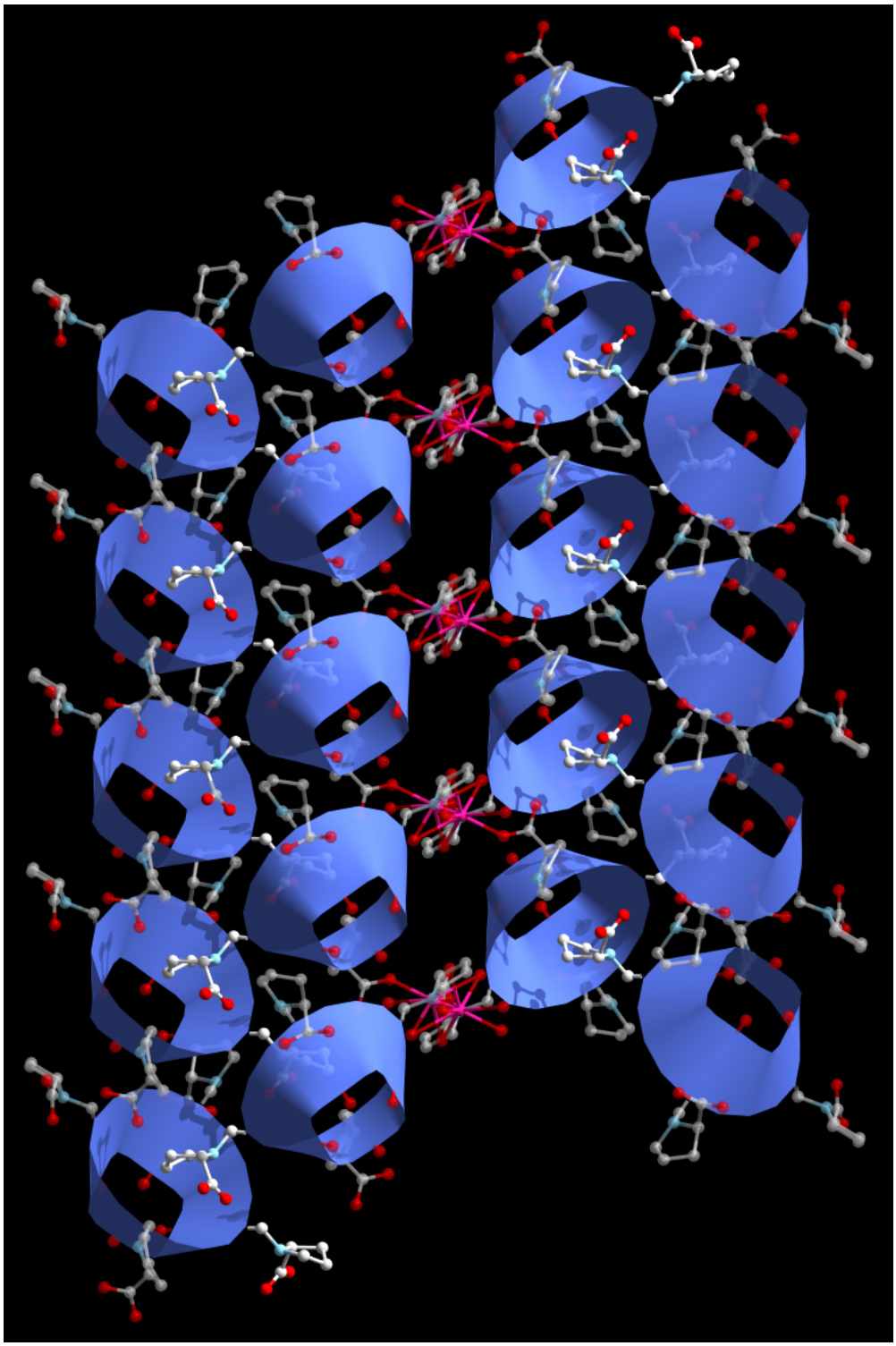

Figure 4.41 Crystal packing of **127a**,**b**-La$(NO_3)_3$ showing self-sorted calixarenes helices (with L-proline on the left helix and D-proline on the right helix) bridged by the lanthanum ions. Here the blue ribbon represents the calixarene structure and protons have been omitted for clarity.

4.7 Proposed mechanism of gelation

The theories for the formation of fibrils from molecules and formation of the gel-phase from the solution phase are described in detail elsewhere.[94–96] This section will be concerned with how the calixarene units can possibly be assembled into fibrils and eventually the fibrous structures observed in the presence of electrolytes.

A possible arrangement of proline calix[4]arene **127** into self-assembled fibres in the presence of an electrolyte can be carefully extrapolated from the crystal structure of **127a**,**b**-$La(NO_3)_3$ (Figure 4.41). Assuming the calix[4]arene adopts a cone conformation, it is possible for the proline moieties from one calixarene molecule to include within the cavity of another calixarene molecule. Hydrogen bonds between the carboxylate of the proline and the electron deficient methylene of $Ar–CH_2–Pro$[97] and C–H···π interactions between hydrophobic ring of proline and the aromatic rings of the calixarene (Figure 4.40) could aid the self-inclusion process (especially in an aqueous solution). The resulting fibrils could then be bundled into fibres mediated by carboxylate-cation binding of the fibrils. Although the anions have not been explicitly observed during this investigation (including x-ray crystal structures), the anions must be involved in the self-assembled structures as the nature of the anion dictates if a gel will form and exerts influence over the hydrogel fibre morphology. The amine/ammonium centre of the proline is also of importance as this would explain the pH-responsive ability (i.e. gel-sol transition at high pH) of proline calixarene **127**. Further work is required to elucidate the role of the anion and proline calix[4]arene **127** in the formation of gel fibres.

4.8 Conclusions

A specific ion effect has been observed for the formation of hydrogels by proline calix[4]arene **127**. Further investigation has shown that the ability to form a hydrogel and the thermostability of the hydrogels formed correlated with the Hofmeister series for anions. Hydrogels were formed by **127** in the presence of chaotropic anions including chloride, however the most stable hydrogels were those formed with nitrate and bromide anions (both of which are chaotropes).

Characterisation of the hydrogels by AFM showed that calix[4]arene **127** self-assembled into fibres and that the morphology was dependent on the electrolyte. In addition, cryo-TEM showed that a solution of **127**, in the presence of selected anions below the minimum gelation concentration, self-assembled into fibres. The **127**-electrolyte hydrogels were largely thermoreversible and pH-responsive. Investigations into the self-assembly behaviour of **127** in the presence of lanthanum nitrate revealed that the self-assembly process was most likely under kinetic control.

A racemate of L-proline calix[4]arene (**127a**) and D-proline calix[4]arene (**127b**) produced a hydrogel of lower stability than the pure enantiomers. A 1:1 ratio of each enantiomer produced the least stable hydrogel, leading to the crystallisation of the gel. Remarkably, the x-ray crystal structure of **127a**,**b**-$La(NO_3)_3$, crystallised from the hydrogel, revealed self-sorting of the enantiomers: each enantiomer self-assembled into helical strands with lanthanum atoms bridging the strands. A preliminary mechanism for the formation of the hydrogel was presented based on this crystal structure, however further investigation is required to elucidate a more complete mechanism.

4.9 Experimental

4.9.1 General remarks

Reagents were used as purchased from the manufacturer or supplier. Experimental details for the synthesis of L-proline calix[4]arene (**127a**) and D-proline calix[4]arene (**127b**) are described in Chapter 2.

4.9.2 Gelation in the presence of electrolytes

The gelation ability of calix[4]arene **127a** in the presence of select electrolytes was investigated by the tube inversion method.[98] In a typical experiment, an aqueous solution of the electrolyte (stock solution, 0.1 M) was added to an equal volume of an aqueous solution of **127a** (stock solution, 0.04 M). Samples were prepared in a glass vial (2 mL, outer diameter = 0.5 cm).

4.9.3 Gel-sol transition studies

The gel-sol transition temperature ($T_{gel\text{-}sol}$) was determined by the dropping-ball method[26, 98] with each system determined in duplicate. Gels were prepared in a glass vial (7 mL, outer diameter 2 cm). A steel ball (110 mg, 3 mm diameter) was carefully placed on top of the gel to avoid disturbing the surface. The vials were then placed in a thermostated water bath (17 cm evaporating dish) heated on a Torrey Pines Scientific hot plate stirrer (model HS30-2) at 10 °C/hour from room temperature to a maximum of 85 °C.

4.9.4 Physical characterisation

Atomic force microscopy micrographs were obtained by Dr Thomas Becker. Thin films of hydrogels were placed onto freshly cleaved mica discs (Grade V-4, SPI Supplies, Pennsylvania, USA). The samples were imaged with Tapping Mode at room temperature using a Dimension 3100 Atomic Force Microscope (Bruker, Santa Barbara, USA) with standard silicon Tapping Mode cantilevers (type NSC-15, Mikromasch, Spain and type NCH, NanoWorld, Switzerland). The cantilevers were cleaned with an UV/ozone cleaner (BioForce Nanosciences, Iowa, USA) immediately prior to measurements. AFM data were processed using Gwyddion[99] version 2.26.

Cryo-transmission electron microscopy micrographs were obtained with the assistance of Dr. Matthias Floetenmyer, Centre for Microscopy and Microanalysis, University of Queensland. Samples were placed on to a copper grid, (coated with a carbon film) vitrified in liquid ethane using a Vitrobot Mark IV (FEI Company) and cryogenically transferred in liquid nitrogen to the cryo-TEM holder, which was then inserted into the microscope (FEI Tecnai G2). The temperature of the sample was maintained at approximately −175 °C to prevent crystallisation of ice. Data was processed using IMOD version 3.4.7.[100]

Variable temperature experiments were acquired on a Bruker Avance^{TM} III 400 NanoBay (^{1}H 400 MHz, ^{13}C 100 MHz) spectrometer.

Diffraction patterns of crystals of **127a**, **127a**-$MgCl_2$, and **127a**,**b**-$La(NO_3)_3$ were obtain and analysed by Dr Brian W. Skelton at the School of Biomedical, Biomolecular and Chemical Sciences, University of Western Australia, Australia.

UV-visible spectra were acquired on a GBC UV/VIS 916 spectrometer.

4.10 References

1 Aoki, M.; Nakashima, K.; Kawabata, H.; Tsutsui, S.; Shinkai, S. *J. Chem. Soc., Perkin Trans. 2* **1993**, (3), 347–354.

2 Kawabata, H.; Aoki, M.; Murata, K.; Shinkai, S. *Supramol. Chem.* **1993**, *2* (1), 33–39.

3 Xing, B.; Choi, M.-F.; Xu, B. *Chem. Commun.* **2002**, (4), 362–363.

4 de Loos, M.; Feringa, B. L.; van Esch, J. H. *Eur. J. Org. Chem.* **2005**, (17), 3615–3631.

5 Žinić, M.; Vögtle, F.; Fages, F. *Top. Curr. Chem.* **2005**, *256*, 39–76.

6 Cai, X.; Liu, K.; Yan, J.; Zhang, H.; Hou, X.; Liu, Z.; Fang, Y. *Soft Matter* **2012**, *8* (14), 3756–3761.

7 Zheng, Y.-S.; Ji, A.; Chen, X.-J.; Zhou, J.-L. *Chem. Commun.* **2007**, (32), 3398–3400.

8 Zhou, J.-L.; Chen, X.-J.; Zheng, Y.-S. *Chem. Commun.* **2007**, (48), 5200–5202.

9 Zheng, Y.-S.; Ran, S.-Y.; Hu, Y.-J.; Liu, X.-X. *Chem. Commun.* **2009**, (9), 1121–1123.

10 Vreekamp, R. H.; Verboom, W.; Reinhoudt, D. N. *Recl. Trav. Chim. Pays-Bas* **1996**, *115* (7–8), 363–370.

11 Dudic, M.; Colombo, A.; Sansone, F.; Casnati, A.; Donofrio, G.; Ungaro, R. *Tetrahedron* **2004**, *60* (50), 11613–11618.

12 Fujii, S.; Sanada, Y.; Nishimura, T.; Akiba, I.; Sakurai, K.; Yagi, N.; Mylonas, E. *Langmuir* **2012**, *28* (6), 3092–3101.

13 Zhang, J.; Guo, D.-S.; Wang, L.-H.; Wang, Z.; Liu, Y. *Soft Matter* **2011**, *7* (5), 1756–1762.

14 Haines, S. R.; Harrison, R. G. *Chem. Commun.* **2002**, (23), 2846–2847.

15 Kazakova, E. K.; Morozova, Y. E.; Prosvirkin, A. V.; Gubanov, E. F.; Timoshina, T. V.; Muslinkin, A. A.; Habicher, W. D.; Konovalov, A. I. *Colloid J.* **2004**, *66* (2), 153–159.

16 Verdejo, B.; Rodriguez-Llansola, F.; Escuder, B.; Miravet, J. F.; Ballester, P. *Chem. Commun.* **2011**, *47* (7), 2017–2019.

17 Lee, J. W.; Samal, S.; Selvapalam, N.; Kim, H.-J.; Kim, K. *Acc. Chem. Res.* **2003**, *36* (8), 621–630.

18 Freeman, W. A.; Mock, W. L.; Shih, N. Y. *J. Am. Chem. Soc.* **1981**, *103* (24), 7367–7368.

19 Hwang, I.; Jeon, Woo S.; Kim, H.-J.; Kim, D.; Kim, H.; Selvapalam, N.; Fujita, N.; Shinkai, S.; Kim, K. *Angew. Chem. Int. Ed.* **2007**, *46* (1–2), 210–213.

20 Smith, D. K. *Chem. Soc. Rev.* **2009**, *38* (3), 684–694.

21 Raynal, M.; Bouteiller, L. *Chem. Commun.* **2011**, *47* (29), 8271–8273.

22 Hirst, A. R.; Coates, I. A.; Boucheteau, T. R.; Miravet, J. F.; Escuder, B.; Castelletto, V.; Hamley, I. W.; Smith, D. K. *J. Am. Chem. Soc.* **2008**, *130* (28), 9113–9121.

23 Chen, J.; Kampf, J. W.; McNeil, A. J. *Langmuir* **2010**, *26* (16), 13076–13080.

24 Muro-Small, M. L.; Chen, J.; McNeil, A. J. *Langmuir* **2011**, *27* (21), 13248–13253.

25 Buerkle, L. E.; von Recum, H. A.; Rowan, S. J. *Chem. Sci.* **2012**, *3* (2), 564–572.

26 de Loos, M. Hydrogen-bonded low molecular weight gelators. Dissertation, University of Groningen, Groningen, Netherlands, 2005.

27 Raghavan, S. R.; Cipriano, B. H. Gel Formation: Phase Diagrams Using Tabletop Rheology and Calorimetry. In *Molecular gels: materials with self-assembled fibrillar networks*, Weiss, R. G.; Terech, P., Eds. Springer: Dordrecht, The Netherlands, 2006; pp 241–252.

28 Debnath, S.; Shome, A.; Dutta, S.; Das, P. K. *Chem. Eur. J.* **2008**, *14* (23), 6870–6881.

29 Gschneidner, K. A., Jr. Physical Properties of the Rare Earth Metals. In *CRC Handbook of Chemistry and Physics* [Online] 91st (Internet Version 2011) ed.; Haynes, W. M., Ed. CRC Press/Taylor and Francis: Boca Raton, FL, 2010; pp. 4-127–4-132. http://www.hbcpnetbase.com/ (accessed 5 December, 2010).

30 Lewith, S. *Arch. Exp. Pathol. Pharmakol.* **1887**, *24* (1–2), 1–16.

31 Hofmeister, F. *Arch. Exp. Pathol. Pharmakol.* **1888**, *24* (4–5), 247–260.

32 Hofmeister, F. *Arch. Exp. Pathol. Pharmakol.* **1888**, *25* (1), 1–30.

33 Limbeck, R. *Arch. Exp. Pathol. Pharmakol.* **1888**, *25* (1), 69–86.

34 Hofmeister, F. *Arch. Exp. Pathol. Pharmakol.* **1890**, *27* (6), 395–413.

35 Hofmeister, F. *Arch. Exp. Pathol. Pharmakol.* **1891**, *28* (3–4), 210–238.

36 Münzer, E. *Arch. Exp. Pathol. Pharmakol.* **1898**, *41* (1), 74–96.

37 Kunz, W.; Henle, J.; Ninham, B. W. *Curr. Opin. Colloid Interface Sci.* **2004**, *9* (1–2), 19–37.

38 Zhang, Y.; Cremer, P. S. *Curr. Opin. Chem. Biol.* **2006**, *10* (6), 658–663.

39 Collins, K. D.; Washabaugh, M. W. *Q. Rev. Biophys.* **1985**, *18* (04), 323–422.

40 Zhang, Y.; Cremer, P. S. *Annu. Rev. Phys. Chem.* **2010**, *61* (1), 63–83.

41 Lo Nostro, P.; Ninham, B. W. *Chem. Rev.* **2012**, *112* (4), 2286–2322.

42 Ninham, B. W.; Duignan, T. T.; Parsons, D. F. *Curr. Opin. Colloid Interface Sci.* **2011**, *16* (6), 612–617.

43 Boström, M.; Williams, D. R. M.; Ninham, B. W. *Curr. Opin. Colloid Interface Sci.* **2004**, *9* (1–2), 48–52.

44 Ninham, B. W.; Yaminsky, V. *Langmuir* **1997**, *13* (7), 2097–2108.

45 Koelsch, P.; Motschmann, H. *Curr. Opin. Colloid Interface Sci.* **2004**, *9* (1–2), 87–91.

46 Edwards, S. A.; Williams, D. R. M. *Curr. Opin. Colloid Interface Sci.* **2004**, *9* (1–2), 139–144.

47 Kunz, W.; Lo Nostro, P.; Ninham, B. W. *Curr. Opin. Colloid Interface Sci.* **2004**, *9* (1–2), 1–18.

48 Parsons, D. F.; Bostrom, M.; Nostro, P. L.; Ninham, B. W. *Phys. Chem. Chem. Phys.* **2011**, *13* (27), 12352–12367.

49 Boström, M.; Parsons, D. F.; Salis, A.; Ninham, B. W.; Monduzzi, M. *Langmuir* **2011**, *27* (15), 9504–9511.

50 Boström, M.; Tavares, F. W.; Finet, S.; Skouri-Panet, F.; Tardieu, A.; Ninham, B. W. *Biophys. Chem.* **2005**, *117* (3), 217–224.

51 Kunz, W. *Curr. Opin. Colloid Interface Sci.* **2010**, *15* (1–2), 34–39.

52 Lo Nostro, P.; Ninham, B. W.; Milani, S.; Lo Nostro, A.; Pesavento, G.; Baglioni, P. *Biophys. Chem.* **2006**, *124* (3), 208–213.

53 Tadeo, X.; Pons, M.; Millet, O. *Biochemistry* **2006**, *46* (3), 917–923.

54 Salis, A.; Cugia, F.; Parsons, D. F.; Ninham, B. W.; Monduzzi, M. *Phys. Chem. Chem. Phys.* **2012**, *14* (13), 4343–4346.

55 Sinn, C. G. Ion Binding to Polymers and Lipid Membranes in Aqueous Solutions. Doctor Rerum Naturalium Dissertation, University of Potsdam, Postdam, 2004.

56 Schott, H. *Colloids Surf.* **1984**, *11* (1–2), 51–54.

57 Collins, K. D. *Biophys. J.* **1997**, *72* (1), 65–76.

58 Hamm, L. M.; Wallace, A. F.; Dove, P. M. *J. Phys. Chem. B* **2010**, *114* (32), 10488–10495.

59 Nealon, G. L.; Mocerino, M.; Ogden, M.; Skelton, B. *J. Inclusion Phenom. Macrocyclic Chem.* **2009**, *65* (1–2), 25–30.

60 Chen, X.; Flores, S. C.; Lim, S.-M.; Zhang, Y.; Yang, T.; Kherb, J.; Cremer, P. S. *Langmuir* **2010**, *26* (21), 16447–16454.

61 Omta, A. W.; Kropman, M. F.; Woutersen, S.; Bakker, H. J. *Science* **2003**, *301* (5631), 347–349.

62 Tielrooij, K. J.; Garcia-Araez, N.; Bonn, M.; Bakker, H. J. *Science* **2010**, *328* (5981), 1006–1009.

63 Piepenbrock, M.-O. M.; Lloyd, G. O.; Clarke, N.; Steed, J. W. *Chem. Rev.* **2009**, *110* (4), 1960–2004.

64 Steed, J. W. *Chem. Soc. Rev.* **2010**, *39* (10), 3686–3699.

65 Liu, S. Q.; Joshi, S. C.; Lam, Y. C. *J. Appl. Polym. Sci.* **2008**, *109* (1), 363–372.

66 Lloyd, G. O.; Piepenbrock, M.-O. M.; Foster, J. A.; Clarke, N.; Steed, J. W. *Soft Matter* **2012**, *8* (1), 204–216.

67 Piepenbrock, M.-O. M.; Clarke, N.; Foster, J. A.; Steed, J. W. *Chem. Commun.* **2011**, *47* (7), 2095–2097.

68 Shen, J.-S.; Cai, Q.-G.; Jiang, Y.-B.; Zhang, H.-W. *Chem. Commun.* **2010**, *46* (36), 6786–6788.

69 Lloyd, G. O.; Steed, J. W. *Nature Chem.* **2009**, *1* (6), 437–442.

70 Spiller, K. L.; Laurencin, S. J.; Charlton, D.; Maher, S. A.; Lowman, A. M. *Acta Biomater.* **2008**, *4* (1), 17–25.

71 Ekaputra, A. K.; Prestwich, G. D.; Cool, S. M.; Hutmacher, D. W. *Biomacromolecules* **2008**, *9* (8), 2097–2103.

72 Irina, S.; Paul, T.; Sergey, M.; Igor, G. Characterization of Macroporous Gels. In *Macroporous Polymers*, Mattiasson, B.; Kumar, A.; Galaev, I. Y., Eds. CRC Press: Baco Raton, Florida, 2009; pp 211–235.

73 Pogorelov, A.; Selezneva, I. *Bull. Exp. Biol. Med.* **2010**, *150* (1), 153–156.

74 Joubert, L.-M. *Microsc. Microanal.* **2009**, *15* (Suppl. S2), 1308–1309.

75 Brizard, A.; Oda, R.; Huc, I. *Top. Curr. Chem.* **2005**, *256*, 167–218.

76 Ryan, D. M.; Anderson, S. B.; Senguen, F. T.; Youngman, R. E.; Nilsson, B. L. *Soft Matter* **2010**, *6* (3), 475–479.

77 Otten, D. E.; Petersen, P. B.; Saykally, R. J. *Chem. Phys. Lett.* **2007**, *449* (4–6), 261–265.

78 Buck, R. P.; Singhadeja, S.; Rogers, L. B. *Anal. Chem.* **1954**, *26* (7), 1240–1242.

79 Rodik, R. V.; Klymchenko, A. S.; Jain, N.; Miroshnichenko, S. I.; Richert, L.; Kalchenko, V. I.; Mély, Y. *Chem. Eur. J.* **2011**, *17* (20), 5526–5538.

80 Amanokura, N.; Yoza, K.; Shinmori, H.; Shinkai, S.; N. Reinhoudt, D. *J. Chem. Soc., Perkin Trans. 2* **1998**, (12), 2585–2592.

81 Ablett, S.; Clark, A. H.; Rees, D. A. *Macromolecules* **1982**, *15* (2), 597–602.

82 Hirst, A. R.; Smith, D. K.; Feiters, M. C.; Geurts, H. P. M. *Chem. Eur. J.* **2004**, *10* (23), 5901–5910.

83 Côte, M.; Nicholls, T.; Knight, D. W.; Morgan, I. R.; Rogueda, P. G. A.; King, S. M.; Heenan, R. K.; Griffiths, P. C. *Langmuir* **2009**, *25* (15), 8678–8684.

84 Das, R. K.; Kandanelli, R.; Linnanto, J.; Bose, K.; Maitra, U. *Langmuir* **2010**, *26* (20), 16141–16149.

85 Lin, J. B.; Dasgupta, D.; Cantekin, S.; Schenning, A. P. H. J. *Beilstein J. Org. Chem.* **2010**, *6*, 960–965.

86 Čaplar, V.; Frkanec, L.; Vujičić, N. Š.; Žinić, M. *Chem. Eur. J.* **2010**, *16* (10), 3066–3082.

87 Cicchi, S.; Ghini, G.; Lascialfari, L.; Brandi, A.; Betti, F.; Berti, D.; Baglioni, P.; Di Bari, L.; Pescitelli, G.; Mannini, M.; Caneschi, A. *Soft Matter* **2010**, *6* (8), 1655–1661.

88 Čaplar, V.; Žinić, M.; Pozzo, J.-L.; Fages, F.; Mieden-Gundert, G.; Vögtle, F. *Eur. J. Org. Chem.* **2004**, *2004* (19), 4048–4059.

89 Becerril, J.; Escuder, B.; Miravet, J. F.; Gavara, R.; Luis, S. V. *Eur. J. Org. Chem.* **2005**, *2005* (3), 481–485.

90 Braga, D.; d'Agostino, S.; D'Amen, E.; Grepioni, F. *Chem. Commun.* **2011**, *47* (18), 5154–5156.

91 Kumar, D. K.; Jose, D. A.; Das, A.; Dastidar, P. *Chem. Commun.* **2005**, (32), 4059–4061.

92 Shannon, R. *Acta Crystallogr. Sect. A: Found. Crystallogr.* **1976**, *32* (5), 751–767.

93 Safont-Sempere, M. M.; Fernández, G.; Würthner, F. *Chem. Rev.* **2011**, *111* (9), 5784–5814.

94 Liu, X. Y. *Top. Curr. Chem.* **2005**, *256*, 1–37.

95 Schmelzer, J. W. P. Kinetics of Nucleation, Aggregation and Ageing. In *Molecular Gels*, Weiss, R. G.; Terech, P., Eds. Springer Netherlands: Dordrecht, The Netherlands, 2006; pp 131–160.

96 Li, J.-L.; Yuan, B.; Liu, X.-Y.; Wang, X.-G.; Wang, R.-Y. *Cryst. Growth Des.* **2011**, *11* (7), 3227–3234.

97 Petrova, M.; Muhamadejev, R.; Vigante, B.; Cekavicus, B.; Plotniece, A.; Duburs, G.; Liepinsh, E. *Molecules* **2011**, *16* (9), 8041–8052.

98 Takahashi, A.; Sakai, M.; Kato, T. *Polym. J. (Tokyo, Jpn.)* **1980**, *12* (5), 335–341.
99 Nečas, D.; Klapetek, P. *Cent. Eur. J. Phys.* **2012**, *10* (1), 181–188.
100 Kremer, J. R.; Mastronarde, D. N.; McIntosh, J. R. *J. Struct. Biol.* **1996**, *116* (1), 71–76.

5 Templated crystallisation in hydrogels

5.1 Crystallisation in gels

Templated crystallisation of inorganic materials under the influence of organic and bioorganic structures has been studied previously[1–3] and a short overview of templated crystallisation is covered in section 1.2.4. Of the many 'templates' available (e.g. monolayers, polymers, surfactants), gels are of interest here as both a template and medium for crystallising inorganic minerals. This could potentially lead to new materials and a better understanding of biomineralisation processes.

5.1.1 Crystallisation in hydrogels

5.1.1.1 Calcium carbonate

Hydrogels have been shown to play an important role in biomineralisation systems. Investigations by Levi-Kalisman et al.[4] on the nacreous layer of the shell of *Atrina serrata* (a bivalve mollusc) by cryo-TEM led to the proposal of a model for the nacreous layer. This model depicted layers of the β-chitin framework incorporating Asprich glycoproteins alternating with silk fibroin gel phases. Keene et al.[5] showed that the addition of silk fibroin hydrogels to a crystallisation system (comprising nacre specific peptide and β-chitin) changed the environment in which the calcium carbonate crystallised. The addition of silk fibroin hydrogel to the nacre specific peptide and β-chitin crystallisation system gave particles of amorphous calcium carbonate and vaterite (with habits resembling the shape of 'sunny-side up' fried eggs) adhered to the β-chitin; in the absence of the hydrogel, polycrystalline

aragonite was obtained. The authors proposed that the hydrogel modulated the activity of the peptide (or a component in the natural system was missing). Silk fibroin is known to have inhibitory effects on calcium carbonate crystallisation,[6] however, the diffusion control exerted by silk fibroin hydrogels should also be considered.[7] Recent work by Khalifa et al.[8] on the operculum of *Balanus amphitrite* suggests that a hydrogel matrix is important for the mineralisation of calcium carbonate. Here, the authors showed that the hydrogel occupied the space in which calcite particles were to form; as the particles grew they excluded water and compressed gelator molecules. The nucleating agents were believed to be the gelator molecules and the low concentration of highly acidic proteins (rich in Asx and Glx). From this, they also postulate that hydrogels may play a wider role in biomineralisation in general.

It is of no surprise that much of the literature on crystallisation in hydrogels (in the laboratory) has been extensively focused on the application of hydrogels as mimics for organic matrices in biomineralization systems. In 'biologically-controlled'[9, 10] or 'matrix-mediated'[11] biomineralisation processes, organisms use organic frameworks to control the orientation, size, and shape of the biomineral. Calcium carbonate, one of the most common and widely studied biominerals,[12] has been crystallised in a variety of gels including carrageenan;[13] agarose;[14–16] agarose with poly(aspartic acid), aspartic acid, and ethylenediaminetetraacetic acid inhibitors;[17] agarose on self-assembled monolayers (to direct orientation of crystals);[18] agar;[19] gelatin xerogels entrapped with poly(L-aspartic acid) or poly(L-glutamic acid);[20] polyacrylamide hydrogels;[21] sodium acrylate hydrogels (seeded with calcium carbonate);[22] sodium alginate nanospherical hydrogels;[23] self-assembled collagen;[24] hydrogels comprised of a hydrogelator with Ca^{2+}-binding domains (i.e. carboxylates);[25] porous poly(hydroxyethylmethyacrylate) hydrogels templated on sea urchin spines;[26] and silica hydrogels containing chromium(VI)[27] and magnesium.[28] Most of these gels are composed of macromolecular gelators and were shown to impact the morphology, polymorph, particle size, and orientation on the calcium carbonate.

As crystals grow within a gel, they may incorporate or exclude the gel fibres. Building on their earlier work,[15] Li et al.[14] showed that calcite single crystals grown in agarose hydrogel had a continuous three-dimensional network of nanofibres

throughout the crystal. This is similar to the occlusion of organic macromolecules (particularly proteins) into biominerals.[29–32] Li et al. proposed that a physical mechanism (rather than a chemical mechanism such as epitaxial matching) was operating at the organic fibre-inorganic mineral interface. In this case, high- and low-energy facets of calcite surrounded the curved fibres.

5.1.1.2 **Calcium phosphate**

Crystallisation of calcium phosphate in hydrogels has also garnered interest. Using a model biomineralisation system consisting of propionic acid in polyacrylamide hydrogels, Yokoi et al.[33] studied the effect of propionic acid (as a simple substitute for proteins) on the crystallisation of calcium phosphate. They found that the propionic acid adsorbed onto the (100) face where the Ca^{2+} ions were situated. This resulted in spherical particles rather than the fibrous or plate-like morphology observed in the absence of propionic acid.

Wang, et al.[34] have successfully prepared composites of bacteriophages layered with nanocrystals of hydroxyapatite. A gel-like substance was obtained after $CaCl_2$ was added to bacteriophage and centrifuged; the gel-like substance was then added to a Na_2HPO_4 solution. Acidic amino acid residues (Asp and Glu) along the surface of the bacteriophage chelated Ca^{2+} in solution, pre-organising the bacteriophage in to fibrous bundles (leading to the gel-like substance) and creating a local super-saturation of Ca^{2+} on the bacteriophage surface. This allowed hydroxyapatite to crystallise between bacteriophage bundles. The authors also noted that the chirality of the helices of the protein coating the bacteriophage was transferred to the hydroxyapatite nanocrystals.

Crystallisation in gels also opens up an avenue for new composite materials. Schnepp et al.[35] prepared a hydrogel-calcium phosphate composite. The self-assembled thermoresponsive hydrogel (prepared by dephosphorylation of **166**, Figure 5.1, by a phosphatase) was placed into a solution of calcium chloride and calcium phosphate and was allowed to mineralise. The authors found that calcium phosphate mineralised around the hydrogel fibres and not in the space in between fibres. By tuning the level of mineralisation, the viscoelaticity, thermostability, and stiffness of the hydrogel-calcium phosphate composite could be tuned.

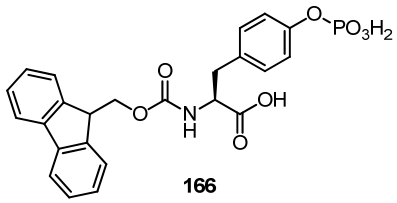

166

Figure 5.1 A masked gelator. Cleaving the phosphate group leads to a hydrogel.[35]

5.1.1.3 **Other inorganic minerals**

Despite the recent literature focused on the use of hydrogels as mimics for biomineralisation, other authors have investigated other inorganic minerals in hydrogels. Sperka conducted an early survey of crystallisation in silica gels (the paper did not specify which minerals were studied).[36] Later Achilles[37] studied the crystallisation of calcium oxalate in agar-agar gel matrices with artificial and natural urine, mimicking the growth of calcium oxalate in the gel medium along the urinary tract. Imai and Oaki[38–40] found that crystallisation of $K_2Cr_2O_7$ in gel media provided the ability to tune the chirality of inorganic crystals. The authors postulated that this occurred due to the crystal–organic stereochemical recognition. Jiang et al.[41] have reported the synthesis of silica nanotubes in a hydrogel (although much of the literature reports silica nanostructures prepared in organogels, refer to section 5.1.2). The chiral features of hydrogel fibres (formed from the self-assembly of bolaamphilphile **167**, Figure 5.2) were transcribed onto the inside of the nanotubes.

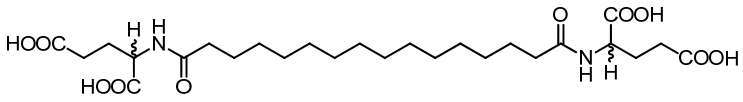

167

Figure 5.2 Bolaamphiphilic hydrogelator utilised by Jiang et al.[41] for sol-gel transcription to silica nanotubes.

5.1.2 Crystallisation in organogels

Much of the published literature on crystallisation in organogels involved sol-gel transcription to synthesise silica nanostructures—in particular nanotubes.[2, 42–46] The key feature here is the preparation of the organogel from low molecular weight organogelators (such as those in Figure 5.3). Typically, tetraethoxysilane is condensed in the organogel and calcined to leave the silica nanostructures. Recently Lin et al.[47] reported chiral double helical strands of silica tubes prepared from sugar-

lipid-based amphiphilic organogel (**168**). The twist of the helix was dependant on the twist of the gel fibres, hence the enantiomer of the gelator. Kim et al. were also successful in preparing single stranded helical silica nanotubes using chiral amphiphilic organogelators, **169**[48, 49] and **170**.[50] Organogels with chiral fibrils were prepared by a 1:1 mixture of the neutral and cationic organogelator with the same chirality (e.g. (1*S*,2*S*)-**169a** and (1*S*,2*S*)-**169b**). The neutral organogelators determined the rotation of the helix of the fibres. The cationic gelators (with diminished gelation ability) provided cationic charge on the surface of the gel fibres. This was consistent with the authors obtaining non-helical silica nanotubes if racemic neutral organogelator (±)-**169a** was used in the organogel mixture. Craythorne et al.[51] have also reported silica nanotubes, albeit achiral, prepared from a sugar-based gelator (**171**). Silica nanotubes have potential applications in medicine[52, 53](such as drug delivery and imaging), hydrogen storage, and sensors.[45]

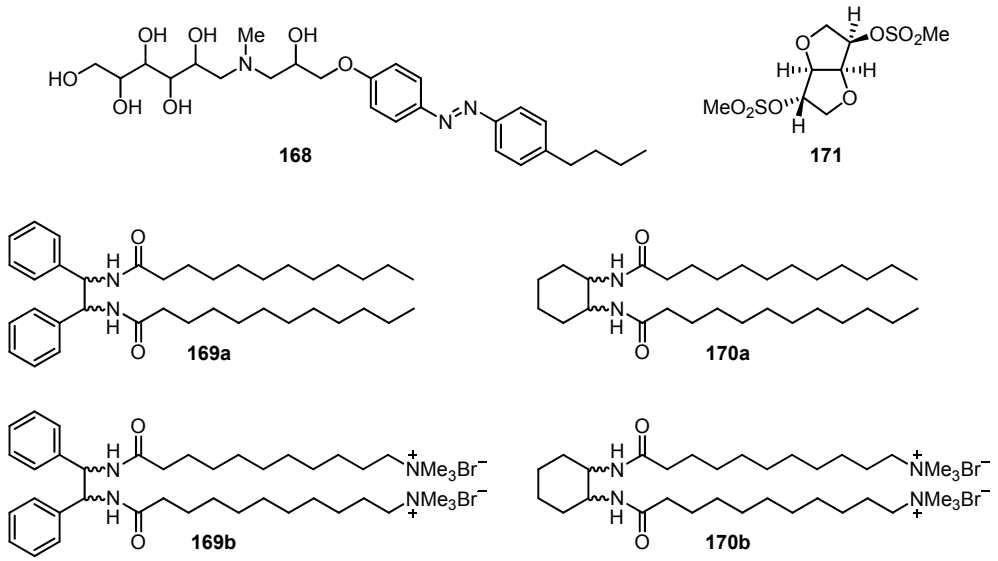

Figure 5.3 Example of organogelators employed in the production of silica nanotubes by a sol-gel transcription process.[47, 50, 51]

5.1.3 Motivation for crystallisation in hydrogels

From the review of literature on crystallisation in hydrogels, it appears that there has been little application of low molecular weight hydrogels as templates for controlled crystallisation. Hydrogels of proline calix[4]arene **127a** had potential as a template for crystallisation of inorganic minerals. Calcium carbonate is a well studied mineral and would have been a suitable model mineral, however the **127a** hydrogels

transition into solutions at pH >7. Barium sulfate is another well-studied mineral with a single known polymorph. Therefore, barium sulfate was selected as the model mineral for crystallisation in a hydrogel.

5.2 Barium sulfate crystallisation in a hydrogel

Barium sulfate was crystallised in a **127a**-$LiNO_3$ hydrogel. The hydrogel was prepared from separate solutions of proline calix[4]arene **127a**/$BaCl_2$ and $LiNO_3$. Barium sulfate (at a target supersaturation ratio of ~25) was crystallised by diffusing sodium sulfate into the hydrogel (Figure 5.4). The supersaturation selected here was identical to that used previously in the study of aspartic acid and glutamic acid functionalised calix[4]arenes (refer to Chapter 3). The barium chloride levels at the supersaturation of interest, was not capable of producing a hydrogel with **127a.** Hydrogels comprised of chloride as an electrolyte component tended to have lower stability—often crystallising as very thin plates. From previous work (refer to section 4.2.2), the anion that produced the strongest hydrogels was nitrates, thus $LiNO_3$ was selected as the electrolyte component of the hydrogel. Lithium cations were shown to have minimal impact on the crystallisation of barium sulfate (Jones, F. Curtin University, Perth, Australia. Personal communication, 2010). In a typical experiment (refer to Table 5.1 for more details), the **127a**-$LiNO_3$ hydrogel loaded with barium chloride was allowed to stand for two hours before sodium sulfate was allowed to diffuse into it. The opaque/cloudy gels phase appeared to remain stable for at least 12 hours and some gel fragments were observed up to seven days. With slight agitation the gels fragments dissolved into solution, allowing for the recovery of the barium sulfate precipitate.

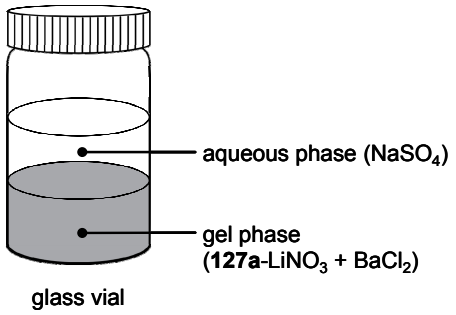

Figure 5.4 Experiment set-up for crystallisation of barium sulfate in a hydrogel (**127a**-$LiNO_3$).

Table 5.1 Concentration of additives used in the crystallisation of barium sulfate in **127a**-$LiNO_3$ hydrogel and associated experiments. Here, c = concentration and I = ionic strength.

Experimental conditions	c / $\times 10^{-3}$ mol L^{-1}				I
	$BaCl_2$	Na_2SO_4	**127a**	$LiNO_3$	/ $\times 10^{-3}$
No additives (blank)	0.25	0.25	0	0	1.5
Solution, **127a**	0.25	0.25	20	0	1.5
Solution, $LiNO_3$	0.25	0.25	0	25	26.5
Solution, $LiNO_3$	0.25	0.25	0	50	51.5
Hydrogel, **127a**-$LiNO_3$	0.25	0.25	20	25	26.5
Hydrogel, **127a**-$LiNO_3$	0.25	0.25	20	50	51.5

Barium sulfate grown in the presence of **127a** (Figure 5.6b) exhibited only small changes in morphology compared to the control, with highly twinned particles and minor development of the (100) and (210) faces which in control experiments exist as rounded (*hk*0) faces (as shown in Figure 5.6a). When crystallised in the presence of $LiNO_3$, barium sulfate crystallised with a hexagonal morphology with more rounded (100) and (210) faces and a much shorter *c*-axis (Figure 5.6c). In contrast, work by Jones and Ogden[54] showed that monovalent cations such as Na^+ and K^+ *lengthened* the *c*-axis. However, this result was obtained at 75 °C and it is unclear whether the differences in the morphology observed in this work were a result of the temperature or the presence of nitrate anions. It is clear that the presence of $LiNO_3$ has a similar impact on barium sulfate morphology to that of lowering the supersaturation.[54] This may also be an ionic strength effect.

Barium sulfate grown in the presence of **127a**-$LiNO_3$ (20:25 mM) hydrogel (Figure 5.5f,g) showed well defined (100) and (210) faces unlike the (*hk*0) face of the control experiment (Figure 5.5a). Doubling the concentration of the $LiNO_3$ in the **127a**-$LiNO_3$ hydrogel produced much smaller barium sulfate particles with

orthorhombic morphology (Figure 5.5h,i). The barium sulfate particles grown in the **127a**-$LiNO_3$ hydrogel with the lower level of $LiNO_3$, 25 mM, (Figure 5.5d) resembled those grown in the absence of the calixarene; some particles had a reduced *c*-axis length. However, barium sulfate crystals grown in the hydrogel with higher $LiNO_3$ content, 50 mM, (Figure 5.5e) were much smaller and had a different morphology compared to those grown in the absence of calixarene **127a**.

(a)

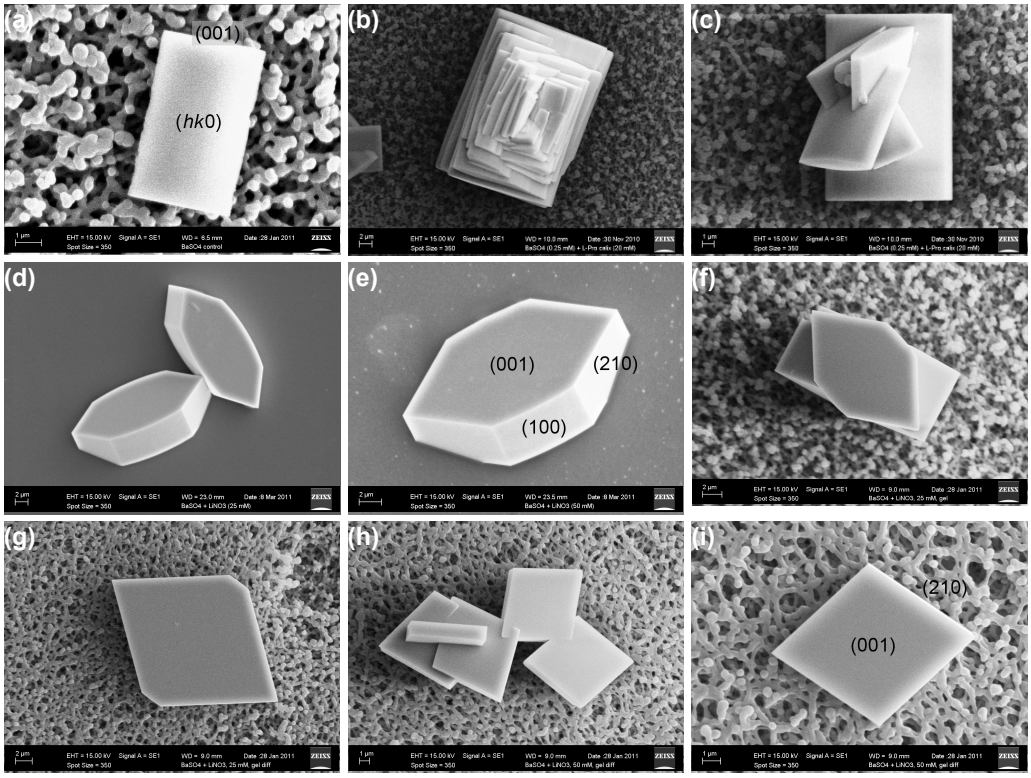

Figure 5.5 SEM micrographs showing barium sulfate grown in a **127a**-$LiNO_3$ hydrogel. (a) $BaSO_4$ grown in the absence of both L-proline calix[4]arene **127a** and $LiNO_3$ (control); in the presence of (b, c) **127a** (20 mM), (d) $LiNO_3$ (25 mM), (e) $LiNO_3$ (50 mM), (f, g) **127a** (20 mM)/ $LiNO_3$ (25 mM) hydrogel; and (h, i) **127a** (20 mM)/$LiNO_3$ (50 mM) hydrogel. Here the background of micrographs a–c and f–i are of the filter membrane.

The SEM micrographs suggested that the hydrogel has some impact on the morphology of the barium sulfate with some influence also from the lithium nitrate. The morphology observed for barium sulfate crystallised in **127a**-$LiNO_3$ (20:25 mM) hydrogel was similar to that crystallised in the presence of $LiNO_3$ but the absence of the hydrogel. Under these conditions, the similarity between the morphology of barium sulfate in the presence of $LiNO_3$ and that in the hydrogel suggested that the hydrogel itself did not have a significant impact on the final morphology. Doubling

the $LiNO_3$ level in the hydrogel resulted in particles with orthorhombic morphologies and significantly shortened *c*-axes (Figure 5.6d), which are slightly different to barium sulfate crystallised in the presence of an equivalent level of $LiNO_3$ (in the absence of the hydrogel). These particles had morphologies resembling the synthetic barium sulfate particles produced by Hopwood et al.[55] They proposed that the observed barium sulfate particles, in the absence of additives, were largely under the influence of changes in the ionic strength. However, the bulk ionic strengths (Table 5.1) used in this study were lower than those used by Hopwood et al. (I = 0.6 M). In addition, the morphologies of barium sulfate crystallised in the hydrogels (Figure 5.6c,d) resembled barium sulfate crystallised at even lower supersaturation (3.63 and 2.14 respectively) by Jones and Ogden.[54] This then suggests that the most significant impact of the hydrogel is that it reduces the diffusion of ions through the aqueous phase, resulting in slower crystallisation kinetics. From previous gel studies (as reported in section 4.2.1) it was observed that with a higher concentration of the electrolyte, the **127a**-electrolyte hydrogel appeared to be stronger, possibly due to the increased density of gel fibres. Changes in gel fibre density will affect the mobility of ions and therefore the diffusion of sodium sulfate from the aqueous phase into the gel phase. The impact of polymer content in a hydrogel on calcium carbonate is known;[21] the calcium carbonate habit was influenced by diffusion control with no specific impact from the polymer itself. This could explain the apparent lower supersaturation of the **127a**-$LiNO_3$ (20:50 mM) hydrogel compared with the hydrogel at half the $LiNO_3$ content. As a consequence the Ba^{2+}:SO_4^{2-} ratio is expected to impact on the crystallisation of barium sulfate,[56] however it is difficult to determine Ba^{2+}:SO_4^{2-} ratio in hydrogel systems.

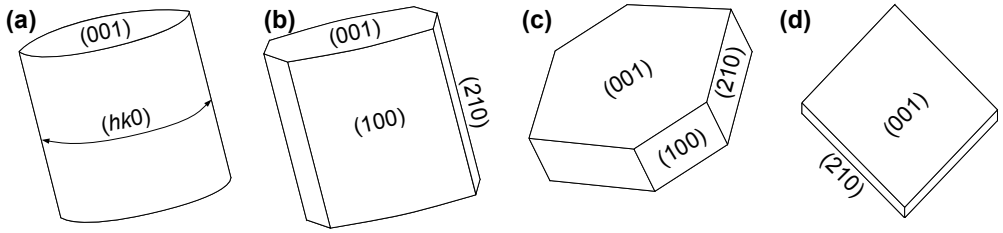

Figure 5.6 Tentative assignment of crystal faces to barium sulfate particles crystallised (a) in the absence of any additives and in the presence of (b) **127a**, (c) $LiNO_3$ and **127a**-$LiNO_3$ (20:25 mM) hydrogel, (d) **127a**-$LiNO_3$ (20:50 mM) hydrogel.

5.3 Conclusions

Proline calix[4]arene hydrogels, with lithium nitrate electrolyte, were shown to have subtle influence over the final morphology of barium sulfate and the impact related to the level of the electrolyte present. With $LiNO_3$ levels at 25 mM, **127a**-$LiNO_3$ hydrogels produced barium sulfate particles with morphology similar to those grown in the absence of the calixarene; these particles have a hexagonal morphology. However, doubling the $LiNO_3$ content in **127a**-$LiNO_3$ hydrogel resulted in smaller barium sulfate particles with an orthorhombic morphology.

5.4 Experimental

5.4.1 General remarks

Reagents were used as purchased from the manufacturer or supplier. MilliQ water, having a resistance of 0.055 cm/Ω, was used throughout crystallisation experiments. Hydrogelators **127a** was prepared by methods described in Chapter 2.

5.4.2 Crystallisation in proline calix[4]arene gels

Gels were prepared in a 20 mL glass vials. $LiNO_3$ was added to $BaCl_2$ and L-proline calix[4]arene (**127a**) solution to form a hydrogel and allowed to equilibrate for two hours. Then a Na_2SO_4 solution was carefully layered above the gel and the vial allowed to stand for seven days.

5.4.3 Characterisation of barium sulfate

Gels were carefully dissolved by swirling the vial. The mixture was filtered through a 0.2 μm filter membrane. Filter membranes were dried, gold coated, and the morphology examined under a scanning electron microscope (Zeiss Evo 40XVP).

5.5 References

1 Sommerdijk, N. A. J. M.; de With, G. *Chem. Rev.* **2008**, *108* (11), 4499–4550.

2 van Bommel, K. J. C.; Friggeri, A.; Shinkai, S. *Angew. Chem. Int. Ed.* **2003**, *42* (9), 980–999.

3 Behrens, P.; Baeuerlein, E., Eds. *Handbook of Biomineralization: Biomimetic and Bioinspired Chemistry*. Wiley-VCH GmbH and Co. KGaA: Weinheim, Germany, 2007; Vol. 2.

4 Levi-Kalisman, Y.; Falini, G.; Addadi, L.; Weiner, S. *J. Struct. Biol.* **2001**, *135* (1), 8–17.

5 Keene, E. C.; Evans, J. S.; Estroff, L. A. *Cryst. Growth Des.* **2010**, *10* (12), 5169–5175.

6 Addadi, L.; Joester, D.; Nudelman, F.; Weiner, S. *Chem. Eur. J.* **2006**, *12* (4), 980–987.

7 Falini, G.; Albeck, S.; Weiner, S.; Addadi, L. *Science* **1996**, *271* (5245), 67–69.

8 Khalifa, G. M.; Weiner, S.; Addadi, L. *Cryst. Growth Des.* **2011**, *11* (11), 5122–5130.

9 Weiner, S.; Dove, P. M. An Overview of Biomineralization Processes and the Problem of the Vital Effect. In *Biomineralization*, Dove, P. M.; De Yoreo, J. J.; Weiner, S., Eds. Mineralogical Society of America: Washington, D.C., 2003; Vol. 54, pp 1–29.

10 Veis, A. Mineralization in Organic Matrix Frameworks. In *Biomineralization*, Weiner, S.; De Yoreo, J. J.; Dove, P. M., Eds. Mineralogical Society of America: Washington, D.C., 2003; pp 249–289.

11 Mann, S. Organic Matrix-Mediated Biomineralization. In *Biomineralization: Principles and Concepts in Bioinorganic Materials Chemistry*, Oxford University Press: Oxford, 2001; pp 89–124.

12 Lowenstam, H. A. *Science* **1981**, *211* (4487), 1126–1131.

13 Kosanović, C.; Falini, G.; Kralj, D. *Cryst. Growth Des.* **2010**, *11* (1), 269–277.

14 Li, H.; Xin, H. L.; Muller, D. A.; Estroff, L. A. *Science* **2009**, *326* (5957), 1244–1247.

15 Li, H.; Estroff, L. A. *Adv. Mater.* **2009**, *21* (4), 470–473.

16 Borah, B. M.; Lakshmi, H.; Das, G. *Mater. Sci. Eng., C* **2008**, *28* (7), 1173–1182.

17 Boggavarapu, S.; Chang, J.; Calvert, P. *Mater. Sci. Eng., C* **2000**, *11* (1), 47–49.

18 Li, H.; Estroff, L. A. *J. Am. Chem. Soc.* **2007**, *129* (17), 5480–5483.

19 Oaki, Y.; Hayashi, S.; Imai, H. *Chem. Commun.* **2007**, (27), 2841–2843.

20 Falini, G.; Fermani, S.; Gazzano, M.; Ripamonti, A. *J. Chem. Soc., Dalton Trans.* **2000**, (21), 3983–3987.

21 Helbig, U. *J. Cryst. Growth* **2008**, *310* (11), 2863–2870.

22 Guo, Y.; Yang, L.; Yang, X.; Zhang, X.; Zhu, S.; Jiang, K. *Macromol. Biosci.* **2003**, *3* (3–4), 163–168.

23 Wang, T.; Leng, B.; Che, R.; Shao, Z. *Langmuir* **2010**, *26* (16), 13385–13392.

24 Yang, L.; Ye, F.; Xing, R.; Zhang, B.; Ren, Q. *Supramol. Chem.* **2008**, *20* (8), 761–763.

25 Estroff, L. A.; Addadi, L.; Weiner, S.; Hamilton, A. D. *Org. Biomol. Chem.* **2004**, *2* (1), 137–141.

26 Cheng, X.; Gower, L. B. *Biotechnol. Prog.* **2006**, *22* (1), 141–149.

27 Sánchez-Pastor, N.; Gigler, A. M.; Cruz, J. A.; Park, S.-H.; Jordan, G.; Fernández-Díaz, L. *Cryst. Growth Des.* **2011**, *11* (7), 3081–3089.

28 Fernández-Díaz, L.; Putnis, A.; Prieto, M.; Putnis, C. V. *J. Sediment. Res.* **1996**, *66* (3), 482–491.

29 Metzler, R. A.; Tribello, G. A.; Parrinello, M.; Gilbert, P. U. P. A. *J. Am. Chem. Soc.* **2010**, *132* (33), 11585–11591.

30 Gotliv, B. A.; Kessler, N.; Sumerel, J. L.; Morse, D. E.; Tuross, N.; Addadi, L.; Weiner, S. *ChemBioChem* **2005**, *6* (2), 304–314.

31 Seto, J.; Zhang, Y.; Hamilton, P.; Wilt, F. *J. Struct. Biol.* **2004**, *148* (1), 123–130.

32 Fu, G.; Valiyaveettil, S.; Wopenka, B.; Morse, D. E. *Biomacromolecules* **2005**, *6* (3), 1289–1298.

33 Yokoi, T.; Kawashita, M.; Ohtsuki, C. *IOP Conf. Ser. Mater. Sci. Eng.* **2011**, *18* (19), 192012.

34 Wang, F.; Cao, B.; Mao, C. *Chem. Mater.* **2010**, *22* (12), 3630–3636.

35 Schnepp, Z. A. C.; Gonzalez-McQuire, R.; Mann, S. *Adv. Mater.* **2006**, *18* (14), 1869–1872.

36 Sperka, G. *Prog. Colloid Polym. Sci.* **1988**, *77*, 207–210.

37 Achilles, W. *Scanning Microsc.* **1991**, *5* (4), 1001–1017.

38 Imai, H.; Oaki, Y. *CrystEngComm* **2010**, *12* (6), 1679–1687.

39 Oaki, Y.; Imai, H. *J. Am. Chem. Soc.* **2004**, *126* (30), 9271–9275.

40 Imai, H.; Oaki, Y. *Angew. Chem. Int. Ed.* **2004**, *43* (11), 1363–1368.

41 Jiang, J.; Wang, T.; Liu, M. *Chem. Commun.* **2010**, *46* (38), 7178–7180.

42 Jung, J. H.; Park, M.; Shinkai, S. *Chem. Soc. Rev.* **2010**, *39* (11), 4286–4302.

43 Jung, J. H.; Shinkai, S. *Top. Curr. Chem.* **2004**, *248*, 401–411.

44 Gronwald, O.; Shinkai, S. "Inorganic" Combinatorial Chemistry Utilizing Sol-Gel Transcription of Gelatinous Organic Superstructures. In *Macromolecular Nanostructured Materials*, Ueyama, N.; Harada, A., Eds. Springer: Heidelberg, Germany, 2004; Vol. 78, pp 101–117.

45 Yang, X.; Tang, H.; Cao, K.; Song, H.; Sheng, W.; Wu, Q. *J. Mater. Chem.* **2011**, *21* (17), 6122–6135.

46 Estroff, L. A.; Hamilton, A. D. *Chem. Mater.* **2001**, *13* (10), 3227–3235.

47 Lin, Y.; Qiao, Y.; Gao, C.; Tang, P.; Liu, Y.; Li, Z.; Yan, Y.; Huang, J. *Chem. Mater.* **2010**, *22* (24), 6711–6717.

48 Jung, J. H.; Ono, Y.; Shinkai, S. *Chem. Eur. J.* **2000**, *6* (24), 4552–4557.

49 Jung, J. H.; Ono, Y.; Hanabusa, K.; Shinkai, S. *J. Am. Chem. Soc.* **2000**, *122* (20), 5008–5009.

50 Kim, T. K.; Jeong, E. D.; Oh, C. Y.; Shin, M. S.; Kim, J.-P.; Jung, O.-S.; Suh, H.; Khan, F. R. N.; Hyun, M. H.; Jin, J. S. *Chem. Pap.* **2011**, *65* (6), 863–872.

51 Craythorne, S. J.; Pollock, C. L.; Blake, A. J.; Nieuwenhuyzen, M.; Marr, A. C.; Marr, P. C. *New J. Chem.* **2009**, *33* (3), 479–483.

52 Son, S. J.; Bai, X.; Lee, S. B. *Drug Discov. Today* **2007**, *12* (15–16), 650–656.

53 Son, S. J.; Bai, X.; Lee, S. B. *Drug Discov. Today* **2007**, *12* (15–16), 657–663.

54 Jones, F.; Ogden, M. I. *CrystEngComm* **2010**, *12* (4), 1016–1023.

55 Hopwood, J. D.; Mann, S.; Gooday, A. J. *J. Mar. Biol. Assoc. U. K.* **1997**, *77* (4), 969–987.

56 Kucher, M.; Babic, D.; Kind, M. *Chem. Eng. Process.* **2006**, *45* (10), 900–907.

6 Conclusions and suggestions for future work

From this project, it has been shown that amino acid functionalised calixarenes are versatile molecules with many interesting properties. Two of the three acidic amino acid functionalised calix[4]arenes synthesised and investigated, L-aspartic acid and L-glutamic acid functionalised calix[4]arenes (**124a** and **124b** respectively), were able to alter the morphology of calcium carbonate and barium sulfate. In addition, these calix[4]arenes were able to influence the growth kinetics of barium sulfate. The iminodiacetic acid functionalised calix[4]arene (**124c**) showed little activity on calcium carbonate compared with the other two calix[4]arenes.

The L-proline calix[4]arene (**127a**) exhibited several behaviours of interest in supramolecular chemistry. NMR studies showed that the calix[4]arene **127a** interacts with small molecules such as *tert*-butyl alcohol, *N*-methylpyrrolidinone, and tetrahydrofuran. Interestingly, calix[4]arene **127a** was shown to be capable of forming hydrogels in the presence of electrolytes. Further investigations showed that gel formation was mainly influenced by the anion and the most thermostable hydrogels formed with anions towards the 'chaotropic' end of the Hofmeister's series for anions. Characterisation of the hydrogels by AFM showed that calix[4]arene **127a** self-assembles into fibrous structures in the gel phase. Fibrous structures were also observed by cryo-TEM for calix[4]arene **127a** in the presence of an electrolyte under sub-gel conditions. Fortuitously, single crystal structures were obtained for material crystallised from the hydrogels including one for a racemic mixture of L-proline and D-proline calix[4]arenes in the presence of $La(NO_3)_3$.

Bridging interests in both crystallisation of minerals and gel materials, an attempt was made to utilise L-proline calix[4]arene-$LiNO_3$ hydrogels for template crystallisation. Barium sulfate was selected as the model mineral. The results showed the lithium nitrate had the dominant impact on the morphology of barium sulfate, however the hydrogel did impact the crystallisation of barium sulfate by diffusion control of the ions in solution.

This project has opened some interesting avenues for future work. The application of acidic amino acid functionalised calix[4]arenes as crystal growth modifiers can be extended to functionalisation with short peptides comprising acid amino acids (e.g. Asp-Asp-Asp). This would allow the impact of pre-organisation offered by calixarenes to be studied. On the other side of the calix[4]arene, the alkyl chain could potentially be lengthened (e.g. octyl chain) or removed. This could potentially alter the surfactant properties of the calixarenes and offers the opportunity to tether amino acid functionalised calixarenes onto surfaces to allow for study of crystallisation on surfaces. With respect to the calixarene scaffold, higher calixarenes (such as calix[6]arene and calix[8]arenes) could also be investigated. The increased conformational mobility offered by these calixarenes may allow a greater degree of freedom for the attached amino acid functionality to interact with the crystal surface.

Other work in this project on proline and sarcosine functionalised calix[4]arenes showed that such motifs are responsive to anions. This could form the basis of anion-tuneable calixarene hydrogelators. Work by other groups on proline calix[4]arene hydrogels (refer to section 4.1.1), showed that single amino acids could influence the hydrogel morphology. Further work can extend this to the impact of the stereochemistry of the amino acid on the gel morphology and the impact of both the amino acid and electrolyte on gel formation and hydrogel properties.

Appendix A — Crystal data and structure refinement information

Table A.1 Crystal data and structure refinement information for mmcy04 (**127a**•THF).

Identification code	mmcy04
Empirical formula	$C_{56}H_{68}N_4O_{13}$
M_r / g mol^{-1}	1005.14
Crystal description	block
Crystal colour	colourless
Crystal dimensions / mm	0.58 × 0.33 × 0.24
F(000)	12864
Crystal system	cubic
Space group	F432
Cell parameters	a = 36.2659(2) Å, α = 90 °
	b = 36.2659(2) Å, β = 90 °
	c = 36.2659(2) Å, γ = 90 °
Volume / Å^3	47697.5(5)
Z	24
Density, calculated / Mg m^{-3}	0.84
Absorption coefficient, μ / mm^{-1}	0.489
Temperature / K	150(2)
Radiation type	Cu K_α
Wavelength, λ / Å	1.54184
θ range for data collection / °	3.45 < θ < 67.28
Index ranges	−16 < h < 16, −16 < k < 15, −19 < l < 19
Reflections collected	144414
Independent reflections	[R(int) = 0.0475]
Completeness to θ = 67.28	99.9%
Absorption correction	Semi-empirical from equivalents
Max. and min. transmission factor	1.000 and 0.859
Refinement method	Full-matrix least-squares on F^2
Data / restraints / parameters	2160 / 9 / 172
Goodness-of-fit on F^2	1.363
Final R indices [I>2σ(I)]	R_1 = 0.0984, wR_2 = 0.3022
R indices (all data)	R_1 = 0.1055, wR_2 = 0.3121
Largest diff. peak and hole / e Å^{-3}	0.300 and −0.371

Table A.2 Crystal data and structure refinement information for mm39 (**127a**-$MgCl_2$).

Identification code	mm39
Empirical formula	$C_{52}H_{96}Cl_2MgN_4O_{30}$
M_r / g mol^{-1}	1352.54
Crystal description	plate
Crystal colour	colourless
Crystal dimensions / mm	0.46 × 0.25 × 0.15
F(000)	1444
Crystal system	tetragonal
Space group	$P4$
Cell parameters	a = 14.12420(10) Å, α = 90°
	b = 14.12420(10) Å, β = 90°
	c = 16.61700(10) Å, γ = 90°
Volume / Å^3	3314.98(4)
Z	2
Density, calculated / Mg m^{-3}	1.355
Absorption coefficient, μ / mm^{-1}	1.728
Temperature / K	100(2)
Radiation type	Cu K_α
Wavelength, λ / Å	1.54184
θ range for data collection / °	$2.66 < \theta < 67.13$
Index ranges	$-25 < h < 25$, $-30 < k < 30$, $-43 < l < 43$
Reflections collected	40081
Independent reflections	[R(int) = 0.0278]
Completeness to θ = 67.13	99.8%
Absorption correction	Semi-empirical from equivalents
Max. and min. transmission factor	1.000 and 0.766
Refinement method	Full-matrix least-squares on F^2
Data / restraints / parameters	5900 / 3 / 450
Goodness-of-fit on F^2	1.091
Final R indices [I>2σ(I)]	R_1 = 0.0826, wR_2 = 0.2396
R indices (all data)	R_1 = 0.0833, wR_2 = 0.2406
Largest diff. peak and hole / e Å^{-3}	1.074 and −0.852

Table A.3 Crystal data and structure refinement information for mm39 (**127a**-$La(NO_3)_3$).

Identification code	mmcy08
Empirical formula	$C_{52}H_{72.60}La_{0.40}N_4O_{18.80}$
M_r / g mol^{-1}	1110.10
Crystal description	spear
Crystal colour	pale mauve
Crystal dimensions / mm	0.32 × 0.15 × 0.07
F(000)	4694
Crystal system	monoclinic
Space group	$C2/c$
Cell parameters	a = 35.5856(13) Å, α = 90°
	b = 9.6028(3) Å, β = 99.056(3)°
	c = 35.8812(9) Å, γ = 90°
Volume / Å^3	12108.5(7)
Z	8
Density, calculated / Mg m^{-3}	1.219
Absorption coefficient, μ / mm^{-1}	0.363
Temperature / K	100(2)
Radiation type	Mo K_α
Wavelength, λ / Å	0.71073
θ range for data collection / °	$2.98 < \theta < 67.56$
Index ranges	$-41 < h < 42$, $-11 < k < 11$, $-41 < l < 42$
Reflections collected	22605
Independent reflections	[R(int) = 0.0502]
Completeness to θ = 67.56	97.7%
Absorption correction	Semi-empirical from equivalents
Max. and min. transmission factor	1.000 and 0.805
Refinement method	Full-matrix least-squares on F^2
Data / restraints / parameters	10475 / 199 / 701
Goodness-of-fit on F^2	1.101
Final R indices [I>2σ(I)]	R_1 = 0.1120, wR_2 = 0.3427
R indices (all data)	R_1 = 0.1864, wR_2 = 0.3743
Largest diff. peak and hole / e Å^{-3}	1.624 and −0.126